MODEL DEVELOPMENT FOR NUMERICAL SIMULATION OF THE BEHAVIORS OF pH-STIMULUS RESPONSIVE HYDROGELS

YEW YONG KIN

(B.Eng. (Hons.), Universiti Teknologi Malaysia)

A THESIS SUBMITTED

FOR THE DEGREE OF DOCTOR OF PHILOSOPHY

DEPARTMENT OF MECHANICAL ENGINEERING

NATIONAL UNIVERSITY OF SINGAPORE

2006

SUMMARY

The modulation of the swelling ability of the hydrogel in responses to pH and electric stimuli enables us to dynamically control the conversion of electrochemical energy into mechanical energy, thereby obtaining effective diffusivity and permeability of the solutes or performing mechanical work.

In this thesis, a chemo-electro-mechanical model is developed to simulate the deformation characteristics of the pH-stimuli responsive hydrogel based on multi-field effects formulation, and it is termed the Multi-Effect-Coupling of pH-Stimulus (MECpH) model. This model accounts for the ionic fluxes within both the hydrogel and surrounding solution, the coupling between the ionic diffusion, electric potential, and mechanical deformation in the hydrogel. The model also incorporates the relationship between the concentrations of the ionizable fixed charge groups and the diffusive hydrogen ion, which follows a Langmuir isotherm theory, into the Poisson-Nernst-Planck system. On top of that, the finite deformation has been considered in the formulation of mechanical equilibrium equation.

In order to validate the MECpH model, one-dimensional steady-state simulations of the hydrogel deformation with salt concentration, pH and electric potential as the main stimuli are carried out via a meshless Hermite Cloud method and Newton-Raphson iterative procedure. The numerical results are compared with available experimental data. The simulations show a satisfactory agreement with the experiment data from open literature qualitatively and quantitatively. The steady-state

behaviors of swelling equilibrium of hydrogel are demonstrated here in the context of nonlinear chemoelectromechanical theories.

In addition, the behaviors of the hydrogel are considerably dependent on it bathing environment, as well as the physical and chemical nature of the hydrogel. The significances of those factors on the equilibrium deformation can be inferred by tracking the changes of the average curvature or dimension of the hydrogel. The illustrated results are analyzed and discussed with the support of the experimental data from other research groups. Those simulation results are confirmed to be quantitatively consistent with the real measured data. Present studies prove that the MECpH model is accurate, efficient and numerically stable for providing a possible simulating tool for analysis of the nonlinear behavior of the pH-sensitive hydrogel.

ACKNOWLEDGEMENTS

I owe a great debt of gratitude to my supervisor, Prof Lam Khin Yong, who provided me with continuous encouragement and support. It has been a great learning experience for me to work with him. Assoc Prof Ng Teng Yong and Dr Li Hua were instrumental in helping me start my work in Institute of High Performance Computing (IHPC). They have continually lent support through the many years, as well as giving meticulous criticism of my works.

This work was largely written and created at IHPC, where I have spent a large part of my research. The work would not be in successful completion if not the help and encouragement from my friends and staffs in IHPC. I am indebted to many of them; many fruitful discussions have contributed to form most part of the dissertation.

I am fortunate in that I had expert guidance all this while in the field, and I would like to take this opportunity to thank those who have set me on the right road.

Dissertation is not written without a lot of family support. They have given me their unflagging support during those difficult years. My debt to them can never be repaid.

Finally, I would also like to thank the National University of Singapore and the Institute of High Performance Computing for giving financial support.

TABLE OF CONTENTS

LIST OF FIGURES

LIST OF TABLES

LIST OF SYMBOLS

c_k	interior ionic concentration of species k
$\overline{c}_k$	ionic concentration of species k in exterior solution
c^s_{m0}	total ionizable groups per unit solid volume
c_f	fixed charge concentration
D_k	diffusion coefficient of the k^{th} species
D_0	diffusion coefficient in the pure solvent
$\mathbf{D}$	material moduli tensor
$\mathbf{D}_{el}$	electric displacement tensor
E_0	Young's modulus
$\mathbf{E}$	strain tensor of solid matrix
$\mathbf{E}_{el}$	electric field tensor
$\mathbf{F}$	deformation gradient tensor
F	Faraday's constant of 96485 C/mol
f_{ij}	frictional drag coefficients between the inter-diffusing i and j components
ΔG	Gibbs free energy
φ	osmotic coefficient
$\mathbf{I}$	identity tensor
I_{el}	electrical current density
J	determinant of deformation gradient
K_a	dissociation constant
k_B	Boltzmann's constant of $1.3807\times10^{-23}\,\text{JK}^{-1}$
M_i	molecular weight of i^{th} component
$\mathbf{N}_k$	flux of the k^{th} ionic species
$\overline{\text{N}}$	mole fraction
n	number of mole
p	pressure
$\mathbf{P}$	first Piola-Kirchhoff stress tensor
$\mathbf{P}_{el}$	electric polarization tensor
R	universal gas constant of $8.314\,\text{J/mol}\cdot\text{K}$
r_k	radius of the diffusing molecule
$\mathbf{S}$	second Piola-Kirchhoff stress tensor

T	absolute temperature, in K
T_c	chemical expansion stress due to the presence of the charge-to-charge electrostatic repulsive forces
U_i	fluid velocity relative to the solid in *i* direction
V_i	volume of i^{th} component
v	partial molar volume
z_k	valence numbers of ionic species *k*
z_f	valence numbers of fixed charge group
v^i	velocity of the i^{th} component
σ	Cauchy stress of the mixture
γ_k	chemical activity coefficient of k^{th} species
ψ	electrostatic potential
υ	Poisson's ratio
ϕ^i	volume fraction of i^{th} component
χ	Flory interaction parameter
ϑ	number of chains
α_i	ratio of the deformed length to the undeformed length in *i* direction, (i=x,y,z)
μ^i	chemical potential of i^{th} component
μ_0^i	chemical potential of i^{th} component at the reference configuration
μ_k^{el}	mobility of of ionic species *k*
ρ^i	mass density of i^{th} component
ρ_{el}	charge density
λ , μ	Lamé constants
λ_D	Donnan partitioning ratio
ε	relative dielectric constant
ε_0	dielectric constant of 8.85418×10^{-12} C^2/Nm^2

CHAPTER 1

INTRODUCTION

1.1 BACKGROUND

1.1.1 Hydrogels and Their Applications

Hydrogels are form of matters that possess both the properties of solid and liquid (Tanaka, 1981; Osada and Gong, 1993). Their structural frameworks are formed from networks of randomly cross-linked macromolecules that embody three different phases, namely, solid matrix network, interstitial fluid and ion. A schematic drawing of the hydrogel structure is shown in Figure 1.1. The solid portion of the hydrogel is a network of cross-linked polymer chains where their three-dimensional structure is usually described as a mesh, with the interstitial space filled up with fluid. Those meshes of networks hold the fluid in place and also impart rubber-like elastic force that will counter the expansion/contraction of the hydrogel, thus providing the solidity to the hydrogel (Osada and Ross-Murphy, 1993). The cross-linked network can be formed physicochemically, for instance, by hydrogen bonding, van der Waals interactions between chains, covalent bond, crystalline, electrostatic interactions or physical entanglements (Lowman and Peppas, 1999). On the other hand, the fluid phase that filled up the interstitial pores of the network gives the hydrogel its wet and soft properties, which resemble, in some respects, to biological tissues (Mow et al.,

1999). The ionic phase is generally composed of a number of mobile ions (counter ions and co-ions due to the presence of electrolytic solvent that surround the hydrogel) and ionizable groups bound to the polymer chains. The ionizable groups will dissociate in solution completely for strong electrolyte or partially for weak polyelectrolyte groups and the network is left with the charged groups fixed to its chains. These fixed charge groups produce electrostatic repulsion force among themselves, which will add influence to the expansion of gel network. It is therefore known that fixed charge density, an important factor in the electrostatic force, will play a substantial role in changing the swelling of a gel.

Various materials, both naturally existing and synthetic, are examples of water swollen polymeric hydrogels. Crosslinked guar gum and collagens are examples of natural polymer that are modified to produce hydrogels. Classes of synthetic hydrogels include PAA — poly(acrylic acid), PHEMA — poly(hydroxyethyl methacrylate), PAM — poly(acrylamide), PVA-PAA — poly(vinyl alcohol) poly(acrylic acid), PAN — poly(acrylonitrile), PAN/PPY poly(acrylonitrile) poly(pyrrole), NIPA — N-isopropylacrylamide, etc. Depending on the physical and chemical characteristics of the polymer, hydrogel can be categorized further into subclasses. For example, hydrogels can be synthesized to be either neutral or ionic, determined by the chemical characteristic of the pendant groups fixed to the matrix. From the point of physical mechanism, if the overall structure of hydrogels is homogeneous, the polymer chains have a high degree of mobility. If it is heterogeneous, there is a great deal of inter-polymer interaction and the polymer chains are virtually immobile at the molecular level (Muhr and Blanshard, 1982). However, the eventual stability of the hydrogel depends on the interaction between its network and the aqueous medium where it is immersed.

Motivated by the pioneering works of Tanaka and his colleagues (Tanaka, 1978, 1981), an entire new class of hydrogels was introduced. Those hydrogels demonstrate the unique property of undergoing discrete or continuous volume transformation in response to infinitesimal changes of external environment conditions, such as pH (Gehrke and Cussler, 1989; Seigel, 1990; Brannon-Peppas et. al., 1991a; Chu et. al., 1995), temperature (Tanaka, 1978, 1979; Marchetti et al., 1990), electric field (Tanaka et. al., 1982), solvent composition (Tanaka et. al., 1980), salt concentration (Ohmine et. al., 1982), light/photon (Irie, 1986; Irie and Kunwatchakun, 1986; Suzuki and Tanaka, 1990), coupled magnetic and electric fields (Suleimenov et al., 2001) and so on. These magnificent features make the hydrogel better known as stimuli-responsive or smart hydrogels.

Due to their unique properties that include swelling behavior, sorption capacities, mechanical properties, permeabilities and surface properties, hydrogels provide the instrumentation for creating functional materials for broad spectrum of applications as they can sense the environmental changes and eventually induce structural changes without a need for an external power source. Artificial muscle (Shahinpoor, 1995; Bar-Cohen, 2001), microfludic control (Beebe, et al., 2000), sensors/actuators (Brock, et. al., 1994), separation process (Andrews, 1986; Galaev and Mattiasson, 2002; Kobayashi, 2003), and chromatographic packing (Tanaka and Araki, 1989) are just few examples of the successful applications of hydrogels. Another exceptional promise of the hydrogels is their biocompatibility and biostability potentials (Park and Park, 1996), suggesting that the hydrogel are also an excellent substitution for the human body tissues or biomimetic applications. There are also extensive exploration of the hydrogels in the medical and pharmaceutical application, such as drug delivery system (DeRossi et. al. 1991; Kwon et al., 1991a; Khare and

Peppas, 1995; Brazel and Peppas, 1999), articular cartilage (Lai et. al., 1991; Noguchi et al., 1991), biomaterial scaffold (Lee et al., 2003), corneal replacement (Hicks et. al., 1997) and tissue engineering (Elbert and Hubbel, 1996; Suh and Matthew, 2000). Peppas (1987), De Rossi et al. (1991), Osada and Gong (1993), Shahinpoor et al. (1998), Peppas et al. (2000a, 2000b) and Dumitriu (2002) have given some notable reviews of these highly maneuverable smart and adaptive structures in their respected fields.

1.1.2 pH-Sensitive Hydrogel

As pH is the most widely utilized triggering signals for modulating physicochemical stimulus-responsive hydrogels, the studies on the behavior of pH-sensitive hydrogel will be the focus of present thesis.

The pH-sensitive hydrogels contain acidic or basic groups bound to the polymer backbone. These pendent groups will be ionized or protonated in response to the external pH changes. Carboxyl, sulfonic, and amino groups are the popular ionizable groups used to prepare pH-sensitive hydrogel. For acidic hydrogels, the pendent groups are unionized below the dissociation constant pK_a. When bathed in pH above the pK_a, the pendent groups start to ionize. As a result, the hydrogels expand enormously as the osmotic pressure is created due to the concentration gradient of ions. Hence, the acidic or basic strength of the pendent groups is an important foctor controlling the magnitude of expansion (Grignon and Scallan, 1980; Cussler et al., 1984). In principle, weak-acid groups such as carboxyl groups exist in the form of —COOH in low pH and deprotonated become —COO^- in high pH solution. In contrast, strong acid groups such as —SO_3^- remain ionized even at low pH. In basic

hydrogels, the pendent groups are unionized above the dissociation constant pK_b of the basic groups. Whereas, the pendent groups are ionized as the environmental pH decrease from the pK_b value, enhancing the swelling degree of the hydrogel (Hirokawa et al., 1985; Katayama and Ohata, 1985; Podual et al., 2000). Likewise, weak-base groups such as —NH_3^+ is deprotonated, forming uncharged —NH_2 when the pH is high, and strong-base groups such as —$N^+(CH_3)_3$ remain ionized even at high pH.

In conclusion, the swelling of the pH-sensitive hydrogel is generally governed by chemical nature of fixed charge groups bound to the network and the swelling agent, which is completely reversible in nature, as depicted in Fig 1.2.

1.2 OBJECTIVES AND SCOPE

Computer simulation is becoming an alternative branch of research complementary to experiments and analytical theory. It offers great deal of advantages, for instance, the freedom to control the parameters of the system and properties of the material, direct access to the microscopic structures and dynamics, and in particular, providing the bridging between the analytical theory and experiment.

All this while, most of the research explorations of these fascinating new materials is based on experimental trial-and-error, which are very time consuming. These have hindered the development of new materials, and delayed the transfer of new applications from the laboratory to the marketplace. The need to bring innovative and high-quality products to market in the shortest time is driving the use of models that can speed up the design and realization process.

On top of that, the experimentalists might find it difficult or impossible to carry out their jobs as intended under extreme environment parameters. In contrast, a computer simulation of the material, for example, in extreme low pressure or high temperature or even an impulse forces or sinusoidal pulse would be completely viable.

Furthermore, in order to precisely controlling the large deformation feature of the hydrogel by means of computer, for example in biomimetic walking machine, a model algorithm is necessary to be implemented in the computer system. With the knowledge of modeling and computational tools in handy, design and simulation of the hydrogel for various engineering application is just one-click apart.

The main purpose of this thesis is to model and simulate the behaviors of hydrogels in response to the changes of solution pH and externally applied electrical field, and explain the experimental phenomena within a theoretical framework. With the proposed numerical technique – Hermite Cloud method, the present mathematical model termed Multi-Effect-Coupling of pH-Stimuli (MECpH) model, is solved numerically to study

- the concentration distributions of different ion species within the hydrogel and outer bath solution.
- the electric potential distribution across the domain of both hydrogel and bathing solution.
- the degree of swelling equilibrium of the pH-sensitive hydrogel in simple and buffer solution.
- the behavior of hydrogel in response to the stimulation of environmental pH and externally applied electric field.
- the distinct effects of the various physical and chemical factors by means of systematically and independently varying their property parameters.

In order to put the metaphor for the law of nature into a useful model, we need to compare the simulation results predicted by the model with those of real experimental measurements. In the first place, it will examine the underlying model. Ultimately, if the model is a successful one, then the experimental results can be interpreted within the theoretical frame work to asses the role of various mechanisms in the observed responses.

It is also noted that the numerical simulations in this thesis only involve one-dimensional steady-state problems. Indeed, the numerical comparisons of the present model reside in how well the predicted results can match experimental data obtained from open literature. The mathematical frameworks could serve as stepping stone for the more complex 2-dimensional and even 3-dimensional analysis. In order to get a generic view of the more involved mathematical ideas, the following section will summarize some of the works done by other researchers related to the modeling of the environmentally-responsive hydrogels.

1.3 LITERATURE SURVEY

1.3.1 Theoretical Model

The swelling behavior of hydrogel can be described by variety of theoretical frameworks. The ultimate goals of all these theoretical models are to predict the swelling behavior, the degree of ionization in the gel, polymer-solvent interaction, the mesh size for solute diffusion, the nature of the diffusive ions and related parameters. Due to the highly nonideal behavior of polymer networks in electrolyte solutions, it is

difficult to exactly predict the behavior. However, the multitude of understanding of charged polymer available also leaves numerous choices for theoretical formulation. The better approach for development of mathematical model with desired accuracy is to correlate the chemical feature of solvent and macromolecule structure of hydrogel available with the swelling and mechanical characteristic desired. Numerous attempts have been made to model the equilibrium swelling behavior of the stimuli-responsive hydrogel.

The first mean-field treatment of gel network systems was given independtly by Flory (1942) and Huggins (1942). The Flory-Huggins theory is traditionally used to calculate the entropy change due to mixing of solvent molecules with chains of the network structure. In 1968, Dusek & Patterson were the first to predict theoretically a discontinuous volume phase transition of polymer gels between the dense and dilute phases, based on the Flory-Huggins theory (Dusek & Patterson, 1968). It was almost 10 years before researchers from MIT discovered it experimentally where a volume transition for partially hydrolyzed polyacrylamide gels in acetone-water mixture as a function of temperature and fluid composition was observed (Tanaka, 1978). Using the Flory-Huggins theory, Tanaka et al. (1980) and Ohmine and Tanaka (1982) demonstrated that the abrupt volume transition is accounted for by osmotic pressure which is a function of pendent ionizable groups and salt concentration. The Flory-Huggins treatment can describe the phase transition qualitatively but it is not quite satisfactory quantitatively. The improved theories based on the Flory-Huggins model have been presented by Hasa et al. (1975) and Konak and Bansil (1989) independently for the polyelectrolyte gels. One of the most obvious failures of Flory-Huggins theory is its inability to predict the scaling behavior of networks in a good solvent. The

studies of gels in good solvents suggest that the interaction has stronger concentration dependence than that assumed in the Flory-Huggins theory.

An extended variant of statistical mechanical treatment similar to Flory-Huggins theory is the Flory-Rehner model (Flory and Rehner, 1943a, 1943b; Flory, 1962). The Flory-Rehner treatment, including its variants, was continuously used with reasonable success where polymer gel swelling equilibrium was described as a balance between solvent, elastic, electrostatic, and ion osmotic pressure (Katchalsky et al., 1951; Katchalsky and Michaeli, 1955; Siegel, 1990; Brannon-Peppas and Peppas, 1991a, 1991b; Wilder and Vilgis, 1998). The initial theoretical framework was used to describe the swelling of neutral, tetrafunctionally crosslinked polymer gels with polymer chains exhibiting a Gaussian distribution (Flory, 1962). The degree of equilibrium swelling was postulated to be governed by the elastic retractive forces of the polymer chains and the thermodynamics compatibility of the polymer and the solvent molecules. The first significant swelling model based on thermodynamic description for polyelectrolyte gels was given by Michaeli and Katchalsky (1957). These models were developed to relate the dependence of the degree of ionization of loosely crosslinked, highly swollen polymethacrylic acid gels with the pH of external medium. Since then, Brannon-Peppas and Peppas (1991a, 1991b) have extended the application of the theory to charged hydrogel by introducing the ionic contribution to the equilibrium swelling characteristic for both anionc and cationic hydrogels. Those theoretical swelling predictions based on thermodynamics treatments have been used extensively to explain the equilibrium swelling of hydrogels. The mentioned models are simple to use, but they can not provide good quantitative results (Siegel, 1990; Chu et al., 1995). Furthermore, many input parameters in the thermodynamic models are

difficult to determine and are often based on the use of several adjustable parameters to match the experimental data.

Other research groups have derived models for swelling of ionic gels based on Donnan theory (Ricka and Tanaka, 1984; Hooper et al., 1990; Basser and Grodzinsky, 1993). For instance, Ricka and Tanaka (1984) used the Donnan theory to model the swelling of weakly charged ionic gels. The given examples include swelling of a poly(acrylamide-co-acrylic acid) copolymer as a function of the ionic composition of the swelling agent. However, this theory is applicable only for monovalent solution with extremely dilute conditions and neglects all polymer-solvent interactions and network parameters. Some comments can be made for this model. The model does have a simple mathematical expression without change of geometry and size of the diffusion medium. For a gel that has a considerable variation in its swelling degree with the pH range of surrounding solution, the model is too far away from reality.

Some researchers have also described the interplay of the mechanism of the volume changes in term of mathematical parameters depending on various controlling effects. Among the theories proposed are the diffusion control mechanism suggested by Nussbaum and Grodzinsky (1981), in which, the proton transport through a charged polyelectrolyte gel was considered as the dominating step for the swelling and is described by continuity equations.

More recently, macroscopic continuum models have been developed to predict the swelling and deswelling kinetics of polymer gels (Nussbaum, 1986; Grimshaw, 1989; Chu et al., 1995). Their approaches were based on the effects of charged species movement, electrodiffusion mechanism, dissociation of fixed charge groups, electro-osmotic drag, and mechanical deformation of the gel network. The membrane was treated as a macroscopic continuum with smooth spatial variations of charge density,

ion concentration, stress, strain and electric field. Segalman et al. (1993) employed the similar approach and solved the two two-dimensional diffusion equations for H^+ and water, along with the polymer momentum balance. A neo-Hookean model was used for the network stress, accounting for large deformations. The swelling or shrinking of a gel disk was modeled as the imbibition/expulsion of solvent with finite elements analysis. De Gennes et al. (2000) and Wallmersperger et al. (2001a, 2001b, 2004) proposed the electrochemical and electromechanical formulations for ionic polymer metal composites and ionic gel respectively.

Based on the foundation laid by Grimshaw (1989), De et al. (2002) developed a modified model that includes the influence of pH buffer solution, and later improved them by incorporating fluid velocity of solute into their formulation (De and Aluru, 2004). From experimental data comparison, they concluded that the fluid velocity of the solute can be safely neglected for the swelling/deswelling kinetics within a wide range of applications.

Borrowing the ideas from the mixture theory (Bowen, 1980), Mow et al. (1980) have developed a biphasic model to describe the deformation of articular cartilage. The proposed biphasic model is consistent with porous media models (Biot, 1956; Bowen, 1980), which describe the intrinsically incompressible and nondissipitative solid-fluid interaction. The triphasic (Lai et al. 1991) and quadriphasic (Huyghe and Janssen, 1997) mechano-electrochemical model were introduced to include the electrochemical effects into the biphasic mixture model, and to study the transport of electrolytes in charged porous biological tissue. Based on first law of thermodynamics for an irreversible thermodynamic law, the governing equations of triphasic mechano-electrochemical mixture were reformulated by Hon et al. (1999).

Recently, there are also engrossments in molecular simulations for studies of volume phase transitions of polyelectrolyte gels. Aalberts (1996) studied a simplified, defect-free lattice network in two-dimensions, in which, the solvent or counterions are not explicitly simulated and an effective polymer-polymer interaction was described by a square-well potential. The ionic groups within the network are excluded from the simulations, but a hydrogen ion (or counterion) pressure was modeled, as a first approximation, to exert a force inversely proportional to the gel volume. However, these conventional simulation methodologies are not effective at dealing with the topological complexity, large size, and long relaxation times encountered in these systems. There are other newer methodologies introduced recently and can be found in the reviews by Kremer (1998) and Escobedo and Pablo (1999). For example, Schneider and Linse (2003) used the Monte Carlo simulation to study the swelling mechanism of polyelectrolyte where the electrostatics and chain connectivity are simultaneously treated in a consistent manner. Most of the molecular simulations mentioned above only pursuing a perfect or defect-free network with assumption of equal length chains.

1.3.2 Chemically Driven Hydrogels

Katchalsky (1949) and Kuhn et al. (1950) were the first to introduce the stimuli-responsive polymer gels. The crosslinked, water-soluble polyelectrolytes gel may be chemically contracted or expanded like a synthetic muscle. They should also be credited as the first to report the ionic chemomechanical deformation of polyelectrolytes such as polyacrylic acid (PAA) and polyvinyl chloride (PVA) systems. They have shown that the deformation mechanism of ionizable polymeric molecules

depended on the degree of ionization of charged group bound to the molecular chain. Tanaka (1978, 1981) proved experimentally the existence of phase transition in partially ionized acrylamide gels at specific concentration of acetone-water mixture, in a manner analogous to the vapor/liquid phase transition observed with pure fluids.

The possibilities of using polymeric gels as muscles or actuators for chemomechanical engines and turbines were originally discussed by Steinberg et al. (1966), and Sussman and Katchalsky (1970). They also proposed few theoretical models for the physiochemical behavior of the chemomechanical engines which are capable of converting chemical energy directly into mechanical work or reversibly.

Tanaka and Fillmore (1979) introduced a theory for the kinetics swelling of an spherical poly(acrylamide) gel in water and defined the diffusion coefficient as a ratio of longitudinal bulk modulus of the network over the friction coefficient. Experimental data were also given to support their theoretical analysis. Tanaka and his groups also discussed that the discontinuity of the volume phase transition could even be degraded to zero by appropriately varying the degree of ionization, resulting in a critical point at zero osmotic pressure (Tanaka, 1981). Tanaka and his colleagues (Tanaka, 1981) pointed out that the sudden collapses of ionic polymer gels in acetone-water mixtures under infinitesimal changes in external conditions, including temperature change (Tanaka, 1978), solvent composition change (Tanaka et al., 1980), DC electric field application (Tanaka, 1981; Tanaka et al., 1982) and salt concentration (Ohmine and Tanaka, 1982), were due to the phase transition phenomena of the polymer gels. Based on the experimental observations, they also presented a mathematical modeling for deformation of polyelectrolyte gels in electric field originated from the mean field theory formulated by Flory and Huggins (Tanaka and Fillmore, 1979; Tanaka et al., 1982). The model was later extended by Peters and Candau (1986) to include the effect

of shear modulus. Theoretical studies of the gel swelling and collapse were also intensively pursued in the early stage by other groups, for instance, Khokhlov (1980) and Ilavsky (1981).

1.3.3 Electrically Driven Hydrogels

The observation of swelling and shrinking of PVA-PAA polyelectrolyte gel induced by electric field was first reported by Hamlen et al. (1965). They tried to give some insight of the swelling and shrinking behaviors of the polymer fiber impregnated with platinum by associating it to the changes of pH of the surrounding solution when an electric field of 5V was applied. In this case, the solution became either alkaline or acidic depending on the direction of the current. If the solution becomes alkaline it forces the polymer gel to expand. Otherwise, the polymer gel contracts as the solution becomes acidic. The magnitudes of deformation are found to be almost the same as those obtained using dilute sodium hydroxide and hydrochloric acid. Fragala et al. (1972) successfully fabricated the electrically-controlled artificial muscles based on weak acid polymer which is a typical pH-sensitive polymer based on the works of Katchalsky and Kuhn (1949, 1950).

Grodzinsky, Melcher and Yannas also involved in a series of experiments with collagen based membrane, which is a protein polyelectrolyte found in the extracellular specimens as a major component of vertebrate connective tissue, under the control of an applied electric field (Yannas and Grodzinsky, 1973; Grodzinsky, 1974; Grodzinsky and Melcher, 1976). Subsequently, this leaded them to study the electromechanochemical transduction process, where changes in pH and concentration gradient induced by electric fields applied across the collagen membrane were

exploited to produce tensile force (Grodzinsky and Shoenfeld, 1977, 1980). Grodzinsky and his groups (1974, 1976) are also the first to contribute towards the electrochemistry formulation of deformation of charged polyelectrolyte membranes by utilizing continuum model. The mechanical deformation in polyelectrolyte gels is specified to be induced from the changes in intramembrane ionic strength driven by electric field. An electrokinetic model, coupled with convection, diffusion and migration of ions was proposed.

With the goal of developing artificial organ components, De Rossi et al. (1985, 1986) took the bold step in studying the contractile behavior of electrically driven polyelectrolyte gel. They believed the rate limiting processes, that control gel swelling and contractile phenomena in charged polymer networks in the presence of electric fields, comprise of electrodiffusion, electroosmosis and polymer deswelling. They laid out five primary effects on polyelectrolyte gel due to electricity flow, which are: (a) orientation of polar species; (b) deformation of polarizable species and resulting orientation of induced dipoles; (c) deviation of dissociation of weak acids and bases and promotion of separation of ion pairs by external fields (second Wien effects); (d) redistribution of mobile charged species which cause alteration in free energy, and (e) electrochemical reaction at interfaces. They had presented a series of papers (Dario and De Rossi, 1985; De Rossi et al., 1987, 1988a, 1988b; Domenici et al., 1989) on the development of 'skin like' tactile sensors and 'muscle like' actuators by mimicking the electromechanical transduction properties of biological tissue and studying the chemomechanical conversion phenomena.

At the same time, Osada and his groups (Osada and Hasebe, 1985) claimed to be the first to offer an electrically activated artificial muscle system which undergoes contraction under isothermal condition when electric current is running across the

water-swollen polyelectrolyte gels and the rate of volume change is proportional to the electric current. The contraction was believed to be induced from the electrophoretic migration of hydrated ions and concomitant water exudation. They further observed that there were occurrences of protonization of carboxylic groups in water swollen poly(methacrylic acid) (PMAA) gel (Osada et al., 1987), i.e. a decrease of pH of the gel, when a stress was applied (a reverse chemomechanical reaction). Base on the numerous experimental observations, they drew the conclusions that the contraction or expansion of the gel is due to the electrophorectic and electro-osmotic transport of ionic species and water molecules (Osada et al., 1987; Kishi and Osada, 1989; Kishi et al., 1990; Osada et al., 1991).

Nussbaum (1986) and Grimshaw (1989) who were under the supervision of A.J. Grodzinsky proposed some plausible continuum models. They treated the membrane as a macroscopic continuum with smoothed spatial variations in charges density, ion concentration, stress, strain and electric field. Within the framework of the continuum principle, they incorporated the effect of the movement of charged species, electrodiffusion mechanism, dissociation of membrane charge groups, intramembrane fluid flow and mechanical deformation of the membrane matrix into their formulation. Proven with experiment results, they suggested that the electrodiffusion is the dominant mechanism for electrically induced swelling. They also offered a dynamic model to describe the interaction between solvent and polymer gel network frame where two internal state variables is used to describe the system (Grimshaw et al., 1990).

Shiga and his group (1990, 1992a, 1992b) tried to explain the deformation behavior of sodium acrylate–acrylamide copolymer gels (PAA gels) from the point of view of osmotic pressure based on the Flory's theory and conformational change of

polymer network due to the changes of the pendent polyion. These two factors competed with each other and determined the deformation of polymer gel. However, the behavior can be changed with the application of electric field. They also gave a quantitative calculation of the bending, derived from the simple osmotic pressure difference on the basis of Donnan equilibrium. Doi et al. (1992) studied the deformation of ionic gels in buffer solutions when an electric field was applied.

Segalman et al. (1992a, 1992b, 1993) and Brock et al. (1994) presented a series of papers on application and numerical analysis of electrically controlled ionizable polymeric gel as active materials in adaptive structures. They offered theoretical predictions based on the finite element analysis by solving one-dimensional (gel sphere) and two-dimensional (gel disk) collapse of an ionic polymeric gel, considering expansion and contraction of polymer matrix, transportation of fluid into and out of the polymer network, and the coupled effects between the two phenomena.

Shahinpoor et al. (1998) did an excellent review on the mathematical modeling and application of ionic polymer-metal composite (IPMC). They had investigated the dynamics of IPMC in an quasi-statistical electric field (Shahinpoor , 1995; Shahinpoor and Kim, 1998). Recently, Nemat-Nasser and Li (2000) presented a modeling of the electromechanical response of ionic polymer-metal composites based on electrostatic attraction/repulsion forces of IPMCs.

1.4 LAYOUT OF DISSERTATION

The feasibility of controlling the expansion and contraction of a hydrogel will be demonstrated within a theoretical framework in this thesis, and a mathematical

model will be constructed to interpret the trends of experimental results extracted from open literatures. To be specific, the model is used to investigate the impacts of changing hydrogel properties or environmental parameters on the swelling equilibrium of the pH-responsive hydrogels. The discussions in this dissertation try to offer some insight into the deformation mechanism of a hydrogel which is highly dependent on it own properties and medium where it resides. The long range goal of present work is to develop a mathematical model to express the equilibrium swelling of pH-sensitive hydrogels, and subsequently to solve the systems of equations to asses the role of the various mechanisms observed in the experimental results such that they can be interpreted in a comprehensible theoretical manner.

In Chapter 2, a few representative mathematical models proposed by past researchers are reviewed. Concepts applicable to uncharged and charged polymer gels are discussed. Finally, a chemoelectromechanical coupling model is developed to predict the combined effects of pH and electric fields stimuli on the crosslinked, charged hydrogels behavior. Electrodiffusion is the key to understanding and modeling of a charged hydrogel and its surrounding environment, in which ions transport by diffusion under concentration gradient, and migration due to electrical potential gradients. In the present of fixed charge groups in the hydrogel, the dissociation/associate mechanism was also taken into consideration. The linear and finite deformation mechanical equilibrium equations are derived to describe the swelling mechanics of the expanding/contracting hydrogels. Chapter 3 describes the numerical technique used to solve the set of nonlinear multi-field equations presented in chapter 2.

In this thesis it is demonstrated that, under the proper conditions, the swelling of hydrogel can be controlled by bath pH and electrical field applied across the

hydrogel. Steady state experimental comparison and parametric study are presented in Chapter 4 for the effect of pH stimulation and Chapter 5 for the coupling effects of chemical and electrical stimulation. Discussions of the phenomenological behaviors of the hydrogel immersed in chemically and electrically induced environments are also presented in Chapter 4 and Chapter 5. In addition, Young's modulus associated with the degree of crosslinking, concentration of the pendent ionizable groups, initial dimension of hydrogel, ionic strength and solution compositions which have distinct influences on the deformation of the hydrogel network will be discussed.

This dissertation will end with concluding remarks in Chapter 6. The limitations of the present MECpH model are also discussed and further works are recommended.

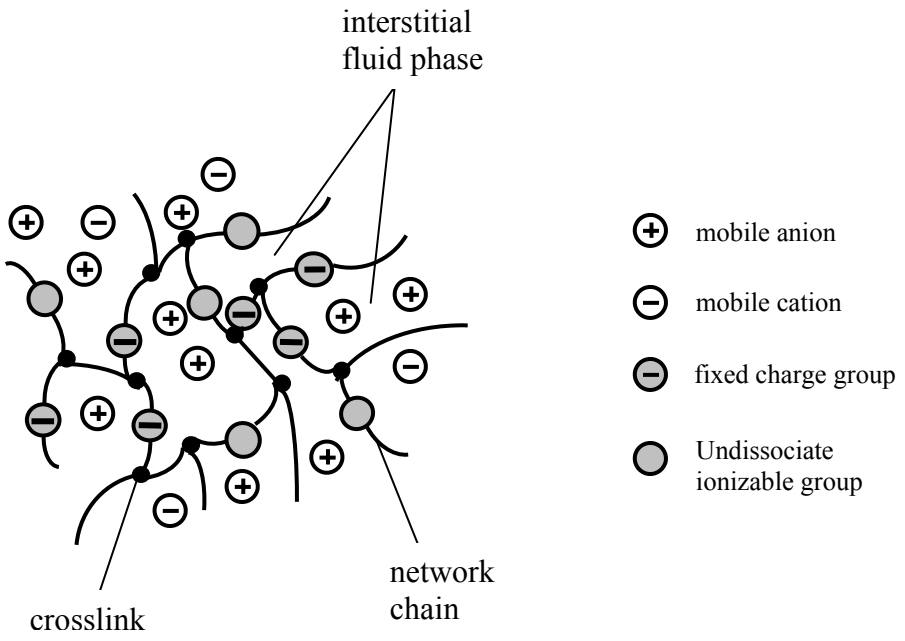

Figure 1.1 Schematic representation of hydrogel structures.

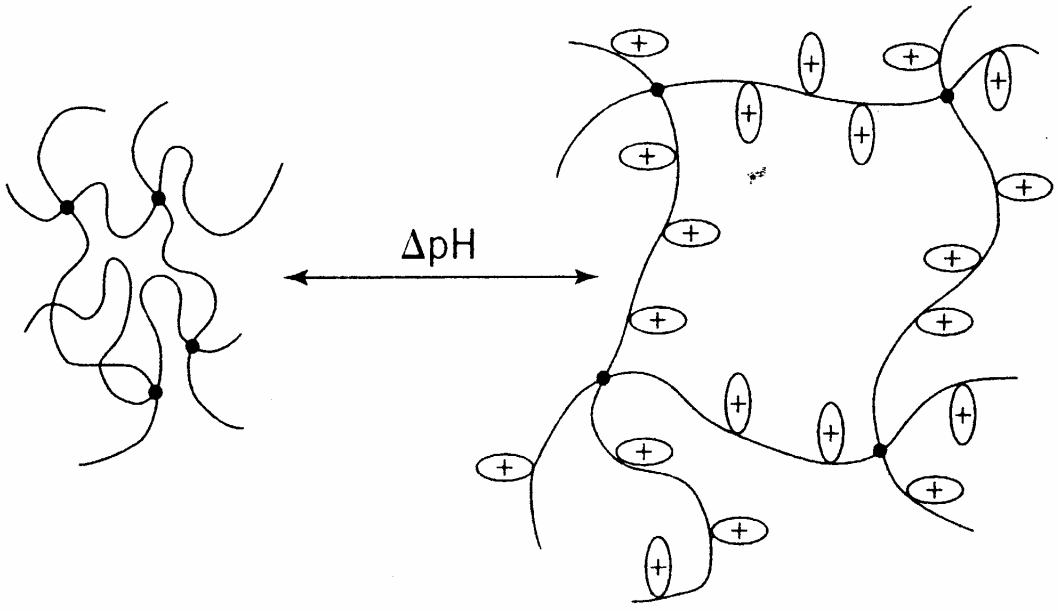

Figure 1.2 Reversible expansion or contraction of ionic hydrogel when pH changes [Lowman and Peppas, 1999].

CHAPTER 2

DEVELOPMENT OF MATHEMATICAL MODEL FOR SWELLING OF pH-SENSITIVE HYDROGELS

2.1 OVERVIEW

For a responsive hydrogel, the degree of swelling/shrinking is dependent upon ionizable groups and network structure of the hydrogel and related parameters plus the nature of environment solvent composition, pH, temperature etc., in which there is an intimate interaction between mechanical, chemical and electrical fields.

In this chapter, a general phenomenological model is developed to predict the effects of chemical milieu and applied electric voltage on the swelling behavior of hydrogel. The proposed electrodiffusion equations based on Poisson-Nernst-Planck (PNP) formulation are obtained from combining the diffusion equation, pendent ionizable groups dissociation reaction and spatial charges. The PNP equations are then coupled with mechanical finite deformation equation to solved for the profiles of ionic, electric and deformation within both hydrogel and bathing solution domain in response to chemical and electric potential changes. Prior to the presentation of the mathematical model, a few of the significant mathematical models are reviewed to make this chapter a self-consistent discussion.

2.2 REVIEW OF EXISTING THEORETICAL MODELS

Only the representative models from the literatures are reviewed herein as general discussions. The two extensively used theoretical description for charged polymer gel or polyelectrolyte or hydrogel are the thermodynamics formulation based on the works of Flory, Huggins, Rehner, etc. (Katchalsky et al., 1951; Katchalsky and Michaeli, 1955; Flory, 1962; Dusek & Patterson, 1968; Hasa et al., 1975; Tanaka, 1978; Tanaka et al., 1980; Ohmine and Tanaka, 1982; Konak and Bansil, 1989; Siegel, 1990; Brannon-Peppas and Peppas, 1991a, 1991b; Wilder and Vilgis, 1998), and multiphasic theory by the Mow's group (Lai et al. 1991; Huyghe and Jann, 1997; Gu et al., 1998; Hon et al., 1999; Sun et al., 1999; Zhou et al., 2002).

2.2.1 Thermodynamics Model

The swelling of hydrogel immersed in a solution is basically described as a mixing of an analogous linear polymer with the solvent; the swollen gel is in fact a polymer solution although an elastic rather than viscous one (Flory, 1962). The mixing tendency is a function of compatibility between polymer and solvent, which is decided by their thermodynamic properties. The mixing tendency drives solvent into the polymer network and expands the polymer network. As the swelling increases, the chains between network junctions are elongated and an elastic retractive force in the gel is then developed to oppose the swelling process. When an equilibrium state of swelling is attained, the elastic retractive force will balance with the swelling expansion force.

The earliest theory was developed by Flory and Rehner (1943) for a neutral, crosslinked polymer system where the polymer chains react in the solid state and the macromolecular chains exhibit Gaussian distribution. Generally, thermodynamics model assumes three sources of Gibbs free energy that will contribute towards the total free energy of the hydrogel-solvent system, namely free energy of hydrogel-solvent mixing, elastic free energy due to the deformation of polymer network and the ionic free energy due to mobile ions (Flory, 1962).

Firstly, the free energy of mixing represents the entropy change as a result of mixing of the polymer chains with surrounding solvent. If the solvent and hydrogels are relatively compatible, the free energy of mixing favors the swelling of the hydrogel. Otherwise, if both are relatively incompatible, the contribution of the mixing entropy will be suppressed. Secondly, the elastic retraction of the cross-linked network of hydrogels will discourage the swelling as the hydrogel stretches to greater extend. Thirdly, the osmotic pressure originated from concentration differences of mobile ions between the hydrogels and aqueous bathing solution, which tends to swell the hydrogels.

The total change in the Gibbs free energy ΔG of ionic hydrogels can be expressed as the sum of mixing ΔG_{mix}, elastic $\Delta G_{elastic}$ and ionic free energies ΔG_{ion}.

$$\Delta G = \Delta G_{mix} + \Delta G_{elastic} + \Delta G_{ion} \tag{2.1}$$

By taking the derivatives of each term in Equation (2.1) with respect to the number of solvent molecules in the system, an expression for the total chemical potential $\Delta\mu$ of the system due to mixing $\Delta\mu_{mixture}$, the network elastic deformation $\Delta\mu_{elastic}$ and ionic potential $\Delta\mu_{ion}$, is derived as

$$\Delta\mu = \mu - \mu^0 = \left(\frac{\partial \Delta G_{mix}}{\partial n}\right)_{p,T} + \left(\frac{\partial \Delta G_{elastic}}{\partial n}\right)_{p,T} + \left(\frac{\partial \Delta G_{ion}}{\partial n}\right)_{p,T} \qquad (2.2)$$
$$= \Delta\mu_{mixture} + \Delta\mu_{elastic} + \Delta\mu_{ion}$$

where μ is the chemical potential of the solvent within the hydrogels-solvent mixture and μ^0 is the chemical potential of the pure solvent. At equilibrium state, when the total Gibbs free energy is minimized, the chemical potential within hydrogels μ is equal to that of the exterior bathing solution $\bar{\mu}$ (i.e. $\mu = \bar{\mu}$). Substituting this condition in Equation (2.2) and writing $\Delta\bar{\mu}_{ion}$ for $\bar{\mu} - \mu^0$, therefore, we have

$$\Delta\bar{\mu}_{ion} - \Delta\mu_{ion} = \Delta\mu_{mixture} + \Delta\mu_{elastic} \qquad (2.3)$$

In general,

$$\Delta\bar{\mu}_{ion} \equiv \bar{\mu} - \mu^0 = \varphi RT \ln \bar{\mathrm{N}} \qquad (2.4)$$

where φ is the osmotic coefficient and $\bar{\mathrm{N}}$ the mole fraction of the solvent in exterior solution. In dilute solutions $\varphi \cong 1$ and $\ln \bar{\mathrm{N}} \cong -\mathrm{v}\sum_k \bar{c}_k$. Therefore, we may write

$$\Delta\bar{\mu}_{ion} \cong -\mathrm{v}RT\sum_k \bar{c}_k \quad \text{and} \quad \Delta\mu_{ion} \cong -\mathrm{v}RT\sum_k c_k \qquad (2.5)$$

where the summation includes all mobile ionic species only.

$$\Delta\bar{\mu}_{ion} - \Delta\mu_{ion} = \mathrm{v}RT\sum_k (c_k - \bar{c}_k) \qquad (2.6)$$

where c_k is the interior ionic concentration of species *k*, and $\bar{c}_k$ is the ionic concentration of species *k* in exterior solution. v is the solvent partial molar volume. It is noted that the Equation (2.6) is equivalent to Van't Hoff's law for osmotic pressures of dilute solutions. Therefore, we can consider the ionic contribution to chemical potential as consequence from osmotic pressure gradient in hydrogels-solvent system (Seigel, 1990).

In the resulting Equation (2.3), the mathematical expressions of chemical potential of mixing and elastic deformation, $\Delta\mu_{mixture}$ and $\Delta\mu_{elastic}$, are required for equilibrium analysis of hydrogels. Usually they are obtained by examining the contribution of mixing and elastic deformation towards the system equilibrium, based on various assumptions and theories.

The free energy of mixing is generally described by the Flory-Huggins lattice theory of polymer solutions (Huggins, 1942; Flory, 1942; 1962). By differentiating the free energy of mixing with respect to the number of moles of solvent in the hydrogel, we can obtain the chemical potential of mixing as

$$\Delta\mu_{mixture} = RT[\ln(1-\phi)+\phi+\chi\phi^2] \tag{2.7}$$

where ϕ is the volume fraction of the swollen gel, χ the Flory interaction parameter which ranges from 0 to 1, R the universal gas constant and T the absolute temperature. The χ parameter depends on the compatibility of the hydrogel and solvent, hence it is also an indicator of the compatibility level of the mixing hydrogel-solvent system. For an instance, a low value of χ is associated with the tendency of the hydrogel-solvent mixing and therefore it indicate the increase of swelling degree. A constant interaction parameter is often used in majority of the simulations done. However, recent experiments have proven that it is indeed a function of polymer volume fraction (Erman and Flory, 1986; Mikos and Peppas, 1988).

As to account for the presence of solvent during network formation, the modified statistical theory of polymer elasticity is utilized to quantify the elastic contribution. The theory assumes that the cross-linked network of the polymer chains is in the form of Gaussian random-walk configuration with an initial configuration representing a state of a

maximal probability or configuration entropy. By stretching, compressing or swelling, the network is distorted, and results in formation of cross-linked chains with less probable configurations. This decreases the configuration entropy of the chains and increases the free energy. In general, the internal energy is negligibly affected by practically any deformation process of interest. For the succinct of present discussion, the theory will only consider an ideal network which is also adopted by most research works. Each cross-link point of the ideal network joins to four polymer chains and all chains terminate at two different cross-linked points. In other words, there are no "dangling" ends or single-chain loops. Further, it is assumed that the topological entanglements between chains have negligible influence on the network elastic properties of the network.

The actual geometry of the network formation can be of any types of shape. A rectangular prism is chosen as an example for the present purpose. The corresponding chemical potential of elasticity deformation is given by

$$\Delta\mu_{elastic} = \vartheta RT \sum_{i=x,y,z} (\alpha_i - \frac{1}{2\alpha_i}) \frac{\partial \alpha_i}{\partial n} \tag{2.8}$$

where ϑ is the number of chains, the subscript *i* denotes the spatial direction. For example, α_x designates the ratio of the deformed length to the undeformed length in the *x* direction. For free isotropic swelling, the deformation ratio can be considered as

$$\alpha_x = \alpha_y = \alpha_z = \left(\frac{\phi_0}{\phi} \right)^{1/3} \tag{2.9}$$

Substituting Equation (2.8) into Equation (2.9), the chemical potential of elastic deformation is given by

$$\Delta\mu_{elastic} = \bar{v} RT \rho_0 \left[\left(\frac{\phi}{\phi_0} \right)^{1/3} - \frac{1}{2} \left(\frac{\phi}{\phi_0} \right) \right] \tag{2.10}$$

where ρ_0 is the density of polymer chains in the network at formation, i.e. $\rho_0 = \vartheta / V_0$ in which V_0 is the hydrogel volume at formation, $\bar{\nu}$ the partial molar volume of water. It is note that ϕ_0 / ϕ is the ratio of the volume of the hydrogel after swelling to that before swelling. In more complete form, the elastic potential can be calculated by

$$\Delta\mu_{elastic} = RT\left(\frac{\bar{\nu}}{V_0 \bar{M}_c}\right)\left(1-\frac{2\bar{M}_c}{\bar{M}_n}\right)\phi_0\left[\left(\frac{\phi}{\phi_0}\right)^{1/3} - \frac{1}{2}\left(\frac{\phi}{\phi_0}\right)\right] \tag{2.11}$$

where $\bar{M}_c$ is the molecular weight of the polymer chains between cross-links, whereas $\bar{M}_n$ is the average molecular weight of the polymer chains before cross-linking.

In general, the ionic concentrations within hydrogels is not known directly, but it can be expressed in term of exterior bathing solution ion concentration using Donnan theory and a isotherm reaction of the ionizable groups. With these assumptions, the chemical potential equation still has two unknowns, the solid volume fraction of polymer at equilibrium ϕ and Donnan partitioning ratio λ_D. Electroneutrality inside the hydrogel provides an additional condition containing the same unknowns. The system of two nonlinear equations can then be solved for ϕ and λ_D using the Newton method.

For example, the interior ion concentrations can be determined by the concentrations of exterior bathing solution based on the assumption of Donnan equilibrium as

$$\lambda_D = \left(\frac{c_k}{\bar{c}_k}\right)^{1/z_k} \tag{2.12}$$

A further assumption made in Equation (2.12) is that the activities and concentrations are in dilute condition where they are equal for each phase. By introducing Donnan

equilibrium Equation (2.12) into the Equation (2.6), the ionic chemical potential is obtained in terms of bath concentrations as follows

$$\Delta\bar{\mu}_{ion} - \Delta\mu_{ion} = \bar{v}RT\sum_{k}[(\lambda_D{}^{z_k} - 1)\bar{c}_k] \tag{2.13}$$

Substituting the Equations (2.7), (2.11) and (2.13) into the Equation (2.3), an equilibrium governing equation for the swelling hydrogels is derived as

$$\bar{v}RT\sum_{k}[(\lambda_D{}^{z_k} - 1)\bar{c}_k] = RT[\ln(1-\phi) + \phi + \chi\phi^2] + RT\left(\frac{\bar{v}}{V_0\bar{M}_c}\right)\left(1 - \frac{2\bar{M}_c}{\bar{M}_n}\right)\phi_0\left[\left(\frac{\phi}{\phi_0}\right)^{1/3} - \frac{1}{2}\left(\frac{\phi}{\phi_0}\right)\right] \tag{2.14}$$

The governing equation above can be solved if both the volume fraction of hydrogels at equilibrium ϕ and the Donnan partitioning ratio λ_D are given. In order to obtain the two variables, an additional equation is required and it is the constraint condition of bulk electroneutrality for the hydrogels. If c_f denotes the fixed charge concentration of the hydrogels, the electroneutrality condition is

$$c_f + \sum_{k} z_k(\lambda^{z_i} - 1)\bar{c}_k = 0 \tag{2.15}$$

where c_f is signed according to the valence of the fixed charge groups. By solving numerically the two nonlinear Equations (2.14) and (2.15), the swelling behavior of the hydrogel is simulated.

For electrolyte solution of symmetrical salt ($z:z$) with concentration lower than the fixed charge concentration, counterion of concentration $c_+ = c_f / z$ diffuses into hydrogel in order to neutralize the fixed charge groups. Hence, the Donnan ratio λ_D can be determined from Equation (2.15) as

$$\lambda_D = \left(\frac{c_f}{z\bar{c}_+} \right)^{1/z} \tag{2.16}$$

In the case where the concentration of the outer electrolyte solution is higher than the fixed charge concentration, the concentration difference of mobile ion between the domain inside and outside of the hydrogel is comparable with the fixed charge concentration, the Donnan ratio λ_D can be determined as

$$\lambda_D = 1 - \frac{c_f}{\sum z_k^2 \bar{c}_k} \tag{2.17}$$

Thermodynamics model of the ionic hydrogels offers a simple method for predicting the equilibrium swelling characteristic of the hydrogels. However, it will only become more effective in providing more consistent qualitative and quantitative results if some improvements are made in the formulation. First, a rigorous statement of Donnan equilibrium would require concentrations in Equation (2.12) to be replaced by chemical activities (Overbeek 1956), as the chemical activity coefficients are assumed to be unity in the ideal theory. Secondly, the osmotic coefficient g in Equation (2.4) should be considered instead of fixing it to a unity. Thirdly, the ideal Donnan theory prescribes swelling as a function of the concentrations and valences of the ions in the outer solution, but independent of ϕ. This seems unlikely, since nonidealities in ionic interactions will take place when the volume fraction of polymer is appreciable (Siegel et al. 1991). Further, the statistical theory of polymer elasticity is limited to ideal cases. Problem may occur if the swelling of hydrogel is in the range of large deformation, the chains are short, chains entanglements or random cross-linking occurs, as the Gaussian statistics is insufficient to describe the real situation. Furthermore, most of the theories of polyelectrolyte gel

proposed are still based on the affine model (Flory, 1962). The model, which states that the end-to-end distance of a chain scales linearly with the linear extension of the gel, was originated from the pioneering work of Flory and Rehner (1943a, 1943b). Therefore, the application of non-Gaussian statistic is inevitable and hence the molecular level simulation seems to be more realistic (Konak and Bansil, 1989; Prange et al., 1989; Schneider and Linse, 2003; Mann et al., 2004). This will complicate the solution as it needs additional experimentally determined parameters. For more discussions of the polyelectrolyte gel theories, an excellent collection of works edited by Dusek (1993a, 1993b) is a good direction to start with.

Even though Flory-Huggins theory is able to model the phenomenological effect of the solvent-hydrogel mixing system, it is still far from convincing when compared quantitatively with experimental data. One of the reasons is that the χ parameter is assumed to be a constant in most cases while many researchers proved that χ is also dependent on the volume fraction of swollen hydrogels. The second reason is that the random-mixing polymer-solution model does not account for orientation-dependent interactions (i.e. hydrogen bonds) and thus often fails to describe correctly phase behavior in aqueous solutions. Therefore, usually this model is used to estimate qualitatively the swelling of hydrogels, instead of pursuing the quantitative accuracy. On top of that, most of the thermodynamic treatments rely on the use of several adjustable parameters to match experimental data and provide reliable extrapolations over a limit range of conditions.

2.2.2 Mixture Theory – Multiphasic Mechano-Electrochemical Model

Mow et al. (1980) formulated a biphasic mixture theory for articular cartilage where the collagen–proteoglycan matrix is described as an incompressible porous-permeable solid matrix, and the interstitial fluid as incompressible. Later on, Mow and his co-workers (Lai et al., 1991; Gu et al., 1998; Sun et al., 1999) developed the triphasic mechano-electrochemical model to describe the mechano-electrochemical behavior of the charged-hydrated soft tissues, by combining the physico-chemical theory for ionic and polyionic (proteoglycan) solutions with the fluid-solid biphasic theory. The charged-hydrated soft tissue is considered as a mixture composed of: (1) an intrinsically incompressible, porous-permeable-charged solid matrix phase, (2) an intrinsically incompressible interstitial fluid phase, and (3) ion phase with 2 monovalent ion species, anion and cation. The model is based on the assumption that the driving forces for the movements of water and neutral salt in the charged hydrogels are gradients of their chemical potentials. Further, the stress in the solid matrix network and the chemical potentials of the interstitial fluid and ions are related to the Helmholtz energy functions in accordance with the laws of energy balance and entropy. The continuum mechanics and the second law of thermodynamics are the principal grounds for this theory. A brief description of the triphasic theory is given as follows, where only monovalent electrolyte and infinitesimal deformations are considered here for the sake of simplicity.

Saturation condition

$$\phi^s + \phi^w + \phi^+ + \phi^- = 1 \tag{2.18}$$

where $\phi^i (i = w, s, +, -)$ is the volume fraction (i.e. $\phi^i = dV^i / dV$) and the superscripts *s, w, +, –* represent the solid matrix, fluid phase, cation and anion species, respectively. Usually, ϕ^+ and ϕ^- are neglected as they are considerably small when compared with solidity ϕ^s and porosity of tissues ϕ^w.

Continuity equations

If the chemical reaction is neglected, the conservation of mass for each component is written as

$$\frac{\partial \rho^i}{\partial t} + div(\rho^i v^i) = 0 \qquad (i = w, s, +, -) \qquad (2.19)$$

where ρ^i is the apparent mass density and is related to its true density ρ_T^i by $\rho^i = \phi^i \rho_T^i$. v^i is the velocity of the i^{th} component. By using both the saturation condition of (2.18) and continuity equation of (2.19), and assuming that the mass density remains unchanged, the continuity equation for mixture is derived as

$$div(\phi^s v^s + \phi^w v^w + \phi^+ v^+ + \phi^- v^-) = 0 \qquad (2.20)$$

By neglecting the small contribution of the ionic volume fraction $\phi^k (k = +, -)$, the Equation (2.20) is simplified as

$$div(\phi^s v^s + \phi^w v^w) = 0 \qquad (2.21)$$

This model further assumes that the total amount of fixed charge groups remain unchanged. The fixed charge density c^f also is conserved at all time during deformation

$$\frac{\partial \phi^w c^f}{\partial t} + div(\phi^w c^f v^s) = 0 \qquad (2.22)$$

Hence, the distribution of fixed charge density can be defined as a function of the deformation as

$$c^f = \frac{c_0^f}{(1+\mathrm{tr}(\mathbf{E})/\phi_0^w)} \tag{2.23}$$

in which c_0^f is the fixed charge density at the reference state which is assumed to remain unchanged with the ionic environment, and ϕ_o^w is the volume fraction of interstitial water content which is assumed to be homogeneous throughout the whole system.

Electroneutrality condition

In addition to the continuity equation, the electroneutrality condition is also imposed as

$$\sum_i z^k c^k + z^f c^f = 0 \tag{2.24}$$

where z^k and z^f are the valence numbers of ionic species k and the fixed charge respectively, and c^k and c^f are the corresponding charge densities. This equation is to be obeyed at all time.

The conservation of ions and fixed charges, with the electroneutrality conditions (2.24) yield an additional equation as

$$div(I_{el}) = 0 \tag{2.25}$$

where the electrical current density $I_{el} = F\phi^w[c^+(v^+ - v^s) - c^-(v^- - v^s)]$, and F is the Faraday's constant.

Momentum equation

A few assumptions made for development of the triphasic theory can be summarized: (1) gravitational effect is neglected and the body force is taken to be zero, (2) effect of magnetic filed is absent, (3) the gradients of the chemical/electrochemical

potentials are considered as the driving forces and they are balanced by the frictional forces between each phase. Thus, the momentum equations are derived as

Tissue: $$\nabla \cdot \sigma = 0 \tag{2.26}$$

Fluid phase: $$-\rho^w \nabla \mu^w + f_{ws}(v^s - v^w) + f_{w+}(v^+ - v^w) + f_{w-}(v^- - v^w) = 0 \tag{2.27}$$

Cation: $$-\rho^+ \nabla \overline{\mu}^+ + f_{+s}(v^s - v^+) + f_{+w}(v^w - v^+) + f_{+-}(v^- - v^+) = 0 \tag{2.28}$$

Anion: $$-\rho^- \nabla \overline{\mu}^- + f_{-s}(v^s - v^-) + f_{-w}(v^w - v^-) + f_{-+}(v^+ - v^-) = 0 \tag{2.29}$$

where σ is the total stress of the mixture (tissue), $\overline{\mu}^+$ and $\overline{\mu}^-$ are electrochemical potentials for cations and anions, respectively, and $\overline{\mu}^w$ is the chemical potential for the fluid phase. f_{ij} is defined as the frictional drag coefficients per unit tissue volume between the inter-diffusing *i* and *j* components. Following the classical mixture theory, the frictional coefficients are assumed to be symmetric, i.e. $f_{ij} = f_{ji}$.

Constitutive equations

For an isotropic hydrated charged tissue with infinitesimal deformation, the total mixture stress and chemical potentials for the interstitial fluid phase and salt are given by

$$\sigma = -p\mathbf{I} - T_c\mathbf{I} + \sigma^e = -p\mathbf{I} - T_c\mathbf{I} + \lambda e\mathbf{I} + 2\mu\mathbf{E} \tag{2.30}$$

$$\mu^w = \mu_0^w + [p - RT\phi(c^+ + c^-) + B_w e]/\rho_T^W \tag{2.31}$$

$$\mu^+ = \mu_0^+ + (RT/M_+)\ln(\gamma_+ c^+) + F\psi/M_+ \tag{2.32}$$

$$\mu^- = \mu_0^- + (RT/M_-)\ln(\gamma_- c^-) - F\psi/M_- \tag{2.33}$$

$$T_c = a_0 c^f \exp\{-\kappa(\gamma_\pm/\gamma_\pm^*)[c^+c^-]^{1/2}\} \tag{2.34}$$

where *p* is the pressure of the fluid phase, T_c is the chemical expansion stress due to the presence of the charge-to-charge electrostatic repulsive forces in the solid phase, and it

depends explicitly on the fixed charge concentration, σ^e is the elastic stress of the solid phase, μ_0^i the chemical potential per unit mass of *i*-component at the reference configuration, λ_s and μ_s are the Lamé constants of solid matrix, γ_+ and γ_- are the activity coefficients of cation and anion respectively, $\gamma_\pm$ is the mean activity coefficient (i.e. $\gamma_\pm = (\gamma_+\gamma_-)^{1/2}$), M_+ and M_- are the molecular weights of the cation and anion respectively, ϕ is the osmotic coefficient and ψ is defined as the electrical potential, a_0, κ and B_w are the material constants. *F*, *R* and *T* refer to the Faraday constant, universal gas constant and absolute temperature respectively.

Boundary condition

The boundary of the triphasic mixture is assumed to be fixed to the solid matrix network. The interstitial fluid and ions are allowed to exchange freely at the interface between the boundary and exterior solution. For quasi-static conditions, the chemical potentials μ^i and μ^w are continuous across this boundary, and the total stress vector ($\boldsymbol{\sigma} \cdot \mathbf{n}$) of the tissue mixture at such a boundary must be equal to the traction vector acting on the mixture due to the momentum balance. Thus, for the triphasic theory, it is natural to express the momentum equation in term of the total stress $\boldsymbol{\sigma}$ and the two chemical potentials μ^i and μ^w.

There are a few deficiencies about the mixture model. Firstly, the computational domain confined within the hydrogels only, and the exterior bathing solution is excluded from the domain of interest. In other words, the responses of the solid displacement, ion concentrations, and fluid and ion velocities to the external stimuli are solved only for the hydrogels domain, without regard to the concomitant changes in the bathing solution.

Secondly, the triphasic model assumes that the solid deformations are small and a linear strain-displacement relation is sufficient to describe the hydrogel displacement. In fact, the deformations of hydrogel are often appreciable and should be described by large deformation theories. Thirdly, an assumption of an "electroneutrality" condition is made in this model. Thus, this model is only applicable to particular cases. In fact, the existences of ionic diffusion and fixed charge result in a distribution of electric potential although it is usually smaller compared with externally applied electric fields. Further, the model still lack rigorousness for treatment of chemical reaction between phase and electrostatic interaction. However, it will be a demanding job to extend this model to capture extra phenomenological behaviors of interest as the model is complex and computationally expensive.

2.3 DEVELOPMENT OF MULTI-EFFECT-COUPLING pH-STIMULUS (MECpH) MODEL FOR pH-SENSITIVE HYDROGELS

2.3.1 Overview

Most of the theoretical formulations in the preceding sections are either oversimplified, hence confined it applicability to certain cases, or so complex that they are inflexible for expanding to account for additional parameters that are significant as proven by experiment works. Therefore, we have seek for a theoretical formulations with

clear vision in fundamental background, possible extension and robust in wide range of application.

A mathematical model, termed Multi-Effect-Coupling pH-stimulus (MECpH), is developed to simulate the behavior of the pH-sensitive hydrogels in response to infinitesimal changes in environmental conditions. The model is based on the Poisson-Nernst-Planck (PNP) system coupled with a finite deformation mechanical equation.

Usually the Nernst-Planck flux system is used to describe the transport mechanisms of ionic species in a solution. It is obvious that the Nernst-Planck system is insufficient as it includes only the gradient effects of the concentrations and electrical potential. Over the past few decades, numerous researchers chose the simplified model by assuming electroneutrality conditions or a constant field. Those conditions are two widely used assumptions, as they are the two limiting cases of specific dimensionless parameters that related to the ratio of the Debye length to membrane thickness. Therefore, these assumptions when applied in Nernst-Planck system is not sufficiently accurate for some electrolytic solutions, especially for the presently considered hydrogels with fixed charges, but are found commonly in the description of biological systems like thin membranes. A more rigorous model is required to include the variation of the electric potential according to the spatial distribution of the electric charges, for which the relationship between the electrical potential and the various ionic fluxes is considered by coupling with the Poisson equation, to form the PNP system. According to this system, the drift of an ionic species strongly influences that of all other ions dissolved in the electrolytic solution. Further, the model couples the mechanical equilibrium equations with the PNP equations to simulate the deformation of hydorgels.

One of the important contributions that the present model makes is to incorporate a relation between the fixed charge attached to the long-molecular chain network and the diffusive hydrogen ions, which was done based on the Langmuir absorption isotherm with consideration of the hydrogen ion bound by the fixed charge attached on the polymer chains of hydrogels. Secondly, a finite deformation formulation has been incorporated into the model mathematics.

The MECpH models for pH-responsive hydrogels is able to simulate the concentration profiles of all diffusive ionic species, electric-potential distribution and mechanical deformation of the hydrogels swollen in the bathing solution of varying conditions.

2.3.2 Electrochemical Formulation

There are several possible approaches to simulate the ion permeation at atomistic level, that include all-atom molecular dynamics simulation (Alder and Wainwright, 1959; Allen and Tildesley, 1987; van Gunsteren and Berendsen, 1990; Muller-Plathe, 1991; Tonsing and Oldiges, 2001, 2002a, 2002b; Victorov et al., 2002; Cascales et al., 2003), Monte Carlo simulation (Metropolis et al., 1953; Allen and Tildesley, 1987; Lonergan et al., 1995; Binder, 1997; Netz and Dorfmuller, 1997; Snyder et al., 2001, 2002; Valiulin and Skirda, 2001), Brownian dynamics simulation (Chandrasekhar, 1943; Ermak and McCammon, 1978; Cooper et al., 1985; Allen and Tildesley, 1987; Kim and Torquato, 1992; Johansson et al., 1993; Viramontes-Gamboa et al., 1995; Miyata et al., 2002), Eyring or Kramer's rate theory (Eyring, 1936; Lauger, 1973, 1982; Hladky, 1974; Cooper

et al., 1985; Hanggi, 1990; Hille,1992; Syganow and von Kitzin, 1995; Eisenberg, 1999; Laio and Torre, 1999).

Even though the continuum formulations leave out the fine detail of atomic level reality that will become significant at microscopic level, they are very valuable in highlighting fundamental principles in a particularly clear fashion. Further, we are dealing with millions of ion interacting with each other in every time step. Therefore, it is more practical in sense to study the ion transport in hydrogel in a continuum manner. In particular, macroscopic continuum electrostatic calculations are based on the ability to choose infinitesimally small volumes of interest but large enough to cover sufficient number of charge groups, such that meaningful volume charge density can be described in a continuous sense and thus serve to illustrate fundamental principles in a particularly comprehensible way to general (Woodson and Melcher, 1968; Grodzinsky, 1974).

Among the continuum theory formulated for electrodiffusion modeling, Poisson-Nernst-Planck (PNP) equation has been applied with great success for describing the ion transportation phenomena in polyelectrolyte gel (Gulch et al., 2000; Wallmersperger et al., 2001a, 2001b), ion exchange or biological membrane (Helfferich, 1962; Carnay and Tasaki, 1971; Sjodin, 1971; Rubinstein, 1990), biological ion channel (Kurnikova et al., 1999; Syganow and von Kitzin, 1999; Gillespie and Eisenberg, 2001, 2002; Roux et al., 2004), semiconductor (Selberherr, 1984), soil or clay (Samson et al., 1999; Samson and Marchand, 1999) and other porous media (MacGillivray, 1968; MacGillivray and Hare, 1969; Kato, 1995), to name a few.

In the PNP system, the electric field is calculated self-consistently from the average ionic charge densities; ion-ion interactions are thus incorporated approximately at a mean-field level. As what Eisenberg (1999) put it,

"*… the best way to uncover the specific chemical properties of channels is to invoke them as little as possible, seeking to explain with mean field electrostatic first. Then, when phenomena appear that cannot be described the way, by the mean field alone, turn to chemically specific explanations, seeking the appropriate tools (e.g. Langevin, or molecular dynamics) to understand them …*".

With that strategy, we turn our attention to the hydrogel, apply the law of electrodiffusion to it, and see how many of their properties we can predict just in that way.

2.3.2.1 Ionic Flux Equation

Hydrogel consists of network of crosslinked matrix onto which fixed charges are bound and there are mobile co-ion and counter-ion surrounding the mesh network. The flow of fluxes could arise due to gradients of concentration, electrical potential, chemical potential or pressure. The Nernst-Planck equation could be prescribed to express the ionic fluxes in term of gradients of the concentration, potential and pressure gradients. If the mass conservation is considered, the ionic fluxes and concentration of the ionic species can be related by the continuity equation.

The Nernst-Planck equation of transport (Teorell, 1953; Dresner, 1972), describing the flux of ionic species *k* in solution, is given as follows

$$\mathbf{N}_k = -\left(D_k \ \mathrm{grad}(c_k) + z_k \mu_k^{el} F c_k \ \mathrm{grad}(\psi) + D_k c_k \ \mathrm{grad}(\ln \gamma_k) \right) + c_k U_i \quad (k=1, 2, 3, \ldots \beta) \quad (2.35)$$

where $\mathbf{N}_k$ (mol/m^{2}s) is the flux of the k^{th} species and β is the number of species in the system. D_k (m^2/s) is the diffusivity tensor of the k^{th} species, i is the direction of flux flow, c_k (mol/m^3) the concentration of the k^{th} diffusive ionic species, z_k the kth-ionic valence number, μ_k^{el} (m/s·N) the mobility of the k^{th} ion species, ψ (V) the electrostatic potential,

γ_k the chemical activity coefficient of k^{th} species and U (m/s) is the fluid velocity relative to the solid. F, R and T are the Faraday's constant (9.6487×10^4 C/mol), universal gas constant (8.314 J/mol$\cdot$K) and absolute temperature (K), respectively.

The first term on the right hand side of Equation (2.35) represents the diffusive flux based on the concentration gradient in the domain. This term is identical to the Fick's first law of diffusion equation. The spatial distribution of concentration $c_k(\mathbf{x})$ could be a linearly continuous gradient or become rather complicated with an irregular concentration pattern (Katchalsky and Curran, 1965).

The second term represents the migration flux arising from the gradient of the electrical potential. It is applicable when electrostatic forces exist with or without the source of the externally applied electric potential. The electric potential could linearly vary across the domain which is so-called constant field conditions or the distribution could become a Poisson type of equation. Therefore, the concentration profiles are coupled results from the bulk concentration and from its passive distribution in the electric field (Helfferich, 1962). This will be discussed more thoroughly in following section.

The third term is related to the chemical activity coefficient of ions in non-ideal electrolyte solution. There are several semi-empirical equations developed to calculate the chemical activity coefficient. However, the Debye-Huckel model is still the most popular mathematical description to determine the activity coefficient. It should be noted that, if an external electric field is imposed, the rate of the ionic diffusion is much faster than the kinetics of chemical activity. Therefore, the contribution of chemical activity coefficient is relatively much smaller and can be neglected. More studies of the influence of chemical

activity coefficient can be found in the textbook by Bockris and Reddy-Amulya (1998) or the work of Samson et al. (1999) and references there in.

The fourth term refers to the convective flux produced from the gradient in fluid velocity due to electroosmotic solvent flow and usually the term is neglected for simplicity (Grimshaw, 1989). The convection flux is described relative to some convective reference velocity. This reference velocity might be mass average velocity, molar average velocity, volume average velocity, or velocity of the solvent (Cussler, 1997). Nevertheless, for an unstirred solution in vibration-free experimental device, the bulk flow of fluid or hydrodynamic velocity can be eliminated and subsequently the convective flux is neglected (Marchiano and Arvia, 1983).

According to the law of mass conservation, the change in the amount of the species *k* contained in the volume with respect to time *t* is given by the difference between the fluxes entering and leaving the reference volume (Yeager et al., 1983). Thus, the continuity equations of the ionic species *k* is derived as

$$\frac{\partial c_k}{\partial t} + div(\mathbf{N}_k) = \frac{\partial c_k}{\partial t} + div\left\{-\left(D_k \text{grad}(c_k) + z_k \mu_k F c_k \text{ grad}(\psi) + D_k c_k \text{ grad}(\ln \gamma_k)\right) + c_k U_i\right\} = 0$$
$$(k = 1, 2, ..., N) \qquad (2.36)$$

Equation (2.36) involves the unknown mobility μ_k^{el} which can be determined from the Nernst-Einstein relationship as

$$\mu_k^{el} = \frac{D_k}{RT} \qquad (2.37)$$

The diffusion coefficient of solute in hydrogels is usually dependent on a number of factors including the size of the solute in relation to the structure and pore size of the polymer gel, the polymer chain mobility and the water content. Peppeas et al. (2000) have put these into a general form of expressions as

$$\frac{D_k}{D_0} = f(r_k, \phi_s, \xi) \tag{2.38}$$

where D_0 is the corresponding diffusion coefficient of solute in the pure solvent . r_k is the radius of the diffusing molecule, ϕ_s is the volume fraction of polymer in the hydrogel, and ξ is network mesh size. Introduction of the various theoretical models can be found in the reviews by Muhr and Blanshard (1982) and Amsden (1998). However, it is also shown from the measured data that the diffusion coefficient is almost constant with the degree of swelling but it is time dependent (Gehrke and Cussler, 1989).

2.3.2.2 Spatial Charge

For the electrical potential function, there are few possible ways to describe its distribution, including the electroneutrality assumption with null current (Hwang, and Helfferich, 1987; Doi et al., 1992; Samson and Marchand, 1999), or the constant field assumption (Malmivuo and Plonsey, 1995; Gillespie and Eisenberg, 2002). However, the more rigorous treatment is the Poisson equation (Helfferich, 1962; MacGillivray, 1968; MacGillivray and Hare, 1969). We will evaluate each of them and show that electroneutrality and constant field assumptions are indeed the limiting cases of the Poisson equation.

Constant Field

In general, the constant field assumption implies that the electric potential across the system varies linearly, in other words, the electric potential gradient in the hydrogel is constant. This solution was introduced for ion transport through biological membranes (Goldman, 1943; Hodgkin and Katz, 1949). In Goldman-Hodgkin-Katz model, the

membrane is assumed to be uniform, planar, and infinite in its lateral extent. Hence, the potential field ψ and ionic concentration c within the membrane are functions of x only. Then, one can have

$$\frac{\partial^2 \psi}{\partial x^2} = 0 \tag{2.39}$$

If the membrane has a thickness of h,

$$\frac{d\psi}{dx} \approx \frac{\psi(h) - \psi(0)}{h} = \frac{V_m}{h} \tag{2.40}$$

where V_m is the transmembrane voltage.

Constant Current

Following the assumptions of the electroneutrality conserved at every local point for the solution and the global flow of all ions across the boundary yielding a null current, the additional conditions to determine the flux equation (2.35) can be summarized as

Electroneutrality in interior hydrogel: $$\sum_k z_k c_k + z_f c_f = 0 \tag{2.41}$$

Electroneutrality in exterior bathing solution: $$\sum_k z_k c_k = 0 \tag{2.42}$$

Null current: $$\sum_k z_k \boldsymbol{J}_k = 0 \tag{2.43}$$

where c_k is the concentration of the k^{th} ion species either inside or surrounding the hydrogel. c_f is the density of the fixed charge group of the hydrogel.

Poisson Equation

The Poisson equation is a more rigorous approach used to describe the spatial distribution of the electric potential in the domain. In the study of membrane phenomena in physiological electrolytic environments, it is commonly accepted that the electric field

near or in the membrane is of primary importance and that magnetic and electromagnetic phenomena inherently play a second role (Goldman, 1971). Therefore, we can limit the formulation to an electrostatic field and the derivation of the Poisson's equation following the guidelines of Panofsky and Phillips (1964). The fundamental equations that describe the electrostatic field are

$$\nabla \times \mathbf{E}_{el} = 0 \tag{2.44}$$

$$\nabla \cdot \mathbf{E}_{el} = \frac{\rho_{el}}{\varepsilon_0} \tag{2.45}$$

$$\mathbf{E}_{el} \equiv -\nabla \psi \tag{2.46}$$

where $\mathbf{E}_{el}$ is the average macroscopic electric field acting on charges within the medium, ψ is the electric potential, ρ_{el} (C/cm^3) is the average volume charge density and ε_0 the permittivity of free space or dielectric constant (8.85418×10^{-12} C^2/Nm^2). Equations (2.44) to (2.46) are the Maxwell's equations and Equation (2.46) is the consequence from Equation (2.45) which implies that the electrostatic field is irrotational (Panofsky and Phillips, 1964).

Let define the divergence of tensor $\mathbf{E}_{el}$ in term of a scalar potential ψ,

$$\nabla \cdot \mathbf{E}_{el} = \nabla \cdot (-\nabla \psi) = -\nabla^2 \psi \tag{2.47}$$

From the Maxwell's equation of (2.45), Gauss's law proves that

$$\nabla^2 \psi = -\frac{\rho_{el}}{\varepsilon_0} \tag{2.48}$$

Equation (2.48) is the famous Poisson's equation. If the condition of zero charge is imposed, i.e. $\rho_{el} = 0$, the Poisson equation will be reduced to Laplace's equation

$$\nabla^2 \psi = 0 \tag{2.49}$$

Equation (2.49) is equivalent to Equation (2.39), which is the consequence of imposing constant field assumption.

From the Maxwell's Equation (2.44),

$$\nabla \times \mathbf{E}_{el} = \nabla \times (-\nabla \psi) = 0 \tag{2.50}$$

The curl law of Equation (2.44) will make sure that $\mathbf{E}_{el}$ could be represented as the gradient of a scalar. Hence, it works out that $\nabla \times \mathbf{E}_{el} = 0$ permits $\mathbf{E}_{el} \equiv -\nabla \psi$; in return, $\mathbf{E}_{el} \equiv -\nabla \psi$ guarantees $\nabla \times \mathbf{E}_{el} = 0$. In addition, we can conclude that ψ can be determined by just one differential equation, i.e. Poisson equation, because ψ is a scalar. However, the determination of tensor $\mathbf{E}_{el}$ requires the presence of both the divergence and curl conditions.

In real case, the source of electric field is separated into two types, specifically, true free charge ρ_{el} and polarization (or bound) charge ρ_P because of the material medium. Therefore, the Poisson's equation (2.48) becomes

$$\nabla^2 \psi = -\nabla \cdot \mathbf{E}_{el} = -\left(\frac{\rho_{el} + \rho_P}{\varepsilon_0} \right) \tag{2.51}$$

For the purpose of derivation, it is more convenient to express ρ_P in term of the divergence of the polarization $\mathbf{P}_{el}$, in which Equation (2.51) is provided as

$$-\nabla \cdot \left(\mathbf{E}_{el} + \frac{\mathbf{P}_{el}}{\varepsilon_0} \right) = -\frac{\rho_{el}}{\varepsilon_0} \tag{2.52}$$

Therefore, we can now define the electric displacement $\mathbf{D}_{el}$ (C/m^2) by

$$\mathbf{D}_{el} = \varepsilon_0 \mathbf{E}_{el} + \mathbf{P}_{el} \tag{2.53}$$

and subsequently Gauss's law in tem of $\mathbf{D}_{el}$ is given as

$$\nabla \cdot \mathbf{D}_{el} = \rho_{el} \tag{2.54}$$

For medium with linear dielectrics, the polarization is $\mathbf{P}_{el} = \varepsilon_0(\varepsilon - 1)\mathbf{E}_{el}$ and Equation (2.53) becomes

$$\mathbf{D}_{el} = \varepsilon\varepsilon_0\mathbf{E}_{el} \tag{2.55}$$

where ε is the relative dielectric constant of the surrounding medium. After some substitution and rearrangement, the general Poisson's equation is given as

$$\nabla^2\psi = -\frac{\rho_{el}}{\varepsilon\varepsilon_0} \tag{2.56}$$

The true free charge ρ_{el} is a function of the concentration of all ions in solution and it can be calculated from

$$\rho_{el} = F\left(\sum_k z_k c_k + z_f c_f\right) \tag{2.57}$$

The Poisson equation is used to describe the spatial distribution of the electric potential in the domain and it is given as

$$\nabla^2\psi = -\frac{F}{\varepsilon\varepsilon_0}\left(\sum_k z_k c_k + z_f c_f\right) \tag{2.58}$$

The Poisson equation embodies a mean field potential ψ that approximates the ion-ion and ion with fixed charge interactions. Note that ψ is in general the sum of all externally applied potentials and diffusion potential. This potential, or potential of mean force, acts as the mean electrical driving force on the ion. It is not the instantaneous potential, but rather the mean potential about which the instantaneous potential fluctuates (Cooper et al., 1985). It can be shown that the electroneutrality and constant field hypotheses are in fact the special cases of the Poisson equation. The electroneutrality with null current assumption is applicable only when the concentrations are high while the

constant field hypotheses are valid for low concentrations (MacGillivray, 1968; MacGillivray and Hare, 1969).

If one needs to add the screening condition at microscopic level, the Poisson equation (2.56) can be conveniently extended to Poisson-Boltzmann equation. The Poisson-Boltzmann approach is a mean-field approximation that includes the electrostatic of the system through the Poisson equation and the effect of entropy, because of the mobility of the counterions, through the Boltzmann distribution of statistical mechanics. Thus, if $\rho(\mathbf{x}) = \rho_{fixed}(\mathbf{x}) + \rho_{mobile}(\mathbf{x})$ is the charge density as a function of position, the Poisson equation is

$$\nabla^2 \psi = -\frac{\rho_{fixed}(\mathbf{x}) + \rho_{mobile}(\mathbf{x})}{\varepsilon \varepsilon_0} \tag{2.59}$$

When only one species of ion (with charge q) is mobile, than according to statistical mechanics, the relative probability of finding an ion at a position $\mathbf{x}$ is given by the Boltzmann expression, $\exp(-q\psi(\mathbf{x})/k_B T)$, where k_B is Boltzmann's constant ($1.3807 \times 10^{-23}\,\mathrm{JK}^{-1}$)and T is the absolute temperature. Then, the charge density profile is given by

$$\rho_{mobile}(\mathbf{x}) = qc_0 \exp(-q\psi(\mathbf{x})/k_B T) \tag{2.60}$$

where c_0 is the ion density (in ions per volume) at a point where the electrostatic potential vanishes. Poisson equation (2.56) is now expand into Poisson-Boltzmann equation

$$\nabla^2 \psi(\mathbf{x}) = -\rho_{fixed}(\mathbf{x})/\varepsilon - qc_0 \exp(-q\psi(\mathbf{x})/k_B T)/\varepsilon \tag{2.61}$$

The main drawback of the Poisson-Boltzmann model is that at short distance (e.g., within a few tenths of a nanometer) from the membrane surface the approximation of

continuous charge densities breaks down because of the atomistic nature of the system (Guldbrand *et al.*, 1984; Redondo and Laser, 2004).

2.3.2.3 Fixed Charge Group Interaction

The ability of charged hydrogel to achieve large volume transition is facilitated by the weakly acidic or weakly basic groups bound to the polymer chain, which are strongly dependent on the dissociation constant. These groups are readily ionizable and sensitive to the effects of environment pH of their swelling medium (Katchalsky, 1949; Fragala et al., 1972; Tanaka et al., 1980; De Rossi et al., 1985). For example, the weak-acidic of carboxyl groups will exist in the form of RCOOH when H^+ concentration is higher than the dissociation constant K_a, whereas in medium where H^+ concentration is lower than K_a, the pendent groups will be charged and become $RCOO^-$. The whole process can be summarized as

$$RCOOH \rightleftharpoons RCOO^- + H^+ \tag{2.62}$$

The hydrogen ion H^+ is the important controller in the electrochemical modulation of the swelling of the pH-sensitive hydrogel. A relation between the fixed charge group and the diffusive hydrogen ion was developed based on the Langmuir absorption isotherm (Grimshaw et al., 1990). For the case of single site single ion binding mechanism, the equilibrium constant is defined as

$$K_a = \frac{[RCOO^-][H^+]}{[RCOOH]} \tag{2.63}$$

The total ionizable fixed charge groups of the dry gel is determined from titration process per volume of solid polymer (Grimshaw, 1989) and given as

$$c_{m0}^{s} = \frac{\text{moles of ionizable group}}{\text{volume of solid polymer}} = \frac{n}{V^{s}} \tag{2.64}$$

The quantities of ionic concentrations in Equations (2.35) and (2.36) are averaged over the interstitial fluid volume. Therefore, we need to convert the total ionizable groups c_{m0}^{s} into unit of fluid volume where

$$c_{m0} = c_{m0}^{s} \frac{V^{s}}{V^{f}} = \frac{c_{m0}^{s}}{H} \tag{2.65}$$

where H is the hydration of the hydrogel and defined as the ratio of fluid volume V^{f} to solid volume V^{s} as

$$\begin{aligned} H &= \frac{\text{fluid volume}}{\text{solid volume}} \\ &= \frac{V^{f}}{V^{s}} \end{aligned} \tag{2.66}$$

Now, the reaction isotherm can be written as

$$K_{a} = \frac{c_{f} c_{\mathrm{H}^{+}}}{c_{m0} - c_{f}} \tag{2.67}$$

After rearranging the equation, the concentration of the fixed charge groups bound on the polymer chains c_{f} can be determined as

$$c_{f} = \frac{K_{a} c_{m0}}{K_{a} + c_{\mathrm{H}^{+}}} = \frac{c_{m0}^{s}}{H} \frac{K_{a}}{K_{a} + c_{\mathrm{H}^{+}}} \tag{2.68}$$

Thus we had a relation between the fixed charge density and the diffusive hydrogen ion, whereby the concentration of the fixed charge group is calculated as a function of the concentration of total ionizable groups in the dry gel c_{m0}^{s} and concentration of free ion hydrogen c_{H} (Siegel et al., 1991, 1990).

For a basic hydrogel, the calculation of fixed charge groups c_f based on Langmuir isotherm relation will become

$$c_f = \frac{c_{m0}^s}{H} \frac{c_{\mathrm{H}^+}}{K_a + c_{\mathrm{H}^+}} \tag{2.69}$$

One should note that the fixed charge groups are bound to the network chain, hence become immobile. In normal cases, the profiles of the fixed charge groups can only be modified by chemical reaction (Shibayama and Tanaka, 1993; Shiga et al., 1992a, 1992b).

2.3.3 Mechanical Formulation

As discussed before, hydrogels are able to take up solution in which they are immersed and expand until equilibrium is attained. In this section, the equations describing the mechanics of a charged and swollen hydrogel are given.

At equilibrium state, the swelling stress is balanced by the elastic retractive force exerted by crosslinking solid matrix of the hydrogel in order to maintain the current hydration state. The total swelling stress could be the components due to the stretching of electrostatic effects, polymer-solvent and polymer-solute interactions, and entropic effects (Flory, 1962). However, it is assumed that the swelling stress arising from the entropic effects (e.g. thermal motion, solvent interactions) reaches steady state faster than the ionic diffusion or water flow. Thus the swelling pressure is assumed to be state function of a set of ionic environment, membrane fixed charge and hydration.

The balance of linear momentum leads to the following equation of motion (Malvern, 1969)

$$\text{div}\boldsymbol{\sigma} + \mathbf{b} = \rho \frac{\partial^2 \mathbf{u}}{\partial t^2} \tag{2.70}$$

where ρ is the mass density, t the time variable and **u** the displacement of the solid phase, $\boldsymbol{\sigma}$ the total stress tensor of the interior hydrogel, and **b** the body tensor that is not of interest in present work.

If the effect of the inertial term is dropped from the equilibrium equation, as found to be negligible from the experimental work of Tanaka and Filmore (1979), and body force of the hydrogel is omitted from the equilibrium equation of (2.70), the equation becomes

$$\text{div}\boldsymbol{\sigma} = 0 \tag{2.71}$$

As there are only three first-order partial differential equations from equilibrium equation, they are insufficient to solve the six independent unknown stress components. In general, the constitutive equation, that embodies the stress-strain behavior of the material, is considered. The constitutive equation for multiphasic mixture (Lai et al., 1991) is expressed as

$$\boldsymbol{\sigma} = -(p + T_c)\mathbf{I} + \boldsymbol{\sigma}_e \tag{2.72}$$

where p is the osmotic pressure, T_c is the chemical-expansion stress exerted on the solid but will be dropped from the present formulation. The is the elastic restoring stress σ_e can be determined from

$$\sigma_e = \lambda(tr\mathbf{E})\mathbf{I} + 2\mu\mathbf{E} \tag{2.73}$$

where λ and μ are the Lamé's coefficients of the solid matrix which can be related to the Young's modulus E_0 and Poisson's ratio ν in the form of

$$\lambda = \frac{\nu E_0}{(1+\nu)(1-2\nu)} \tag{2.74}$$

$$\mu = \frac{E_0}{2(1+\nu)} \tag{2.75}$$

And $\mathbf{E}$ is the strain tensor of solid matrix. For small deformation, strain tensor $\mathbf{E}$ can be written in term of displacement gradients as

$$E_{jk} = \frac{1}{2}\left(\frac{\partial u_j}{\partial x_k} + \frac{\partial u_k}{\partial x_j}\right) \qquad j,k = 1,2,3 \tag{2.76}$$

The osmotic pressure p is contributed from the tendency of the hydrogel to absorb additional solvents which appear as the concentration difference between the interior hydrogel and the external medium (Helfferich, 1962; Katchalsky and Curran, 1965). Hence the osmotic pressure can be calculated according to

$$p = RT\sum_k (c_k - \overline{c}_k) \tag{2.77}$$

where $\overline{c}_k$ is the concentration of the k^{th} ion species in external solution and c_k the concentration of k^{th} ion species within the hydrogel.

By substitution of Equations (2.72) and (2.73) into Equation (2.71), and neglecting the effects of inertial force, body force and chemical-expansion stress, the mechanical equation can be expressed as

$$\text{div}\left[-(p)\mathbf{I} + \lambda(tr\mathbf{E})\mathbf{I} + 2\mu\mathbf{E}\right] = 0 \tag{2.78}$$

For simplicity, we will take the one-dimensional formulation in x-direction as exemplary case. The linear deformation equation describing the mechanical equilibrium can be written in the term of displacement component as

$$\frac{\partial}{\partial x}\left\{(2\mu+\lambda)\left(\frac{\partial u}{\partial x}\right)-p\right\}=0 \tag{2.79}$$

The work of, like, Tanaka et al. (1982) and De-Rossi et al. (1985) or the more recent modeling of Sun et al. (1999), De et al. (2002) and Zhou et al. (2002), assume the linear elasticity in their formulations as in Equation (2.79) which is only appropriate for small deformation.

When an elastic body undergoes very large deformation, the difference between the initial and deformed configurations can not be neglected as is done for the case of linear elasticity. For geometrically nonlinear analysis, the second Piola-Kirchhoff stress and the Green-Lagrangian strain are used as the stress and the strain measures, respectively (Malvern, 1969; Belytschko et al., 2000). The governing equation for large deformation analysis using a total Lagrangian description is given as follows,

$$\mathrm{Div}\mathbf{P}+\mathbf{b}=\rho\frac{\partial^2\mathbf{u}}{\partial t^2} \tag{2.80}$$

where $\mathbf{P}$ is the first Piola-Kirchhoff stress tensor. Comparing with Equation (2.70), the Cauchy stress $\boldsymbol{\sigma}$ have been replace with first Piola-Kirchhoff stress $\mathbf{P}$. The 1st and 2nd Piola Kirchhoff stress are related to the Cauchy stress as

$$\mathbf{P}=J\mathbf{F}^{-1}\cdot\boldsymbol{\sigma} \quad \text{and} \quad \mathbf{S}=J\mathbf{F}^{-1}\cdot\boldsymbol{\sigma}\cdot\mathbf{F}^{-T} \tag{2.81}$$

where $\mathbf{F}$ is the deformation gradient tensor,

$$\mathbf{F}=F_{ij}=\frac{\partial x_i^{Deformed-configuration}}{\partial X_j^{Initial-configuration}}=\delta_{ij}+\frac{\partial u_i}{\partial X_j}=\mathbf{I}+\nabla\mathbf{u} \tag{2.82}$$

where **u** is the displacement vector from the initial configuration **X** to the deformed configuration **x**, in which $\mathbf{x} = \mathbf{X} + \mathbf{u}$ and **I** is identity tensor. J is the determinant of deformation gradient **F** and can be compute as

$$J = \det \mathbf{F} \tag{2.83}$$

For general Kirchhoff model, the 2nd Piola-Kirchhoff stress tensor **S** is given as

$$\mathbf{S} = \mathbf{DE} \tag{2.84}$$

where **D** is the material moduli tensor and several elastic constitutive relations can be chosen. For isotropic elastic material the material moduli tensor can be written

$$\mathbf{D} = \lambda \mathbf{I} \otimes \mathbf{I} + 2\mu \boldsymbol{I} \tag{2.85}$$

where λ and μ are the Lame's constants. $\boldsymbol{I}$ is the fourth-order symmetric identity tensor which is defined as $1/2\left(\delta_{ik}\delta_{jl} + \delta_{il}\delta_{jk}\right)$. The Green-Lagrange strain **E** in Eq.(33) is defined as

$$\mathbf{E} = \tfrac{1}{2}(\mathbf{F}^{\mathrm{T}}\mathbf{F} - \mathbf{I}) \tag{2.86}$$

If the body force vector **b** and the inertial force $\rho \frac{\partial^2 \mathbf{u}}{\partial t^2}$ are omitted, Equation (2.80) can be simplified as

$$\mathrm{Div}\mathbf{P} = 0 \qquad \text{in } \Omega \tag{2.87}$$

After substitution, the mechanical equilibrium equation is given as

$$\mathrm{Div}(-J\mathbf{F}^{-1} p\mathbf{I} + \mathbf{FS}) = 0 \tag{2.88}$$

where the 2nd Piola-Kirchhoff stress in term of displacement can be conveniently represented as a matrix equation expressing a six-element column matrix of stresses in terms of a six-element column matrix of strain as

$$\begin{bmatrix} S_{11} \\ S_{22} \\ S_{33} \\ S_{23} \\ S_{13} \\ S_{12} \end{bmatrix} = \begin{bmatrix} \lambda+2\mu & \lambda & \lambda & 0 & 0 & 0 \\ \lambda & \lambda+2\mu & \lambda & 0 & 0 & 0 \\ \lambda & \lambda & \lambda+2\mu & 0 & 0 & 0 \\ 0 & 0 & 0 & \mu & 0 & 0 \\ 0 & 0 & 0 & 0 & \mu & 0 \\ 0 & 0 & 0 & 0 & 0 & \mu \end{bmatrix} \begin{bmatrix} E_{11} \\ E_{22} \\ E_{33} \\ 2E_{23} \\ 2E_{13} \\ 2E_{12} \end{bmatrix} \tag{2.89}$$

Based on the Lagrangian formulation, in which variables are described in the undeformed configuration,the equilibrium governing equation for analysis of one-dimensional finite deformation problem is expanded from Equation (2.88) as follows,

$$\frac{\partial S}{\partial X} + \frac{\partial S}{\partial X}\frac{\partial u}{\partial X} + S\frac{\partial^2 u}{\partial X^2} = J\frac{\partial p}{\partial x} \tag{2.90}$$

And, the 2nd Piola-Kirchhoff stress $\mathbf{S}$ for one-dimensional finite deformation is given as

$$S = \left(\frac{\lambda+2\mu}{2}\right)\left[\left(\frac{\partial u}{\partial X}\right)^2 + 2\frac{\partial u}{\partial X}\right] = \frac{\lambda+2\mu}{2}\left(\frac{\partial u}{\partial X}\right)^2 + \frac{\lambda+2\mu}{2}\left(\frac{\partial u}{\partial X}\right) \tag{2.91}$$

After substituting Equation (2.91) into Equation (2.90) and rearranging the resulting equation, the 1-D equilibrium governing equation in term of the displacement is given as follows,

$$\left(\lambda+2\mu\right)\left[\frac{\partial^2 u}{\partial X^2} + 3\frac{\partial u}{\partial X}\frac{\partial^2 u}{\partial X^2} + \frac{3}{2}\left(\frac{\partial u}{\partial X}\right)^2\frac{\partial^2 u}{\partial X^2}\right] = J\frac{\partial p}{\partial x} \tag{2.92}$$

The corresponding boundary conditions are prescribed as

$$\mathbf{u} = \mathbf{G} \text{ in } \Gamma_g \tag{2.93a}$$

$$\mathbf{P}\cdot\mathbf{N} = \mathbf{H} \text{ in } \Gamma_h \tag{2.93b}$$

where $\boldsymbol{N}$ is the unit outward normal vector in the initial configuration, $\boldsymbol{G}$ is the prescribed displacement vector and $\mathbf{H}$ is the surface traction vector.

2.3.4 Computational Domain and Boundary Conditions

In this section, the appropriate electrochemical and mechanical boundary conditions are specified to fully describe pertinent problems. In the experimental work conducted by Beebe and his team (Beebe et al., 2000a; De et al., 2002), the hydrogels were fabricated in the microchannel with upper and lower surface covered with glasses. Hence, the deformation of hydrogels in axial direction is confined and swelling only occurs in the radial direction. Due to the constraints, the swelling/shrinking equilibrium of a cylindrical hydrogel can be modeled as a one-dimensional problem along the diameter of the hydrogel. The surrounding bath concentrations are constants, together with homogenous properties assumption, which further reduce the problem into a symmetrical consideration about the axis of the hydrogel. Due to the axisymmetric consideration, only half of the hydrogel diameter is determined in the simulation, as shown in Figure 4.1. The computational domain thus consists of three sub-domains, namely, the interior hydrogel, bathing medium and boundary effect. The boundary effect domain refers to the hydrogel-solution interface.

Since it is an axisymmetric problem, the Neumann type of the electrochemical boundary conditions will be taken to ensure the continuity inside the hydrogel and Dirichlet boundary conditions at the solution boundaries as prescribed by the experiment. In general, in a system of k ions, there are only $k-1$ independent ionic concentrations. The k-th concentration is determined from electroneutrality condition. On the other hand, the boundary conditions for mechanical equilibrium are defined within the hydrogel. Those boundary conditions prescribed here are as listed in Figure 4.1. As usual, all the

simulations are assumed to take place under ambient temperature or it will be stated otherwise. Applications of the mentioned boundary conditions are further presented in Chapter 4.

In the simulations of the pH and electric driven hydrogel, the hydrogel strip is assumed to be centered between a pair of electrodes and aligned parallel to them, in which a DC electric field is applied across the computational domain as shown in Fig. 5.1. We are going to calculate the degree of swelling of the charged hydrogels under the stimulation of chemical milieu and DC electric field after attaining it equilibrium state.

Since there are potential applied across the hydrogel, the symmetric solution is no longer relevant in this case. The computational domain has to cover the whole area of interest, from cathode on the left region to anode on the right. The parametric studies shall be restricted to case where the concentration conditions are identical in both region of anode and cathode, i.e. $c = c_{left} = c_{right}$. The electric boundary conditions are given as prescribed by the applied electric potential. As usual, all the simulations are assumed to take place under ambient temperature or it will be stated otherwise.

2.3.5 Equivalent Non-Dimensional MECpH Model for One-Dimensional Steady-State Problems

A set of nonlinear coupled electrochemical and mechanical equations has been developed to predict the swelling/deswelling equilibrium of hydrogel. Modeling equilibrium behavior of pH-responsive hydrogel requires an accurate description of the

diffusion of hydrogen ions into and out of the hydrogel. This requirement also takes into account the chemical reactions of the hydrogen ions with fixed charge groups and the buffering effect on hydrogen ion diffusion. Equations (2.35) and (2.58) are collectively known as Poisson-Nernst-Planck (PNP) system, which is a system of nonlinear partial differential equations for which an analytical solution is not feasible and can only be solved with numerical methods. PNP continuum electrodiffusion theory attempts to represent the average ion fluxes in term of densities or potential gradients. Hence, from the difference in concentration and potential across the hydrogel, the equilibrium swelling/shrinking degree can be calculated from the finite deformation mechanical equation (2.92).

The equilibrium swelling/deswelling process has been modeled using the steady-state Nernst-Planck equation, the Poisson equation and the mechanical equilibrium, collectively known as MECpH system. The set of equations is amenable by numerical solution. Nevertheless, appropriate approximations can significantly decrease the amount of computer time necessary to obtain a solution of meaningful accuracy. Some assumptions and approximations have been made in the numerical models which have been discussed in Sections 2.3.2 and 2.3.3.

First, the effect of diffusion coefficients is not considered in the equilibrium model as they affect only the rate of diffusion but not the final equilibrium state. Moreover, it is observed in experiments that the diffusion coefficient varies only slightly with changes in degree of swelling (Gehrke and Cussler, 1989). Secondly, the convection terms in the flux equations are negligible as fluid pressure remains constant across the hydrogel and the fluid velocity is unchanged with hydrogel swelling. This assumes that the change in concentration profiles, due to convective flow of ions is much smaller than the calculated

concentrations (Grimshaw, 1989). Thirdly, it is also assumed that the flux due to the chemical reaction of ions is much smaller than the net diffusion and migration fluxes. Therefore, the contribution of chemical activity coefficient to the flux becomes insignificant. Moreover, the chemical activity coefficients of ionic species will always equal to unity in the dilute condition (Bockris and Reddy-Amulya, 1998). Lastly, the hydrogel properties under consideration are assumed to be homogeneous. Therefore, the swelling equilibrium is considered to be isotropic. Although the actual dielectric constants of ions depend on the species and applied electric current, they are chosen to be equal to each other for simplication. Besides that, any electrolytic processes due to the imposition of the external electric field have been disregarded by limiting to low-range voltages in simulations.

The governing equations can be rewritten in non-dimensional form by introducing a set of dimensionless parameters for the present problem

$$\tilde{x} = \frac{x}{L_{ref}}, \qquad \tilde{u} = \frac{u}{L_{ref}}, \qquad \tilde{c}_k = \frac{c_k}{c_{ref}}, \qquad \tilde{c}_f = \frac{c_f}{c_{ref}}, \qquad \tilde{\psi} = \frac{\psi}{\psi_{ref}} = \frac{F\psi}{\eta RT} \tag{2.94}$$

where $\tilde{x}$, $\tilde{u}$, $\tilde{c}_k$, $\tilde{c}_f$, $\tilde{\psi}$ are the dimensionless variables of coordinates, displacement, diffusive ionic concentration, fixed charge density and electric potential respectively. L_{ref} , c_{ref} , ψ_{ref} and η are the characteristic length, concentration, electric potential and weighted coefficient respectively. There are many reasons to recast the governing equations into a non-dimensional form, but the main purpose is to get more insight of the significance of each variable parameter and also to overcome the problem of solving the variables with different units and scales.

In steady state analysis, the time derivative $\frac{\partial c_k}{\partial t}$ in Equation (2.36) is removed. This significantly reduces the computational cost when solving the system of coupled nonlinear partial differential equations as we have saved computational time in solving the additional k continuity equations (2.36). Thus the final form of the non-dimensional system of partial differential equations after dropping the tildes can be written as:

Electrochemical equations,

$$\frac{\partial^2 c_k}{\partial x^2} + \eta z_k \frac{\partial c_k}{\partial x}\frac{\partial \psi}{\partial x} + \eta z_k c_k \frac{\partial^2 \psi}{\partial x^2} = 0 \qquad (k = 1,2,3,\ldots N) \qquad (2.95)$$

$$\frac{\partial^2 \psi}{\partial x^2} = -\frac{F^2}{\varepsilon\varepsilon_0 RT}\frac{L_{ref}^2 c_{ref}}{\eta}\left(\sum_{k=1}^{N} z^k c^k + z^f c^f\right) \qquad (2.96)$$

For acidic hydrogel, the fixed charge concentration is calculated as

$$z_f c_f = -\frac{1}{H}\left(\frac{c_{m0}^s K}{K + c_{\mathrm{H}^+}}\right) \qquad (2.97)$$

and the fixed charge concentration formula for basic hydrogel is

$$z_f c_f = \frac{1}{H}\left(\frac{c_{m0}^s c_{\mathrm{H}^+}}{K + c_{\mathrm{H}^+}}\right) \qquad (2.98)$$

Mechanical deformation equations,

$$(2\mu + \lambda)\frac{\partial}{\partial x}\left(\frac{\partial u}{\partial x}\right) - c_{ref} RT \frac{\partial}{\partial x}\left(\sum_{k=1}^{N}(c^k - \bar{c}^k)\right) = 0 \qquad (2.99)$$

or

$$(2\mu + \lambda)\left(\frac{\partial^2 u}{\partial X^2} + 3\frac{\partial u}{\partial X}\frac{\partial^2 u}{\partial X^2} + \frac{3}{2}\left(\frac{\partial u}{\partial X}\right)^2 \frac{\partial^2 u}{\partial X^2}\right) - c_{ref} RTJ \frac{\partial}{\partial x}\left(\sum_{k=1}^{N}(\bar{c}^k - \bar{c}^{k'})\right) = 0 \qquad (2.100)$$

depending on the range of hydrogel deformation.

It is noted that, in the present model, a few assumptions have been made as discussed in precedent section, in which the chemical reaction and the convection transport of ionic species are neglected. The equilibrium mechanical deformation Equation (2.99) or Equation (2.100) are coupled with PNP equations (2.95) and (2.96) and fixed charge groups dissociation activity Equation (2.97) or Equation (2.98) through the hydration H parameter. These equations complete the MECpH model. Thus, there are k Nernst-Planck equations (2.95) linking the $k+1$ variables $c^1, c^2, \ldots, c^k, \psi$. The additional relation linking the $k+1$ variables is the Poisson equation (2.96). If the fixed charges are specified as a material property, and if appropriate boundary conditions are specified, these equations construct a complete specification of an electrodiffusion problem; that is, there are $k+1$ variables and corresponding equations. In principle, these equations can be solved for the concentration and the flux of each mobile ion as well as the electric potential. However, these equations are obviously nonlinear because of the coupled terms $\frac{\partial c_k}{\partial x}\frac{\partial \psi}{\partial x}$ and $c_k \frac{\partial^2 \psi}{\partial x^2}$ in Equation (2.95), which complicates the solution of MECpH system.

Owing to the simplified form of MECpH as in Equations (2.95) to (2.100), numerical simulation can easily cover a wider range of possible situations. For instance, the wide concentration range is chosen to examine the limiting behavior of those curves beyond the particular range of interest. In general, this system of equations is coupled and nonlinear, and has no closed-form analytical solution. However, the advancements in numerical techniques have offered a mean to solve the system of equations for approximated solutions with excellent accuracy.

2.4 REMARKS

In general, thermodynamics models consider the Gibbs free energy as the contributor towards the total free energy of the hydrogel-solvent system, whereas multiphasic models are based on the assumption that the driving forces for the movements of water and neutral salt in the charged hydrogels are gradients of their chemical potentials. In addition, the stress in the solid matrix network and the chemical potentials of the interstitial fluid and ions are related to the Helmholtz energy functions in accordance with the laws of energy balance and entropy. These models are either oversimplified, and hence confined in applicability to certain cases, or so complex that they are inflexible for expanding to account for additional parameters that are significant as proven by experiment works. Therefore, we have to develop theoretical formulations with sound fundamental basis, possible extension and robust in wide range of application. The presently developed MECpH model takes into consideration the chemical, electrical and mechanical multi-field interaction of the hydrogel-solvent system in a consistent manner with the incorporation of fixed charge binding reaction and large deformation of hydrogel in the formulation.

The main concenpts of chemomechanical or electromechanical machines are based on the modulation of the solvating ability of the polymer networks by pH-stimuli that enables the dynamic control of the swelling forces. Thereby, ones can obtain effective diffusibility or permeability of the solutes, as well as mechanical energy from the hydrogel. In addition, the presence of the electrostatic potential that is locally induced in the electrolytic solution by the movement of all ionic species is an important phenomena occurring in ionic diffusion, but not in neutral molecular diffusion. In an ionic solution,

the local electroneutrality is preserved. During the diffusion, all ions do not drift at the same speed as some ions tend to diffuse at a higher rate. However, any excess charges transferred by the faster ions result in the building up of a local electric field, also called the diffusion potential, which slows down the faster ions, and reciprocally accelerates the slower ionic particles. In addition, the diffusion potential has to be accounted for even in cases where an external electrical field is applied to the system, with the diffusion potential being superimposed onto the external field, as shown in Fig. 5.2.

The interaction between the hydrogel elastic network and chemical medium will strongly influence the degree of response of the hydrogel. The ionizable polymer fractions in the hydrogel are capable of associating and dissociating themselves and this characteristic is the determinant of the physico-chemical properties of the hydrogels. When immersed in a suitable solution, the electrolytic composition of the surrounding solution will diffuse into the gel and this will determine the dissociation/association of the polyelectrolyte fraction of the hydrogels. Chemical reactions arise as a result from the reversible processes of dissociation/association between the diffusive ions and the ionizable groups in the gel and subsequently redistribute the ionic concentration within the hydrogel. The redistributions of ionic concentrations of the hydrogel generate both the electrostatic field and the osmotic pressure due to the difference of ionic concentrations between the hydrogel and surrounding environment. The osmotic pressure will exert influence on the degree of expansion or contraction of the hydrogel. The swelling or shrinking subsequently redistributes the ion concentration of the hydrogel interior. These processes will go on until a steady state is achieved.

In this chapter, the formulated electrochemical and mechanical equations that coupled together through the hydration H parameter (collectively known as multi-effect-

coupling of pH-stimulus model, abbreviated as MECpH) are able to describe the phenomenological process as mentioned above. In addition to that, the MECpH model do has some advantages that make it more attractive over other models in some way as described in following paragraph.

- The computational domains of interest cover both the hydrogels and exterior bathing solution. The model is able to predict the distributions of concentration of all diffusive ionic species, electric potential in both the hydrogels and surrounding solution simultaneously.
- MacGivllivary (1968) pointed out that the electroneutrality and constant field assumptions are in fact nothing new but two limiting cases of a certain dimensionless parameter which is related to the ratio of the Debye length to membrane thickness. In order to account for the electrical coupling of various ionic fluxes, the Poisson equation provides a more scrupulous approach to the problem.
- Physically, the distribution of the fixed charge is a function related to the material properties and hydration of the hydrogels. In the MECpH model, the Langmuir absorption isotherm is used to derive the profile fixed charge concentration as a function of the hydration, the diffusive hydrogen ion H^+ concentration, and the concentration of fixed charge per solid volume.
- This model can easily incorporates multiple ionic species. Unlike other models where only two monovalent ion species, an anion and a cation, are considered.
- This model is in more concise form and readily applicable for numerical implementation as compared with other models.

CHAPTER 3

DEVELOPMENT OF NOVEL MESHLESS METHODOLOGY

3.1 OVERVIEW

The earliest precursor of meshless methods can be traced back to the smooth particle hydrodynamics (SPH) method (Lucy, 1977; Gingold and Monaghan, 1977). The method was originally used for modeling non-axisymmetric phenomena in astrophysics where there are large numbers of particles interacting with each others. The collective movement of those particles is similar to the movement of a liquid, or gas flow, and it may be modeled by the governing equations of classical Newtonian hydrodynamics.

There are number of parallel paths proposed to construct meshless approximations which are emerging recently. An excellent review of recent development in meshless methods can be found in the works of Duarte (1995), Beltyschko et al. (1996) and Boresi et al. (2003). Thus far, those methods which have established as the representative meshless methods include smooth particle hydrodynamics (SPH) (Monaghan, 1982,1988; Swegle et al., 1994), the finite difference method with arbitrary irregular grids (Jensen, 1980; Liszka and Orkisz, 1980), diffuse element method (Nayroles et al., 1992), element free Galerkin (EFG) method (Belytschko et al., 1994; Lu et al., 1994; Krongauz, 1996; Krongauz and Belytschko, 1996, 1997), reproducing kernel particle hydrodynamics (RKPM) (Liu, W.

K. et al., 1995a, 1995c, 1996a, 1996b), finite point method (Onate et al., 1996a, 1996b), partition of unity methods (PUM) (Melenk and Babuska, 1996), *hp*-meshless clouds (Duarte and Oden, 1996; Liszka *et al.*, 1996), boundary node method (Mukherjee and Mukherjee,1997a; Chati et al., 1999), meshless local Petrov-Galerkin (MLPG) method (Atluri and Zhu, 1998; Atluri, 2004), local boundary integral equation (LBIE) method (Zhu et al., 1998), finite cloud method (Aluru, 2000; Aluru and Li, 2001), the point interpolation method (PIM) (Liu and Gu, 2001), finite spheres (De and Bathe, 2000, 2001), *h*M-DOR method (Ng et al., 2003a, 2003b), Hermite-cloud (Li et al., 2003), to name a few.

Although meshless methods originated about twenty years ago, the meshless methods only started to attract sufficient attention in the late 1990s, motivated by the shortcomings arising in the use of finite element methods (FEM) or other conventional computational methods such as finite volume method (FVM) or finite difference methods (FDM). Most of the shortcomings are related to mesh generation. Mesh generation is very time-consuming in many situations, e.g., when solving excessive mesh distortion, as in large deformation or crack propagation, continuous remeshing is required; when the domain has complicated geometry, especially those that require two or three-dimensional modeling; when there are mixing of energy domain or scaling, especially in microelectricalmechanical system (MEMS) and the evolving nanoelectricalmechanical system (NEMS); when a Lagrangian formulation is employed, especially with non-linear PDE's. These drawbacks become more profound when treating moving discontinuities problems (Belytschko et al., 1996).

Further, meshless techniques offer the privilege of flexibility in the selection of approximating functions when constructing the window functions (e.g., the flexibility to use non-polynomial window functions) that is not appreciable in FEM (Babuska et

al., 2002). More discussions on the shortcomings of the more thoroughly developed FEM methods can be found in the book written by Liu (2002). As meshless techniques require only sets of scattered points representing the domain of interest, meshless techniques do not require the generation of a mesh for complex two- and three-dimensional structures. No connectivity information among the scattered sets of nodes is required, unlike finite element, boundary element or classical finite difference techniques.

Meshless techniques are also appealing because of their potential in adaptive techniques, where a user can simply add more points in a particular region to obtain more accurate results. Meshless techniques are especially attractive for emerging technologies such as microelectromechanical systems (MEMS) and nanoelectromechanical system (NEMS), where multiphysics and multiscale analyses are a common requirement. Both multiphysics and multiscale analyses are radically simplified by dealing with nodes or points rather than of a mesh (Aluru and Li, 2001).

Based on the classical smooth particle hydrodynamics (Lucy, 1977; Gingold and Monaghan, 1977), Monaghan extended the practices of SPH by proposing the idea of kernel approximation as a more rational basis to SPH formulation in his later works (Monaghan, 1982, 1988, 1992). Various improvements of SPH have been developed through the years. One of the notable advancement is the reproducing kernel particle method (RKPM) (Liu et al., 1995a-c, 1996a, 1996b, 1997; Gosz and Liu, 1996; Gunther and Liu, 1998).

In order to fully exploit the potential of collocation-based techniques, we have proposed a novel true meshless technique – the Hermite-Cloud method (Li et al., 2003), which combines the Hermite interpolation theorem (DeVore and Lorentz, 1993) with the point collocation technique. This method is an extension of the classical RKPM

developed by Liu *et al.* (1995a-c, 1996a, 1996b, 1997; Gosz and Liu, 1996). The key idea behind the classical RKPM is the construction of the approximate solutions for the unknown functions by reproducing kernels with selection of a suitable corrected kernel function. The main contribution of the classical RKPM is the development of the corrected kernel function, which consists of a correction function and a kernel function. Reproducing kernels refer to a class of mathematical operators that can reproduce the function itself by integration transform over the whole domain of interest. It is analogous to the popular examples such as the Fourier and Laplace transforms. With the selection of different forms of window functions in the formulation of correction function, various outcomes will be obtained.

The Hermite-Cloud method combines the Hermite theorem for the construction of the interpolation functions with the point collocation technique for discretization of the partial differential equations (PDE) and their boundary conditions. The distinguished differences between the RKPM and Hermite-Cloud method are:

1. With the implementation of Hermite interpolation theorem, the shape functions are constructed for the unknown functions and the corresponding first-order derivatives.
2. A fixed kernel is used which is in parallel path as the finite cloud method proposed by Aluru and his group (2000, 2001).
3. A set of auxiliary conditions are required to generate a set of complete equations for the governing partial differential boundary value (PDBV) problem.

3.2 HERMITE CLOUD METHOD

The main characteristic of the reproducing kernel method is its ability to reproduce a given function by integration transform over the domain of interest, which has the same attribute as a Fourier or Laplace transform. For example, if we take a two-dimensional case, the reproducing kernel expression can be written as the product of the window function, $\bar{W}(x-p, y-q)$, with the unknown function of $u(x, y)$, and integrated over the defined domain, Ω,

$$u^h(x, y) = \int_\Omega \bar{W}(x-p, y-q)u(p, q)dpdq \tag{3.1}$$

where $u^h(x, y)$ is the approximation of function $u(x, y)$.

In order to exactly reproduce the real function, an ideal window functions should fulfill two conditions: (1) it is compact in nature, i.e. $\bar{W}(x-p, y-q) = 0$ outside the Ω domain, and (2) its integral over the Ω domain should be unity, i.e. $\int_\Omega \bar{W}(x-p, y-q)dpdq = 1.0$. However, an ideal window function that simultaneously satisfies both conditions hardly exist. Hence, it is often demanding to select a suitable function to exactly reproduce the unknown function $u(x, y)$. Instead of finding the best choice of window function, we can modify the window function so that the reproducing conditions can be satisfied, as proposed in reproducing kernel method (RKM). Following the key ideas of the RKM (Liu *et al.*, 1995a, 1995b, 1996a), by employing a correction function $C(x, y, p, q)$ and a kernel function $K(x-p, y-q)$, the corrected window function is in the form of

$$\bar{W}(x-p, y-q) = C(x, y, p, q)K(x-p, y-q) \tag{3.2}$$

Substituting Equation (3.2) back into Equation (3.1), the approximate unknown function can be rewritten as

$$u^h(x,y) = \int_{\Omega} C(x,y,p,q)K(x-p,y-q)u(p,q)dpdq \tag{3.3}$$

If a fixed kernel technique is used instead of the classical moving kernel, Equation (3.3) can be represented as

$$u^h(x,y) = \int_{\Omega} C(x,y,p,q)K(x_k-p,y_k-q)u(p,q)dpdq \tag{3.4}$$

where the kernels are centered at points (x_k, y_k). The correction function $C(x,y,p,q)$ is typically expressed as a linear combination of independent basis functions. However, basis function of arbitrary function can be selected as long as they are independent functions. The highest order polynomial terms in the correction function $C(x,y,p,q)$ will be determined by the order of accuracy of the approximation needed to reproduce. As rules of thumb, the numbers of term to be include is equal to the highest order derivative terms contained in the governing PDE of interest is usually considered. Thereupon, the correction function $C(x,y,p,q)$ can be defined as a product of a β^{th}-order row basis function vector $\mathbf{B}(p,q)$ and a β^{th}-order column correction coefficient vector $\mathbf{C}^*(x,y)$, where β is the order of polynomial to be included as the basis function. The correction function can be summarized as

$$C(x,y,p,q) = \mathbf{B}(p,q)\mathbf{C}^*(x,y) \tag{3.5}$$

A linearly independent basis for a one-dimensional quadratic PDE problem is given as

$$\mathbf{B}(p) = \{b_1(p), b_2(p), \ldots, b_\beta(p)\} = \{1, p, p^2\} \qquad (\beta = 3) \tag{3.6}$$

and for a two-dimensional quadratic PDE problem by

$$\mathbf{B}(p,q) = \{b_1(p,q), b_2(p,q), \ldots, b_\beta(p,q)\} = \{1, p, q, p^2, pq, q^2\} \qquad (\beta = 6) \tag{3.7}$$

The correction coefficient vector is provided as

$$\mathbf{C}^{*T}(x,y) = \{c_1, c_2, \cdots, c_\beta\} \tag{3.8}$$

The unknown correction coefficients can be determined by satisfying the following reproducing conditions

$$b_i(x,y) = \int_{\Omega} \mathbf{B}(p,q)\mathbf{C}^*(x,y)K(x_k - p, y_k - q)b_i(p,q)dpdq \qquad (i = 1,2,...,\beta) \qquad (3.9)$$

In order to solve the correction coefficient vector $\mathbf{C}^*(x,y)$, the reproducing conditions of Equation (3.9) is written in matrix form as

$$\mathbf{M}\mathbf{C}^*(x,y) = \mathbf{B}^T(x,y) \qquad (3.10)$$

where $\mathbf{M}$ is a symmetric moment matrix associated with the fixed kernel centered at point (x_k, y_k). In fixed kernel approximation, the moment matrix $\mathbf{M}$ is independent of x and y, i.e. a constant in the prescribed kernel supported domain. Each element in the moment matrix are given as

$$M_{ij} = \int_{\Omega} b_i(x-p, y-q)K(x-p, y-q)b_j(p,q)dpdq \ \ (i,j = 1,2,...,m) \qquad (3.11)$$

From Equation (3.10), the correction coefficient vector $\mathbf{C}^*(x,y)$ eventually can be solved in the form of

$$\mathbf{C}^*(x,y) = \mathbf{M}^{-1}\mathbf{B}^T(x,y) \qquad (3.12)$$

Substituting Equations (3.5) and (3.12) into Equation (3.4), the approximation solution $u^h(x,y)$ of the unknown function can be computed as

$$u^h(x,y) = \int_{\Omega} \mathbf{B}(p,q)\mathbf{M}^{-1}\mathbf{B}^T(x,y)K(x_k - p, y_k - q)u(p,q)dpdq \qquad (3.13)$$

If the domain of interest is represented by N_T distinct nodes, the approximation $u^h(x,y)$ in Equation (3.13) can be given in discrete form as

$$u^h(x,y) = \sum_{n=1}^{N_T} (\mathbf{B}(x_n, y_n)\mathbf{M}^{-1}\mathbf{B}^T(x,y)K(x_k - x_n, y_k - y_n)\Delta S_n)u_n \qquad (3.14)$$

where N_T is the total number of points sprinkled over both the interior computational domain Ω and along its edges. The subscript n denotes the n^{th} node in the domain and

u_n is unknown nodal value at *n*-th node. ΔS_n is the nodal volume associated with the n^{th} node which is usually set to unity.

If a shape function $N_n(x,y)$ is defined in similar manner as the trial function in finite element method, Equation (3.14) can be represented as

$$u^h(x,y) = \sum_{n=1}^{N_T} N_n(x,y)u_n \tag{3.15}$$

where the shape function is calculated as

$$N_n(x,y) = \mathbf{B}(x_n,y_n)\mathbf{M}^{-1}\mathbf{B}^T(x,y)K(x_k - x_n, y_k - y_n)\Delta S_n \tag{3.16}$$

In discrete form, the reproducing or consistency conditions of Equation (3.9) is given as

$$b_i(x,y) = \sum_{n=1}^{np} \mathbf{B}(x_n,y_n)\mathbf{C}^*(x,y)K(x_k - x_n, y_k - y_n)\Delta S_n \qquad (i = 1,2,...,\beta) \tag{3.17}$$

Therefore, if a linear independent basic function $\mathbf{B}(p,q) = [1, p, q]$ is considered, the discretized reproducing conditions of equation (3.16) can be expressed as

$$1.0 = \sum_{n=1}^{N_T} \mathbf{B}(p,q)\mathbf{M}^{-1}\mathbf{B}^T(x,y)K(x_k - p, y_k - q)\Delta S_n = \sum_{n=1}^{N_T} N_n(x,y) \tag{3.18a}$$

$$x = \sum_{n=1}^{N_T} (\mathbf{B}(p,q)\mathbf{M}^{-1}\mathbf{B}^T(x,y)K(x_k - p, y_k - q)\Delta S_n)x_n = \sum_{n=1}^{N_T} N_n(x,y)x_n \tag{3.18b}$$

$$y = \sum_{n=1}^{N_T} (\mathbf{B}(p,q)\mathbf{M}^{-1}\mathbf{B}^T(x,y)K(x_k - p, y_k - q)\Delta S_n)y_n = \sum_{n=1}^{N_T} N_n(x,y)y_n \tag{3.18c}$$

The property of Equation (3.18a) is also known as the concept of partition of unity (Melenk and Babuska, 1996). The fixed kernel approach is able to reproduce exactly any function that is included in the definition of the basis function $\mathbf{B}(x,y)$, if all the reproducing conditions in Equations (3.18) are satisfied simultaneously.

Following the concept of the Hermite interpolation theorem, the first-order derivatives of the unknown real function $u(x,y)$ will be treated as an additional unknown function

$$v_x(x,y) = \frac{\partial}{\partial x} u(x,y) \tag{3.19a}$$

$$v_y(x,y) = \frac{\partial}{\partial y} u(x,y) \tag{3.19b}$$

Hence, the first-order differential functions may also be computed in an analogous discretization procedure as Equation (3.15). Thus the discrete approximation is given by

$$v_x^h(x,y) = \sum_{m=1}^{N_s} M_m(x,y) v_{xm} \tag{3.20a}$$

$$v_y^h(x,y) = \sum_{m=1}^{N_s} M_m(x,y) v_{ym} \tag{3.20b}$$

where $N_S (\leq N_T)$ is the total number of nodes covering the domain of interest for the first-order differential functions. In similar notation as Equation (3.15), v_{xm} and v_{ym} denote the first-order differential of the unknown nodal values u_m with respect to x and y. While $M_m(x,y)$ are the shape functions associated with the first-order differential functions $v_x(x,y)$ and $v_y(x,y)$. Note that there are differences between the constructions of shape functions $M_m(x,y)$ and $N_n(x,y)$. In particular, the former shape functions are composed of $(\beta - 1)$ terms of polynomial in the construction of the basis functions, an order lower than the polynomial terms in the basis functions of the latter.

Following the Hermite interpolation theorem, a true meshless approximation $u^h(x,y)$ of the unknown real function $u(x,y)$ can now be constructed as follows

$$u^h(x,y)=\sum_{n=1}^{N_T}N_n(x,y)u_n+\sum_{m=1}^{N_S}(x-\sum_{n=1}^{N_T}N_n(x,y)x_n)M_m(x,y)v_{xm}+\sum_{m=1}^{N_S}(y-\sum_{n=1}^{N_T}N_n(x,y)y_n)M_m(x,y)v_{ym} \tag{3.21}$$

With the implementation of the Hermite-based interpolation approximation, we can directly compute the approximate solutions of both the unknown function and its first-order differential function. It is noteworthy to point out the potential of Hermite approximation in improving the computational accuracy. Therefore, the increase of accuracy of the approximate solutions and its first-order derivatives justifies the shortcoming of having additional unknown functions in the computation.

With the introduction of the additional unknown functions, $v_x(x,y)$ and $v_y(x,y)$, we need to impose auxiliary conditions, so as to formulate a set of complete PDBV equations. Based on the definitions of $v_x(x,y)$ and $v_y(x,y)$ in Equations (3.19), the auxiliary conditions are developed naturally by differentiating the approximate solution $u^h(x,y)$ of Equation (3.21) with respect to the indicated spatial variable, which can be expressed as

$$\begin{aligned}u^h_{,x}(x,y)=&\sum_{n=1}^{N_T}N_{n,x}(x,y)u_n+\sum_{m=1}^{N_S}[1-\sum_{n=1}^{N_T}(N_{n,x}(x,y)x_n)]M_m(x,y)v_{xm}\\&-\sum_{m=1}^{N_S}[\sum_{n=1}^{N_T}(N_{n,x}(x,y)y_n)]M_m(x,y)v_{xm}\\&+\sum_{m=1}^{N_S}(x-\sum_{n=1}^{N_T}N_n(x,y)x_n)M_{m,x}(x,y)v_{xm}\\&+\sum_{m=1}^{N_S}(y-\sum_{n=1}^{N_T}N_n(x,y)y_n)M_{m,x}(x,y)v_{ym}\end{aligned} \tag{3.22a}$$

$$
\begin{aligned}
u^h_{,y}(x,y) = &\sum_{n=1}^{N_T} N_{n,y}(x,y)u_n - \sum_{m=1}^{N_S}[\sum_{n=1}^{N_T}(N_{n,y}(x,y)x_n)]M_m(x,y)v_{xm} \\
&+ \sum_{m=1}^{N_S}[1-\sum_{n=1}^{N_T}(N_{n,y}(x,y)y_n)]M_m(x,y)v_{ym} \\
&+ \sum_{m=1}^{N_S}(x-\sum_{n=1}^{N_T}N_n(x,y)x_n)M_{m,y}(x,y)v_{xm} \\
&+ \sum_{m=1}^{N_S}(y-\sum_{n=1}^{N_T}N_n(x,y)y_n)M_{m,y}(x,y)v_{ym}
\end{aligned}
\tag{3.22b}
$$

where the comma in the subscript before each variable denote the derivatives with respect to that variable. By considering Equations (3.18)-(3.21), we can induce that the auxiliary conditions are derived as,

$$
\begin{aligned}
\sum_{n=1}^{N_T} N_{n,x}(x,y)u_n - &\sum_{m=1}^{N_S}(\sum_{n=1}^{N_T}(N_{n,x}(x,y)x_n))M_m(x,y)v_{xm} \\
&- \sum_{m=1}^{N_S}(\sum_{n=1}^{N_T}(N_{n,x}(x,y)y_n))M_m(x,y)v_{ym} = 0
\end{aligned}
\tag{3.23a}
$$

$$
\begin{aligned}
\sum_{n=1}^{N_T} N_{n,y}(x,y)f_n - &\sum_{m=1}^{N_S}(\sum_{n=1}^{N_T}(N_{n,y}(x,y)x_n))M_m(x,y)v_{xm} \\
&- \sum_{m=1}^{N_S}(\sum_{n=1}^{N_T}(N_{n,y}(x,y)y_n))M_m(x,y)v_{ym} = 0
\end{aligned}
\tag{3.23b}
$$

Thus far, we have completed the formulation of Hermite-Cloud method. In summary, based on the Hermite interpolation theorem, we need to construct the approximate unknown function $u^h(x,y)$ as in Equation (3.21), and to introduce the first-order differential functions, $v^h_x(x,y)$ and $v^h_y(x,y)$ in Equations (3.20), and then couple the formulation with the constructed auxiliary conditions of Equations (3.23). In a nutshell, the approximate unknown function $u^h(x,y)$ and it various derivatives can be summarized as

$$
\begin{aligned}
u^h(x,y) = &\sum_{n=1}^{N_T} N_n(x,y)u_n + \sum_{m=1}^{N_S}(x-\sum_{n=1}^{N_T}N_n(x,y)x_n)M_m(x,y)v_{xm} \\
&+ \sum_{m=1}^{N_S}(y-\sum_{n=1}^{N_T}N_n(x,y)y_n)M_m(x,y)v_{ym}
\end{aligned}
\tag{3.24a}
$$

$$\frac{\partial}{\partial x}u(x,y) = v_x^h(x,y) = \sum_{m=1}^{N_s} M_m(x,y)v_{xm} \tag{3.24b}$$

$$\frac{\partial}{\partial y}u(x,y) = v_y^h(x,y) = \sum_{m=1}^{N_s} M_m(x,y)v_{ym} \tag{3.24c}$$

$$\frac{\partial^2}{\partial x^2}u(x,y) = \sum_{n=1}^{N_T} N_{n,xx}(x,y)u_n \tag{3.24d}$$

$$\frac{\partial^2}{\partial y^2}u(x,y) = \sum_{n=1}^{N_T} N_{n,yy}(x,y)u_n \tag{3.24e}$$

$$\frac{\partial^2}{\partial x \partial y}u(x,y) = \sum_{n=1}^{N_T} N_{n,xy}(x,y)u_n \tag{3.24f}$$

As mentioned before, the moment matrix **M** is independent of x and y within each support domain, hence we can obtain the derivatives of the shape function by directly differentiating the basis function $\mathbf{B}(x,y)$ vector. Hence, by calling in the Equation (3.16) with a quadratic basis function as in Equation (3.7), the derivatives of the shape function are defined as

$$N_{n,x}(x,y) = \{0 \quad 1 \quad 0 \quad 2x \quad 0 \quad y\}\mathbf{M}^{-1}\mathbf{B}^T(x_n,y_n)W(x_k-x_n,y_k-y_n)\Delta S_n \tag{3.25a}$$

$$N_{n,y}(x,y) = \{0 \quad 1 \quad 0 \quad 0 \quad 2y \quad x\}\mathbf{M}^{-1}\mathbf{B}^T(x_n,y_n)W(x_k-x_n,y_k-y_n)\Delta S_n \tag{3.25b}$$

$$N_{n,xx}(x,y) = \{0 \quad 0 \quad 0 \quad 2 \quad 0 \quad 0\}\mathbf{M}^{-1}\mathbf{B}^T(x_n,y_n)W(x_k-x_n,y_k-y_n)\Delta S_n \tag{3.25c}$$

$$N_{n,yy}(x,y) = \{0 \quad 0 \quad 0 \quad 0 \quad 2 \quad 0\}\mathbf{M}^{-1}\mathbf{B}^T(x_n,y_n)W(x_k-x_n,y_k-y_n)\Delta S_n \tag{3.25d}$$

$$N_{n,xy}(x,y) = \{0 \quad 0 \quad 0 \quad 0 \quad 0 \quad 1\}\mathbf{M}^{-1}\mathbf{B}^T(x_n,y_n)W(x_k-x_n,y_k-y_n)\Delta S_n \tag{3.25e}$$

Equations (3.25) are the first and second derivatives of shape function with respect to x and y. Apparently, Hermite-Cloud has inherited the advantage of fixed kernel technique in determining the derivatives of shape function, whereby the calculation can be done in a straightforward manner. This superiority is due to the unique

characteristics that only a fixed kernel technique moment matrix posses as compared with the classical kernel approximation.

For the choice of window functions to construct the fixed kernel function, it allows user judgment as long as it complies with few conditions (Gingold and Monaghan, 1982; Monaghan, 1982; Beltyschko et al., 1996) as listed below

1. $W(x-y,h)>0$ on a subdomain of Ω, Ω_I (3.26)
2. $W(x-y,h)=0$ outside the subdomain Ω_I (3.27)
3. $\int_\Omega W(x-y,h)dy=1$ (3.28)
4. $W(s,h)$ is a monotonically decreasing function, where $s=\|x-y\|$ (3.29)
5. $W(s,h)\to\delta(s)$ as $h\to 0$, where $\delta(s)$ is the Dirac delta function (3.30)

The first condition is rather to ensure a meaningful description of some physical phenomenal than as a mathematical representation requirement. The second condition or compact support, which ensures that $W(x-y)$ are zero everywhere except in the kernel support domain Ω_I, i.e. the approximation of $u(x)$ will depend only on the values of u at nodes which are within the support domain. The domain over which $W(x-y)$ is nonzero is also known as smoothing domain or influence domain. This approximation property enables the discrete equations, which are generated from local representation of nodes, to be bond in nature.

The third condition ensures the consistency of the integral form representation of the continuum function, although it does not necessarily assure consistency of the discrete form of the approximation. The fourth condition is imposed based on physical considerations that a force exerted by a particle on another particle decreases with distance. The fifth condition ensures that the continuous approximation of equation

(3.1) converge to it exact form. In practical cases, this condition is redundant as being discussed in the work of Beltyschko et al. (1996).

Basically, the kernel function may be constructed by different forms of window functions depending on different PDBV problems. The best choice of window function is still debatable, however, a cubic spline function is considered as one of the more versatile function which is expressed as

$$K(x_k - p, y_k - q) = \frac{1}{(r_x r_y)} W(\frac{x_k - p}{r_x}) W(\frac{y_k - q}{r_y}) \tag{3.31}$$

where $W(z)$ is a cubic-spline window function and is defined as

$$W(z) = \begin{cases} 0 & z < -2 \\ \dfrac{(2+z)^3}{6} & -2 \le z \le -1 \\ \dfrac{2}{3} - z^2\left(1 + \dfrac{z}{2}\right) & -1 \le z \le 0 \\ \dfrac{2}{3} - z^2\left(1 - \dfrac{z}{2}\right) & 0 \le z \le 1 \\ \dfrac{(2-z)^3}{6} & 1 \le z \le 2 \\ 0 & 2 < z \end{cases} \tag{3.32}$$

where $z = (x_k - p)/r_x$ for the x-component, and $z = (y_k - q)/r_y$ for the y-component with r_x and r_y indicating the dilation parameter, as defined in Liu et al. (1995a, 1995b). Fundamentally, the dilation parameters r_x and r_y denote the domain of support or influence, i.e. the cloud size of the fixed kernel point (x_k, y_k) in x- and y-directions, respectively. Thus, the cloud size is more or less arbitrary and is adjusted according to the distribution of nodes, and the accuracy requirements due to the consistency conditions of the reproducing kernel approach. On the other hand, for a given nodal arrangement, the continuity of the dilation parameters is necessary to guarantee the good quality approximation and should correspond to some local information to match

the resolution of the given sampling points (Liu et al., 1995b, 1996). From our experience, the values of $r_x = 1.17\Delta x$ and $r_y = 1.17\Delta y$ are suitable choices for normal nodal distributions in two-dimensional problems. The Δx and Δy are the spacing between nodes in x- and y-directions accordingly. The dilation parameters will be further refined to include more nodes base on whether the consistency condition error exceeds a specific threshold. For random nodes distributions, the shape and size of each cloud can be prescribed arbitrarily.

3.3 DISCETIZATION OF PARTIAL DIFFERENTIAL BOUNDARY VALUE PROBLEMS

As mentioned earlier, we employ the point collocation technique so as to discretize the partial differential boundary value problems (PDBV) equations for generic engineering problems. The general form of the PDBV,

$$L[u(x,y)] = P(x,y) \quad \text{in } \Omega \tag{3.33a}$$

$$u(x,y) = Q(x,y) \qquad \text{on } \Gamma_D \tag{3.33b}$$

$$\frac{\partial}{\partial n}u(x,y) = R(x,y) \quad \text{on } \Gamma_N \tag{3.33c}$$

where L is the differential operator, $u(x,y)$ the unknown real function and n is the outward normal vector. While, Ω the interior domain of the problem described by the PDBV equations, Γ_D the section of the boundary where Dirichlet boundary conditions are imposed, and Γ_N the section of the boundary where Neumann boundary conditions

are specified. By means of the point collocation technique, the PDBV problem is discretized as

$$L[u^h(x_i, y_i)] = P(x_i, y_i) \qquad i=1,2,\ldots, N_\Omega \tag{3.34a}$$

$$u^h(x_i, y_i) = Q(x_i, y_i) \qquad i=1,2,\ldots, N_D \tag{3.34b}$$

$$\frac{\partial}{\partial n} u^h(x_i, y_i) = R(x_i, y_i) \qquad i=1,2,\ldots, N_N \tag{3.34c}$$

where N_Ω , N_D and N_N are the numbers of scattered nodes in the interior computational domain, and along the Dirichlet and Neumann edges of the domain, respectively. The total number of scattered nodes is thus $N_T = (N_\Omega + N_D + N_N)$.

After substituting the approximate solutions of Equations (3.20) and (3.21) into Equations (3.34), we can now solve a complete set of discrete governing equation for the PDBV problem with the introduction of the auxiliary conditions of Equations (3.23). After rearrangement, a set of discrete algebraic equations with respect to the unknown values u_i , v_{xi} and v_{yi} is obtained and can be written in matrix form as

$$[H_{ij}]_{(N_T+2N_S)\times(N_T+2N_S)} \{U_i\}_{(N_T+2N_S)\times 1} = \{F_i\}_{(N_T+2N_S)\times 1} \qquad i, j = 1, 2, ..., (N_T + 2N_S) \tag{3.35}$$

in which $\{U_i\}$ and $\{F_i\}$ are $(N_T + 2N_S)$-order column vectors,

$$\{U_i\}_{(N_T+2N_S)\times 1} = \{\{u_i\}_{1\times N_T}, \{v_{xi}\}_{1\times N_S}, \{v_{yi}\}_{1\times N_S}\}^T \tag{3.36a}$$

$$\{F_i\}_{(N_T+2N_S)\times 1} = \{\{P(x_i, y_i)\}_{1\times N_\Omega}, \{Q(x_i, y_i)\}_{1\times N_D}, \{R(x_i, y_i)\}_{1\times N_N}, \{0\}_{1\times 2N_S}\}^T \tag{3.36b}$$

and $[H_{ij}]$ is a $(N_T + 2N_S)\times(N_T + 2N_S)$ coefficient matrix where

$$[H_{ij}] = \begin{bmatrix} \mathbf{H}^1 & \mathbf{H}^3 \\ \mathbf{H}^2 & \mathbf{H}^4 \end{bmatrix}_{(N_T+2N_S)\times(N_T+2N_S)} \tag{3.37}$$

where the components of $[H_{ij}]$ are given as

$$\mathbf{H}^1 = \begin{bmatrix} [\mathbf{L}N_j(x_i, y_i)]_{N_\Omega \times N_T} \\ [N_j(x_i, y_i)]_{N_D \times N_T} \\ [0]_{N_N \times N_T} \end{bmatrix}_{N_T \times N_T} \tag{3.38a}$$

$$\mathbf{H}^2 = \begin{bmatrix} [N_{j,x}(x_i, y_i)]_{N_S \times N_T} \\ [N_{j,y}(x_i, y_i)]_{N_S \times N_T} \end{bmatrix}_{2N_S \times N_T} \tag{3.38b}$$

$$\mathbf{H}^3 = \begin{bmatrix} [\mathbf{L}((x_i - \sum_{n=1}^{N_T} N_n(x_i, y_i)x_n)M_j(x_i, y_i))]_{N_\Omega \times N_S} & [\mathbf{L}((y_i - \sum_{n=1}^{N_T} N_n(x_i, y_i)y_n)M_j(x_i, y_i))]_{N_\Omega \times N_S} \\ [0]_{N_D \times N_S} & [0]_{N_D \times N_S} \\ [M_j(x_i, y_i)]_{N_N \times N_S} & [M_j(x_i, y_i)]_{N_N \times N_S} \end{bmatrix}_{N_T \times 2N_S} \tag{3.38c}$$

$$\mathbf{H}^4 = \begin{bmatrix} [-(\sum_{n=1}^{N_T} N_{n,x}(x_i, y_i)x_n)M_j(x_i, y_i)]_{N_S \times N_S} & [-(\sum_{n=1}^{N_T} N_{n,x}(x_i, y_i)y_n)M_j(x_i, y_i)]_{N_S \times N_S} \\ [-(\sum_{n=1}^{N_T} N_{n,y}(x_i, y_i)x_n)M_j(x_i, y_i)]_{N_S \times N_S} & [-(\sum_{n=1}^{N_T} N_{n,y}(x_i, y_i)y_n)M_j(x_i, y_i)]_{N_S \times N_S} \end{bmatrix}_{2N_S \times 2N_S} \tag{3.38d}$$

The complete set of linear algebraic equations as above can be solved numerically to obtain $(N_T + 2N_S)$ nodal values for $\{U_i\}$. Accordingly, the approximate solution for the PDBV, $u^h(x, y)$ and the corresponding first-order derivatives $v_x^h(x, y)$ and $v_y^h(x, y)$, can be computed from Equations (3.20) and (3.21).

3.4 NUMERICAL VALIDATIONS

In order to examine the accuracy and convergence characteristics of the true meshless Hermite-Cloud method, numerical comparisons are carried out for several classical two-dimensional partial differential boundary value (PDBV) problems, including the patch test for elasticity, plane stress patch subjected to pure bending,

cantilever beam under pure bending and plane stress patch subjected to temperature field. By using a refined version of the definition of standard error, a global error ξ is defined (Mukherjee and Mukherjee, 1997) for the numerical comparisons as follows,

$$\xi = \frac{1}{|u_{\max}|}\sqrt{\frac{1}{N_T}\sum_{i=1}^{N_T}(u_i^h - u_i)^2} \tag{3.39}$$

where u^h and u designate the approximation and exact solutions, respectively. While, N_T is the total number of nodes in the computational domain and along it edges.

For a plane stress elasticity problem, the stress components are expressed by the displacement components as

$$\sigma_x = \frac{E_0}{1-\mu^2}\left(\frac{\partial u}{\partial x} + \mu\frac{\partial v}{\partial y}\right) \tag{3.40a}$$

$$\sigma_y = \frac{E_0}{1-\mu^2}\left(\frac{\partial v}{\partial y} + \mu\frac{\partial u}{\partial x}\right) \tag{3.40b}$$

$$\tau_{xy} = \tau_{yx} = \frac{E_0}{2(1+\mu)}\left(\frac{\partial v}{\partial x} + \frac{\partial u}{\partial y}\right) \tag{3.40c}$$

where σ_x, σ_y and τ_{xy} are the normal and shear stress respectively. u and v are the displacements in the x and y directions. E_0 and μ is the Young modulus and Poisson ratio of the material accordingly.

Therefore, the plane stress equilibrium equations for an isotropic high order patch can be formulated in terms of displacement as (Xu, 1992)

$$\frac{E_0}{1-\mu^2}\left(\frac{\partial^2 u}{\partial x^2} + \frac{1+\mu}{2}\frac{\partial^2 v}{\partial x \partial y} + \frac{1-\mu}{2}\frac{\partial^2 u}{\partial y^2}\right) + b_x = 0 \tag{3.41a}$$

$$\frac{E_0}{1-\mu^2}\left(\frac{\partial^2 v}{\partial y^2} + \frac{1+\mu}{2}\frac{\partial^2 u}{\partial x \partial y} + \frac{1-\mu}{2}\frac{\partial^2 v}{\partial x^2}\right) + b_y = 0 \tag{3.41b}$$

The body force components acting on the structure are designated as b_x and b_y, which however will not be considered here.

As the point collocation approach requires that the residual of the governing equation be identically zero at each selected node, we can substitute the Hermite Cloud approximations of Equations (3.24) into the governing elasticity equations of (3.41). The discretized form of Equations (3.41) are given as

$$\frac{1}{1-\mu^2}\left(\sum_{i=1}^{N_T} N_{i,xx}(x_j,y_j)u_i\right)+\frac{1}{2(1-\mu)}\left(\sum_{i=1}^{N_T} N_{i,xy}(x_j,y_j)v_i\right)+\frac{1}{2(1+\mu)}\left(\sum_{i=1}^{N_T} N_{i,yy}(x_j,y_j)u_i\right)=0 \tag{3.42a}$$

$$\frac{1}{1-\mu^2}\left(\sum_{i=1}^{N_T} N_{i,yy}(x_j,y_j)v_i\right)+\frac{1}{2(1-\mu)}\left(\sum_{i=1}^{N_T} N_{i,xy}(x_j,y_j)u_i\right)+\frac{1}{2(1+\mu)}\left(\sum_{i=1}^{N_T} N_{i,xx}(x_j,y_j)v_i\right)=0 \tag{3.42b}$$

In general, the natural boundary conditions are prescribed in term of displacements as (Xu, 1992)

$$\frac{E_0}{1-\mu^2}\left[l\left(\frac{\partial u}{\partial x}+\mu\frac{\partial v}{\partial y}\right)+m\frac{1-\mu}{2}\left(\frac{\partial u}{\partial y}+\frac{\partial v}{\partial x}\right)\right]=F_x \tag{3.43a}$$

$$\frac{E_0}{1-\mu^2}\left[m\left(\frac{\partial v}{\partial y}+\mu\frac{\partial u}{\partial x}\right)+l\frac{1-\mu}{2}\left(\frac{\partial u}{\partial y}+\frac{\partial v}{\partial x}\right)\right]=F_y \tag{3.43b}$$

where l and m denote the direction cosines of the outward normal direction of boundary, i.e. the cosines of the angles between the normal stress with the x and y axes, respectively. F_x and F_y denote the external stresses acting on x and y planes, respectively. The discretization of the natural boundary conditions in equations (3.43) are provided as

$$\frac{E_0}{1-\mu^2}\left[l\left(\sum_{i=1}^{N_N} M_i(x_j,y_j)u_{xi}+\mu\sum_{i=1}^{N_N} M_i(x_j,y_j)v_{yi}\right)+m\frac{1-\mu}{2}\left(\sum_{i=1}^{N_N} M_i(x_j,y_j)u_{yi}+\sum_{i=1}^{N_N} M_i(x_j,y_j)v_{xi}\right)\right]=F_x \tag{3.44a}$$

$$\frac{E_0}{1-\mu^2}\left[m\left(\sum_{i=1}^{N_s} M_i(x_j,y_j)v_{yi}+\mu\sum_{i=1}^{N_s} M_i(x_j,y_j)u_{xi}\right)+l\frac{1-\mu}{2}\left(\sum_{i=1}^{N_s} M_i(x_j,y_j)u_{yi}+\sum_{i=1}^{N_s} M_i(x_j,y_j)v_{xi}\right)\right]=F_y \tag{3.44b}$$

where u_x, u_y, v_x and v_y are the independent variables associated with derivatives of displacements u and v, for instance, u_x is the derivatives of displacement u in respect of x direction. Apparently, a quadratic polynomial basis functions is needed for the formulation of kernel function, since we have to solve two second order differential equations simultaneously.

3.4.1 Patch Test for Elasticity

The problem considered in the first example is a standard patch test, as shown in Fig. 3.1(a). The governing equations to be solved are prescribed in Equations (3.42). For the boundary conditions, two uniform stresses are loaded at the right end and at the top of the patch respectively. Additionally, the rectangular patch with $L=9$ and $h=3$ is simply supported at the left and bottom ends with the zero reference point hinged to a surface. The imposing of the boundary conditions is a straightforward process, where the conditions listed below are substituted into Equations (3.44) to construct a set a linear algebra equations,

$$l=-1,\quad m=0,\quad u=0,\quad \tau_{xy}=0 \qquad \text{at } x=0 \tag{3.45a}$$

$$l=1,\quad m=0,\quad \sigma_x=1.0,\quad \tau_{xy}=0 \qquad \text{at } x=9 \tag{3.45b}$$

$$l=0,\quad m=-1,\quad \sigma_y=-0.5,\quad \tau_{xy}=0 \qquad \text{at } y=0 \tag{3.45c}$$

$$l=0,\quad m=1,\quad v=0,\quad \tau_{xy}=0 \qquad \text{at } y=3 \tag{3.45d}$$

Under the conditions of a unity Young modulus and a 0.25 Poisson's ratio, the exact solutions are given by

$$u = \frac{9}{8}x, \tag{3.46a}$$

$$v = -\frac{3}{4}y \tag{3.46b}$$

and their first-order derivatives with respect to x and y are

$$\frac{\partial u}{\partial x} = \frac{9}{8}, \tag{3.47a}$$

$$\frac{\partial u}{\partial y} = 0, \tag{3.47b}$$

$$\frac{\partial v}{\partial x} = 0, \tag{3.47c}$$

$$\frac{\partial v}{\partial y} = -\frac{3}{4} \tag{3.47d}$$

The profiles of the u and v displacements, via uniform nodal distributions, are plotted in Figs. 3.1(b) and 3.1(c), and correspondingly compared with those of a Halton quasi-random nodal distribution (Press *et al.*, 1992) in Figs. 3.1(d) to 3.1(e). The exact solutions for u and v are plotted as lines, while the numerical results generated by the proposed Hermite-Cloud method are displayed in the form of solid points. As observed from the profiles for a uniform nodal distribution of 21×21, the computed results match closely with the exact solutions for both u and v, where the respective global errors of Equation (3.39), ξ ,are 2.13×10^{-9} and 1.58×10^{-9} . The spacing between each nodes for the random distribution is taken as $\Delta = Length/\sqrt{N_T} - 1$. In the Halton distribution case, the results shown in Figs. 3.1(d) and 3.1 (e) also match very well with the exact solutions for both u and v, with respective global errors, ξ, of 1.12×10^{-9} and 1.77×10^{-9}, when 441 nodes are used.

For fewer nodes, the irregular distribution of 25 nodes produce global error of 2.5×10^{-12} for u and 9.81×10^{-12}. Thus in this example, the present HCM method has shown excellent consistency characteristics and high accuracy of the computed approximate solutions when using both uniform and irregular nodal distributions.

3.4.2 Plane Stress Patch Subjected to Pure Bending

The second numerical example is a pure bending patch. The equilibrium equations (3.42) and generalized boundary conditions (3.44) are still applicable in this problem. The patch is supported as shown in Fig. 3.2(a). The hinged zero reference point restricts both horizontal and vertical displacements, and the vertical displacement is also restricted at the hinge on the right end. In brief, the boundary conditions are given in term of displacements as:

$$l=-1,\quad m=0,\quad \sigma_x=\frac{My}{I},\quad \tau_{xy}=0 \qquad \text{at } x=0 \qquad (3.48a)$$

$$l=1,\quad m=0,\quad \sigma_x=\frac{My}{I},\quad \tau_{xy}=0 \qquad \text{at } x=L \qquad (3.48b)$$

$$l=0,\quad m=-1,\quad \sigma_y=0,\quad \tau_{xy}=0 \qquad \text{at } y=-h/2 \qquad (3.48c)$$

$$l=0,\quad m=1,\quad \sigma_y=0,\quad \tau_{xy}=0 \qquad \text{at } y=h/2 \qquad (3.48d)$$

with three additional point constraints

$$u\big|_{x=0,y=0}=0, \qquad (3.49a)$$

$$v\big|_{x=0,y=0}=0, \qquad (3.49b)$$

$$v\big|_{x=L,y=0}=0 \qquad (3.49c)$$

where M is the applied bending moment and y is the distance from the neutral axis. I is the moment of inertia which is defined as $I = (h^3/12)$. L and h are the length and height of the patch test sample respectively.

A rectangular patch of dimensions $L = 8$ and $h = 2$ is considered in this numerical study. A unity bending moment is applied to the patch, and the Young's modulus and Poisson's ratio are taken as unity and 0.25 respectively. The exact solutions are given as (Xu, 1992),

$$u = \frac{M}{E_0 I}(x - \frac{l}{2})y, \tag{3.50a}$$

$$v = \frac{M}{2E_0 I}(xl - x^2 - \mu y^2) \tag{3.50b}$$

and the first-order derivatives with respect to *x* and *y* are written as

$$\frac{\partial u}{\partial x} = \frac{M}{E_0 I} y, \tag{3.51a}$$

$$\frac{\partial u}{\partial y} = \frac{M}{E_0 I}(x - \frac{l}{2}), \tag{3.51b}$$

$$\frac{\partial v}{\partial x} = \frac{M}{E_0 I}(\frac{l}{2} - x), \tag{3.51c}$$

$$\frac{\partial v}{\partial y} = -\frac{\mu M}{E_0 I} y \tag{3.51d}$$

By employing the present Hermite Cloud method, this problem is solved numerically with 21×21 uniform distribution and with Halton quasi-random distribution of 450 nodes, respectively. The profiles of the u and v displacements are plotted in Figs. 3.2(b) and 3.2(c) for uniform nodal distribution and correspondingly in Figs. 3.2(d) and 3.2(e) for quasi-random distribution. The computed results show good correspondence with the exact solutions. For uniform nodal distribution, the respective global errors ξ for u and v are 4.29×10^{-9} and 4.81×10^{-9}. For the quasi-random

nodal distribution, the global errors ξ for u and v are 1.08×10^{-7} and 1.40×10^{-8}, respectively. For coarse distribution of 25 quasi-random nodes, the global errors for u and v are 2.80×10^{-11} and 5.88×10^{-12}.

3.4.3 Cantilever Beam Loader under Pure Bending

The third numerical example considered here is a two-dimensional cantilever beam with a loading of unity bending moment at both ends. The governing differential equations and generalized boundary conditions for this plane stress elasticity problem are provided by Equations (3.42) and (3.44). As depicted in Fig. 3.3(a), one end of the cantilever is fixed. We will employ the modified conditions adopted by Xu (1992), whereby the centre of the fixed end does not move in either the x or y direction. Hence these conditions can be expressed as

$$u\big|_{x=L,y=0} = 0, \tag{3.52a}$$

$$v\big|_{x=L,y=0} = 0 \tag{3.52b}$$

$$l=-1,\quad m=0,\quad \sigma_x=\frac{My}{I},\quad \tau_{xy}=0 \qquad \text{at } x=0 \tag{3.52c}$$

$$l=1,\quad m=0,\quad \sigma_x=\frac{My}{I},\quad \frac{\partial v}{\partial x}=0 \qquad \text{at } x=L \tag{3.52d}$$

$$l=0,\quad m=-1,\quad \sigma_y=0,\quad \tau_{xy}=0 \qquad \text{at } y=-h/2 \tag{3.52e}$$

$$l=0,\quad m=1,\quad \sigma_y=0,\quad \tau_{xy}=0 \qquad \text{at } y=h/2 \tag{3.52f}$$

With reference to the computational model as shown in Fig. 3.3(a), a cantilever beam with dimensions of $L=8$ and $h=2$ is considered with properties of unity

Young modulus and Poisson ratio of 0.25. Under the bending moment of unity, the exact solution (Xu, 1992) is given as

$$u = \frac{M}{E_0 I}(x - l)\, y\,, \tag{3.53a}$$

$$v = -\frac{M}{2E_0 I}[(l - x)^2 + \mu y^2] \tag{3.53b}$$

and their first order derivatives with respect to x and y are written as

$$\frac{\partial u}{\partial x} = \frac{M}{E_0 I} y\,, \tag{3.54a}$$

$$\frac{\partial u}{\partial y} = -\frac{M}{E_0 I}(l - x)\,, \tag{3.54b}$$

$$\frac{\partial v}{\partial x} = \frac{M}{E_0 I}(l - x)\,, \tag{3.54c}$$

$$\frac{\partial v}{\partial y} = -\frac{\mu M}{E_0 I} y \tag{3.54d}$$

In this example, the present Hermite Cloud method is tested with a uniform 25×25 distribution and with Halton quasi-random sequence of 650 scatted nodes, respectively. The numerical solutions of the displacements for both uniform and quasi-random nodal distributions are illustrated in Figs. 3.3(b) to 3.3(e). Similar to the previous two examples, good correspondence between the Hermite Cloud approximations with the exact solutions is achieved. For uniform nodal distribution, the respective global errors ξ for u and v are 1.64×10^{-8} and 4.01×10^{-6}. For the quasi-random nodal distribution, the global errors ξ for u and v are 2.96×10^{-8} and 7.34×10^{-7}, respectively. If coarse distribution of 25 irregular points is used, the global errors for u and v are 3.40×10^{-12} and 7.50×10^{-11}, accordingly.

3.4.4 Patch Subjected to Thermal Stress

The fourth numerical examples considered here is a rectangular patch subjected to thermal stress. The stress components in term of the displacements are given as

$$\sigma_x = \frac{E_0}{1-\mu^2}\left(\frac{\partial u}{\partial x}+\mu\frac{\partial v}{\partial y}\right)-\frac{E_0\alpha T}{1-\mu} \tag{3.55a}$$

$$\sigma_y = \frac{E_0}{1-\mu^2}\left(\frac{\partial v}{\partial y}+\mu\frac{\partial u}{\partial x}\right)-\frac{E_0\alpha T}{1-\mu} \tag{3.55b}$$

$$\tau_{xy} = \tau_{yx} = \frac{E_0}{2(1+\mu)}\left(\frac{\partial v}{\partial x}+\frac{\partial u}{\partial y}\right) \tag{3.55c}$$

The two-dimensional plane-stress equations of equilibrium can be written in terms of the displacements as (Xu, 1992),

$$(1+\mu)\alpha\frac{\partial T}{\partial x} = \frac{\partial^2 u}{\partial x^2}+\frac{1-\mu}{2}\frac{\partial^2 u}{\partial y^2}+\frac{1+\mu}{2}\frac{\partial^2 v}{\partial x\partial y} \tag{3.56a}$$

$$(1+\mu)\alpha\frac{\partial T}{\partial y} = \frac{\partial^2 v}{\partial y^2}+\frac{1-\mu}{2}\frac{\partial^2 v}{\partial x^2}+\frac{1+\mu}{2}\frac{\partial^2 u}{\partial x\partial y} \tag{3.56b}$$

The discretized form of Equations (3.56) are given as

$$\begin{aligned}(1+\mu)\alpha\sum_{i=1}^{N_s}M_i(x_j,y_j)T_{xi}-\left(\sum_{i=1}^{N_T}N_{i,xx}(x_j,y_j)u_i\right)\\ -\frac{1-\mu}{2}\left(\sum_{i=1}^{N_T}N_{i,yy}(x_j,y_j)u_i\right)-\frac{1+\mu}{2}\left(\sum_{i=1}^{N_T}N_{i,xy}(x_j,y_j)v_i\right)=0\end{aligned} \tag{3.57a}$$

$$\begin{aligned}(1+\mu)\alpha\sum_{i=1}^{N_s}M_i(x_j,y_j)T_{yi}-\left(\sum_{i=1}^{N_T}N_{i,yy}(x_j,y_j)v_i\right)\\ -\frac{1-\mu}{2}\left(\sum_{i=1}^{N_T}N_{i,xx}(x_j,y_j)v_i\right)-\frac{1+\mu}{2}\left(\sum_{i=1}^{N_T}N_{i,xy}(x_j,y_j)u_i\right)=0\end{aligned} \tag{3.57b}$$

The patch is subjected to temperature field of function y coordinate

$$T = T_0(1-\frac{y^2}{b^2}) \tag{3.58}$$

where α is the coefficient of thermal expansion, T_0 the reference temperature, and b the distance from the central line.

In general, the natural boundary conditions in the absence of surface forces are prescribed in term of displacements as (Xu, 1992),

$$l\left(\frac{\partial u}{\partial x}+\mu\frac{\partial v}{\partial y}\right)+m\frac{1-\mu}{2}\left(\frac{\partial u}{\partial y}+\frac{\partial v}{\partial x}\right)=l(1+\mu)\alpha T \tag{3.59a}$$

$$m\left(\frac{\partial v}{\partial y}+\mu\frac{\partial u}{\partial x}\right)+l\frac{1-\mu}{2}\left(\frac{\partial u}{\partial y}+\frac{\partial v}{\partial x}\right)=m(1+\mu)\alpha T \tag{3.59b}$$

where l and m denote the cosines of the angles between the normal stress with the x and y axes, respectively. The boundary conditions (3.59) can be presented in discretized form as

$$l(1+\mu)\alpha\left[\sum_{i=1}^{N_D}N_i(x_j,y_j)T_i+\sum_{i=1}^{N_S}(x-\sum_{j=1}^{N_T}N_j(x,y)x_j)M_i(x,y)T_{xi}+\sum_{i=1}^{N_S}(y-\sum_{j=1}^{N_T}N_j(x,y)y_j)M_i(x,y)T_{yi}\right]$$
$$=l\left(\sum_{i=1}^{N_N}M_i(x_j,y_j)u_{xi}+\mu\sum_{i=1}^{N_N}M_i(x_j,y_j)v_{yi}\right)+m\frac{1-\mu}{2}\left(\sum_{i=1}^{N_N}M_i(x_j,y_j)u_{yi}+\sum_{i=1}^{N_N}M_i(x_j,y_j)v_{xi}\right) \tag{3.60a}$$

$$m(1+\mu)\alpha\left[\sum_{i=1}^{N_D}N_i(x_j,y_j)T_i+\sum_{i=1}^{N_S}(x-\sum_{j=1}^{N_T}N_j(x,y)x_j)M_i(x,y)T_{xi}+\sum_{i=1}^{N_S}(y-\sum_{j=1}^{N_T}N_j(x,y)y_j)M_i(x,y)T_{yi}\right]$$
$$=m\left(\sum_{i=1}^{N_N}M_i(x_j,y_j)v_{yi}+\mu\sum_{i=1}^{N_N}M_i(x_j,y_j)u_{xi}\right)+l\frac{1-\mu}{2}\left(\sum_{i=1}^{N_N}M_i(x_j,y_j)u_{yi}+\sum_{i=1}^{N_N}M_i(x_j,y_j)v_{xi}\right) \tag{3.60b}$$

If the structure is simply-supported with the zero reference point hinged to the surface, as depicted in Fig. 3.4(a), the boundary conditions are given by

$$l=-1,\quad m=0,\quad u=0,\quad \tau_{xy}=0 \qquad \text{at } x=0 \tag{3.61a}$$

$$l=1,\quad m=0,\quad \sigma_x=\alpha E_0T_0(\frac{y^2}{b^2}-\frac{1}{3}),\quad \tau_{xy}=0 \qquad \text{at } x=L \tag{3.61b}$$

$$l = 0, \quad m = -1, \quad \sigma_y = 0, \quad \tau_{xy} = 0 \qquad \text{at } y = -b \qquad (3.61c)$$

$$l = 0, \quad m = 1, \quad \sigma_y = 0, \quad \tau_{xy} = 0 \qquad \text{at } y = b \qquad (3.61d)$$

The additional displacement component constraint,

$$v\big|_{x=0,y=0} = 0 \qquad (3.62)$$

For a rectangular patch of the dimensions of $L = 8$ and $2b = 2$ with a Poisson's ratio of 0.25, the exact solutions are derived as

$$u = \frac{2}{3}\alpha T_0 x, \qquad (3.63a)$$

$$v = \alpha T_0[-(1+\mu)\frac{y^3}{3b^2} + \frac{\mu}{3}y + y] \qquad (3.63b)$$

and their corresponding first-order derivatives with respect to x and y can be written as

$$\frac{\partial u}{\partial x} = \frac{2}{3}\alpha T_0, \qquad (3.64a)$$

$$\frac{\partial u}{\partial y} = 0, \qquad (3.64b)$$

$$\frac{\partial v}{\partial y} = \alpha T_0[-(1+\mu)\frac{y^2}{b^2} + \frac{\mu}{3} + 1], \qquad (3.64c)$$

$$\frac{\partial v}{\partial x} = 0 \qquad (3.64d)$$

We first examine the numerical results for the displacements u and v ($T_0 = 298\text{K}$, $\alpha = 0.001$). The profiles of the u and v displacements, based on a 21×21 uniform distribution, are plotted in Figs. 3.4(b) and 3.4(c), whereas those based on calculations using 450 random nodes are depicted in Figs. 3.4(d) and 3.4(e). The displacement profiles in these figures agree well with the exact solutions provided in Equations (3.63). The convergence characteristics of the Hermite Cloud method in this problem are also provided in Figs. 3.4(f) to 3.4(i). As we can observe from the graphs,

the global errors ξ for both the approximate solution and first-order differential decrease monotonically with more refined distribution of nodes. The Hermite Cloud method achieve values of 3.98×10^{-3} and 2.16×10^{-2} for the global errors ξ of computed displacements, with a distribution of 11×11 uniformly scattered nodes. With the increase of nodal number to a 21×21 uniform distribution, the global errors of 1.72×10^{-3} for u and 4.99×10^{-3} for v are obtained. A higher accuracy, with the global errors of 8.55×10^{-4} and 2.20×10^{-3} for u and v, can be achieved with a yet finer uniform nodal distribution of 31×31. Further, in Figs. 3.4(f) to 3.4(g), the convergence rates are found to be 2.03 and 2.55 in the case of uniform distribution, and 1.32 and 1.49 in the case of quasi-random distribution for u and v components respectively. Likewise, the convergence rate of the first-order x-derivative for u and the first-order y-derivative for v are found to be of 2.35 and 2.26 in the case of uniform nodes, and 1.06 and 1.43 in the case of quasi-random nodes respectively, as shown in Figs. 3.4(h) to 3.4(i). Based on these findings, it is clear that the present Hermite-Cloud method is able to achieve an excellent computational accuracy and convergence characteristics for both the approximation of the field-variable solution as well as its first-order derivative.

3.4.5 Heat Conduction with Localized High Gradient

The final example is a steady-state heat conduction problem for a rectangular plate with a heat source, and this is given as

$$\frac{\partial^2 T}{\partial x^2}+\frac{\partial^2 T}{\partial y^2}=-2c^2\operatorname{sech}^2[c(y-3)]\tanh[c(y-3)] \tag{3.65}$$

where c is a free parameter. After implementation of point collocation method, the discrete form of Equations (3.65) is given as

$$\sum_{i=1}^{N_T} N_{i,xx}(x_j, y_j)T_i + \sum_{i=1}^{N_T} N_{i,yy}(x_j, y_j)T_i = -2c^2 \text{sech}^2[c(y_j - 3)]\tanh[c(y_j - 3)] \quad (3.66)$$

where T_i is the temperature at node i.

The boundary conditions for Poisson equation of (3.65) are taken as

$$T = \tanh(3c) \qquad \text{at } y = 0 \text{ and } y = 6 \qquad (3.67a)$$

$$T_{,x} = 0 \qquad \text{at } x = 0 \text{ and } x = 4 \qquad (3.67b)$$

The discrete form of the boundary conditions is provided as

$$\sum_{i=1}^{N_D} N_i(x_j, y_j)T_i + \sum_{i=1}^{N_S}(x - \sum_{j=1}^{N_T} N_j(x, y)x_j)M_i(x, y)T_{xi} + \sum_{i=1}^{N_S}(y - \sum_{j=1}^{N_T} N_j(x, y)y_j)M_i(x, y)T_{yi} = \tanh(3c) \qquad \text{at } y = 0 \text{ and } y = 6 \quad (3.68a)$$

$$\sum_{i=1}^{N_N} M_i(x_j, y_j)T_{xi} = 0 \qquad \text{at } x = 0 \text{ and } x = 4 \qquad (3.68b)$$

where T_{xi} is the independent variable corresponding to the first derivative of T with respect to x at node i. The exact solution for the temperature field is given as

$$T = \tanh[c(y - 3)] \qquad (3.69)$$

and the first derivative of temperature field with respect to y is provided as

$$T_y(x, y) = c \cdot \text{sech}^2[c(y - 3)] \qquad (3.70)$$

The numerical results in Fig. 3.5 are obtained for the case where $c = 10$. With reference to Fig. 3.5(d), a local high gradient occurs in the vicinity of $y = 3$ and its peak value should correspond to the c parameter. With a uniform nodal distribution of 5×31, the solutions from the present Hermite Cloud method matches closely with the exact solution. From the figure, it is obvious that the numerical results from Hermite Cloud method are significantly better than those attained from finite element method

(Belytschko and Lu, 1992). The convergence characteristics for the temperature and its derivative are also plotted in Fig. 3.5(e), and as in the previous example, stable monotonic features are observed. We also note that the global errors ξ of the temperatures solution are higher than the global errors ξ for its corresponding derivatives, but they are both of the same order.

3.5 NUMERICAL SOLUTION OF ONE-DIMENSIONAL STEADY-STATE MECpH MODEL

The MECpH model is constructed from general nonlinear partial differential equations, and hence can be solved with any robust numerical method, such as meshless methods or finite element methods, with a certain degree of care taken to handle the nonlinear nature of the equations. However, meshless methods have their advantages when it comes to solving multiphasic problems and treating moving domain discontinuities as in the hydrogel-solvent system. Furthermore, their advantages become more pronounced, especially in cases of excessive mesh distortion due to large deformation. The presently used Hermite-Cloud method (HCM) is based on the reproducing kernel particle method (RKPM) and combines the Hermite theorem for the construction of the interpolation functions, with point collocation technique for discretization of the partial differential equations (PDE). The HCM stand out from other meshless methods as it possesses several encouraging advantages that are appealing to the present problem, where it does not need any integration procedure for discretization and solves the strong-form equations directly. In addition, the derivatives of the shape function can be readily obtained by differentiating the basis function

directly. Since the interpolation function is of Hermite type, the derivatives of the field function can be handled in a straightforward manner, and the Neumann boundary conditions can be applied easily without any preconditioning.

In order to solve the MECpH system with Hermite Cloud method in present case, the governing equations as prescribed in Section 2.3.5 need to be discretized. Following the procedure in Section 3.3, the spatial discretization for the primary variables, i.e. c^k, ψ, u are

$$c^k(x_i) = \sum_{n=1}^{np} N_n(x_i) c_n^k + \sum_{m=1}^{np} (x - \sum_{n=1}^{np} N_n(x_i) x_n) M_m(x_i) c_{x,m}^k \tag{3.71}$$

$$\psi(x_i) = \sum_{n=1}^{np} N_n(x_i) \psi_n + \sum_{m=1}^{np} (x - \sum_{n=1}^{np} N_n(x_i) x_n) M_m(x_i) \psi_{x,m} \tag{3.72}$$

$$u(x_i) = \sum_{n=1}^{np} N_n(x_i) u_n + \sum_{m=1}^{np} (x - \sum_{n=1}^{np} N_n(x_i) x_n) M_m(x_i) u_{x,m} \tag{3.73}$$

where *np* is the number of nodes scattered in the computational domain of interest. *N* and *M* are the appropriate Hermite Cloud shape functions depending on the highest order of the governing equations. The subscripts before the comma denote the derivatives with respect to the variable. The first order derivatives of the primary variable, i.e. c_x^k, ψ_x, u_x will be considered as separate nodal variables and given according to Hermite Cloud standard as

$$c_x^k(x_i) = \sum_{m=1}^{np} M_m(x_i) c_{x,m}^k \tag{3.74}$$

$$\psi_x(x_i) = \sum_{m=1}^{np} M_m(x_i) \psi_{x,m} \tag{3.75}$$

$$u_x(x_i) = \sum_{m=1}^{np} M_m(x_i) u_{x,m} \tag{3.76}$$

The discretized governing equations to be solved are

$$\begin{aligned}&\sum_{n=1}^{np} N_{xx,n}(x_i) c_n^k + \eta z^k \left(\sum_{n=1}^{np} M_n(x_i) c_{x,n}^k \right) \left(\sum_{n=1}^{np} M_n(x_i) \psi_{x,n} \right) \\ &+\eta z^k \left(\sum_{n=1}^{np} N_n(x_i) c_n^k + \sum_{n=1}^{np} (x - \sum_{m=1}^{np} N_m(x_i) x_m) M_n(x_i) c_{x,n}^k \right) \left(\sum_{n=1}^{np} N_{xx,n}(x_i) \psi_n \right) = 0\end{aligned} \tag{3.77}$$

$$\begin{aligned}&\sum_{n=1}^{np} N_{xx,n}(x_i) \psi_n + \frac{F^2}{\varepsilon \varepsilon_0 RT} \frac{L_{ref}^2 c_{ref}}{\eta} \Bigg[z^f c^f + \sum_{k=1}^{N} z^k \left(\sum_{n=1}^{np} N_n(x_i) c_n^k \right. \\ &\qquad \left. + \sum_{n=1}^{np} (x - \sum_{m=1}^{np} N_m(x_i) x_m) M_n(x_i) c_{x,n}^k \right) \Bigg] = 0\end{aligned} \tag{3.78}$$

$$\begin{aligned}&(2\mu + \lambda) \left(\sum_{n=1}^{np} N_{n,xx}(x_i) u_j + \sum_{m=1}^{np} M_m(x_i) u_x \sum_{n=1}^{np} N_{n,xx}(x_i) u_n \right) \\ &-c_{ref} RT \left(\sum_{k=1}^{N} c_x^k(x_i) - \overline{c}_x^k(x_i) \right) = 0\end{aligned} \tag{3.79}$$

or

$$\begin{aligned}&(2\mu + \lambda) \Bigg[\sum_{n=1}^{np} N_{n,XX}(X_i) u_n + 3 \sum_{m=1}^{np} M_m(X_i) u_X \sum_{n=1}^{np} N_{n,XX}(X_i) u_n + \\ &\frac{3}{2} \left(\sum_{m=1}^{np} M_m(X_i) u_X \right)^2 \sum_{n=1}^{np} N_{n,XX}(X_i) u_n \Bigg] - c_{ref} RTJ \left(\sum_{k=1}^{N} c_x^k(x_i) - \overline{c}_x^k(x_i) \right) = 0\end{aligned} \tag{3.80}$$

The set of equations is non-linear with respect to the unknown concentration, electric potential and displacement. Therefore, an iteration scheme needs to be adopted to find a solution. The Newton-Raphson iteration procedure is used to determine a sequence of approximation solution until the balance equation is satisfied up to a certain degree of accuracy. If the exact solution of the displacement is denoted as u and u^h is an estimate of the exact solution (i.e. guess value for each iterations until δu is within an arbitrary small tolerance), then we can write

$$u^h = u + \delta u \tag{3.81}$$

where δu is the error in the approximation. Analogous expression applied to c^k, ψ, c_x^k, ψ_x, and u_X. Using the standard Newton-Raphson method, the nonlinear system can be linearized and solved in the form of

$$[\mathbf{J}]\{\boldsymbol{\delta}\mathbf{u}\} = \{-\mathbf{R}\} \tag{3.82}$$

where [**J**] is the Jacobian matrix and the right-hand side vector **R** is the residual vector. The components of c^k, ψ, u_X, c_x^k, ψ_x, and u_X are grouped into the column $\{\boldsymbol{\delta}\mathbf{u}\}$.

The residuals R at each node are defined as

$$\begin{aligned} R_{NP}^k(x_i) = &\sum_{n=1}^{np} N_{xx,n}(x_i)c_n^k + \eta z^k \left(\sum_{m=1}^{np} M_m(x_i)c_{x,m}^k\right)\left(\sum_{m=1}^{np} M_m(x_i)\psi_{x,m}\right) \\ &+ \eta z^k \left(\sum_{n=1}^{np} N_n(x_i)c_n^k + \sum_{m=1}^{np}(x - \sum_{n=1}^{np} N_n(x_i)x_n)M_m(x_i)c_{x,m}^k\right)\left(\sum_{n=1}^{np} N_{xx,n}(x_i)\psi_n\right) \end{aligned} \tag{3.83}$$

$$\begin{aligned} R_P(x_i) = &\sum_{n=1}^{np} N_{xx,n}(x_i)\psi_n + \frac{F^2}{\varepsilon\varepsilon_0 RT}\frac{L_{ref}^2 c_{ref}}{\eta}\left[z^f c^f + \sum_{k=1}^{N} z^k \left(\sum_{n=1}^{np} N_n(x_i)c_n^k\right.\right. \\ &\left.\left. + \sum_{m=1}^{np}(x - \sum_{n=1}^{np} N_n(x_i)x_n)M_m(x_i)c_{x,m}^k\right)\right] \end{aligned} \tag{3.84}$$

$$\begin{aligned} R_M(X_i) = &(2\mu + \lambda)\left[\sum_{n=1}^{np} N_{n,XX}(X_i)u_n + 3\sum_{m=1}^{np} M_m(X_i)u_{X,m}\sum_{j=1}^{np} N_{n,XX}(X_i)u_n\right. \\ &\left. + \frac{3}{2}\left(\sum_{m=1}^{np} M_m(X_i)u_{X,m}\right)^2 \sum_{n=1}^{np} N_{n,XX}(X_i)u_n\right] - c_{ref}RTJ\left(\sum_{k=1}^{N} c_x^k(x_i) - \overline{c}_x^k(x_i)\right) \end{aligned} \tag{3.85}$$

together with their auxiliary residuals equations as

$$R_{cx}^k(x_i) = \sum_{n=1}^{np} N_{x,n}(x_i)c_n^k - [\sum_{n=1}^{np} N_{x,n}(x_i)x_n]\sum_{m=1}^{np} M_m(x_i)c_{x,j}^k \tag{3.86}$$

$$R_{\psi x}^k(x_i) = \sum_{n=1}^{np} N_{x,n}(x_i)\psi_n - [\sum_{n=1}^{np} N_{x,n}(x_i)x_n]\sum_{m=1}^{np} M_m(x_i)\psi_n \tag{3.87}$$

$$R_{uX}^{k}(X_i) = \sum_{n=1}^{np} N_{X,n}(X_i)u_n - [\sum_{n=1}^{np} N_{X,n}(X_i)X_n]\sum_{m=1}^{np} M_m(X_i)u_n \tag{3.88}$$

Correspondingly, the Jacobian matrix is obtained as

$$\mathbf{[J]} = \begin{pmatrix} \frac{\partial R_{NP}^k}{\partial \overline{c}^k} & \frac{\partial R_{NP}^k}{\partial \overline{\psi}} & \frac{\partial R_{NP}^k}{\partial \overline{u}} & \frac{\partial R_{NP}^k}{\partial \overline{c}_x^k} & \frac{\partial R_{NP}^k}{\partial \overline{\psi}_x} & \frac{\partial R_{NP}^k}{\partial \overline{u}_x} \\ \frac{\partial R_P}{\partial \overline{c}^k} & \frac{\partial R_P}{\partial \overline{\psi}} & \frac{\partial R_P}{\partial \overline{u}} & \frac{\partial R_P}{\partial \overline{c}_x^k} & \frac{\partial R_P}{\partial \overline{\psi}_x} & \frac{\partial R_P}{\partial \overline{u}_x} \\ \frac{\partial R_M}{\partial \overline{c}^k} & \frac{\partial R_M}{\partial \overline{\psi}} & \frac{\partial R_M}{\partial \overline{u}} & \frac{\partial R_M}{\partial \overline{c}_x^k} & \frac{\partial R_M}{\partial \overline{\psi}_x} & \frac{\partial R_M}{\partial \overline{u}_x} \\ \frac{\partial R_{cx}^k}{\partial \overline{c}^k} & \frac{\partial R_{cx}^k}{\partial \overline{\psi}} & \frac{\partial R_{cx}^k}{\partial \overline{u}} & \frac{\partial R_{cx}^k}{\partial \overline{c}_x^k} & \frac{\partial R_{cx}^k}{\partial \overline{\psi}_x} & \frac{\partial R_{cx}^k}{\partial \overline{u}_x} \\ \frac{\partial R_{\psi x}}{\partial \overline{c}^k} & \frac{\partial R_{\psi x}}{\partial \overline{\psi}} & \frac{\partial R_{\psi x}}{\partial \overline{u}} & \frac{\partial R_{\psi x}}{\partial \overline{c}_x^k} & \frac{\partial R_{\psi x}}{\partial \overline{\psi}_x} & \frac{\partial R_{\psi x}}{\partial \overline{u}_x} \\ \frac{\partial R_{ux}}{\partial \overline{c}^k} & \frac{\partial R_{ux}}{\partial \overline{\psi}} & \frac{\partial R_{ux}}{\partial \overline{u}} & \frac{\partial R_{ux}}{\partial \overline{c}_x^k} & \frac{\partial R_{ux}}{\partial \overline{\psi}_x} & \frac{\partial R_{ux}}{\partial \overline{u}_x} \end{pmatrix} \tag{3.89}$$

Obviously, the components of Jacobian matrix are determined from the differentiation of the residual functions of Equations (3.83) to (3.88) with respect to each variables. Therefore, the solution for the variables are obtained once $\{\mathbf{R}\} \approx \{0\}$ is approximately satisfied. It should be noted that each components in Jacobian matrix (3.89) is a $np \times np$ matrix, thus the Jacobian matrix becomes very large. For the sake of efficiency and storage cost, we have opted for a relaxation approach where the PNP equations will be solved, and the solutions for the concentration and electric potential will be treated as forcing terms in the mechanical deformation equation. The algorithm of the relaxation approach is shown in Figure 3.6.

3.5 REMARKS

Hermite Cloud method (HCM) is based on the similar concept as reproducing kernel method (RKM) (Liu *et al.*, 1995a, 1995b). However, there are few distinct

differences of formulation procedures between HCM and classical RKM, more specifically the Hermite reproducing kernel method (HRKM) by Liu *et al.* (1996b) or the finite cloud method (FCM) by Aluru (2000, 2001) which are intended to enrich the RKM family.

The HCM uses the collocation technique for discretization of the governing partial differential equations (PDEs), which is associated with solving the strong-form PDEs, whereas, the HRKM utilizes Galerkin based discretization method that first converts the PDEs into an integral equation and solves it as weak-form system equations. One of the major concerns in employing Galerkin based meshless method is to evaluate the integrals of the weak form. In dichotomy, the collocation technique possess the advantages of having (1) the character of truly meshless method as no background mesh or cells are needed for the entire procedure of approximation; (2) ease of implementation as the algorithm and coding can be established in a undemanding manner; (3) computationally more effective as the numerical integration is not required; (4) direct implementation of essential boundary conditions. Owing to the vast advantages, collocation based meshless methods have been occupying dominant place in computational mechanics (Fasshauer, 1999).

The Hermite Cloud method employs a fixed reproducing kernel technique rather than the moving reproducing kernel technique to interpolate the scatted nodes in the computational domain. As mentioned erstwhile, the moment matrix of fixed kernel technique is independent of the spatial variables within each support/cloud domain. Therefore, the derivatives of the shape function can be readily obtained by differentiating the basis function directly. This scheme, nonetheless, has somewhat relieved the burden of collocation method that requires consistency of order $2k$ for a

PDEs of order $2k$ as compare with solution by a Galerkin method that only requires consistency of order k.

The difficulties in enforcing the Neumann boundary condition as in FCM (Aluru, 2000; Aluru and Gang, 2001) have been improved significantly through the employment of Hermite-type interpolation (Liu *et al.* 1996b; Liska *et al.*, 1996; Zhang *et al.*, 2000). In Hermite interpolation scheme, the first derivatives of the field function are treated as additional independent variables or degree of freedom. Hence, the derivatives of the field function can be handled in a straightforward. For instance, the Neumann boundary conditions can be applied easily without any preconditioning, in the same way as standard Dirichlet boundary condition. Further, the mixed boundary conditions can also be imposed without any effort (Li *et al.*, 2003). However, we have encountered some trade-off in the Hermite interpolation method where the computation cost is higher as additional variables are introduced into the formulation.

Five sample problems are considered in the numerical studies. The computed results show very good correspondence with the exact solutions, for both the approximate solutions as well as their first-order derivatives. The convergence characteristics and efficiency of the Hermite Cloud method have also been examined in detail, where numerical studies verify that the method is stable and efficient. They also show that computational accuracy of the Hermite Cloud method at discrete points in the domain is significantly refined not only for the approximate solutions, but also for the first-order derivative of the approximate solutions. Therefore, it may be safely concluded that the developed Hermite Cloud method is a very efficient numerical technique for solving general PDBV problems.

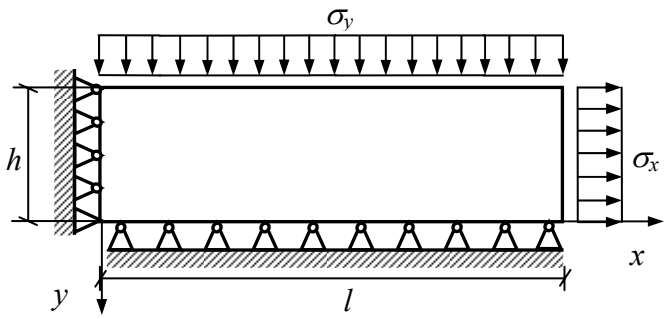

(a). Schematic of the 2D patch under uniform stresses.

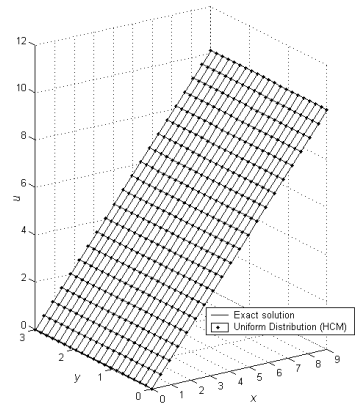

(b). *u*-displacement with uniform nodes.

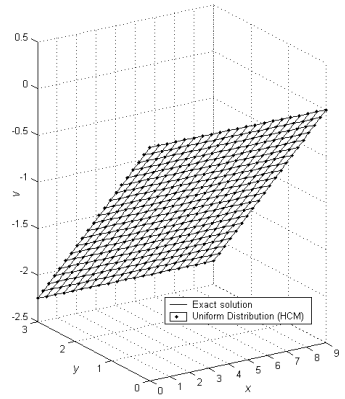

(c). *v*-displacement with uniform nodes.

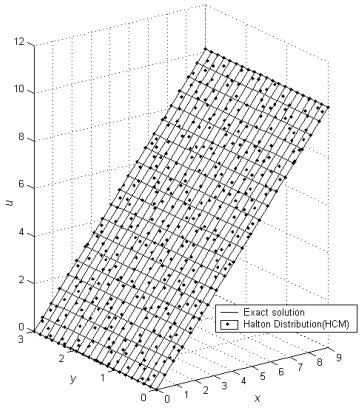

(d). *u*-displacement with quasi-random Halton distribution.

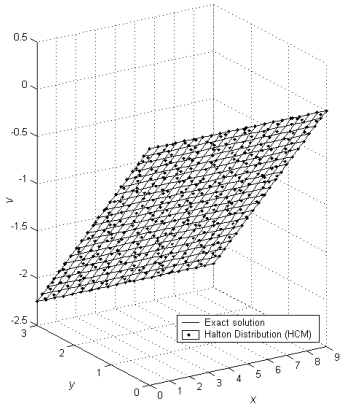

(e). *v*-displacement with quasi-random Halton distribution.

Figure 3.1 Patch test for elasticity.

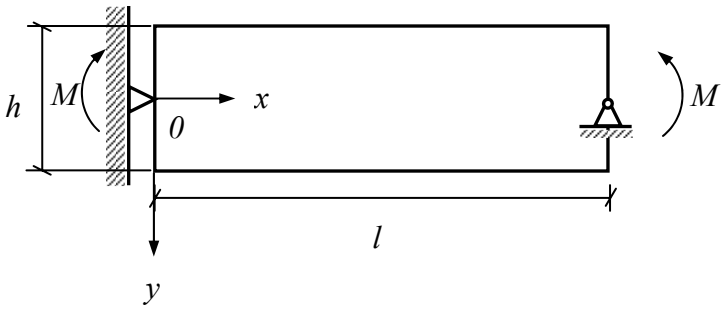

(a). Schematic of the 2D patch subjected to pure bending.

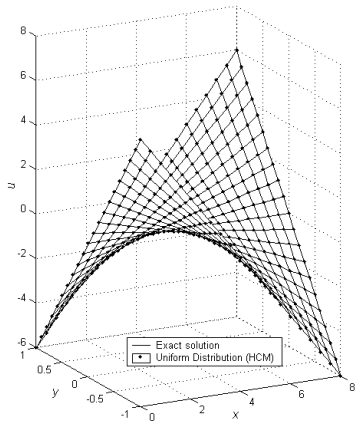

(b). *u*-displacement with uniform nodes.

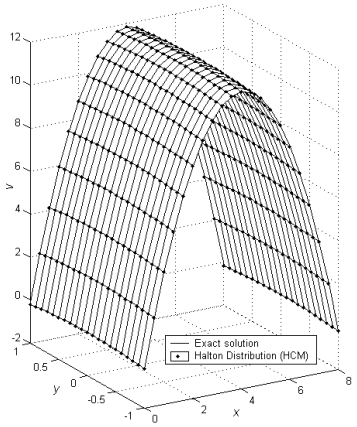

(c). *v*-displacement with uniform nodes.

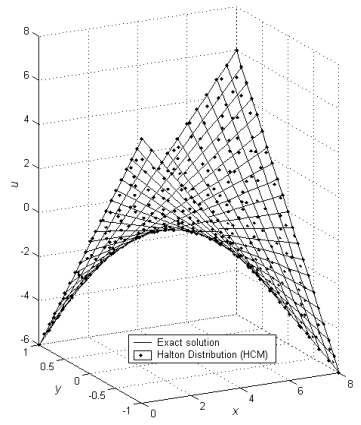

(d). *u*-displacement with quasi-random Halton distribution.

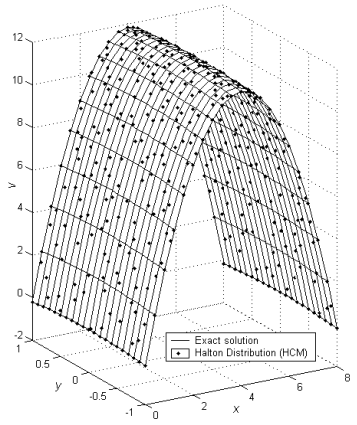

(e). *v*-displacement with quasi-random Halton distribution.

Figure 3.2 Plane stress patch subjected to pure bending.

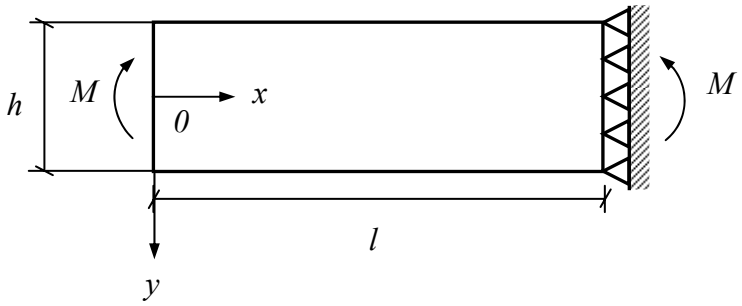

(a). Schematic of the 2D cantilever patch.

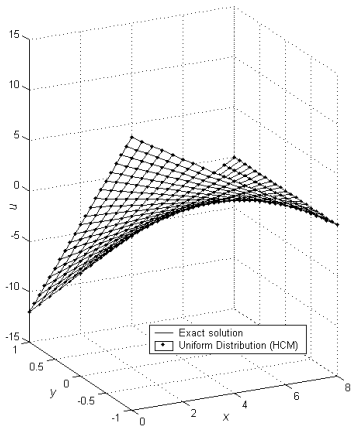

(b). *u*-displacement with uniform nodes.

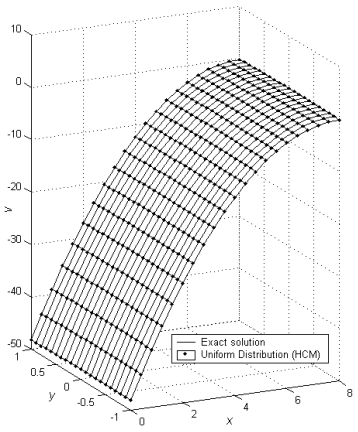

(c). *v*-displacement with uniform nodes.

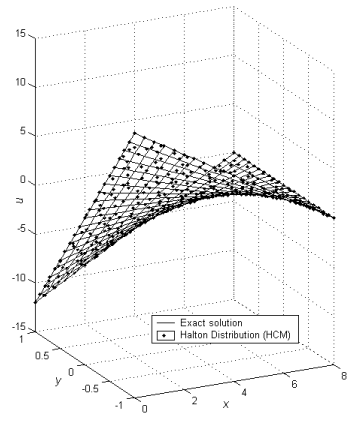

(d). *u*-displacement with quasi-random Halton distribution.

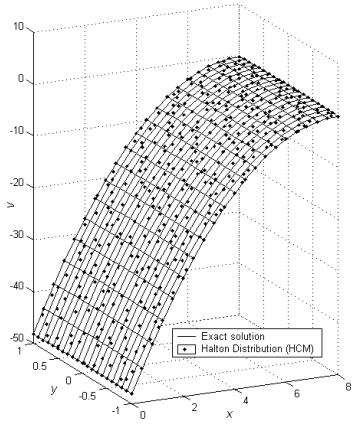

(e). *v*-displacement with quasi-random Halton distribution.

Figure 3.3 2D cantilever beam under pure bending.

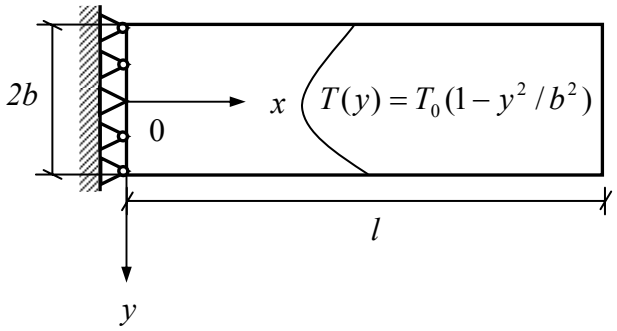

(a). Schematic of the 2D cantilever patch.

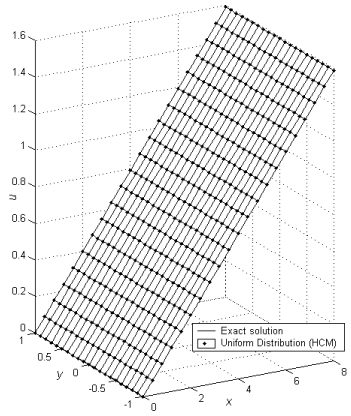

(b). *u*-displacement with uniform nodes.

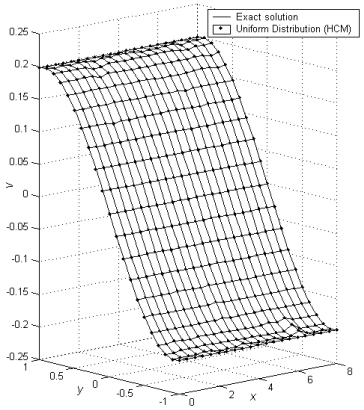

(c). *v*-displacement with uniform nodes.

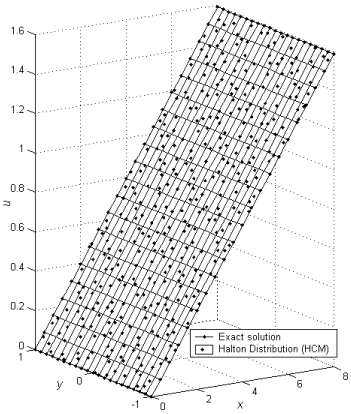

(d). *u*-displacement with quasi-random Halton distribution.

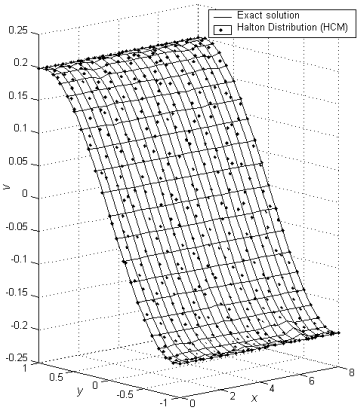

(e). *v*-displacement with quasi-random Halton distribution.

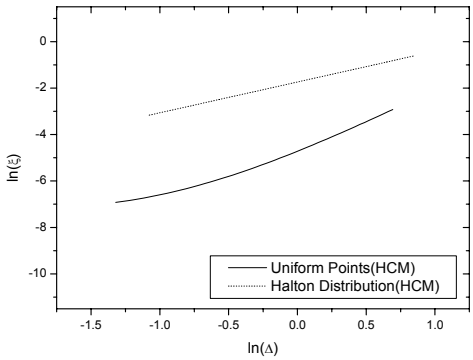

(f). Convergence characteristics for u.

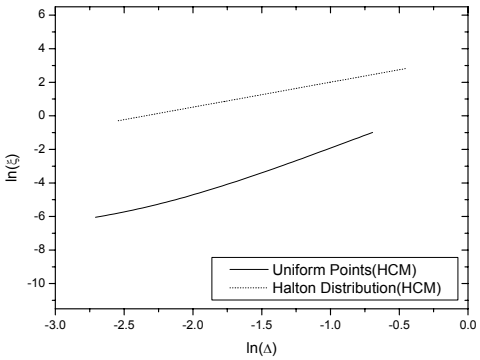

(g). Convergence characteristics for v.

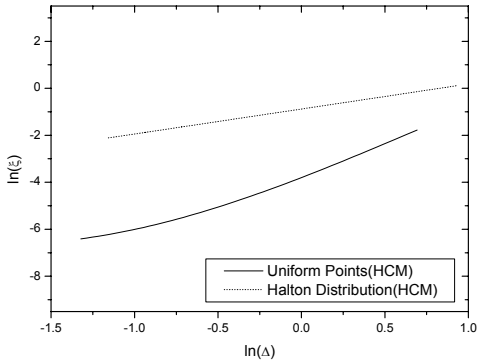

(h). Convergence characteristics for $u_{,x}$.

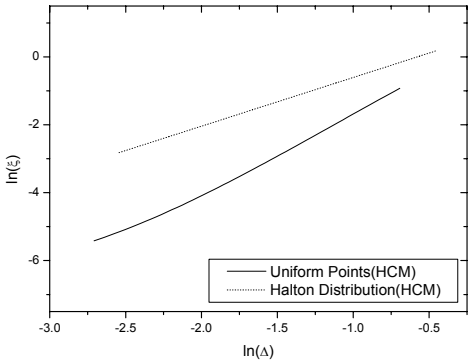

(i). Convergence characteristics for $v_{,y}$

Figure 3.4. Patch subjected to temperature field.

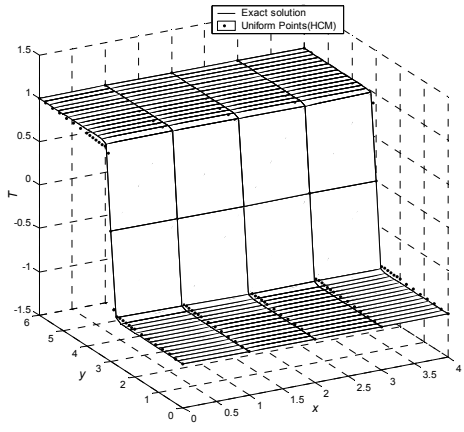

(a). Profile of T.

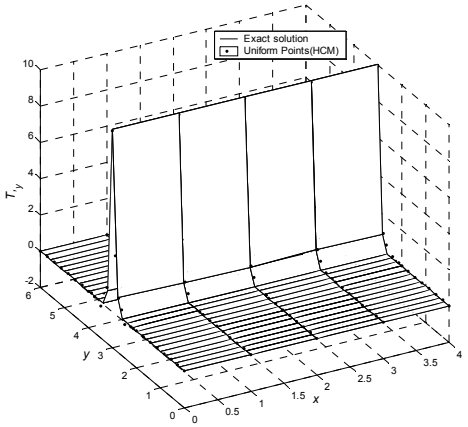

(b). Profile of $T_{,y}$.

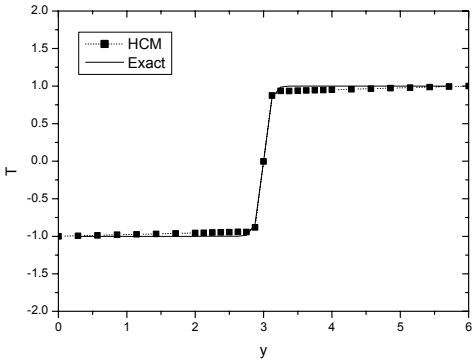

(c). Comparison of Hermite-Cloud results for T, with exact solution and

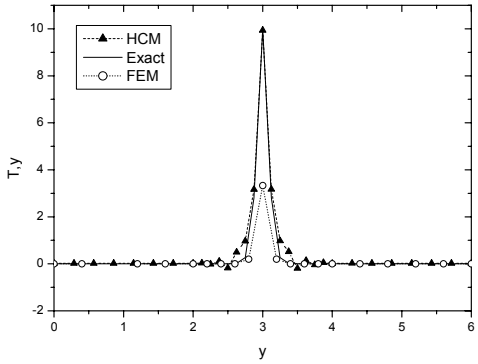

(d). Comparison of Hermite-Cloud results for $T_{,y}$, with exact solution and FEM.

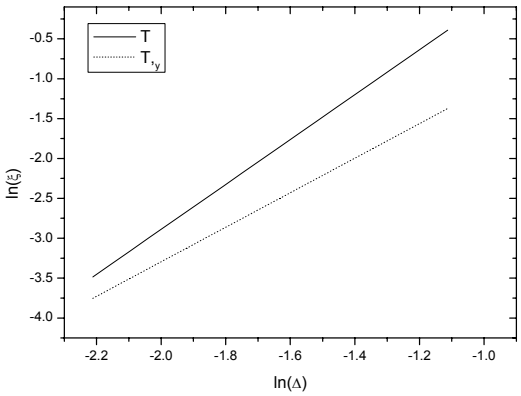

(e). Convergence characteristics for T and $T_{,y}$.

Figure 3.5. Heat conduction with localized high gradient temperature field.

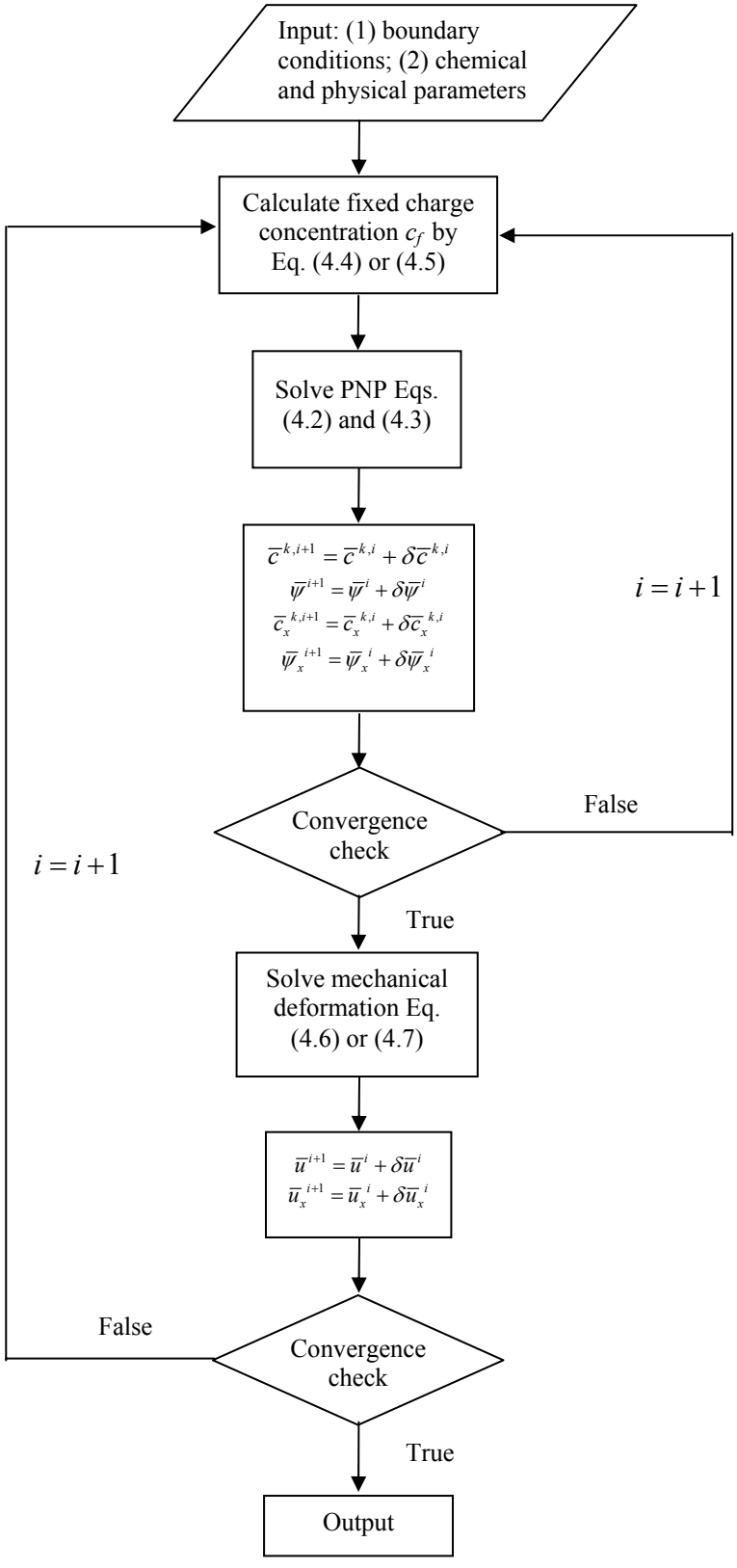

Figure 3.6 Flow chart of relaxation approach for self-consistent MECpH model.

CHAPTER 4

STEADY-STATE SIMULATIONS OF EQUILIBRIUM SWELLING OF pH-SENSITIVE HYDROGEL IN THE PRESENCE OF pH STIMULUS

4.1 OVERVIEW

As introduced in Chapter 1, pH-sensitive hydrogels are polymer networks containing pendent ionizable groups which are usually weak-acid or weak basic. Ionization occurs when the environment pH changes, and hence the pendent groups become charged. The operative of crosslinked, charged hydrogel is mainly pH-dependent. However, chemical nature of fixed charge groups, ionic strength and composition of the bathing solution and crosslinking density, for instance; also greatly affect the hydrogel swelling equilibria (Brondsted and Kopecek, 1992).

Due to their intrinsic swelling property, pH-sensitive hydrogel has been exploited in the development of chemomechanical system, which would convert chemical energy directly into mechanical work, e.g. chemical driven functional actuator and sensors (Osada and Gong, 1993; Beebe et al., 2000a, 2000b). pH-sensitive hydrogel has a significant advantage over conventional microfluidic actuators owing to their ability to undergo abrupt volume changes in response to the surrounding environment without the requirement of an external power source. In addition, the

hydrogel can performs all the sensing, actuating and regulating functions that normally performed by discrete components (valve, sensor, electronic) in a traditional system.

Currently, the medical and pharmaceutical applications of hydrogels have become one of the active fields of research. pH-sensitive hydrogels have been found to be appropriate carriers as swelling-controlled release devices. The ability to control the dynamics of swelling by changing the pH and ionic strength of the external medium provides various opportunities for pH-sensitive hydrogel. For example, the pH of fluid varies considerably along the length of the gastrointestinal tract (1-3 in the stomach and 5-8 in the small intestine), a weak-acidic hydrogel is candidate as an intelligent device to deliver drugs into the small intestines while avoiding release in stomach. Various drug delivery systems of pH-sensitive hydrogels have been reviewed by several researchers (Siegel, 1990; Lowman and Peppas, 1999; Peppas et al., 2000).

Optimizing the design of these systems demands great insight into the underlying mechanisms of the swelling equilibria of the prescribed hydrogels. In this chapter, the emphasis will be placed on the equilibrium swelling properties of pH-responsive hydrogel as functions of various factors that include: environment pH, physical properties of hydrogel, chemical nature of fixed charge groups, ionic strength and composition of swelling medium. Prior to the discussion of the simulation results, a brief historical development of pH-sensitive hydrogel will be presented. Some fine reviews of the experimental and theoretical works can be found in the book edited by Dusek (1993a, 1993b).

4.2 MODEL VALIDATION WITH EXPERIMENTAL RESULTS

The present one-dimensional steady-state simulation results are compared with the experimental data of Beebe and his groups (Beebe et al., 2000a; Johnson et al., 2002; De et al., 2002). In order to illustrate the single-dimensionality of the present problem, we provide here some insights into the experimental procedure. With reference to the experimental work by Beebe et al. (2000a), polymerizable mixture consisting of acrylic acid and 2-hydroxyethyl methacrylate (HEMA) with photoinitiator (3wt%) and ethylene glycol dimethacrylate (1wt%) as crosslinker, was allowed to fill up the microchannel where the experiment was carried out. The microchannel was covered at top and bottom with two pieces of glass. When the mixture reaches a quiescent state, it was then exposed to UV light through a photomask place on top of the channel. The channel was then flushed with water to remove the unpolymerized monomers mixture. The axisymmetric hydrogel in the microchannel is constrained from axial displacement by the cover glasses placed at the two ends. Thus it is reasonable to assume that the hydrogel undergoes displacement mainly in the radial direction. The cylindrical hydrogel, with a diameter of 400μm at dry-state, was placed in a bathing solution with ionic strength of 300mM. It was observed that the hydrogel swollen to a certain degree once submerged in a solution. The instantaneous swelling of the hydrogel is herein referred to as initial hydration state. The hydrogel was presumed to attain an equilibrium swelling state before it was subjected to step changes in the pH of the surrounding solution. The changes in hydrogel volume were observed and the diameters of cylindrical hydrogel structures were measured after reaching equilibrium within their respective pH environments (circular markers in Fig. 4.3). Based on the Hermite-Cloud meshless technique, the

MECpH model, the fully coupled multi-field chemo-electro-mechanical effects of nonlinear partial differential equations, is solved numerically to simulate the responses of the given pH-stimulus-responsive hydrogel. The simulation domain and its pertaining boundary conditions are prescribed in Fig. 4.1.

Simulations are carried out for both finite and linear deformation theory to analyze the magnitude of differences of the predicted results. From Fig. 4.2, the results predicted by both theories give almost identical results. As the swelling of the hydrogel becomes larger, for example the total ionizable fixed charge concentration increases, linear deformation theory predict a slightly greater degree of swelling than the finite deformation simulation.

The square markers in Fig. 4.3 indicate the simulation results obtained, and the solid line is to assist visualization. It is apparent that these results compare very well, both qualitatively and quantitatively, with the experimental data. It is thus concluded that the present MECpH model is accurate and robust to predict the responsive behavior of pH-sensitive hydrogel.

The changes of pH alter the ionization degree of fixed charge groups and the equilibrium state of swelling concurrently. The figure shows that the hydrogel volumes change abruptly in the range from pH 4 to pH 7. It is also distinguished that hydrogels remain almost unchanged from its initial hydrated state diameters in the lower pH solution, and start expanding at pH 4.

As the pH of the bathing solution increases, the ionization of the pendent poly(HEMA) carboxylic acid group on the backbone of the network will increases, where the acid-base equilibrium process is described as

$$RCOOH \rightleftharpoons RCOO^{-} + H^{+} \tag{4.1}$$

As a result, there is an increase in the surplus charge in the hydrogel. In order to maintain neutrality within the hydrogel, more mobile ions with the different sign as the fixed charge groups diffuse into the hydrogel. The concomitant increase in ionic concentration in the interior hydrogel generates greater osmotic pressure, which in turn causes the observable increase in swelling. As the ionization process of the carboxylic acid group approached its saturation stage at pH 7, further increasing of pH after pH 7 does not extend the degree of swelling. More detailed discussions will be presented with supports of the profiles of ionic concentration and electrical potential in succeeding section.

4.3 PARAMETRIC STUDIES OF HYDROGEL PROPERTIES AND ENVIRONMENTAL CONDITIONS

Simulations are worked out to predict the influences of the hydrogel properties and bath conditions on the profiles of ion concentrations and electrical potential distributions, as well as the mechanical displacements. Those chemical and physical parameters used in the simulations, as tabulated in Table 4.1, are obtained from the experimental works of Beebe's groups (Beebe *et al.*, 2000a, 2000b; Johnson *et al.*, 2002, 2004; Yu *et al.*, 2001; Zhao and Moore, 2001) or handbook (Lide, 2002). In this section, the tunable chemical and physical parameters of the hydrogel as well as surrounding environment are exploited.

As shown in Fig. 4.1, a pH-sensitive hydrogel with circular cross-section is immersed in a bath solution consisting of sodium chloride (NaCl) and hydrochloric acid (HCl), which is referred as ideal solution here. In order to investigate the effects

of different buffer contents on the swelling equilibrium of the pH-sensitive hydrogel, two buffer solution – the phosphate buffer and Britton-Robinson buffer are considered.

The advantages of using pH buffers in these experiments are to help stabilization of both the pH and swelling response rate, where the buffer will resists the change in solution pH when small amounts of acid or base are added. In general, a buffer solution is a mixture of weak acid or weak base and its corresponding salt.

For investigations of the effects of buffer content and hydrogel properties on the swelling equilibrium, the cylindrical hydrogels are placed into two systems of the buffered solutions, namely the phosphate buffer and Britton Robinson buffer (Townshend, 1995). The phosphate buffer is prepared with specified ionic strength by controlling NaCl, and the pH of the solution can be regulated by adding certain amount of NaH_2PO_4, Na_2HPO_4, HCl or NaOH. The Britton-Robinson buffer solution is prepared by mixing specified amount of strong base NaOH with the solution containing weak acid CH_3COOH, H_3PO_4 and H_3BO_3 in a proportional amount until a desired pH value is attained. In general, the ionic strength and valence numbers of the ionic species are the two main factors that discern the difference between the phosphate and Briton-Robinson buffers. These effects have clearly been reflected in the PNP equations (2.95) and (2.96) of the present model.

As discussed in Section 2.3.4, the problem domain can be considered as axisymmetry, hence the domain can be reduced to a one-dimensional description, i.e. the swelling will take place along the radial direction of the cylindrical hydrogel, as shown in Fig. 4.1. At the state before swelling, the dry hydrogel has the diameter of $400\mu m$. In general, the diameter of the dry gel is based on the diameter of the circular photomask. However, it is an inevitable consequence that the hydrogel dimensions vary from the size of the photomask after the channel is flushed to remove the

unpolymerized monomers. Light scattering and reflections have been identified by Beebe et al. (2000b) as the possible reasons behind the shift in the hydrogel dimension. Therefore, a boundary-effect domain is defined to describe the hydrogel-solution interface. The length scale of the interface is about 1/20 of the total length of the domain. For example, at the state before swelling, $x(\mu\text{m}) \in [0,200]$ is the interior dry gel domain and $x(\mu\text{m}) \in [300,2000]$ the solution domain. The hydrogel-solution interface, $x(\mu\text{m}) \in [200,300]$, is referred to as the boundary-effect domain. A hyperbolic tangent profile is used to describe the distribution of the fixed-charge concentration ranging from c_f within the hydrogel to zero in the bathing solution. The fixed charge concentration inside the hydrogel is calculated from Equation (2.68) with the values c_{m0}^s and K taken as 1800mM and $10^{-2.0}$ mM, respectively. Based on experimental data obtained by Beebe's research group (Johnson et al., 2002), we note that the Young's modulus of the hydrogel varies with the pH value. In similar manner as the fixed charge concentration, a hyperbolic tangent profile is used to describe the variation of Young's modulus as function of pH solution. This profile consists of three main segments, namely constant Young's modulus values of 0.29MPa when pH<5.5 and 0.21MPa when pH>7.5. In the third segment for 5.5<pH<7.5, the Young's modulus values is assumed to vary linearly from 0.29MPa to 0.21MPa.

Despite the complexity of the swelling behavior of hydrogel at various level of pH environment, much insight can be obtained by independently considering the effects of various hydrogel properties and the chemical conditions of the bath solution. The coupled nonlinear equations of (2.95) to (2.100) are solved numerically with appropriate parameters to understand the underlying mechanism contributed to the swelling characteristic in hydrogels, in order to develop a more predictive model.

4.3.1 Influences of the Ionizable Group Concentration of Hydrogel

In Figs. 4.4, 4.5 and 4.6, the profiles of ionic concentration, electric potential and mechanical displacement are analyzed as function of ionizable fixed charge concentration of hydrogel.

Figures 4.4(a), 4.4(b) and 4.4(c) respectively show the predicted ionic concentration distribution patterns of the hydrogen (H^+), sodium (Na^+) and chlorine (Cl^-) ions, when the hydrogel is submerged in an acidic pH solution of 3.0. The results obtained are intuitively correct in the sense that the PHEMA gel is an acidic hydrogel. The H^+ ion and Na^+ ion distributions are high inside the hydrogel, but decrease in the bath solution; while the inverse of the characteristic is true for the Cl^- ion. the concentration of the H^+ ions is much lower than those of Na^+ and Cl^-. The electroneutrality is conserved at every point in the bath solution which can be proved straightforward from the summation of the concentration profiles of in Fig 4.4. In the interior of the hydrogel, there is a difference between the concentrations of the Na^+ and Cl^- ions, with the Na^+ ions having a higher concentration. This concentration difference between the sodium ions and chlorine ions corresponds closely to the fixed charge concentration shown in Fig. 4.4(d). Figure 4.4(e) illustrates the electric potential distribution. A net difference of drift force between the various ionic concentrations in the hydrogel interior results in a constant electric potential within the hydrogel but it is usually very small (in millivolts). In the bath solution, however, the electric potential distribution is zero since there is electroneutrality in the net total concentration of the various ionic species. Figure 4.4(f) delineates the mechanical displacement in the radial direction of the cylindrical hydrogel. From the profiles, it is obvious that the degree of swelling in hydrogel, from large to small, follows the

sequence of $c_{m0}^{s} = 2400\text{mM}$, $c_{m0}^{s} = 1800\text{mM}$ and $c_{m0}^{s} = 1200\text{mM}$. Inductively, the MECpH model predicts that PHEMA based hydrogels with greater amount of initial fixed charge group will exhibit greater swelling, even though the swelling is very small in acidic solution of Figure 4.4 as compared with basic solution of Figure 4.6.

Figures 4.5 and 4.6 show the profiles of ionic concentrations, electric potential and mechanical displacement of the hydrogel with an initial diameter of 400μm in response to immersion in an neutral solution and alkaline solution of pH 12 respectively, for fixed charge groups at varying initial concentration. It is obvious that the hydrogel exhibits similar characteristic behavior as that of the corresponding acidic bathing solution in Figure 4.4. However, there are quantitative dissimilarities in the degree of swelling between hydrogels when immersed in acidic and alkaline solutions. The PHEMA-based hydrogels do not show significant degree of swelling in acidic solution, while in alkaline solution they expand enormously and frequently reaching more than twice the size of their dry state diameter. On top of that, the differences in degrees of swelling are also obvious between hydrogels with varied initial fixed charge concentration.

The pendent fixed charge groups on the backbone of the network PHEMA, i.e. carboxyl group, will exist in the form of —COO^{-} in basic solution and in the form of —COOH in acidic medium which is summarized as in Equation (4.1).The dissociation constant *K* determines the ionization of the pendent fixed charge groups just like acidic or basic groups of monobasics or monobases. If the concentration of the hydrogen ion H^{+} is lower than the dissociation constant *K*, the carboxyl groups try to release more protons. In order to maintain the electroneutrality, more mobile counter ions (Na^{+} for the present case) will diffuse into the interior hydrogel to compensate the surplus charge. In contrast, the mobile anions will be repulsed from entering the

interior hydrogel. From the interpretation of the profiles of the ionic concentration in the interior hydrogel, it is evident that the concentration of the Na^+ ion is higher whereas that of Cl^- ion is lower for alkaline solution as compared with the acidic solution. As a consequence, the concentration differences between the interior and exterior hydrogel increase tremendously, leading to higher osmotic pressures which effectively create higher degrees of swelling.

Figures 4.7(a) and 4.7(b) show the theoretically predicted dependence of the hydrogel swelling response to the changes of initial fixed charge concentration for an ideal solution. It is clearly observed that a change in fixed charge concentration at dry-state c_{m0}^s strongly affects the swelling equilibrium of the hydrogels at high pH values, whereby a decrease in the c_{m0}^s will dramatically decrease the degree of swelling at high pH values. The concentration of fixed charge at initial stage c_{m0}^s is a function of molar ratios of the comonomers during preparation (Chu et al., 1995). As the molar ratio of carboxylic acid to 2-hydroxyethyl methacrylate decreases, the initial fixed charge density decrease dramatically. The concentration difference thus decreases between the interior hydrogel and exterior solution decreases as a result, which in turn mitigates the osmotic pressure and generates smaller degree of hydrogel swelling. These observations are in accordance to the trend attained in the reported experimental results by Siegel (1990). Figure 4.7(b) nicely characterizes these experimentally observed phenomena where a monotonic swelling is predicted with the increasing of total molar concentration of ionizable groups per volume of solid polymer.

Figure 4.8 shows the relationship between the swelling equilibrium of the hydrogels and the concentration of fixed charge group c_{m0}^s for three different buffer solutions: ideal solution, phosphate buffer and Briton-Robinson buffer. A larger c_{m0}^s

induces greater degree of hydrogel swelling for both the buffer solutions at a higher pH. At low pH level, the swelling degree is almost constant for both the buffer systems. The figure also evidently shows that the achievable swelling equilibrium achievable in the Britton-Robinson system is always higher than that in the ideal solution and phosphate buffer, especially as the initial concentration of fixed charge group c_{m0}^{s} increases higher. The swelling degree of hydrogels bathed with whether ideal solution (only NaCl and HCl are present in solution) or phosphate buffer is almost the same. However, the phosphate buffer shows sign of greater swelling degree as the initial concentration of fixed charge group c_{m0}^{s} increases.

4.3.2 Influences of the Young's Modulus of Hydrogel

Figures 4.9 to 4.11 show the distributions of ionic concentration, electric potential and mechanical displacement as function of normalized Young's modulus value of hydrogel. An ideal bathing solution which consists of NaCl and HCl electrolyte is considered.

The ionic concentration and electric potential profiles show the similar characteristic at large as in Figs. 4.4 to 4.6 for environments of acidic solution (pH3), neutral solution (pH 7) and basic solution (pH12). The cation concentrations (H^+ and Na^+) in the hydrogel are higher than that in bath solution. In contrast, the anion concentration in interior hydrogel is at a lower level than the external solution. Electroneutrality is conserved at every point.

At least, the dissimilarity in swelling response in lower pH and higher pH can tell apart the two different conditions. As discerned from Fig. 4.9, the changes in

Young's modulus values of hydrogel seem to have trivia effects on the swelling degree at low pH. As the hydrogel is still in it compact state at low pH, changes in Young's modulus will not have much impact on it swelling equilibrium. By contrast, the swelling degree is profoundly controlled by changing the Young's modulus if the pH level is high, as noted from Figs. 4.10 and 4.11. These discrete behaviors happen owning to the fact that more fixed charge groups are ionized as the pH increases and so as the swelling magnitude. However, the swelling will soon be constrained from expanding from expanding as the Young's modulus increases. The resistance between expanding and retracting forces will last till a new equilibrium is reached.

Figure 4.12(a) illustrates the dependence of hydrogel swelling on the changes of environment pH as function of the Young's modulus of the hydrogels. The theoretical model predicts that for hydrogels with higher values of Young's modulus, the degree of swelling will decrease at higher pH solution. This characteristic becomes more visible in Fig. 4.12(b) when the normalized Young's modulus is plotted against the diameters of hydrogels at equilibrium state. The swelling magnitude reduces exponentially with the increase of Young's modulus. Usually it is known that the Young's modulus of the hydrogel is strongly dependent on the preparation process, where the modulus is primarily determined by the volume per molar ratio of copolymer mixture which directly quantify the number density of entanglement strands or crosslinking ratio. As the crosslinking content in the polymer network increases, the hydrogel has a higher retraction force and thus creates higher Young's modulus. The phenomenon exists without regards to buffer contents as depicted in Fig. 4.13. The diameters of the swollen hydrogels are plotted against the normalized Young's modulus for both buffer solutions of pH 3 and pH 9. The increases of Young's modulus reduce exponentially the hydrogel swelling for the three different buffer

system as interpreted from the Fig 4.13. Influence of buffer contents on the swelling equilibrium at higher pH is more significant than that at lower pH. When the pH of buffer solutions is low, the degree of hydrogel swelling is almost insignificant as function of the buffer system and Young's modulus. If the pH is high, large differences in swelling degree are observed for different buffer systems. Further, the Britton-Robinson is the unchanging leader in providing the best buffer solution when high swelling scale is needed. It is also noteworthy to point out that the influences of the buffer contents will fade out when the Young's modulus is high enough to diminish the odds.

4.3.3 Influences of the Initial Diameter of Hydrogel

Figures 4.14, 4.15 and 4.16 show the ionic concentration and electric potential profiles, and the mechanical displacement as function of the diameter of the hydrogel at the state before immersion in certain solution. The bathing electrolyte is an electrolyte solution which consists of NaCl and HCl.

For the three different pH buffered conditions of pH3, pH7 and pH12, the concentration of cations are higher inside the hydrogel, whereas the anion densities are lower in comparison with that in the external solution. These are the expected behavior, in view of the negative sign of the ionized charge groups dangling on the network matrix of PHEMA gel. Likewise, electric potential exists as long there are migrations of ions between the exterior and interior of the hydrogel.

Since the initial fixed charge concentration and initial hydration are kept constant against different initial diameters of hydrogel for the simulation of Figs. 4.16

and 4.17, the hydrogels show indistinguishable swelling when they are soaked in electrolyte solution. These characteristics are most clearly depicted in Fig. 4.17 where the hydrations of the swollen hydrogels are plotted against the pH levels and dry gel diameters. As discussed in Section 4.2, the dry gel diameters are determined by the nominal photomask diameters and the hydration is calculated as $H = V^f / V^s$.

In order to study the responsive characteristics of hydrogel bathed in different systems of buffer solutions, several simulations are carried out to model the hydrogels dilation upon soaking in phosphate buffer and Britton-Robinson buffer solutions. Figure 4.18 reveals the comparison of swelling degree of the hydrated hydrogel for the three different buffer solutions at pH level of pH3 and pH9. The figure reinstates the notable independency of swelling magnitudes on the initial diameter of the hydrogel. In parallel to the two case studies in Sections 4.3.1 and 4.3.2, the Britton-Robinson buffer also demonstrates it potentiality in providing the buffer environment solution for voluminous swelling needs.

4.3.4 Influences of the Ionic Strength of Bath Solution

Figures 4.19, 4.20 and 4.21 are plotted to study the characteristics of diffusive ionic species and electrical potential, as well as mechanical deformation of the pH-responsive hydrogel as function of ionic strength conditioning

Since we know that osmotic pressure arises from concentration difference between the interior hydrogel and external solution, the extent of equilibrium swelling can be approximated from examination of the concentration ratio between the interior and exterior of the hydrogel, which is coherent with the definition of Donnan

equilibrium (Flory, 1962; Helfferich, 1962). The osmotic pressure is usually regarded as outward pressure in excess of the surrounding solution pressure that would result in expanding of the hydrogel network. In order to discuss the problems of various bath solution concentrations, it is notationally convenient to introduce the density ratio or better known as Donnan ratio λ_D (Ricka and Tanaka, 1984; Siegel, 1990; Homma et al., 2000),

$$\lambda_D = \left(\frac{c_k}{\overline{c}_k} \right)^{1/z_k} \tag{4.2}$$

where c_k and $\overline{c}_k$ are the concentrations in the hydrogel and external solution of *k*th specie diffusive ion respectively. As the concentrations in the external solutions are maintained at the same density at every point in equilibrium sate, $\overline{c}_k$ will take the boundary values of corresponding ionic species.

The Donnan ratio distributions of the concentration of diffusive Na^+ and Cl^- ions are disclosed in Fig. 4.19. It is evident that the mobile cations, namely hydrogen (H^+) and sodium (Na^+) ions, have higher densities in the interior hydrogel than those in the exterior solution; while the mobile anions, i.e. chloride (Cl^-) ion, show a contrary pattern. However, the requirement of electroneutrality condition is always met in the domains of solution.

As the ionic strength increases, the density ratio of the ions between the interior of the hydrogel and the exterior bath solution decreases (Siegel, 1990). On that account, the osmotic pressure subsides consequently and reduction in hydration is expected. The fixed charge concentration is a function of hydration of the swollen hydrogel, as well as the total ionizable groups per volume of solid polymer and concentration of H^+ ion provided by the outer solution as discussed in Chapter 2. Since increases of ionic strength is controlled by NaCl, the total concentration of H^+ ion and ionizable groups

remain constants. Therefore, it is foreseeable that the redistribution of the fixed charge concentration is now a single function of hydration. Due to the changes in the concentration of fixed charge groups, there will be a concomitant changes in the concentration profiles of the diffusive cations as well as anions. The interaction continues until a new equilibrium state is achieved. These behaviors become more obvious in higher pH solution as noticed from Figs. 4.20 and 4.21.

Figures 4.22(a) and 4.22(b) depict the effects of bath ionic strength on the theoretical equilibrium swelling response of HEMA hydrogels with identical total fixed charge groups and Young's modulus. As predicted, the hydrogel behaves like a hydrophobic polymer at low pH. After pH of 4, fluid content within the hydrogel abruptly increases and results in highly swollen hydrogel. Apart from that, the highest curve is that for a 300mM ionic strength solution while subsequently lower curves represent bath solutions with higher ionic strength, increasing progressively from 300 to 1200mM. At very low ionic strengths, the hydrogen ions play an essential role in the association/dissociation process. Hence, the contribution of the other mobile ion species to the osmotic pressure is minimized. However, as the ionic strength increases, the degree of swelling decreases for high ambient pH. This observation is in accordance to that observed in the experimental results of Siegel and his groups (1988, 1990, 1991).

Figure 4.23 focuses on the dependence of equilibrium swelling on ionic strength of certain buffer systems. Two distinct solutions, namely NaCl/HCl solution and phosphate buffer with a calculated amount of NaCl added to adjust the ionic strength to a desirable level, are compared. The swollen hydrogels show characteristic exponential decrease in degree of swelling as the ionic strength increases for both bathing solution. These behaviors are comparable with the works of Brannon-Peppas

and Peppas (1991a). Both solutions show ineffectual difference in size of swelling. In all likelihood, both solutions do not show enormous difference as the dominant counter ion is essentially the univalent ions which are mainly sodium ion (Siegel et al., 1991). In order to investigate further the effectiveness of multivalent ions in influencing the equilibrium swelling, multivalent ions polyelectrolyte solution will be considered in following section.

4.3.5 Influences of the Ionic Compositions of Bath Solution

The influences of bath compositions on the pH-dependent equilibrium swelling character are shown in Figs. 4.24 to 4.28, which are maintained at 25°C and 300mM of ionic strength. In order to illustrate the characteristic swelling, the bathing solution is assumed to be primarily consists of symmetrical salt (z:z) with varying ionic valencies, i.e. $M^{+1}N^{-1}$, $M^{+2}N^{-2}$ and $M^{+3}N^{-3}$.

Figures 4.24 to 4.26 delineate the profiles of ions (mobile and fixed charges) and electric potential with corresponding mechanical displacement predicted at steady-state. The concentrations of sodium and chloride ions are described in term of Donnan ratio for the sake of apprehensible comparison of osmotic pressure. Once the concentration profiles of the ions are determined, Donnan ratio becomes an elegant tool for estimating quantitatively the swelling of hydrogel when comparing the influence of bath composition of different ion valencies and different ionic densities. Discrepancies in the profiles as well as degree of swelling are not obvious for acidic solution as revealed in Fig. 4.24. However, they still show a trend similar to that of neutral and base solutions as in Figs. 4.25 and 4.26, specifically, concentration of

mobile ions in the hydrogel (or Donnan ratio) peak out as ionic valencies increase, and consequently the equilibrium swelling reduces as predicted. The distribution of fixed charge concentration in Fig. 4.24(d) seems to be the same for all conditions, but in actual case the concentrations are disparate in value from each others, namely, 26.41631 mM ($M^{+3}N^{-3}$), 26.39451 mM ($M^{+2}N^{-2}$) and 26.38594 mM ($M^{+1}N^{-1}$). Therefore, the ionized groups dangling on the hydrogel network tend to elevate as the ionic valencies of the solution increase due to scaling down of equilibrium swelling.

Figures 4.27(a) and 4.27(b) focus on the effects of the ionic valencies on the equilibrium swelling response of an acidic hydrogel at certain pH values. It is observed that the solvent composition strongly influences the swelling behavior. This was documented earlier in few experimental works (Siegel and Firestone, 1988; Siegel, 1990) in which as the salt (solvent) valence of the solution increases, the ion osmotic effect is expected to decrease significantly, since fewer amount of counterions diffused into hydrogel to neutralize the charged groups. These are all consistent with character observed in Figs. 4.27(a) and 4.27(b), where it is clearly noted that the response for the case of highest ionic valency results in the lowest hydrogel deformations. The effects of multivalent salt solution gradually fade out as the ionic concentration increases.

Lets take a step further to explore an asymmetrical salt (Na_2SO_4) solution and compared it with a symmetrical salt (NaCl and Ca_2SO_4) solution as demonstrated in Figure 4.28 for both acidic medium (pH3) and basic medium (pH9). The degree of changes in equilibrium swelling of hydrogel in Na_2SO_4 solution is higher than those in NaCl for base environment even though the counterion species is identical. This can be explained from the difference in sodium ion (counterion) concentration in bathing solution for both cases. To maintain the electroneutrality and ionic strength, sodium ion concentration in Na_2SO_4 electrolyte solution is at a lower level. As a result, the

pressure gradient between the interior and exterior hydrogel tend to increase, leading to higher amount of swelling. In contrary, solution with Ca_2SO_4 shows the lowest degree of swelling. Since fewer divalent than monovalent counterions are required to neutralize the amount of carboxylic acid groups, these create a relatively low concentration gradient and thence the swelling equilibrium.

On the other hand, the differences in swelling degree are insignificant until the ionic strength decrease below 0.6 M as visible in the results of Fig. 4.28(a). Therefore, ionic valencies still play some part in swelling mechanism but on a secondary role as compare to pH condition and ionic strength of the bathing solution (Siegel and Firestone, 1988). The extent of swelling increases exponentially with the decrease of ionic strength regardless of the bath contents at high pH. However, the asymmetrical electrolyte solution shows some symptoms of inclination in swelling at low ionic strength with high pH.

4.4 DISCUSSIONS AND CONCLUSIONS

There are few schools of thoughts on the swelling/deswelling mechanism of the crosslinked, charged hydrogel. They have explained the drastic volume changes in response to changes in the external conditions from the point of views of interaction between water molecule and ion, screening or electrostatic repulsion between ion spheres, short-range hydrophobic interactions (Dobrynin et al., 1996), affinity of polymer network (Flory, 1962) and so on.

We believe that hydrogels, like ionic exchanger found in native charged membranes, contain substantial ionizable groups capable of dissociating and

subsequently attaining net charge in varieties of solvent mediums. These groups are capable of ionizing as a function of electrolyte pH and ionic strength and thereby leaving a net positive or negative charge fixed to the molecule.

The pendent fixed charge on the backbone of the network, i.e. carboxylic group, exists in the form of $RCOO^-$ in basic solution and in the form of RCOOH in acid medium as summarized in Equations (4.1). When the pH of the swelling medium is higher than the pK_a of the weak-acid group bound to the hydrogel network, the chemical reaction will proceed to the forward direction. As a result, the hydrogel will obtain greater fixed charge density. In order to maintain the electroneutrality within the hydrogel, more mobile counter ions (Na^+ if sodium chloride electrolyte solution is added to adjust the ionic strength) will diffuse into the interior of hydrogel to compensate the surplus charge. In vice versa, the mobile ions with charge of the same sign as the fixed charge groups will be repulsed from entering the interior hydrogel. However, besides those compensating counter ions, there are also absorbed counter ions which are accompanied by equivalent amount of co-ions (Helfferich, 1962). From the interpretation of the profiles of the ionic concentration in the interior hydrogel, it is evident that the concentrations of the Na^+ ion is higher whereas Cl^- ion is lower for alkaline solution as compared with acidic solution.

The uptake or sorption of mobile ions that take place upon immersion, will essentially redistribute the mobile ions between two liquid phases, i.e. the interstitial liquid phase of hydrogel and the bathing solution till an equilibrium is attained. As a consequence, the concentration differences between the interior and exterior hydrogel increase tremendously, leading to higher osmotic pressures which create higher degrees of swelling. In the meantime, the elastic retractive force of the polymer

network will react to the ever expanding network. The whole process will carry on back and forth until an equilibrium state is attained.

From the predicted data, it is apparent that swelling behavior of HEMA based hydrogel can roughly be separated into 3 stages: (1) swelling is insignificant (compact and hydrophobic) at pH values lower than 4 regardless of monomer composition, (2) ionization actively takes place within the pH range of 4 and 7 where fluid contents abruptly increase giving rise to highly swollen hydrogel, and (3) binding site of charge group are saturated in environmental pH higher than pH7 and the hydrogel will not expand further even the surrounding pH keep increases.

There are also secondary parameters influencing the expansion and contraction of charged crosslinked hydrogels. In addition to its pH-sensitivity, swelling and deswelling are also dependent on physical and chemical properties of hydrogel as well as the ionic strength and composition of swelling medium. These observations are all consistent with experimental data reported in open literature.

A similar phenomenon is shown for the response characteristics of main ions and electrical potential when the hydrogel is exposed to phosphate and Britton-Robinson buffer systems as compared to HCl/NaCl solution. From quantitative point of view, swelling is almost the same between phosphate buffer and HCl/NaCl solution when all else is held constant. In another study, the equilibrium swelling for samples swollen in Britton-Robinson is predicted to be always relatively larger than those bathed in phosphate buffer system and HCl/NaCl solution. Probably one of the main reasons is that the Britton-Robinson buffer system has lower ionic strength than those of phosphate buffer system and HCl/NaCl solution. However, the identity of buffer ions might also play a detachable role.

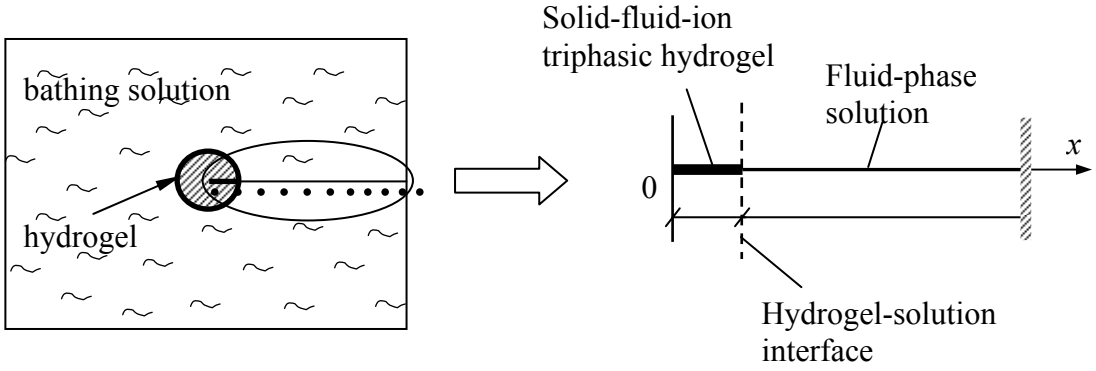

COMPUTATIONAL DOMAIN

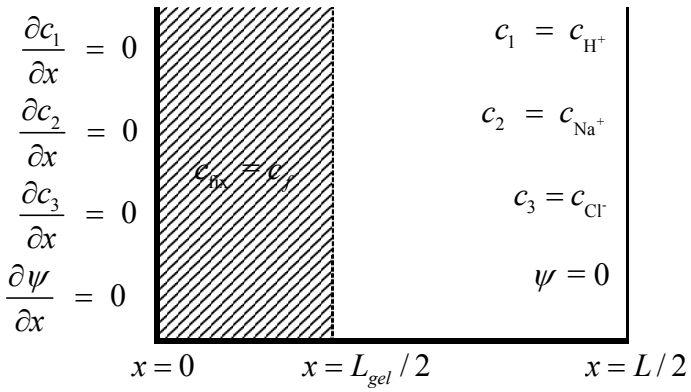

BOUNDARY CONDITIONS

Figure. 4.1 Computational domain and boundaries conditions for the numerical simulations. The shaded areas are the pH-responsive hydrogel.

Table 4.1 Essential chemical and physical parameters used as input data for implementation of the numerical simulations.

K	$10^{-2.0}$ mM
ν	0.45
ε	80
ε_0	8.8542×10^{-12} C^2/Nm^2
F	9.6487×10^4 C/mol
T	298 K
R	8.314 J/mol.K

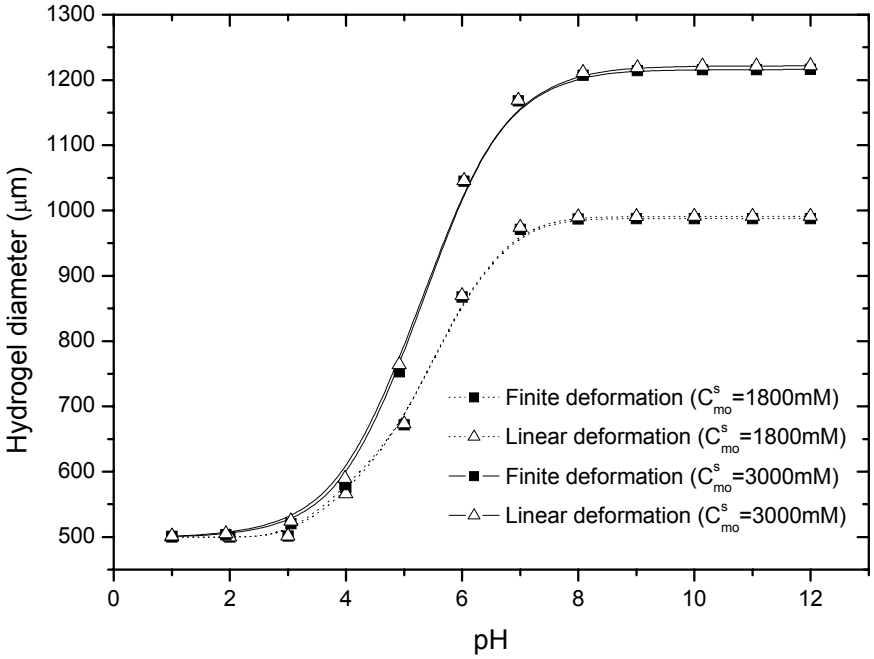

Figure 4.2 Comparison of finite and linear deformation theories.

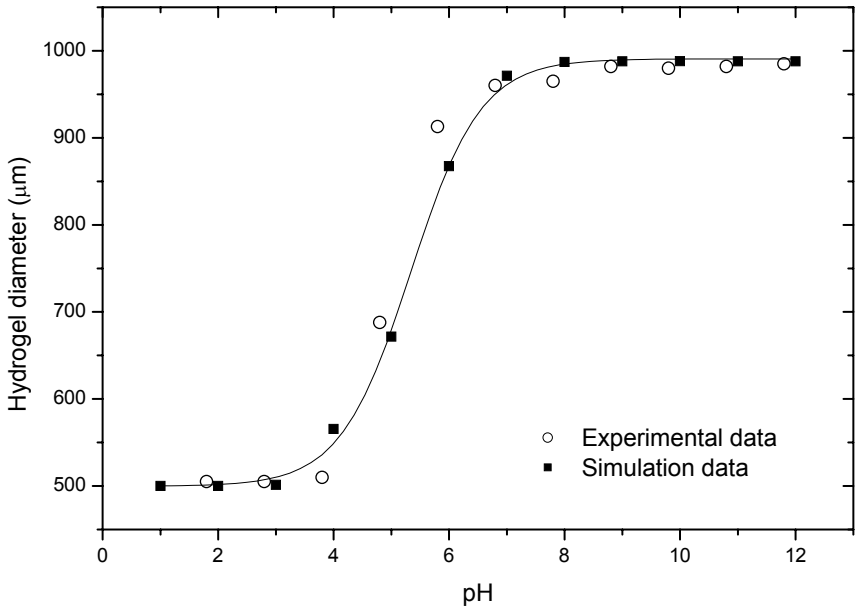

Figure 4.3 Comparison between experimental and numerical results predicted by MECpH model for the equilibrium swelling of PHEMA based hydrogels as a function of pH.

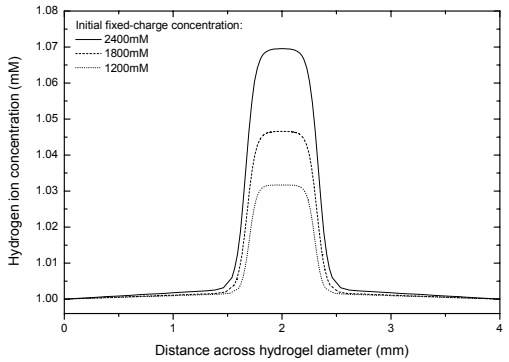

(a) Hydrogen ion (c_{H^+})

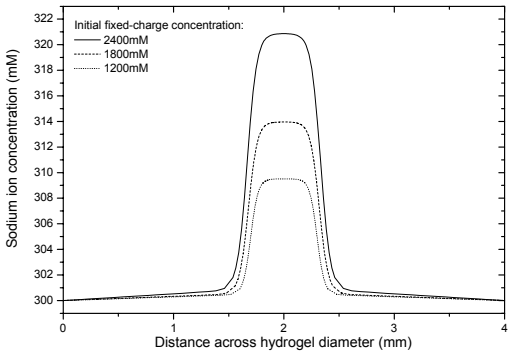

(b) Sodium ion (c_{Na^+})

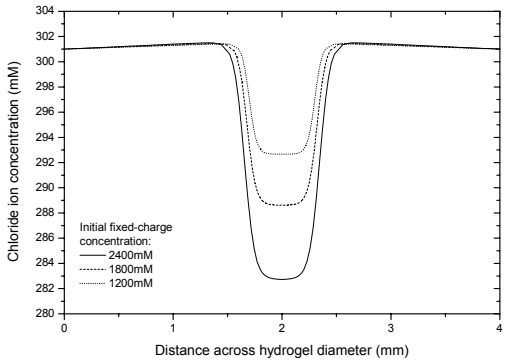

(c) Chloride ion (c_{Cl^-})

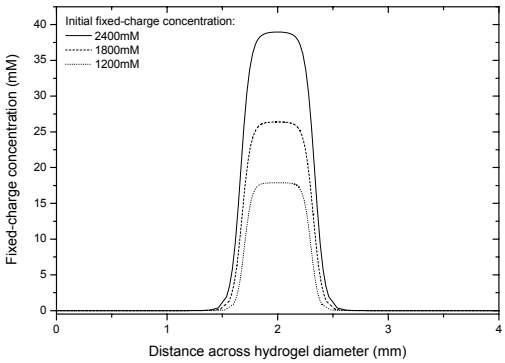

(d) Fixed charge group (c_f)

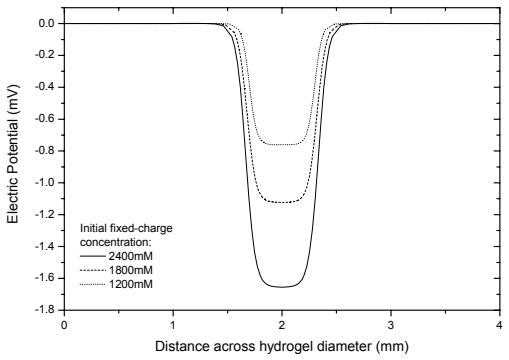

(e) Electric potential (ψ)

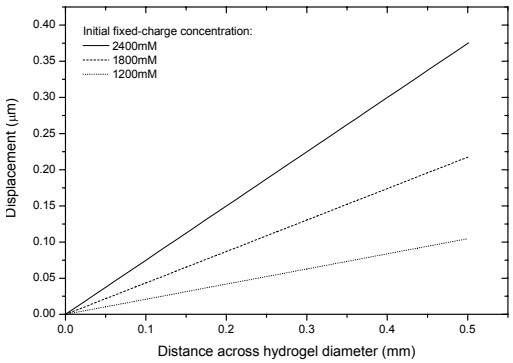

(f) Displacement (u)

Figure 4.4 Profiles of $c_{H^+}, c_{Na^+}, c_{Cl^-}, c_f, \psi$, and u as a function of ionizable fixed charge concentration c_{mo}^s. The PHEMA based hydrogel is equilibrated in an acidic medium of pH3 with NaCl added to control the ionic strength.

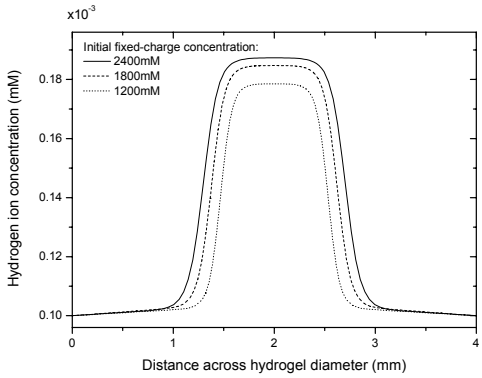

(a) Hydrogen ion (c_{H^+})

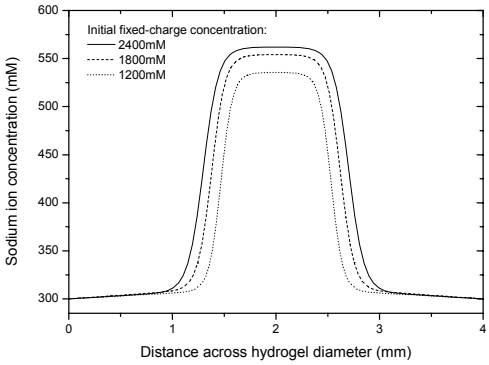

(b) Sodium ion (c_{Na^+})

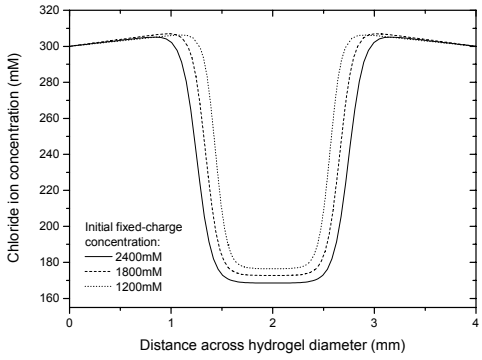

(c) Chloride ion (c_{Cl^-})

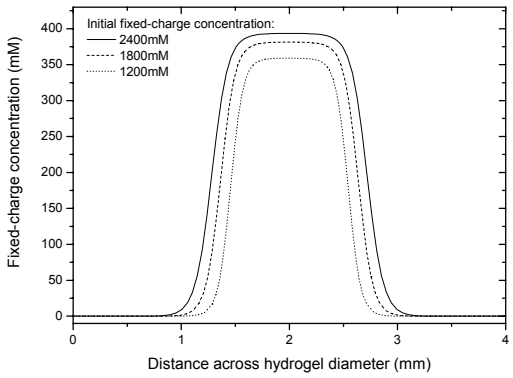

(d) Fixed charge group (c_f)

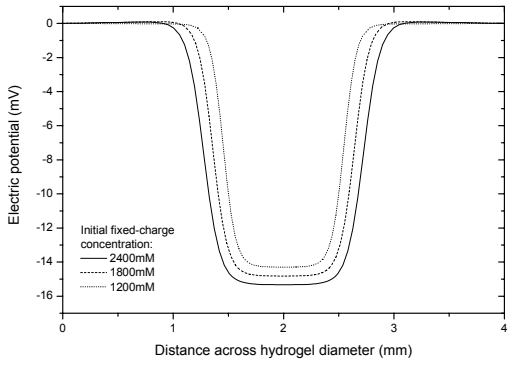

(e) Electric potential (ψ)

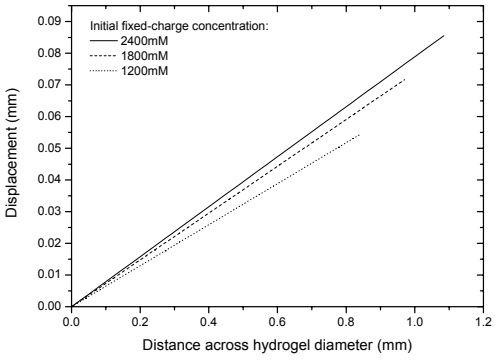

(f) Displacement (u)

Figure 4.5 Profiles of $c_{H^+}, c_{Na^+}, c_{Cl^-}, c_f, \psi$, and u as a function of ionizable fixed charge concentration c_{mo}^s. The PHEMA based hydrogel is equilibrated in a neutral medium with NaCl added to control the ionic strength.

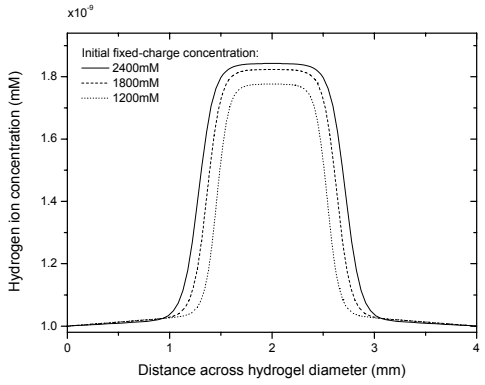

(a) Hydrogen ion (c_{H^+})

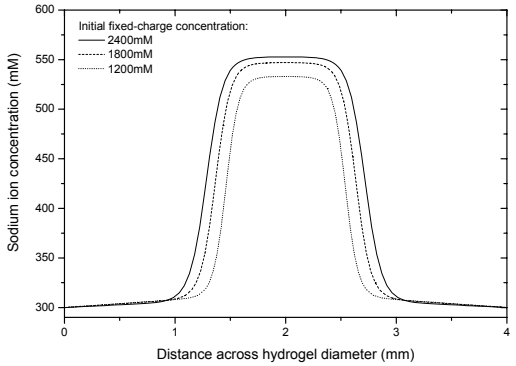

(b) Sodium ion (c_{Na^+})

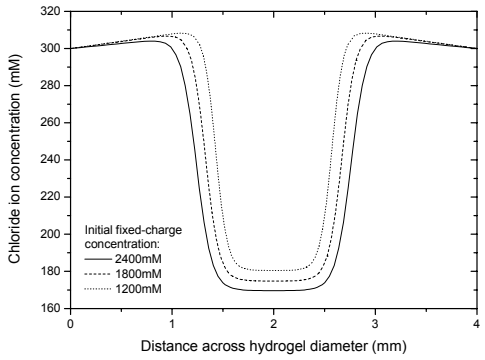

(c) Chloride ion (c_{Cl^-})

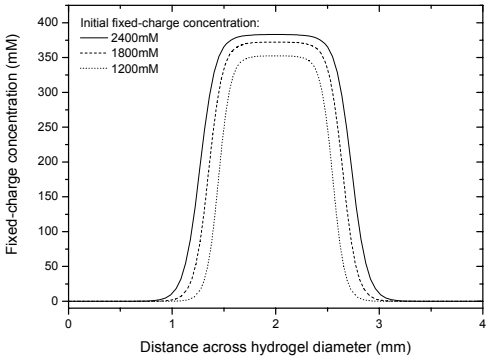

(d) Fixed charge group (c_f)

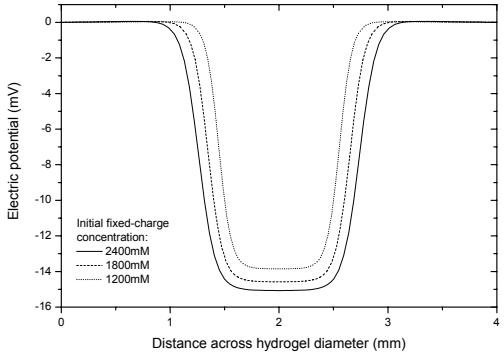

(e) Electric potential (ψ)

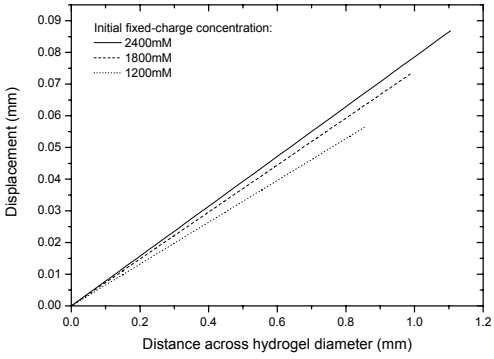

(f) Displacement (u)

Figure 4.6 Profiles of $c_{H^+}, c_{Na^+}, c_{Cl^-}, c_f, \psi$, and u as a function of ionizable fixed charge concentration c_{mo}^s. The PHEMA based hydrogel is equilibrated in a basic medium of pH12 with NaCl added to control the ionic strength.

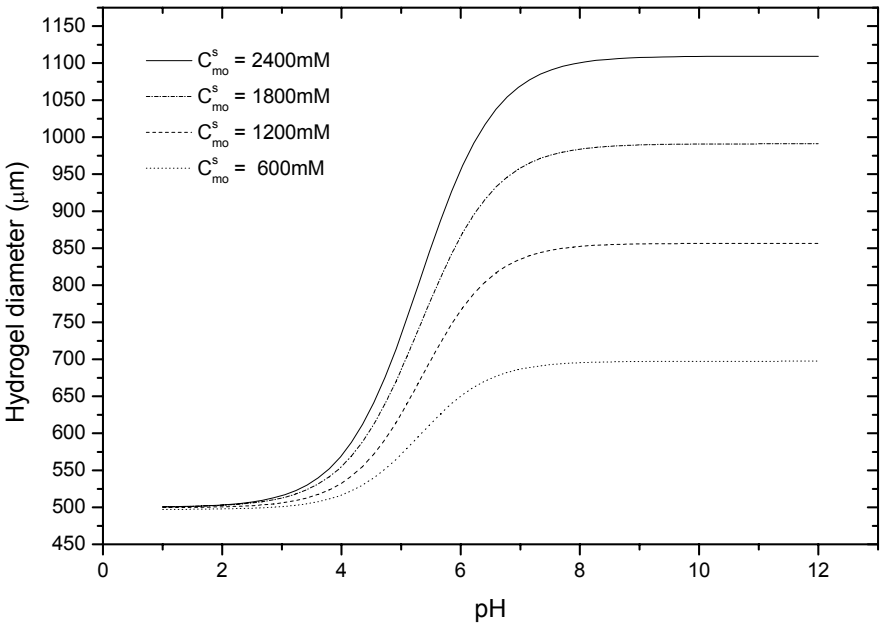

(a)

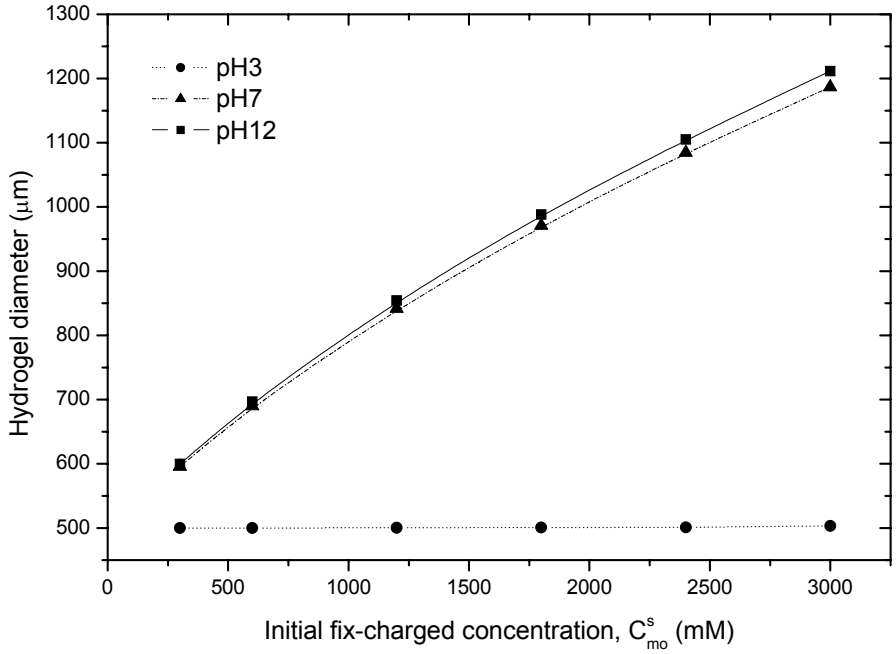

(b)

Figure 4.7 Dependence of swelling degree on (a) bathing pH as a function of ionizable fixed charge concentration c^s_{mo}, and (b) varying ionizable fixed charge concentration c^s_{mo} in acidic, neutral and basic solution.

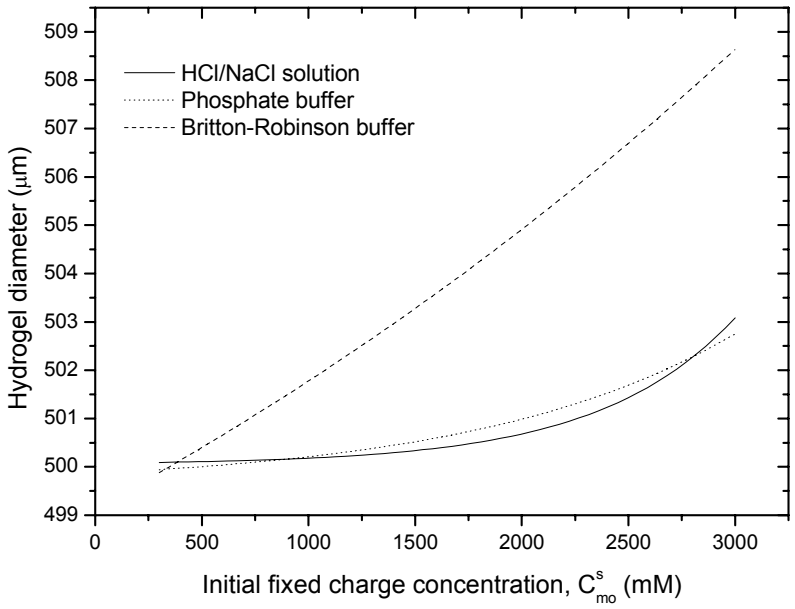

(a)

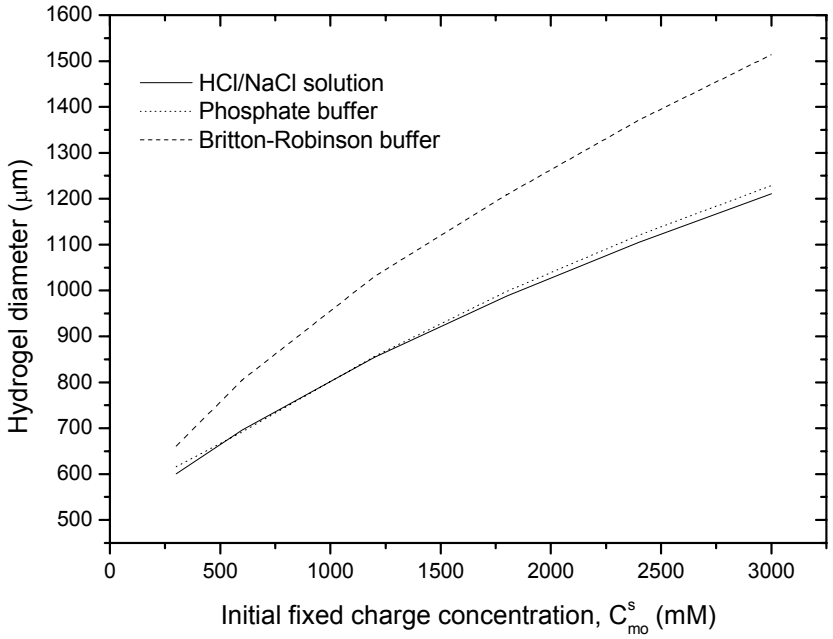

(b)

Figure 4.8 Influences of buffer systems on swelling equilibria as a function of ionizable fixed charge concentration in (a) acidic medium of pH3, and (b) basic medium of pH9.

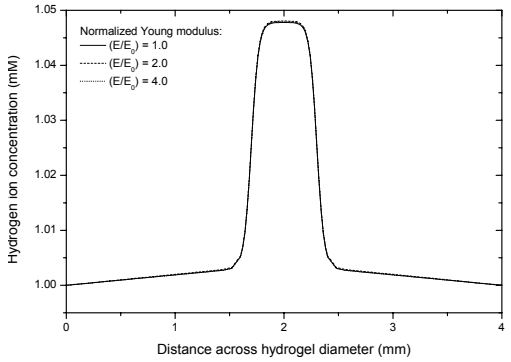

(a) Hydrogen ion (c_{H^+})

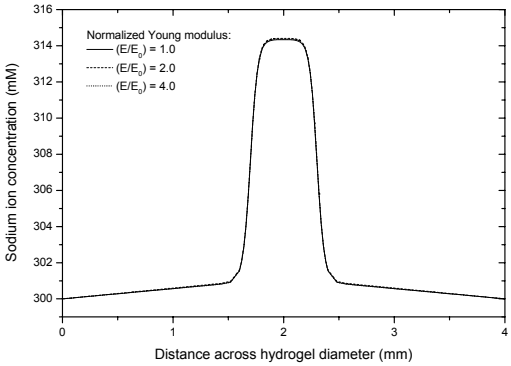

(b) Sodium ion (c_{Na^+})

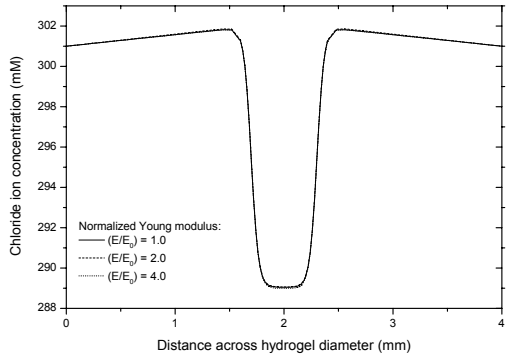

(c) Chloride ion (c_{Cl^-})

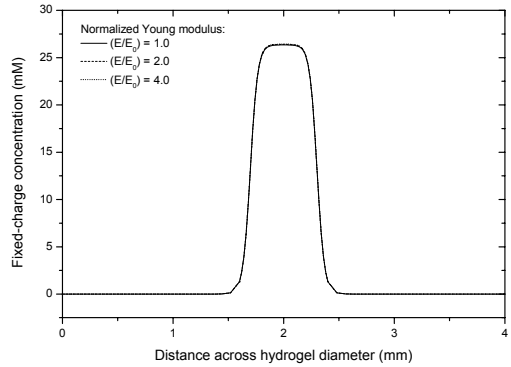

(d) Fixed charge group (c_f)

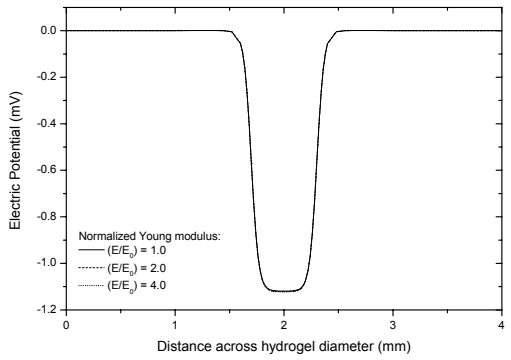

(e) Electric potential (ψ)

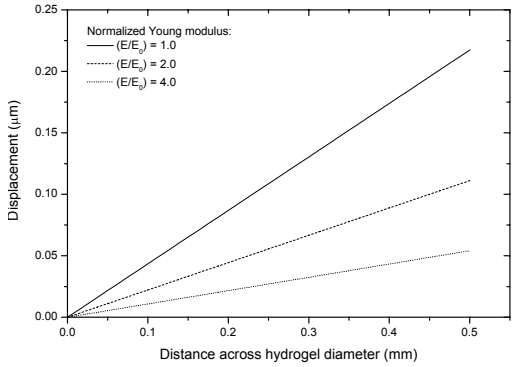

(f) Displacement (u)

Figure 4.9 Profiles of $c_{H^+}, c_{Na^+}, c_{Cl^-}, c_f, \psi$, and u as a function of normalized Young's modulus (E/E_0). The PHEMA based hydrogel is equilibrated in an acidic medium of pH3 with NaCl added to control the ionic strength.

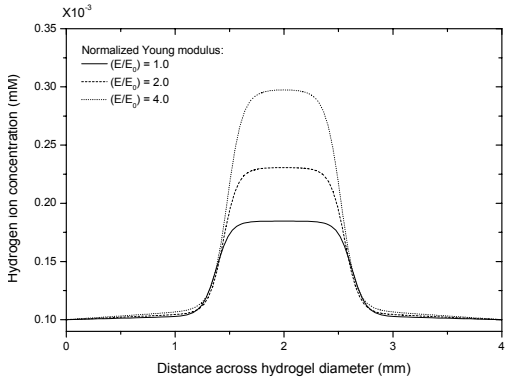

(a) Hydrogen ion (c_{H^+})

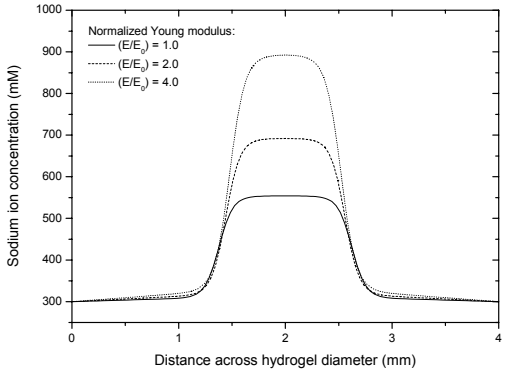

(b) Sodium ion (c_{Na^+})

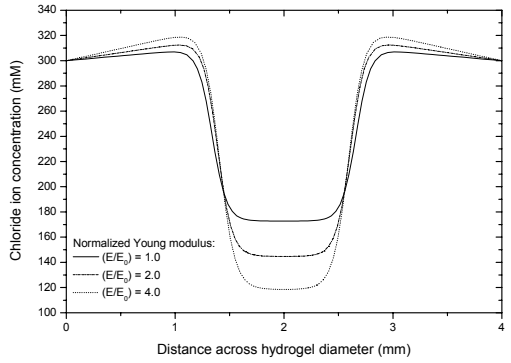

(c) Chloride ion (c_{Cl^-})

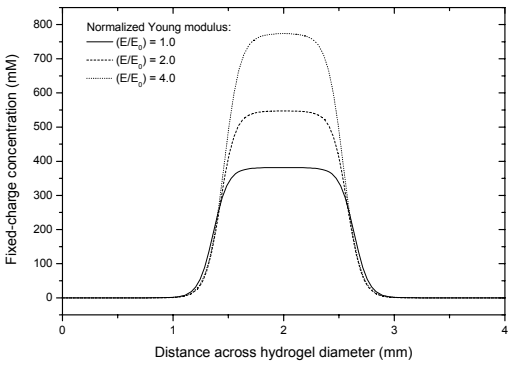

(d) Fixed charge group (c_f)

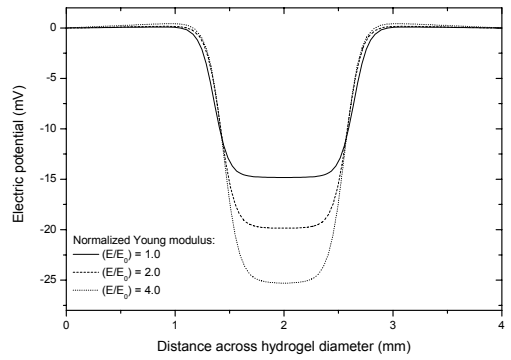

(e) Electric potential (ψ)

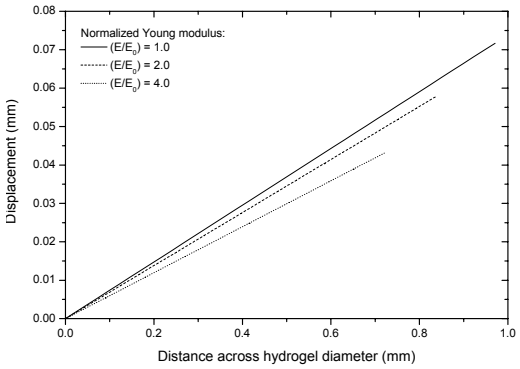

(f) Displacement (u)

Figure 4.10 Profiles of $c_{H^+}, c_{Na^+}, c_{Cl^-}, c_f, \psi$, and u as a function of normalized Young's modulus (E / E_0). The PHEMA based hydrogel is equilibrated in a neutral medium with NaCl added to control the ionic strength.

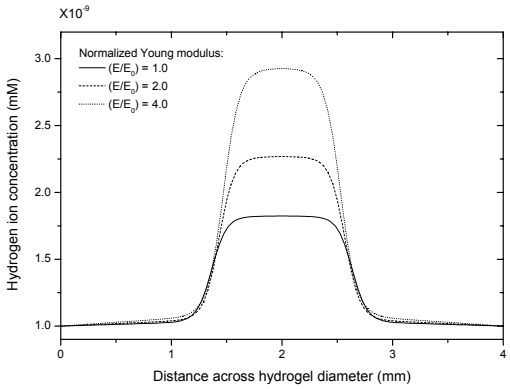

(a) Hydrogen ion (c_{H^+})

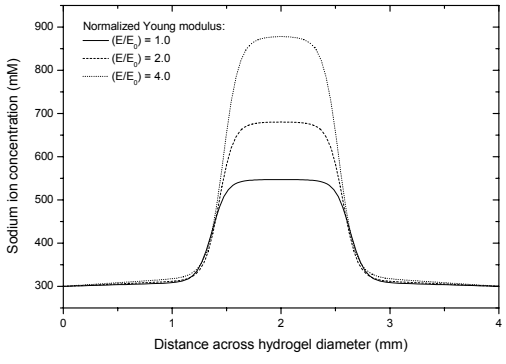

(b) Sodium ion (c_{Na^+})

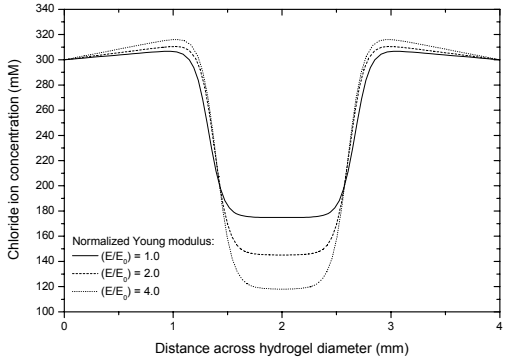

(c) Chloride ion (c_{Cl^-})

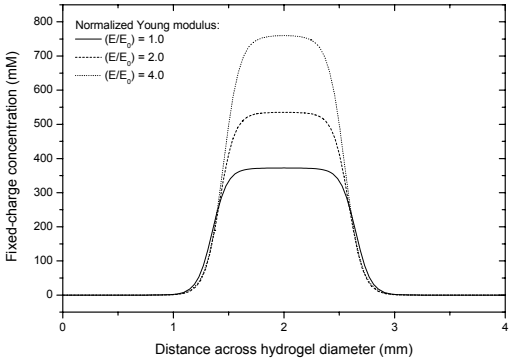

(d) Fixed charge group (c_f)

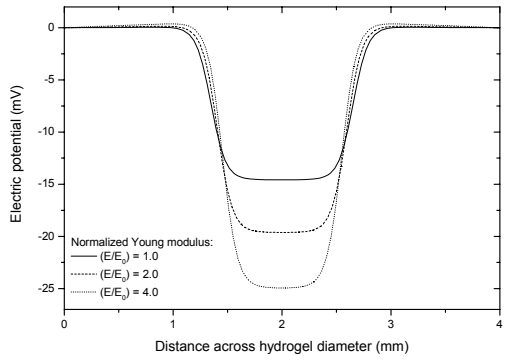

(e) Electric potential (ψ)

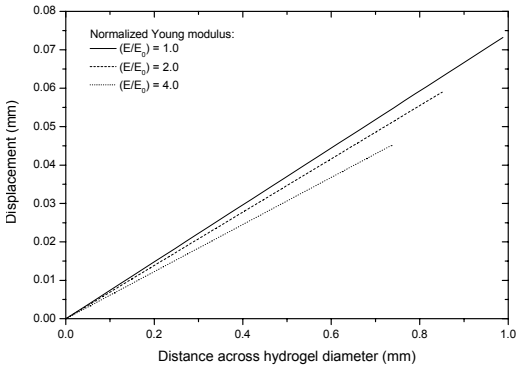

(f) Displacement (u)

Figure 4.11 Profiles of c_{H^+}, c_{Na^+}, c_{Cl^-}, c_f, ψ, and u as a function of normalized Young's modulus (E/E_0). The PHEMA based hydrogel is equilibrated in a basic medium of pH12 with NaCl added to control the ionic strength.

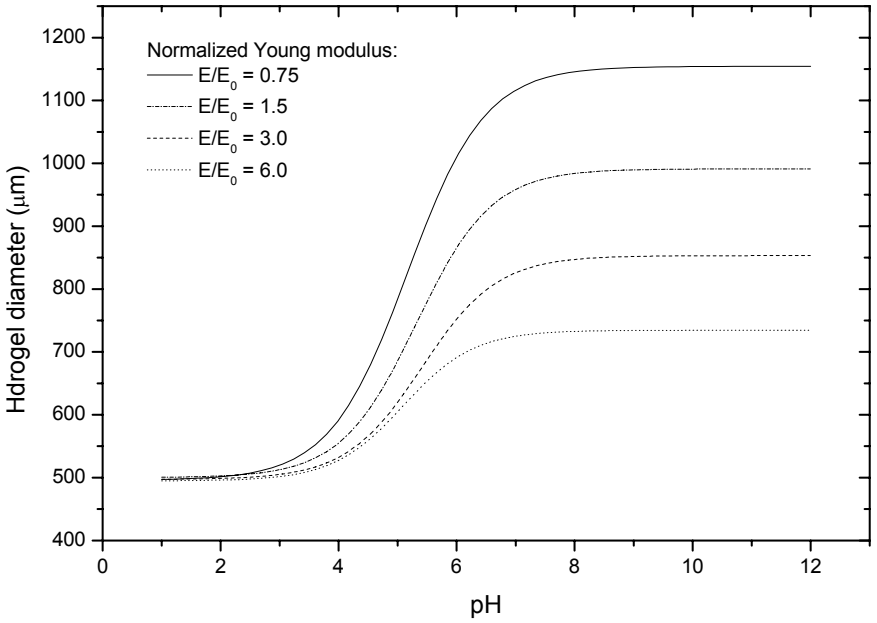

(a)

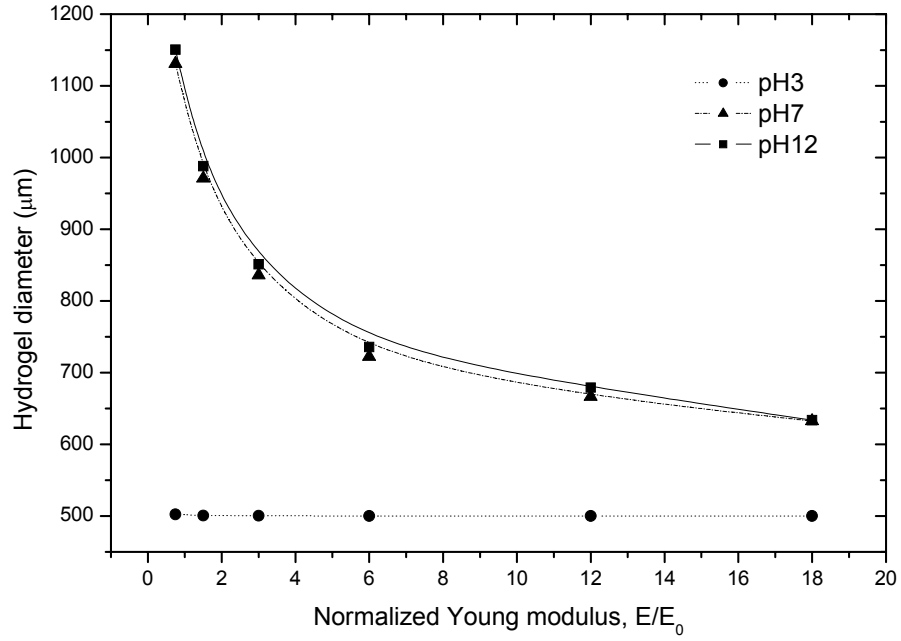

(b)

Figure 4.12 Dependence of swelling degree on (a) bathing pH as a function of normalized Young's modulus (E/E_0), and (b) varying normalized Young's modulus (E/E_0) in acidic, neutral and basic solution.

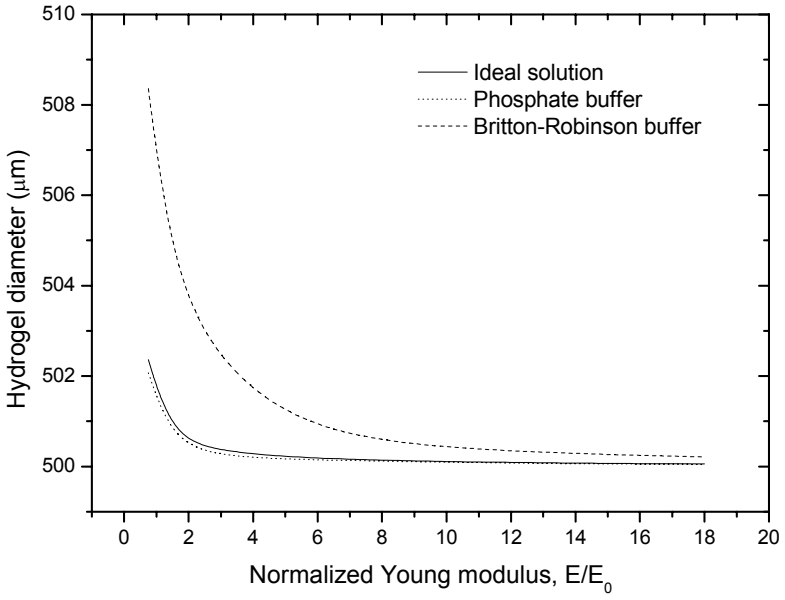

(a)

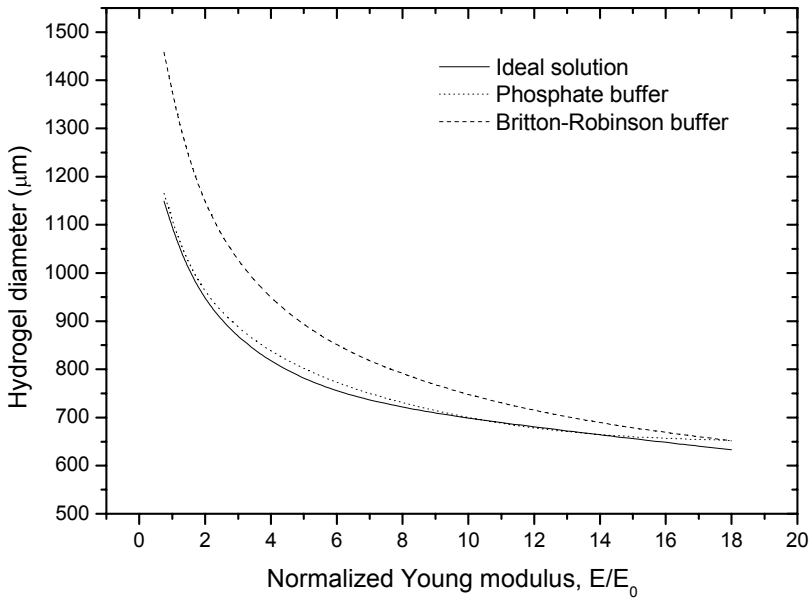

(b)

Figure 4.13 Influences of buffer systems on swelling equilibria as a function of normalized Young's modulus (E / E_0) in (a) acidic medium of pH3, and (b) basic medium of pH9.

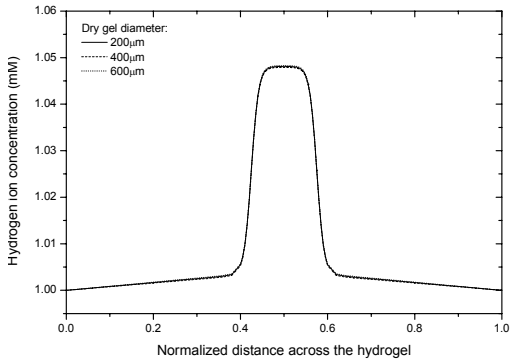

(a) Hydrogen ion (c_{H^+})

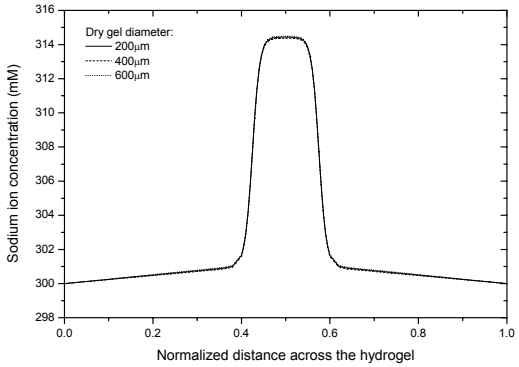

(b) Sodium ion (c_{Na^+})

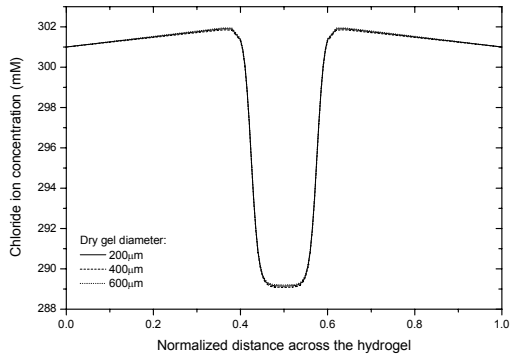

(c) Chloride ion (c_{Cl^-})

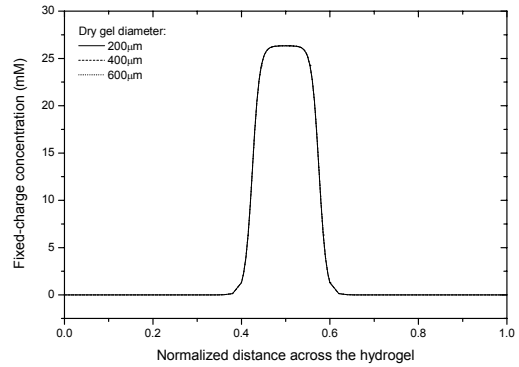

(d) Fixed charge group (c_f)

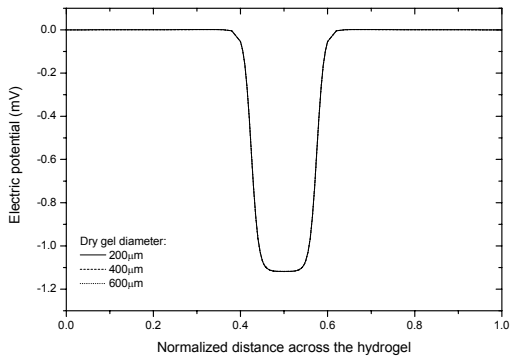

(e) Electric potential (ψ)

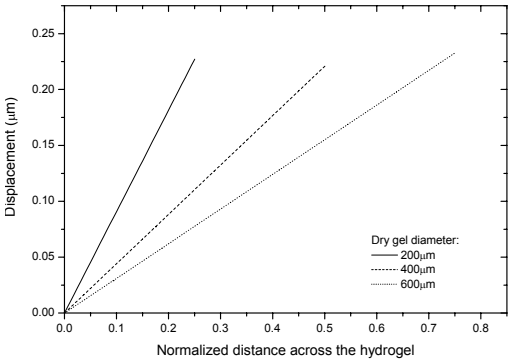

(f) Displacement (u)

Figure 4.14 Profiles of c_{H^+}, c_{Na^+}, c_{Cl^-}, c_f, ψ, and u as a function of initial diameter of hydrogel (dry gel diameter). The PHEMA based hydrogel is equilibrated in an acidic medium of pH3 with NaCl added to control the ionic strength.

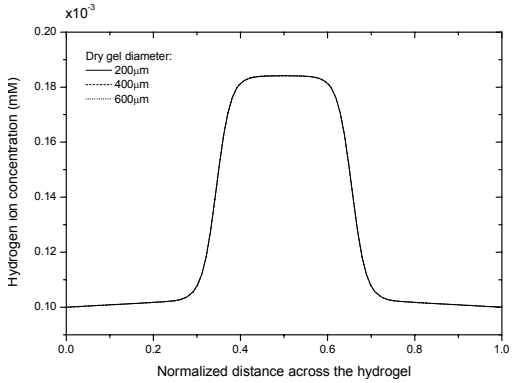

(a) Hydrogen ion (c_{H^+})

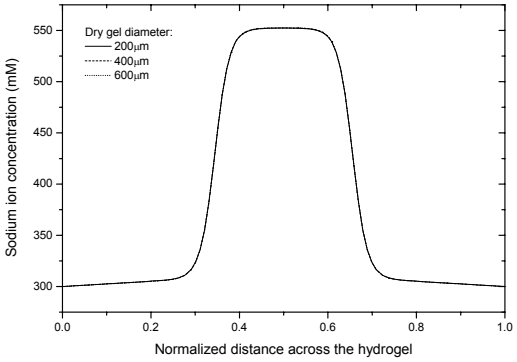

(b) Sodium ion (c_{Na^+})

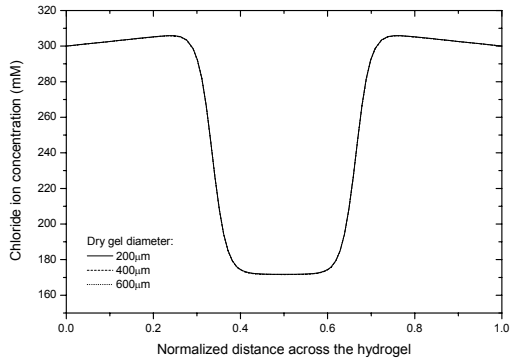

(c) Chloride ion (c_{Cl^-})

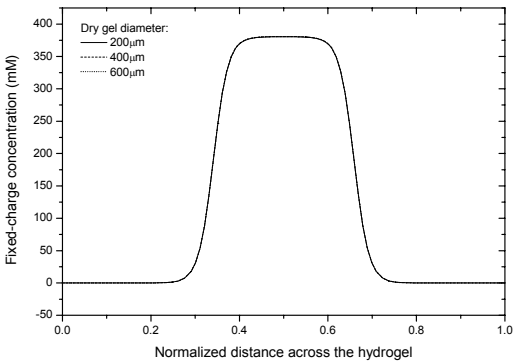

(d) Fixed charge group (c_f)

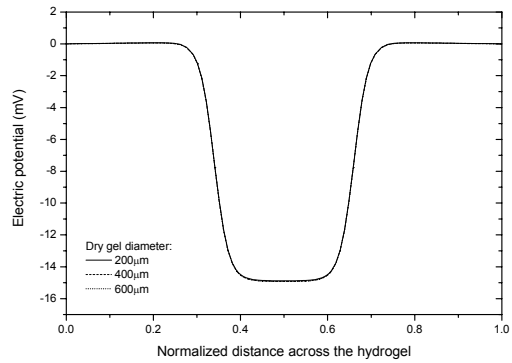

(e) Electric potential (ψ)

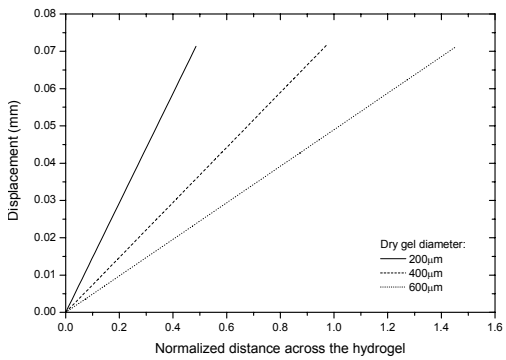

(f) Displacement (u)

Figure 4.15 Profiles of c_{H^+}, c_{Na^+}, c_{Cl^-}, c_f, ψ, and u as a function of initial diameter of hydrogel (dry gel diameter). The PHEMA based hydrogel is equilibrated in a neutral medium with NaCl added to control the ionic strength.

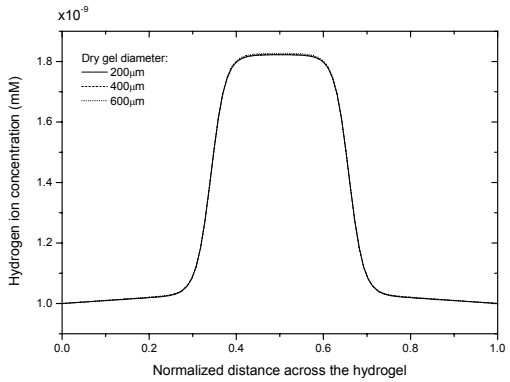

(a) Hydrogen ion (c_{H^+})

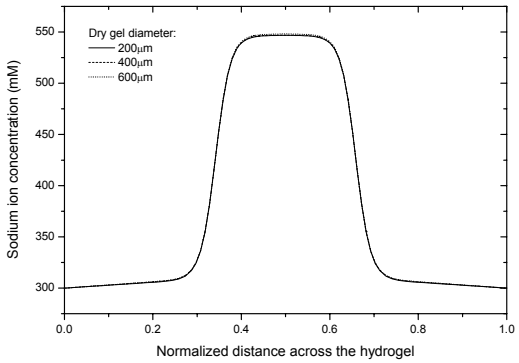

(b) Sodium ion (c_{Na^+})

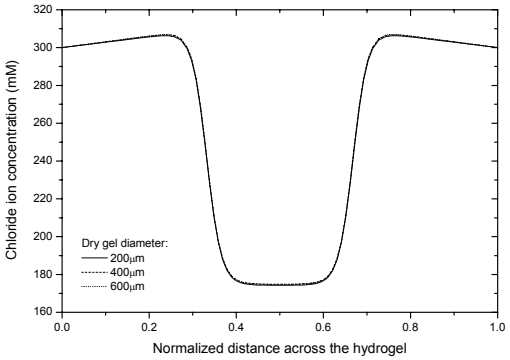

(c) Chloride ion (c_{Cl^-})

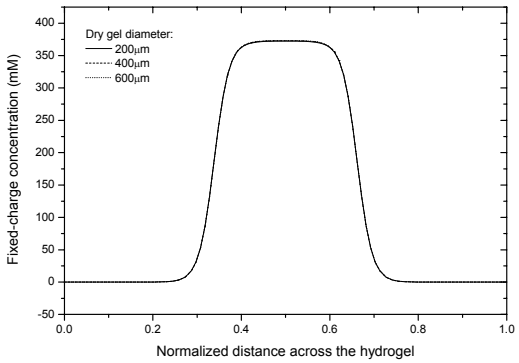

(d) Fixed charge group (c_f)

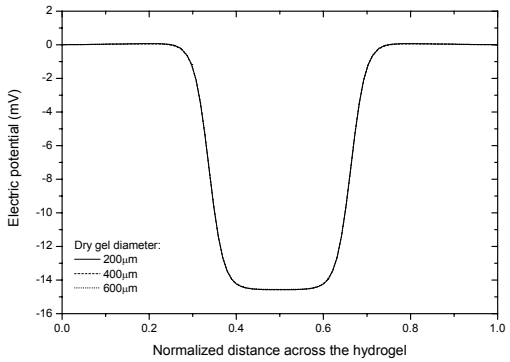

(e) Electric potential (ψ)

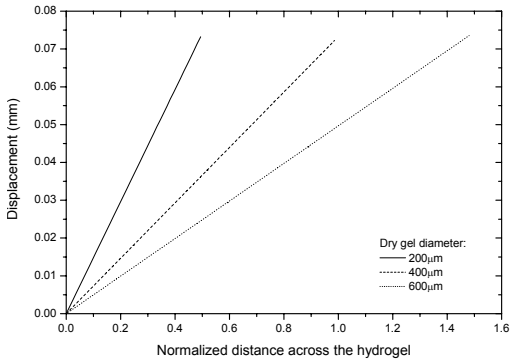

(f) Displacement (u)

Figure 4.16 Profiles of c_{H^+}, c_{Na^+}, c_{Cl^-}, c_f, ψ, and u as a function of initial diameter of hydrogel (dry gel diameter). The PHEMA based hydrogel is equilibrated in a basic medium of pH12 with NaCl added to control the ionic strength.

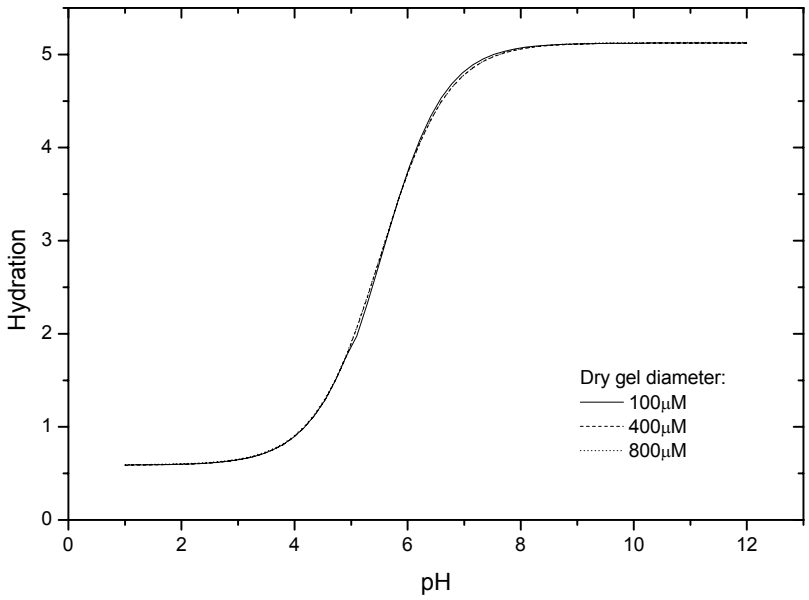

(a)

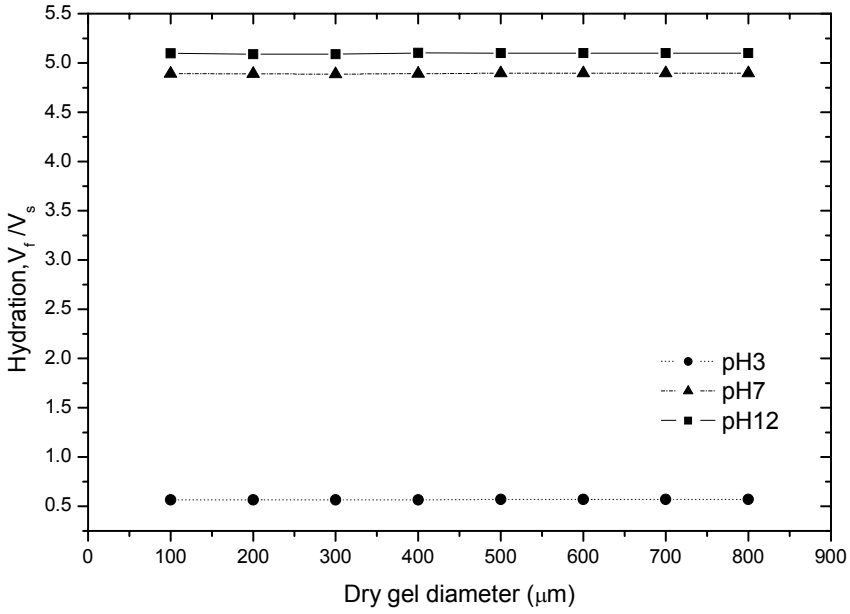

(b)

Figure 4.17 Dependence of hydration parameter on (a) bathing pH as a function of initial diameter of hydrogel (dry gel diameter), and (b) hydrogel diameter at dry state in acidic, neutral and basic solution.

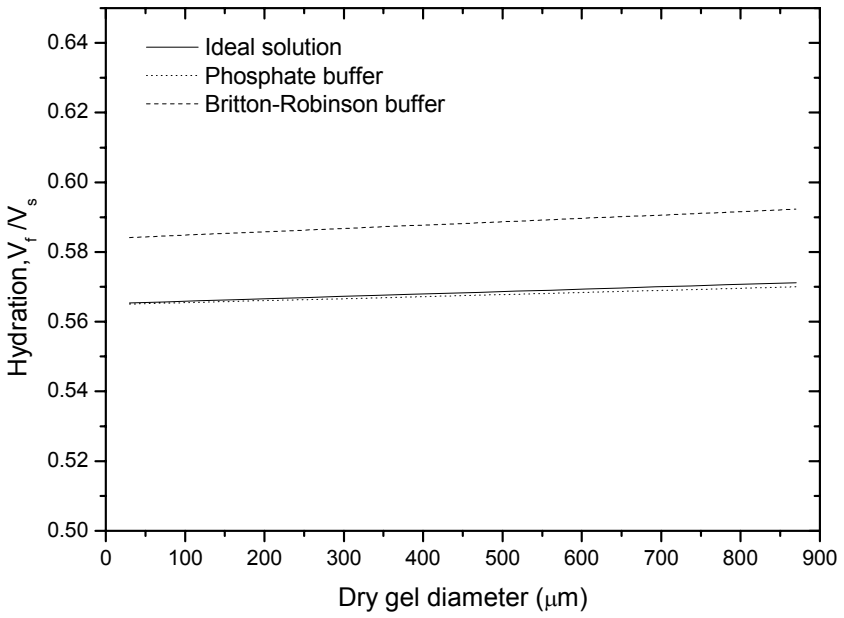

(a)

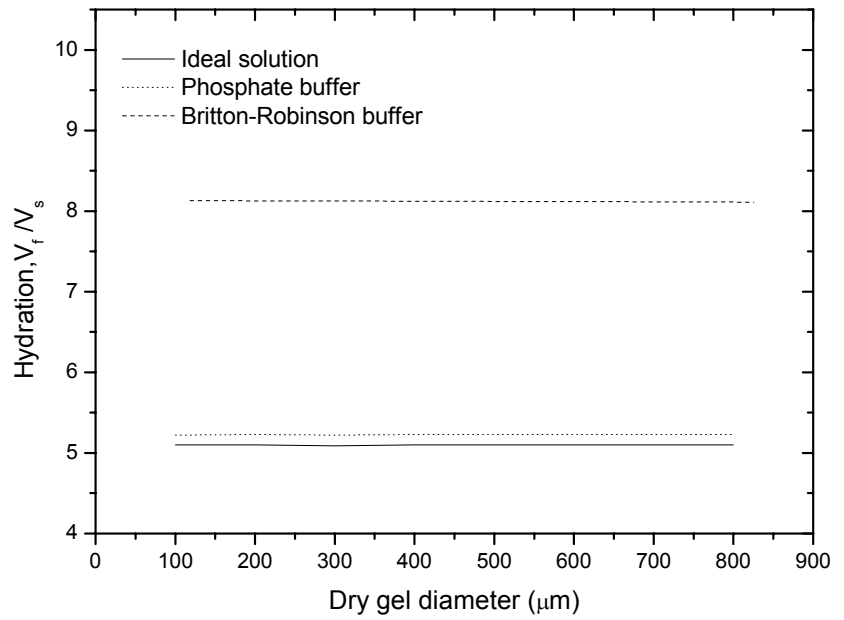

(b)

Figure 4.18 Influences of buffer system on hydration parameter as a function of initial diameter of hydrogel (dry gel diameter) in (a) acidic medium of pH3, and (b) basic medium of pH9.

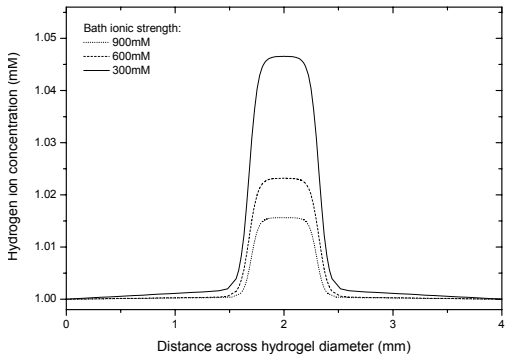

(a) Hydrogen ion (c_{H^+})

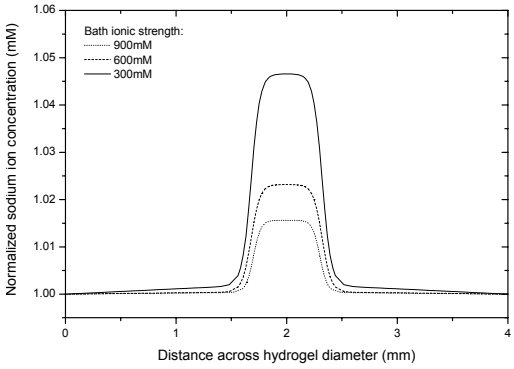

(b) Sodium ion (c_{Na^+})

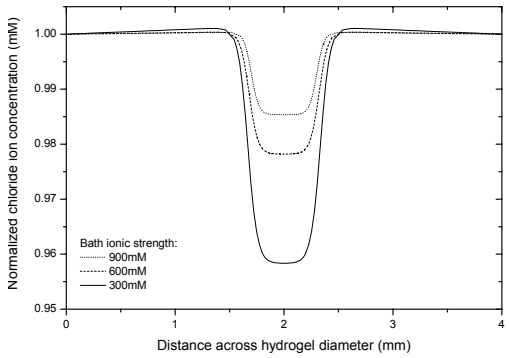

(c) Chloride ion (c_{Cl^-})

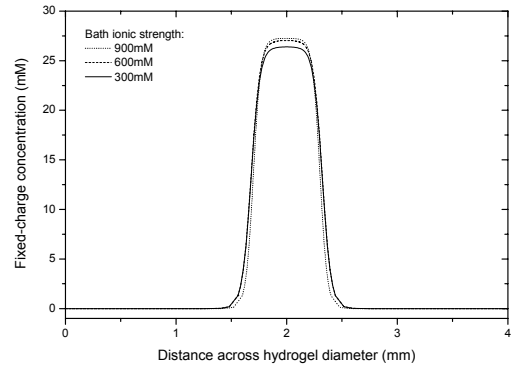

(d) Fixed charge group (c_f)

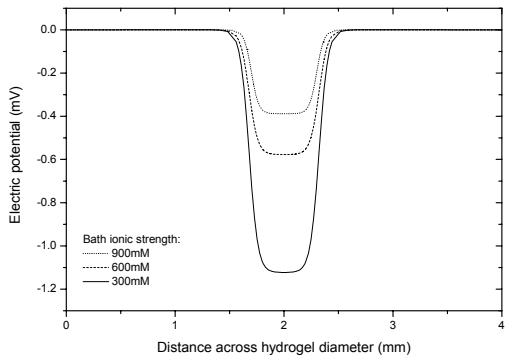

(e) Electric potential (ψ)

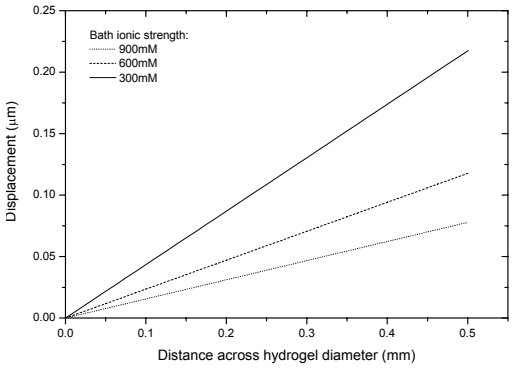

(f) Displacement (u)

Figure 4.19 Profiles of c_{H^+}, c_{Na^+}, c_{Cl^-}, c_f, ψ, and u as a function of swelling medium ionic strength. The PHEMA based hydrogel is equilibrated in an acidic medium of pH3 with NaCl added to control the ionic strength.

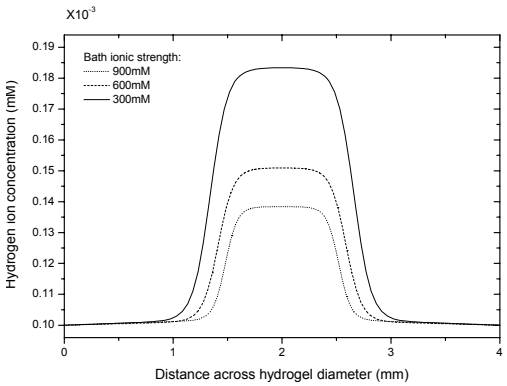

(a) Hydrogen ion (c_{H^+})

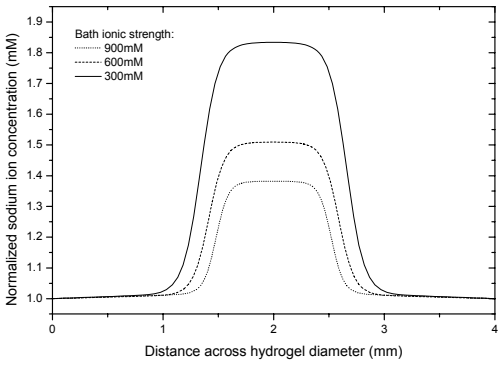

(b) Sodium ion (c_{Na^+})

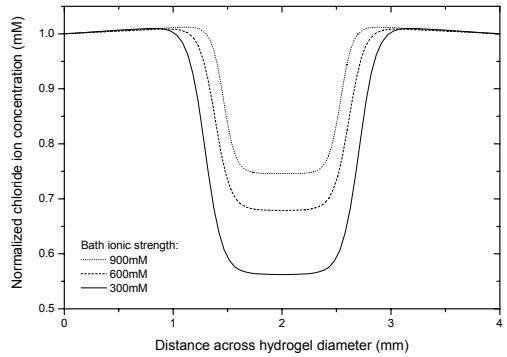

(c) Chloride ion (c_{Cl^-})

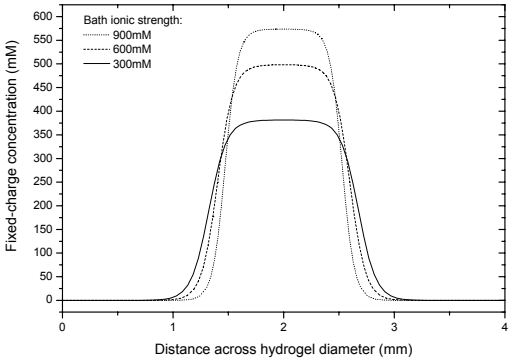

(d) Fixed charge group (c_f)

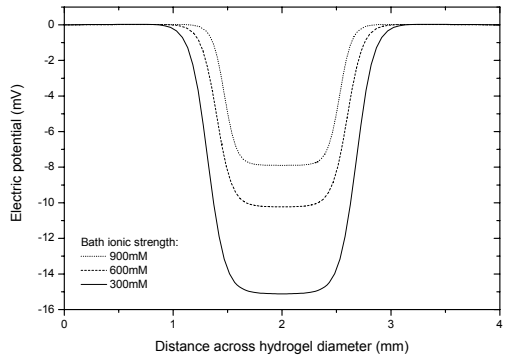

(e) Electric potential (ψ)

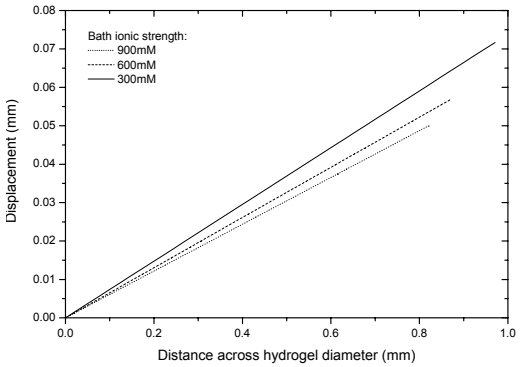

(f) Displacement (u)

Figure 4.20 Profiles of c_{H^+}, c_{Na^+}, c_{Cl^-}, c_f, ψ, and u as a function of swelling medium ionic strength. The PHEMA based hydrogel is equilibrated in a neutral medium with NaCl added to control the ionic strength.

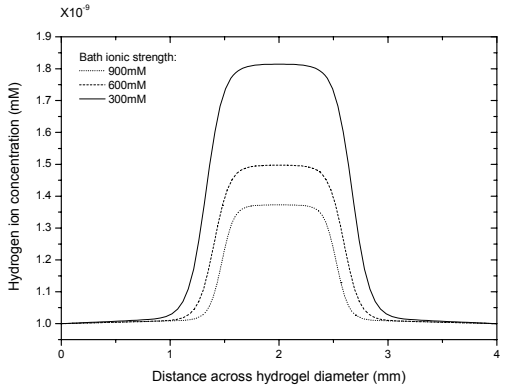

(a) Hydrogen ion (c_{H^+})

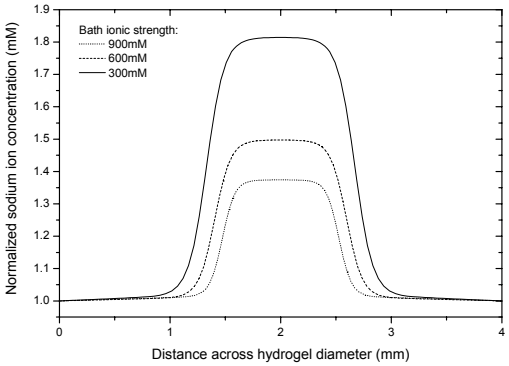

(b) Sodium ion (c_{Na^+})

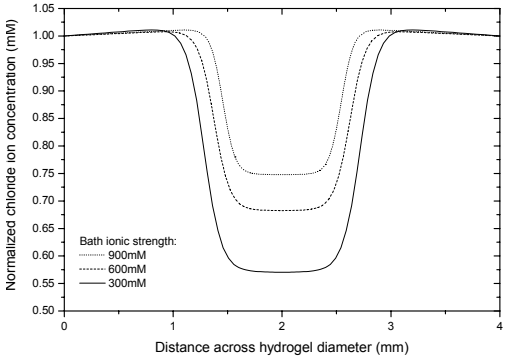

(c) Chloride ion (c_{Cl^-})

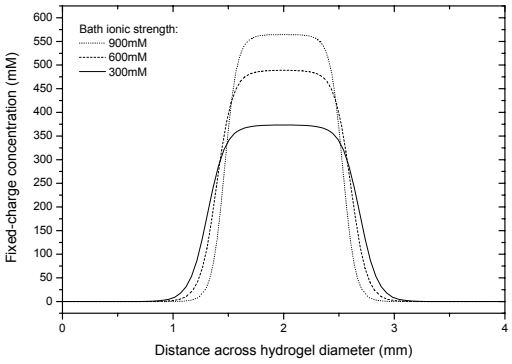

(d) Fixed charge group (c_f)

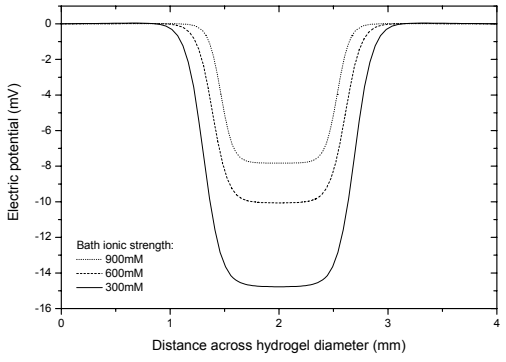

(e) Electric potential (ψ)

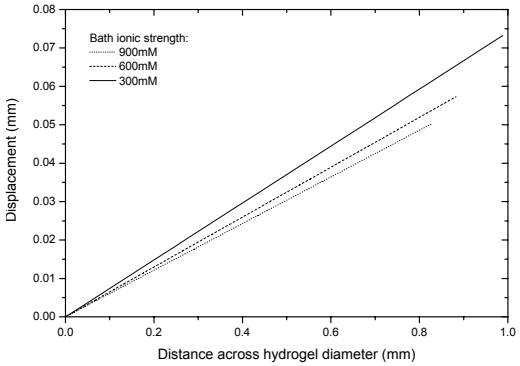

(f) Displacement (u)

Figure 4.21 Profiles of c_{H^+}, c_{Na^+}, c_{Cl^-}, c_f, ψ, and u as a function of swelling medium ionic strength. The PHEMA based hydrogel is equilibrated in a basic medium of pH12 with NaCl added to control the ionic strength.

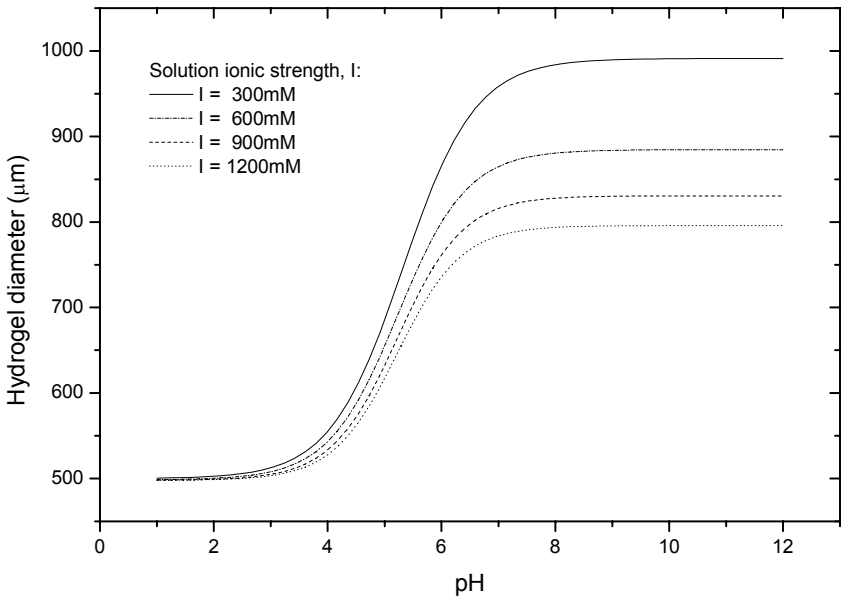

(a)

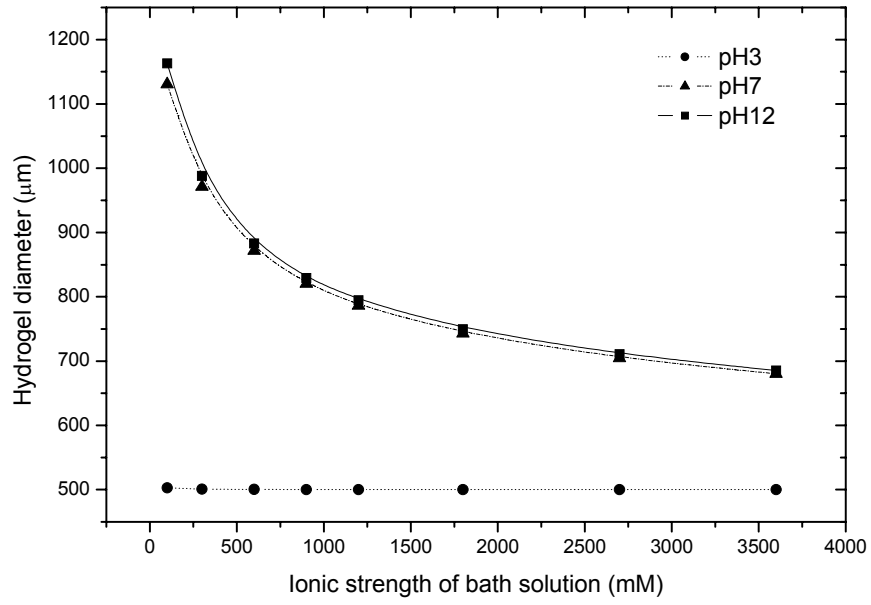

(b)

Figure 4.22 Dependence of swelling degree on (a) bathing pH as a function of ionic strength of swelling medium, and (b) varying ionic strength in acidic, neutral and basic swelling medium.

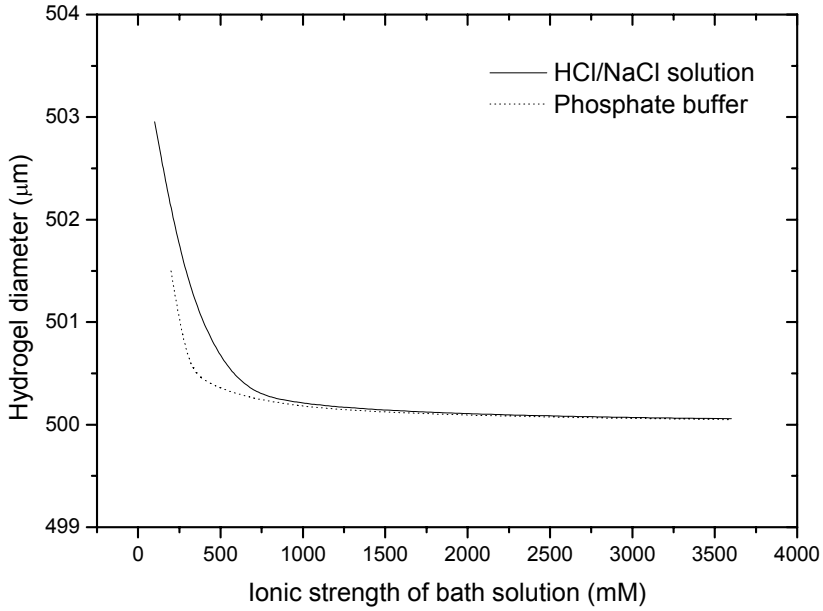

(a)

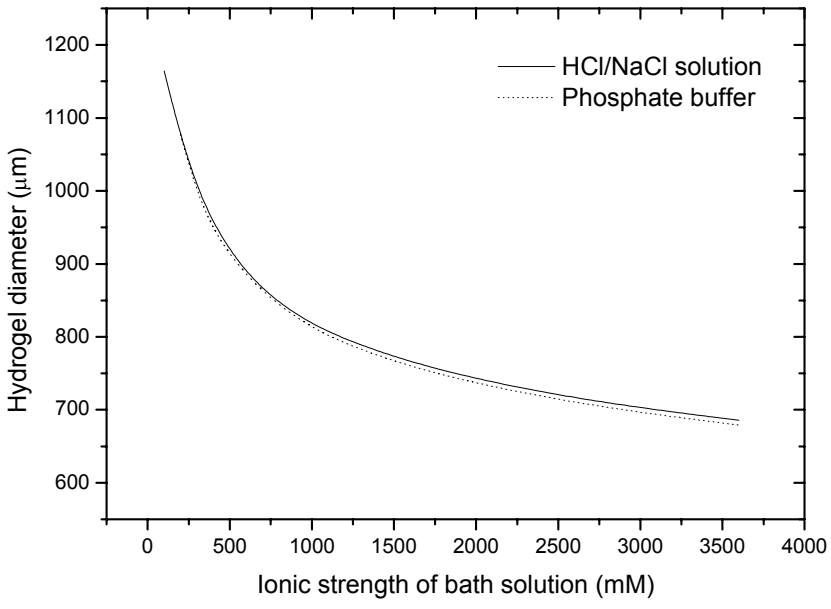

(b)

Figure 4.23 Influences of buffer system on hydration parameter as a function of ionic strength of swelling medium in (a) acidic medium of pH3, and (b) basic medium of pH9.

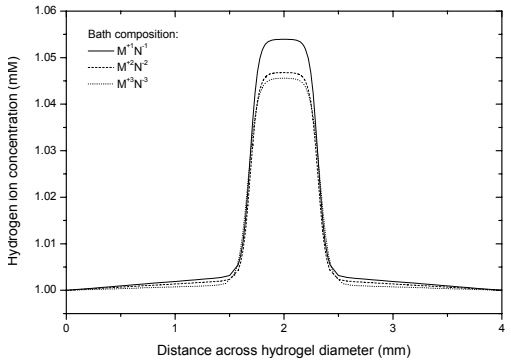

(a) Hydrogen ion (c_{H^+})

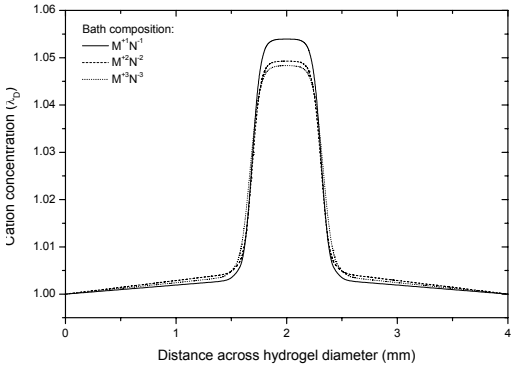

(b) Diffusible cation (c_{M^+})

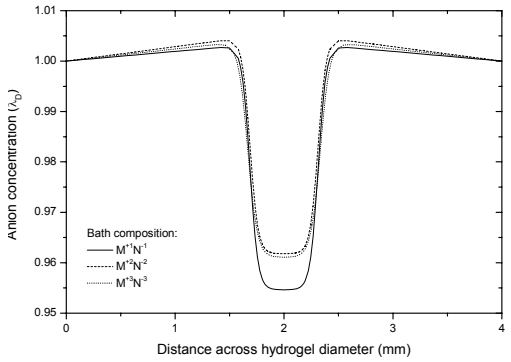

(c) Diffusible anion (c_{N^-})

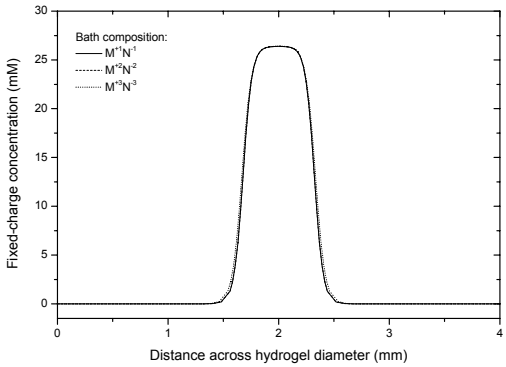

(d) Fixed charge group (c_f)

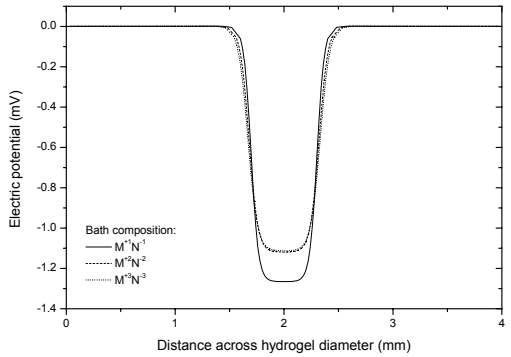

(e) Electric potential (ψ)

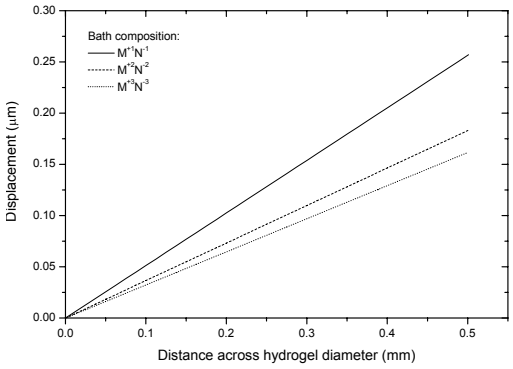

(f) Displacement (u)

Figure 4.24 Profiles of c_{H^+}, c_{M^+}, c_{N^-}, c_f, ψ, and u for particular solvent composition (monovalents, divalents, trivalents). The PHEMA based hydrogel is equilibrated in an acidic medium of pH3.

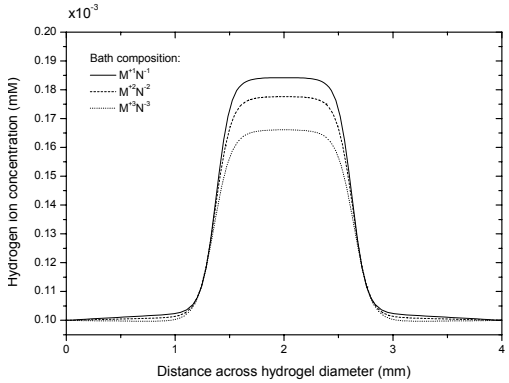

(a) Hydrogen ion (c_{H^+})

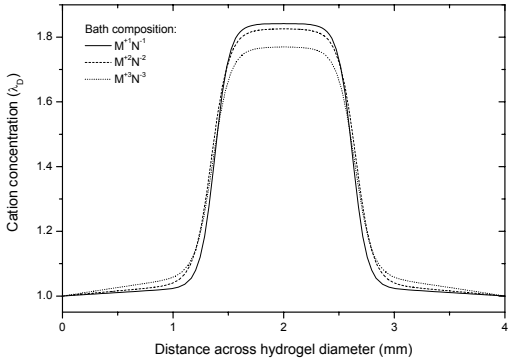

(b) Diffusible cation (c_{M^+})

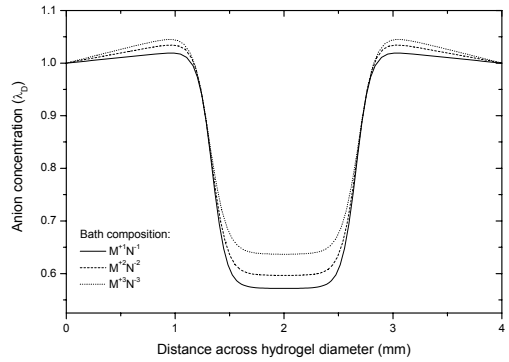

(c) Diffusible anion (c_{N^-})

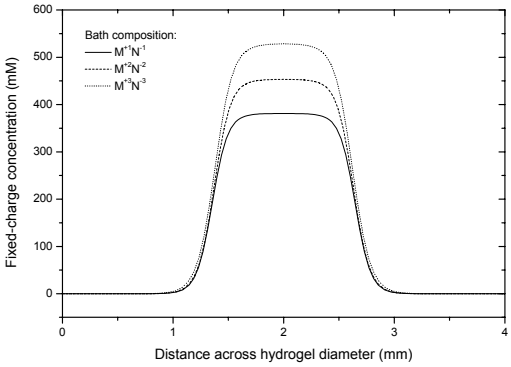

(d) Fixed charge group (c_f)

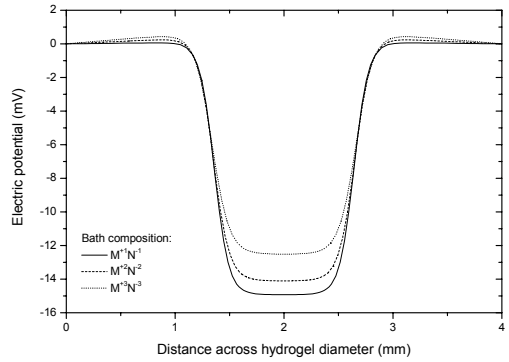

(e) Electric potential (ψ)

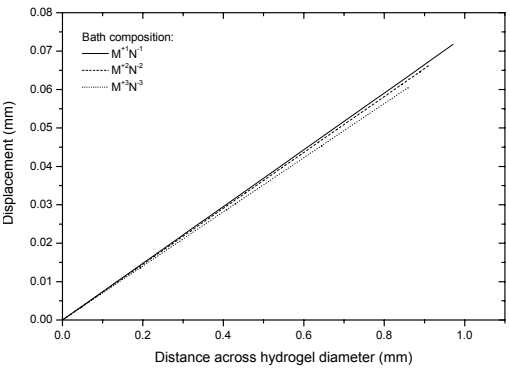

(f) Displacement (u)

Figure 4.25 Profiles of c_{H^+}, c_{M^+}, c_{N^-}, c_f, ψ, and u for particular solvent composition (monovalents, divalents, trivalents). The PHEMA based hydrogel is equilibrated in a neutral medium.

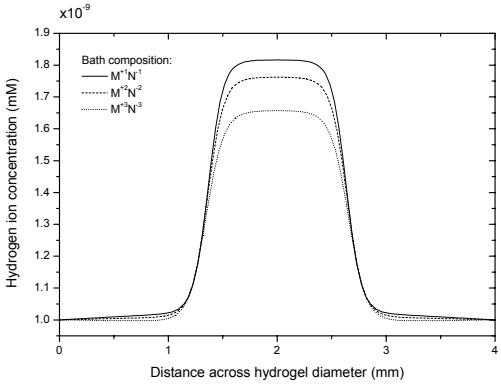

(a) Hydrogen ion (c_{H^+})

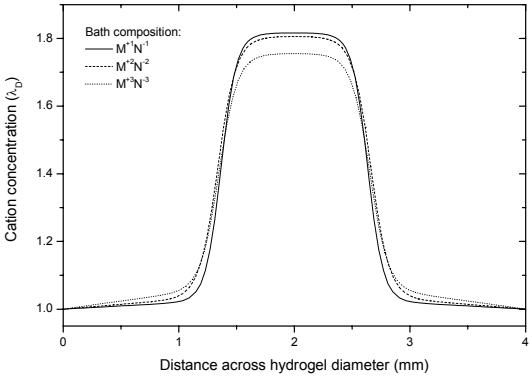

(b) Diffusible cation (c_{M^+})

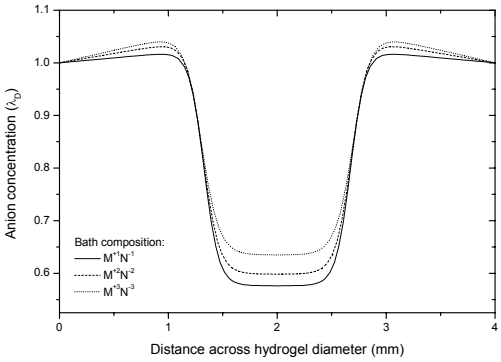

(c) Diffusible anion (c_{N^-})

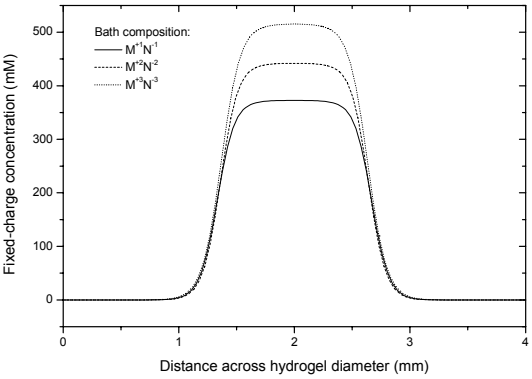

(d) Fixed charge group (c_f)

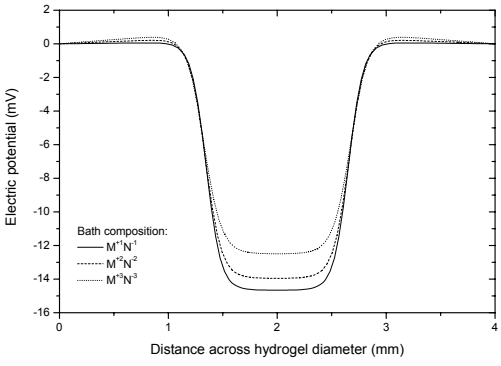

(e) Electric potential (ψ)

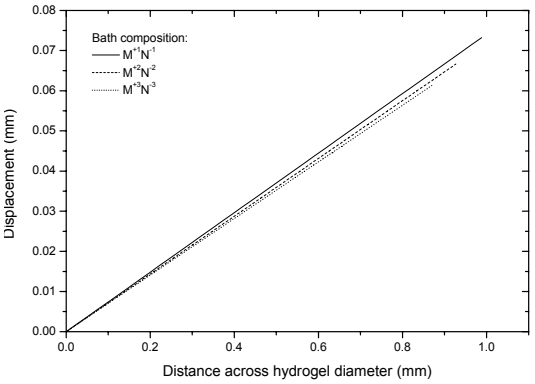

(f) Displacement (u)

Figure 4.26 Profiles of c_{H^+}, c_{M^+}, c_{N^-}, c_f, ψ, and u for particular solvent composition (monovalents, divalents, trivalents). The PHEMA based hydrogel is equilibrated in a basic medium of pH12.

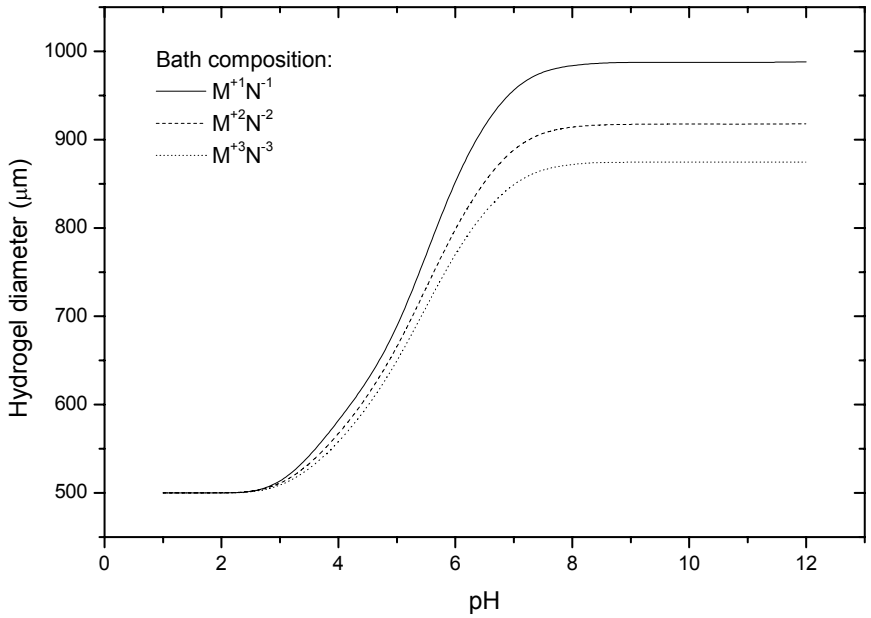

(a)

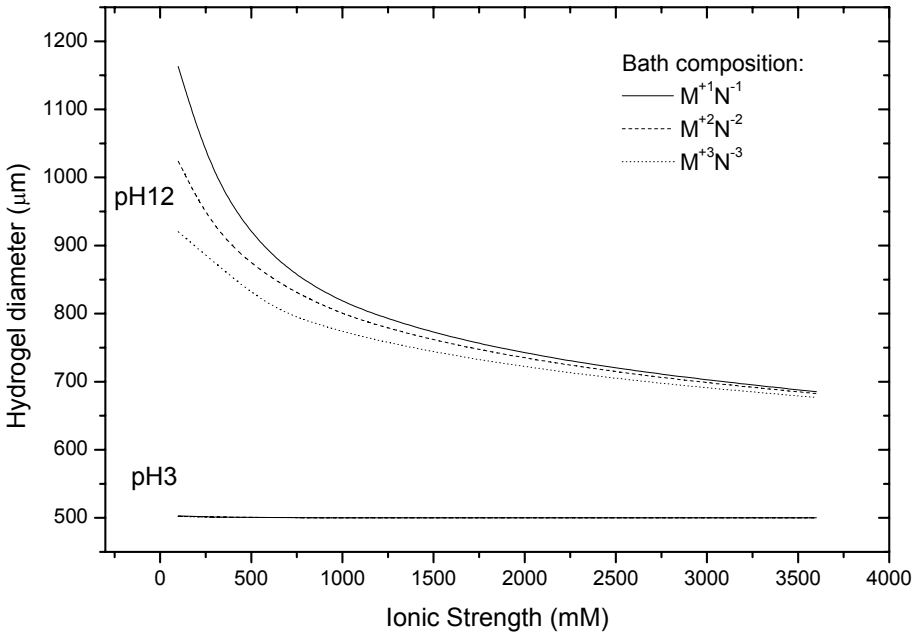

(b)

Figure 4.27 Dependence of swelling degree on (a) solvent composition (monovalents, divalents, trivalents) as a function of bathing pH, and (b) ionic strength of swelling medium in different ionic valencies of bathing solution.

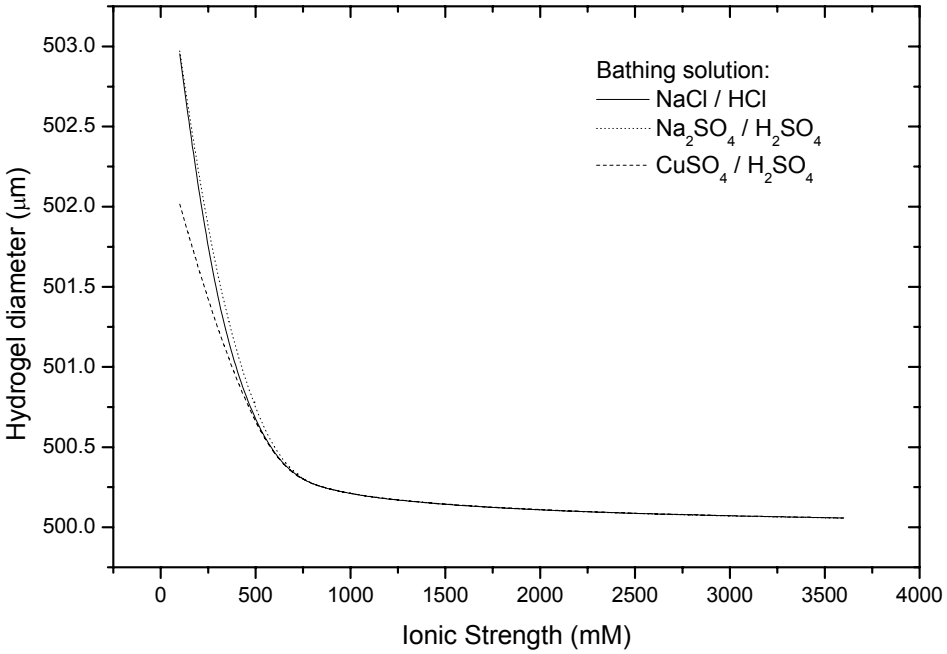

(a)

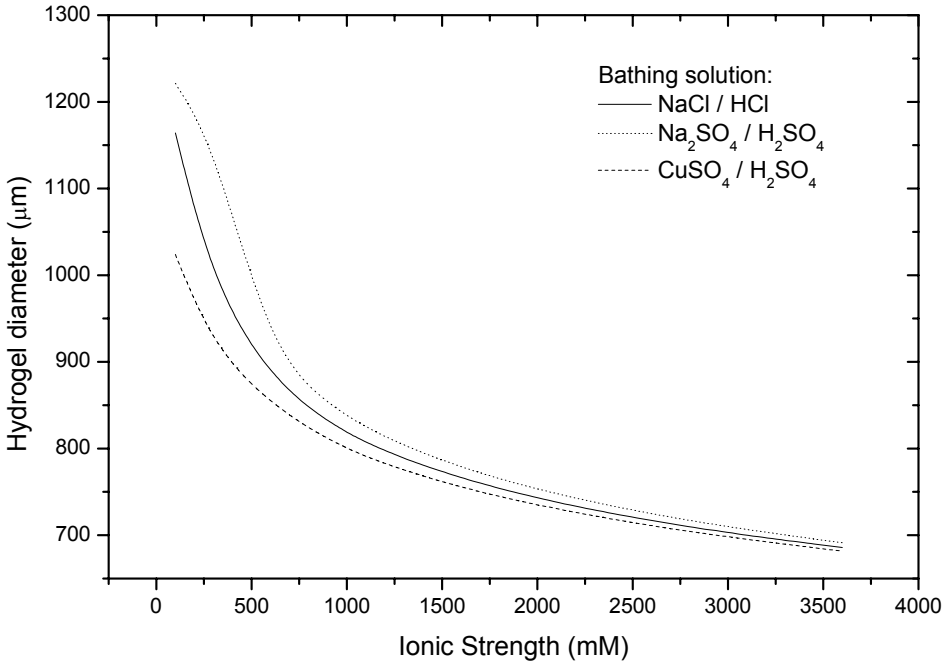

(b)

Figure 4.28 Effects of ionic valencies of bathing solution on swelling equilibria as a function of ionic strength in (a) acidic medium of pH3, and (b) basic medium of pH9.

CHAPTER 5

STEADY-STATE SIMULATIONS OF EQUILIBRIUM SWELLING OF pH-SENSITIVE HYDROGEL IN CONCURRENT PRESENCE OF pH AND ELECTRICAL STIMULI

5.1 OVERVIEW

From the previous chapter, large dimensional changes in crosslinked hydrogels are shown to be induced chemically by altering the chemical milieu, e.g. bath pH, salt concentration, and aqueous solution contents. The volume change of hydrogel can be exploited to build a chemomechanical system which traduces the chemical stimuli into mechanical work.

More recent discoveries (Tanaka et al., 1982) have shown that discontinuous volumetric change in crosslinked water swollen polymer gel can be induced by electric fields. Hypothetically, it is concluded that the effect is primarily due to spatio-temporal pH and salt concentration gradient generated by electric field via an electrodiffusion or electro-osmotic transport mechanism. As demonstrated by the precedent studies of chemomechanical system, swelling or shrinking is caused by conformational changes in ionizable groups fixed to the polymer backbone. The dissociation equilibrium of the ionizable groups is in turn determined by proton and salt concentrations in the bathing solution where changes in those parameters can perturb the system from its

equilibrium state. Therefore, electromechanical response can be invoked, in principle, to induce reversible volume changes in ionizable polymer gels with electric fields.

A chemomechanical system modulated by electric stimulus seems to be particularly intriguing in connection with the fact that electrolytically activated or electrokinetically driven chemomechanical systems could provide a more sensitive and convenient method of controlling the pH and salt solution through physical regulation. The capability for direct conversion of electrical energy into mechanical actuation as well as possessing the mechanical properties resembling biological system indicates the feasibility of designing biomimetic energy-transducing or drug delivery systems with hydrogel (Kajiwara and Ross-Murphy, 1992; Peppas et al., 2000b).

The studies devoted to the experimental observations of hydrogel in response to chemical and electrical stimulation are the subject of many investigations lately. However, the related theoretical or numerical studies of the mechanism governing electrical and chemical coupling to mechanical energy conversion in hydrogel are scarce. The theoretical investigation of electrochemomechanical devices based on water swollen ionic polymer gel under simultaneous presence of electrical and chemical stimuli will serve as the basis of illustration of synthetic analogs of physiological muscles with possible eventual use for orthotics, prosthetics and artificial muscle in robotic. Regarding biological analogies, simultaneous pH (about one pH unit) and electric (approximately 0.14V) gradients are found to exist across the inner mitochondrial membrane and the thylakoid membrane of the Chloroplast as these gradients play an important role in the chemiosmotic ATP synthesis (Cooper and Hausman, 2000).

A short survey of the researches done on the subject has been presented in chronological manner in Section 1.3.3. However, it is by no mean a complete list of publications but a brief introduction to the subject that is of interest.

Even though there are numerous published articles on the swelling/deswelling and bending mechanism of hydrogel subjected to externally applied electric potential, it is still a controversial subject as there are still lack of systematic investigations and discussions of the phenomenological behavior from the theoretical frameworks.

5.2 MODEL VALIDATIONS WITH EXPERIMENTAL RESULTS

5.2.1 Responses of Hydrogel to Externally Applied Electric Field

5.2.1.1 Comparison with Theoretical Calculation

Let us consider a stimuli-responsive hydrogel immersed in a NaCl/HCl bath solution. The concentration of fixed charge groups within the hydrogel c_f is preserved at 10mM. The boundary conditions of Na^+ and Cl^- ions in the solution are set to c_{Na^+} = c_{Cl^-} = 1mM. An external electric field is applied with a constant electric potential of 0.1V at the anode and -0.1V at the cathode. Figure 5.2 shows the comparison of numerical simulations of the MECpH model with those of FEM (Wallmersperger et al., 2001a). Curve 1 depicts the linear variation of electrical potential in the solution before the hydrogel is immersed. Curve 2 shows the superposition of the linear curve 1 over the electrical potentials after the hydrogel is submerged in the solution without externally applied electric field. Curve 3 maps the simulated electric potential in both the hydrogel and exterior solution when an external electric field is applied across the

submerging hydrogel. The plotted curve 3 is quantitatively agreeable for region in the bathing solution but shows dissimilar behavior in the hydrogel region. As noticed from the figure, the gap at the interface between hydrogel and solution grows bigger at the anode side than that near to the cathode side.

5.2.1.2 Comparison with Experimental Data

After pondering on the changes in characteristic of the electric potential profile in electrically stimulated hydrogel which deviates from the purely chemical functioning condition, it is interesting to study the physical changes of hydrogel with the ever-changing external electric field. As pin-pointed in previous section, the distinctive behavior of electrically modulated hydrogel shows difference in swelling strain across the hydrogel, which results in bending of the hydrogel. To examine the bending degree, an average bending curvature κ at the mid point in the direction of the hydrogel thickness h is defined in terms of the swelling strains (Zhou et al., 2002):

$$\kappa = \frac{2(e_1 - e_2)}{h(2 + e_1 + e_2)} \tag{5.1}$$

where e_1 and e_2 assigned to the strains at two ends of the hydrogel thickness.

Attention is given here to the comparison of simulated results by MECpH model with data extracted from experimental work of Zhou et al. (2002). A chitosan/PEG based hydrogel strip with positively charged groups fixed to its polymer network is allowed to swell/shrink in acidic solution under external electric field. The physical parameters pertaining to the experiment are given as $(2\mu + 3\lambda) = 0.12\text{MPa}$, $L_{Gel} = 1\text{mm}$, $\varepsilon = 80$, $c^s_{mo} = 20\text{mM}$, $c_k = 5\text{mM}$. The two electrodes that exert electric potential on the hydrogel are separated at a distance of 20mm and the initial fluid volume fraction upon immersion is taken as 0.8. As discussed in Section 2.3.3,

implementation of finite deformation theory becomes prevalent when geometrical nonlinearity becomes significant (Liew et al., 2002). The calculated average curvature κ of the bending hydrogel is plotted in Fig. 5.3 against the externally applied electric potential for both nonlinear and linear results. The bending curvatures predicted from linear and finite deformation theories are identical under low voltage conditions. However, the results for both theories differ significantly as the applied voltage increases. Figure 5.3 shows that the finite deformation gives more accurate prediction then the linear deformation theory at high voltage application. Further, the predicted results obtained from finite deformation are closely comparable with the experimental measurements. The MECpH model predicts a monotonically increasing average curvature κ with electric field. To summarize, the bending degree of the hydrogel strip is linearly controlled by the applied electric voltage. This linear relationship could be an advantage in the design of actuator devices.

5.2.2 Responses of Hydrogel to Coupling Effects of Chemically and Electrically Induced Environment Condition

5.2.2.1 Comparison with Experimental Data

The material under study is an interpenetrating polymer networks (IPNs) hydrogel composed of polymethacrylic acid (PMAA) and poly(vinyl alcohol) (PVA). Interpenetrating polymer networks (IPNs) are a combination of two or more network polymers synthesized in juxtaposition to form interpolymer complex (Abe et al., 1977). Under the complexation mechanism, the different macromolecules interact with each other through such secondary binding forces as Coulombic force, hydrogen bond, van

der Waals force and hydrophobic interaction. Often, the crosslinking is used to increase the extent of mixing of the networks (Bischoff and Cray, 1999). Carboxylic acid groups in PMAA accumulate negative fixed charge density through dissociation when the pH of the swelling medium increases above it pK_a value of 5.5.

The dimension of the hydrogel is given as $20 \times 5 \times 0.2 mm^3$. For the calculation of the swelling ratio, we assume that the PMAA/PVA IPN hydrogel strip with an initial ionizable fixed charge concentration of 1100mM is immersed in a 0.8wt % NaCl aqueous solution until an equilibrium state is attained. The equilibrium swelling of hydrogel is calculated according to the formula of

$$\text{Swelling of hydrogel}(\%) = \left(\frac{W_s - W_d}{W_d} \right) \times 100 \tag{5.2}$$

where W_s and W_d are defined as weights of swollen and dry sates respectively as given by Kim et al. (2004). The numerical results from the simulation of the IPN hydrogel swelling in different pH environments are plotted in Fig. 5.4. The simulated results are qualitatively coherent with the experiment results, although there are some deviations in the swelling ratio within the transition phase. However, the mismatch in the swelling ratio in the transition phase is expected as the swelling is highly dependent on various conditions of the experiment and measurement.

For the investigation of bending mechanism, one ends of the hydrogel is fixed and placed between two electrodes as illustrated by Kim and his colleagues (Kim et al., 2003). When a constant voltage of 15V is applied across the hydrogel, the gel starts to bend towards the negative electrode. The equilibrium bending angle, as calculated in Fig. 5.5, is assumed to be the degree of angle measured from the mid-plane of the hydrogel at vertical position to the tip of hydrogel after deflection. The curvature of the deflected hydrogel is presumed to be uniform. As observed from Fig. 5.5, the value of

the calculated bending angle departs slightly from the data obtained from experiment of Kim and his co-workers (Kim et al., 2003) at pH lower than 3 and pH greater than 10. One must appreciate that the mechanical properties of hydrogels depend on the environmental conditions in which they are tested, as well as the way the mechanical test is conducted and the value are part of the assumptions made. Since PVA is identified as the main contributor to the mechanical strength of the IPN hydrogel (Kim et al., 1999), mechanical properties determined by Fei et al. (2002) for poly(vinyl alcohol)/poly(acrylic acid) (PVA/PAA) are used as reference range. For pH less than 6, a Young's modulus of 3.0MPa is used, and a Young's modulus of 1.35MPa is used for pH greater than 8. As for those pH between 6 and 8, the Young's modulus is assumed to vary linearly. A universal value of 0.43 (Johnson et al., 2004a) is used for the Poisson's ratio in the simulation.

5.2.2.2 Analysis of the Characteristics of Hydrogel at Steady-State

In order to discern the responsive characteristics of diffusive ion species, electrical potential and mechanical deformation of pH-sensitive hydrogels, numerous simulations are carried out at varying pH environment and external electric potential as shown in Figs. 5.6 to 5.9. Those figures disclose the ionic and electric field profiles inside and outside of the hydrogel which can be used to infer the mechanical behavior of the hydrogel. The profiles in the hydrogel and solution are plotted as a function of the distance from the anode.

The configurations of the PHEMA based hydrogel are similar to those mentioned in Chapter 4 or it will be stated otherwise. The dissociation constant $pK_a \approx 5.0$, fixed charge density $c_{mo}^s = 1200\text{mM}$, dry state gel thickness of 400μm and

Young's modulus value that varies with the pH are used for the numerical simulation. For pH less than 5.5, a Young's modulus of 0.29MPa is used, and a Young's modulus of 0.21MPa is used for pH greater than 7.5. As for those pH between 5.5 and 7.5, the Young's modulus is assumed to vary linearly. The ionic strength of the solution is 300mM and it is controlled by adjusting the NaCl concentration in the electrolyte solution.

Figures 5.6, 5.7 and 5.8 show the distributions of the diffusive ions, fixed charge group and electric potential inside and outside the hydrogel as a function of externally induced electric field for three different pH solutions: acidic, neutral and alkaline solutions accordingly. Further, a closer look at the osmotic pressure gives an estimation of the swelling degree and the strain offers the explanation of the bending phenomenal.

It is evident that the concentrations of mobile cations, i.e. the hydrogen (H^+) and sodium (Na^+) ions, in both hydrogel and solution on the anode side decrease as the external electric potential is augmented. In contrast, the concentrations near to the cathode side increase with increasing electric density. The similar behavior is also observed for chloride (Cl^-) ion. As expected, the concentrations of mobile cations are higher in the interior hydrogel than those in the exterior solution. However, the differences in concentrations of mobile cations at the hydrogel-solution interface near to the anode side increase and coexist with the decrease of differences in cation concentrations near to cathode side as the external electric potential augmented. The inverse traits occur to the anion concentration where the differences of concentration between hydrogel and solution are smaller at the anode region than differences determined at the cathode region.

The concentration of fixed charge groups decreases as the system is boosted with higher density of electric field, especially for pH greater than 4. The declining in fixed charge density is linked to the increase in hydration of the hydrogel as the electric field density increases. However, the electrically stimulated swelling degree is considerably smaller than the extent of swelling when the hydrogel is excited by pH. These will be discussed in more detail in upcoming section. Another phenomenal worth noted is the inclining charge concentration away from the cathode in acidic solution as shown in Fig. 5.6(d) which is in contrast to the neutral and basic solution. This will be explored further in following paragraph when the hydrogel is under larger density of electric field.

The differences of electric potential between the hydrogel and solution are more obvious in the neutral and basic solutions as shown in Figs. 5.7(e) and 5.8(e). This is due to the larger amounts of mobile ions diffusing into the hydrogel, creating a larger ion drift (potential of migration) in the hydrogel.

The osmotic pressure is generated from the variation in concentration between the hydrogel and bathing solution. Since there is no electric gradient generated to alter the distribution of concentration for the condition without external electric field, it is expected that the osmotic pressure will be the same on both sides of cathode and anode. As the electric potential across the hydrogel rises, the gradient of the osmotic pressure increases concomitantly due the redistribution of ion. The larger osmotic pressure near to the anode as compared to the cathode side is responsible for locally different swelling degrees which collaterally induce the bending mechanism of the hydrogel in a solution with external electric field. For the strain plot as a function of coordinate from the anode in Fig. 5.6(e), it is self-explanatory that the applied voltage has altered the swelling characteristic of the hydrogel where the boundary region of the hydrogel near

to the anode undergoes swelling process whereas at the cathode side the hydrogel shrinks. However, in pH solution larger than 5, the large swelling and bending mechanisms occur coinstantaneously. Both sides of the boundary regions undergo swelling state but in different degrees of magnitudes, as shown in Figs. 5.7(f) and 5.8(f). The dissimilarity in strain at both sides of the hydrogel boundary proves the existence of the bending mechanism.

From Fig. 5.9, we delve into the typical responses of mobile ions, fixed charge groups and eventually mechanical deformation of the hydrogel under the control of high density electric field. The H^+ ion concentration in Fig. 5.9(a) is normalized by it corresponding boundary concentrations. It is profound that the concentration differences between the interior hydrogel and surrounding solution are larger for higher pH due to the release of hydrogen ions from the ionization of the carboxyl groups bound to the hydrogel network. The concentration profiles for diffusive cations and anions also show the resemblance trend due to the requirement of larger amount of cations to neutralize the negatively charged group. The influx of anions is the concomitant effects of the migration of cations into the hydrogel. As remarked from Fig 5.9(d), the fixed charge densities remain consistent for hydrogels bathed in solutions of pH7 and pH12. In contradiction, the fixed charge density decreases if plotted from the anode side to cathode side in pH3 solution. This nonuniformity in the fixed charge distribution can be related to the distribution of hydrogen ion in the hydrogel. As constant electric potential is applied across the hydrogel, the H^+ ions and mobile ions are attracted to the cathode or anode, while the pendent charge groups remain fixed to the network matrix (Kurauchi et al., 1991; Shibayama and Tanaka, 1993). This results in larger amount of the fixed charge groups gather near to the anode as compare with the region near to the cathode.

On the anode side of the system, higher negativity is induced (hyperpolarisation) whereas depolarization occurs on the cathode side when an electric potential is applied across the system. The hyperpolarisation and depolarisation are responsible for the redistribution of spatial profiles of the ionic concentration. The larger concentration gaps between the interior hydrogel and surrounding solution result in higher electric potential difference at the anode side. These are also the reason leading to the higher osmotic pressure at the anode than at cathode. As a consequence, differences in local swelling degree develop across the hydrogel as can be interpreted from the slope of the strain value in Fig. 5.9(f). Further, the figure also implies that the polyacids hydrogel is bending towards the cathode side as shown in Fig. 5.1. As larger electric potential is applied across the hydrogel, the hydrogel swells slightly while making distinct degree of bending angle as observed from Figs. 5.10 and 5.11.

At pH lower than dissociation constant pK_a of carboxylic acid groups, i.e. 5.0, there are limited amount of cations and their pairing anions inside the hydrogel as noticed from Fig. 5.6. As the solution rises to high pH condition, more carboxylic acid groups dissociate and become negatively charged groups, $RCOO^-$. More cations diffuse into the hydrogel matrix due to conservation of electroneutrality. The increases of concentration within the hydrogel widen the concentration differences at hydrogel-solution interface between the anode and the cathode sides, leading to larger bending of the hydrogel strip. There are precipitous increases in bending curvature of the hydrogel within the range of pH4 and pH7 where the ionizations of carboxyl groups are active. These phenomenological attributes are summarized in Figs. 5.10(b) and 5.11(b). In the following sections, key parameters that govern the bending and swelling characteristics of charged hydrogel, if an electric field is imposed across their thickness at different level of pH equilibrium, are further identified.

5.3 PARAMETRIC STUDIES OF HYDROGEL PROPERTIES AND ENVIRONMENTAL CONDITIONS

The presently developed MECpH model for pH-responsive hydrogels is able to simulate the concentration distributions of all diffusive ionic species, as well as the electric-potential distribution and mechanical deformation of the hydrogels, in response to changes of pH of the bath solution coupled with ever-changing electric voltage. Recent methods of preparing polymer gels make it possible for the fabrication of the hydrogels with a wide range of properties such as structure, Young's modulus, degree of cross-linking, softening point, etc. It is thus also rational to investigate separately the effects of the various physical factors by means of systematically and independently varying the various properties while keeping the other conditions constant. These investigations will be carried out in similar conditions and hydrogel configurations to precedent simulations in Section 5.2.2.2, the hydrogel is orientated in parallel to the electrodes in controlled aqueous solution as shown in Fig. 5.1. A constant electric field is externally applied across the system. Both environmental pH and electric potential have been studied extensively as they are the external electrochemical stimuli that can be easily modulated to control the deformation of hydrogel.

5.3.1 Influences of the Ionizable Fixed Charge Concentration of Hydrogel

The total molar of fixed charge groups concentration at preparation stage of the hydrogel c_{m0}^{s}, which can be determined from titration procedure, are investigated to

ascertain it relationship with swelling deformation of hydrogel strip. The dependence of swelling behavior of hydrogel on the c_{m0}^{s} is shown in Figs. 5.12 to 5.16, correlated with various combination of electrochemical stimuli, surrounding pH and externally applied electric field.

The hydrogel starts to swell when the surrounding pH solution is higher than pH4 and reaches its maximum stretching around pH7. The transitional large volume expansions are attributed to the ionization of the charged groups bound to the hydrogel networks. The ionization process of the charged groups also plausibly explain the increase in volume swelling as the total ionizable charge groups per volume of solid gel increase. The swelling behaviors still prevail even under high intensity electric potential of 0.5V are shown in Fig. 5.12(a). There are some dissimilarity in the bending character of the hydrogel since the increase in total ionizable charge groups does not always corresponds with greater bending curvature, as observed from Fig. 5.12(b). At low pH solution, augmenting the total ionizable charge groups increase the bending curvature of the hydrogel strip. However, the bending curvature decreases when increasing the amount of total ionizable charge groups if the hydrogel is functioning in high pH solution. As depicted in Figs. 5.13 and 5.14, these trends become more obvious when the applied electric potential is increased further. The applied electric field intensity is believed to be the limiting factor of the difference in strain energy at both hydrogel-solution interfaces.

It should also be noted that the bending curvature can be linearly controlled by the intensity of the applied electric field if the bathing solution is an acidic medium. While in basic bathing solution, the increases of bending curvature gradually slow down as the electric potential increases. The application of electric potential across the hydrogel other than altering the distribution of the ionic species and henceforth

inducing hydrogel bending, also acts as catalyst boosting the swelling degree of the hydrogel immersed in basic bathing solution. As for the hydrogel equilibrated in acidic solution, the volume swelling increases as the electric potential is elevated but starts showing sign of contraction when the applied electric potential is higher than 0.6V. The predicted results are plotted in Figs. 5.13(a) and 5.14(a).

Figures 5.15 and 5.16 show the deformation characteristics of the hydrogel as a function of total ionizable charge groups for acidic and basic solutions respectively. Volume expansion of hydrogel multiplies monotonically with addition of total ionizable charged groups when submerged in acidic solution. On the other hand, the hydrogel shows evidence of slowing down in the swelling magnitude in basic solution as visible in Figs. 5.15(a) and 5.16(a). In strong acidic condition, the bending curvature of the hydrogel increases linearly with increasing total ionizable charge groups; whereas in strong basic solution, the bending angle increases significantly with the increase of ionizable charge groups. After the ionizable charge concentration reaching the optimal value of around 600mM, the bending gradually shows sign of reverse bending.

The concentration of the counter ion in the hydrogel increases with the concentration of the ionic group even if the concentration of the outer solution remains constant. The bending of the hydrogel, however, does not increase after certain angle of deflection because the free mobile ions do not increase as the condensation of counter ion occurred. As a result, the osmotic pressure did not change largely. This explains why the redistribution of the ionic concentration in the hydrogel, due to ionic transport, played an important role in determining the deformation mechanism.

5.3.2 Influences of the Young's Modulus of Hydrogel

Figures 5.17 to 5.21 demonstrate the degree of swelling and bending curvature of the hydrogel as a function of Young's modulus of the hydrogel strip for various pH solutions and applied electric potential. The Young's modulus property is directly influenced by amount of crosslinkers added during polymerization process. The Young's modulus can be lower by reducing the portion of the cross linker. High percentage of cross-linking agents will obstruct the motility of the network matrices, thereby strengthen the Young's modulus.

Figure 5.17(a) shows that the abrupt volume transition range is the same whether the system with or without an externally applied electric field, i.e. spanning from pH4 to pH7. Below this range, the swelling degree is trifling as the present of ionized groups is inappreciable; whereas above this range most of the carboxylic acid groups are ionized and volume swelling does not change much. The hydrogel also shows an impetuous stepping up of bending in a narrow range but the range is shifted to pH lower than expected for volume swelling, i.e. pH3 to pH6 as revealed in Fig. 5.17(b).

As the Young's modulus increases, the hydrogel becomes more restricted from stretching volumetrically even with more intensified electric field. These are established evidence in both strong acidic and basic solutions especially in the acidic solution as demonstrated in Figs. 5.18(a) and 5.19(a). On the other hand, the bending curvature always increases linearly with applied electric potential for hydrogel bathed in acidic solution whereas hydrogel equilibrated in basic solution shows gradual insensitivity towards electric field intensity as the externally applied electric potential icreases. The bending behaviors are plotted quantitatively in Figs. 5.18(b) and 5.19(b).

The downtrend of Young's modulus from the given experimental value E_0, i.e. $E / E_0 < 1$, causes a sharp increase in swelling and bending of hydrogel as shown in Fig. 5.20. As discussed before, the Young's modulus can be lowered by reducing the density of crosslinkers while keeping other moieties constant. By reducing the crosslinker ratio, high swelling high bending hydrogel can be prepared but at the cost of structural stability. If the Young's modulus is a large value, the deformation of the hydrogel will thence subjected to more confinement from the rigidity of the hydrogel network, whether it is stimulate with strong acidic or basic solution as shown in Figs. 5.20 and 5.21. However, the behavior of hydrogel in the acidic solution shows differenced if the hydrogel is of low Young's modulus property (highly flexible) where the decreases of Young's modulus results in large degree of swelling but small in bending. These could be due to the concomitant occurence of swelling and bending that influence each other which are clearly demonstrated in the present case. As the hydrogel is in precipitous increasing of volume at low Young's modulus, the fixed charge groups become more sparsely distributed. At certain point, the hydrogel exists in large swollen state in which the distribution of fixed charge groups gradually becomes dominant factor and subside the influence of the Young's modulus. These phenomena have been shown in real experiments of Fei et al. (2002).

5.3.3 Influences of the Initial Thickness of Hydrogel

In the process of miniaturizing the specimen, such as the hydrogel strip for the purpose of fitting into microscale system, the deformation behavior of the hydrogel might differ from the bulk condition. Figs. 5.22 to 5.26 investigate the dominance of

the thickness of hydrogel before bathing in solution, i.e. a dry gel thickness, of 300mM NaCl solution and room temperature of 25°C. Swelling degree of the hydrogel is defined in terms of hydration H, volumetric ratio of fluid V_f to solid V_s, in current studies and the same initial hydration for each sample hydrogels is assumed.

From Figs. 5.22(a) to 5.26(a), it is self-explanatory that changes in hydration of hydrogels are predicted to be relatively small as the diameters of hydrogel varies. Even though that the external electric field does amplify the swelling equilibrium of the hydrogel, it is only to a small extend. These concluding behaviors are clearly expressed in Figs. 5.25(a) and 5.26(a). One of the reasons is that the osmotic pressure is the main driving force in the swelling mechanism. As the concentration in the bathing solution is kept unchanged in all case and the other hydrogel properties (e.g. total ionizable charged groups and Young's modulus) are constant values, the osmotic pressure that depends on the concentration gradient at the boundary between the hydrogel and the bath solution should remain constant.

As a polyacids hydrogel, the hydrogel tends to experience greater swelling pressure on the side near to anode than that on the side near the cathode, hence, the hydrogel tend to bend towards the cathode when subjected to electric potential. Unlike the volume swelling, the degree of bending is notably affected by the changes of thickness of the hydrogel strip, as proved by the simulation results in Figs. 5.23(b) to 5.26(b). The average curvature of the hydrogel in equilibrium state decreases with the thickening of the hydrogel strip. It is noted that the thinner the hydrogel strip the larger the flexure of the curvature (Fei et al., 2002; Zhou et al., 2002). Since the osmotic pressure remains unchanged, we can infer that the thicker the strip the smaller the strain gradient at the two boundaries of the hydrogel. In other words, the larger the thickness of the hydrogel the harder the strip tends to bend with the same driving force.

5.3.4 Influences of the Ionic Strength of Bath Solution

The effects of the ionic strength of the bathing solution on the deformation behavior of hydrogel in response to electric stimuli are accounted by varying the concentration of NaCl and plotted in Figs. 5.27 to 5.31.

From Fig. 5.27, it is apparent that PHEMA based hydrogel swelling is scant, still exist in compact and hydrophobic form, at pH values lower than 4 regardless of electrolyte concentration in the outer solution. In spite of that, the hydrogel starts to show its sensitivity towards the concentration of the surrounding solution as the pendent ionizable groups start to deprotonate. In this region of high pH solution, the magnitude of the equilibrium swelling increases with the decrease of the medium ionic strength. That is not the case when it comes to the bending mechanism. At high pH environment, the bending degree of the hydrogel strip increases with increasing ionic strength of the bathing medium, which becomes clearer when cross-referring with the plotting of the bending curvature versus the ionic strength of the bathing solution of Fig. 5.31(b).

Figures 5.28 and 5.29 study the impact of surrounding ionic concentration on the deformation behavior of the PHEMA based hydrogel as a function of electric field intensity for both acidic and basic environments. Samples were equilibrated separately in acidic and basic solution, and both samples show identical behavior at large where the degree of swelling increases with applied electric potential. Since the electric potential forces are exerted across the hydrogel, bending of the PHEMA hydrogel towards the cathode is expected. If the bathing solution is an acidic solution instead, a linear increase in the degree of swelling with applied electric potential is observed.

While the bending curvature in basic solution will be in full force at initial stage but it gradually flatten out as the applied voltage intensified.

As shown in Figs. 5.30(a) and 5.31(a), the hydrogels in both acidic and basic solutions experience larger swelling degree of swelling in lower ionic concentration and decrease sharply with additional ionic concentration. The transitional ionic concentration is reasonably estimated at 900mM. In general, the increase of mobile ions in the surrounding solution leads to decreases of osmotic pressure at the hydrogel-solution interface and hence limits the swelling force. In spite of that, the uniqueness in the behavior of the hydrogel equilibrated in acidic solution differs itself from the basic condition. As observed from Figs. 5.30(a) and 5.31(a), the hydrogel show a transitional trend in it swelling equilibria at ionic concentration of approximately 900mM. For the acidic swelling medium, the shrinking are steeper as the intensity of electric potential increases when the ionic strength changes coinstantaneously from low to higher level, whereas the rate of shrinking of hydrogel in basic medium is almost the same under different external electric potential. Another notable characteristic is the changes in volume dilations are not clearly observable when the ionic strength is approximately higher than 1200mM for hydrogels bathed in acidic solution. The bending curvature of the hydrogel also experiences an optimal bending at approximately 900mM if the swollen medium is an acidic solution. In other words, the bending curvature decreases gradually for ionic concentrations less than 900mM and also for ionic concentrations above 900mM. As described above, the increase of the ionic concentration in solution induces the increase of the free ions moving from the surrounding solution into the hydrogel network. As a result, the bending curvature of the hydrogel could increase. However, if the ionic strength of the solution is greater than the optimal concentration, the shielding effect of the polyions by the ions in the ionic solution occurs, which leads

to reduction in the electrostatic repulsion of the polyions by the screening of fixed charges and bring about a decrease in the degree of bending (Flory, 1962). As for the case where the hydrogel is bathed in basic solution of Fig. 5.31, the gradual toning down of bending curvature with lower NaCl concentration could be attributed to a more highly swollen state.

5.3.5 Influences of the Ionic Compositions of Bath Solution

Figures 5.32 to 5.35 show the influences of the compositions of bathing solution on the deformation behaviors of the PHEMA hydrogel in response to chemical and electric coupled stimulation. The bathing solution is assumed to be primarily consisting of electrolyte solutions with varying ionic valencies, i.e. NaCl, Na_2SO_4 and $CaSO_4$, preserved at constant ionic strength of 300mM and room temperature (25°C).

In general, the counterions decrease concurrently with the increase of ionic valencies, which leads to the decrease in osmotic pressure and thus the swelling degree (Homma et al., 2001). On the other hand, the bending of hydrogel which is induced from different in localized swelling also depends on the valence of the ions (Kurauchi et al., 1991).

Figures 5.32(a) and 5.33(a) show the degree of swelling of PHEMA hydrogels as function of applied electric potential in three different types of aqueous solution: NaCl, Na_2SO_4 and $CaSO_4$ electrolyte solution. In general, swelling equilibria are improved by increasing the voltage at the two electrodes. Nevertheless, the presences of different types of salt in the aqueous solution surrounding the hydrogel also post

some deterministic effects on the swelling equilibria. As observed from the figures, Na_2SO_4 salt solution provides an ideal medium for larger swelling degree for both acid and basic conditions. As discussed in Chapter 4, the concentration of sodium ion needed in Na_2SO_4 salt solution is lower compared to NaCl salt solution if both aqueous solutions are to maintain under the same ionic strength. That explains the occurrence of higher degree of swelling in the former condition. At low electric field intensity, lesser amount of multivalent (Cu^{2+}) than monovalent (Na^+) counterions are required to neutralize the charged groups fixed to the hydrogel matrix, therefore, smaller swelling degree is expected. Since the pH is lower than the dissociation constant, the ionizable charged groups still exist in the form of RCOOH. Therefore, ion diffusion is the rate limiting process. As the applied electric potential intensified, more mobile ions diffuse into hydrogel. However, multivalent ions are facing with stiffer competition from other ionic species to enter the hydrogel because of the repulsive electrostatic force. For example, one mole of divalent sulfate ion (SO_4^{2-}) will be accompanying by one mole of divalent copper ion (Cu^{2+}) or two mole of monovalent sodium ion (Na^+) into the hydrogel to conserve the electroneutrality. The later combination has a greater concentration gradient at the hydrogel-solution interface, which explains the steeper growth in the swelling degree. When the pH environment is higher than the dissociation constant, the fixed charge group is ionized and forms $RCOO^-$. Coinstantaneously, counterions will diffuse into the hydrogel to neutralize the fixed charged groups or accompanied with the co-ions. The application of electric potential accelerates the drifting of free ions. As a multivalent ion, copper ion reaches it condensation sooner than the monovalent sodium ion. The osmotic pressure and hence swelling equilibrium does not change substantially after counterions reach condensation stage.

The electric field applied across the hydrogel amplifies the concentration gap between the cathode and anode sides of hydrogel-solution interfaces. Consequently, the average curvature of the hydrogel in acidic solution increases proportionally with applied electric potential as depicted in Fig. 5.32(b). On the other hand, MECpH model has predicted a dominant dependent of bending curvature on swelling equilibrium of hydrogel when the medium is a basic solution. As a result, the bending rate tend to slow down as swelling degree get larger with the increase of applied voltage. The relationship can be observed from Fig. 5.33.

The sharp decrease in the plots of the swelling degree versus bathing ionic strength in Figs. 5.34(a) and 5.35(b), with various compositions of salt solution under applied voltage of 0.5V, shows the high dependence of salt concentration. For the PHEMA hydrogel equilibrated in acidic solution, the swelling degree becomes insignificant after reaching a transitional value of 1200mM which corresponds with the density of ionizable charged groups of the hydrogel regardless of the type of electrolyte solution. Likewise, the swelling volume flat off to a certain value after an initial sharp decrease when the hydrogel is surrounded by basic environment. Nonetheless, the copper sulfate aqueous solution shows a slower decrease with ionic strength in comparison with the sodium chloride and sodium sulfate aqueous solutions.

When an electric field is applied across the hydrogel, the hydrogel starts to bend toward the cathode. For hydrogel samples in acidic solution, there is an abrupt change in the average curvature after the optimal ionic strength is obtained and the curvature does not change much even the ionic strength increases as revealed in Fig. 5.34(b). On top of that, different salt compositions give different maximum values of bending curvature which depends on the valence of the counter ions (Kurauchi et al., 1991). In basic medium, the bending curvature increases gradually which contrast to

the precipitate increasing in acidic medium as shown in Fig. 5.35(b). Once again, swelling degree does impose it influence in the bending curvature of the hydrogel, hence it is a counterbalancing process before the steady state is attained.

5.4 DISCUSSIONS AND CONCLUSIONS

A charged crosslinked hydrogel swollen in aqueous solution can perform three types of deformations under a constant electric potential, namely shrinking, swelling and bending. The quantitative and qualitative deformations depend on the factors including environment pH, ionic strength and composition of solution, chemical nature of fixed charge groups, Young's modulus which can be correlated directly with crosslinking density, and initial dimension of the gel.

Generally, the swelling or shrinking of the hydrogels depends on the balance of the dissociation/association state of ionic groups bound to the backbone of the polymer networks. If the pendent ionizable groups are of weak-acid group, these hydrogels swell at pH higher than the pK_a value, and shrink at pH lower than the pK_a value. The large changes in volume are results of the development of a large osmotic swelling force in the presence of the ions.

The bending and flapping behaviors are considered to be a general property of charged hydrogels in the presence of externally applied voltage. It is generally believed that the characteristic mechanical deformation of a charged polymer hydrogel under an electric field is attributed to the localized swelling of the hydrogel where expansion is developed near the positive electrode and contraction near the negative electrode if the

hydrogel contains weak-acidic pendent groups as elucidated in Fig. 5.1, and the opposite observation for hydrogel with weak-basic pendent group.

It is shown that, when an electric field is applied on an anionic hydrogel swollen in the aqueous solution, the ion concentration is redistributed in both hydrogel and swelling medium. Consequently, the osmotic pressure differences developed within the hydrogel produces measurable difference in swelling degree. Therefore, it is strongly believed that the voltage induces the shift of ions and concomitant expansion of one side of the hydrogel when the osmotic pressure increases and contraction of the other sidewhen the osmotic pressure decreases that are not observable for conditions without applied voltage. The system becomes more complex in nature when considering the dissociation reactions of fixed charge groups where the reversible protonization-deprotonization reactions take place in the system.

The numerically computed profiles of the concentration of ionic species, electric potential, fixed charge density, osmotic pressure and strain for several configurations of hydrogel properties and surrounding conditions enable us to better understand the causes and effects of experimentally observed nonlinear behaviors, such as the volume transition, bending mechanism and shift of mobile ion.

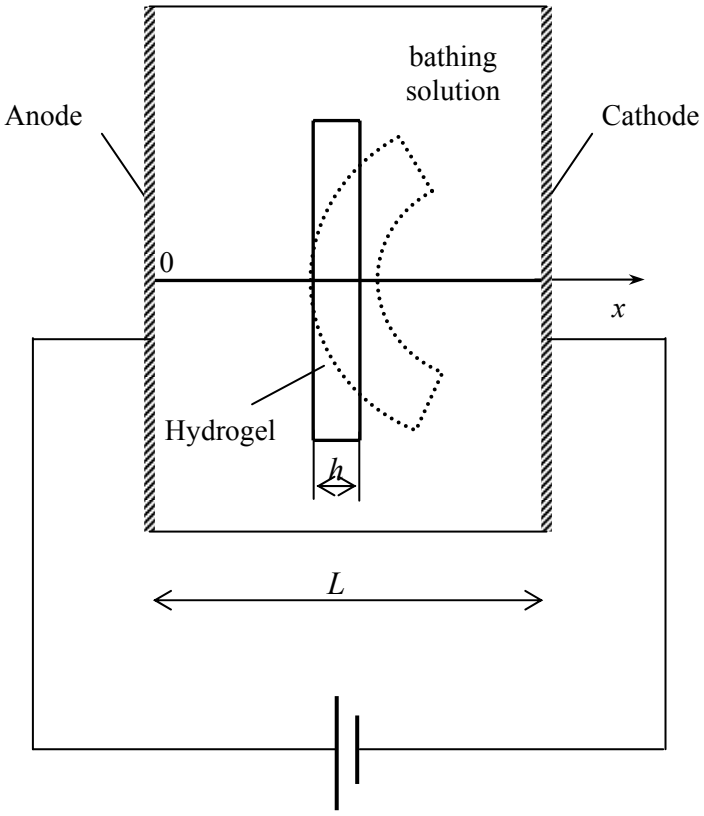

(a)

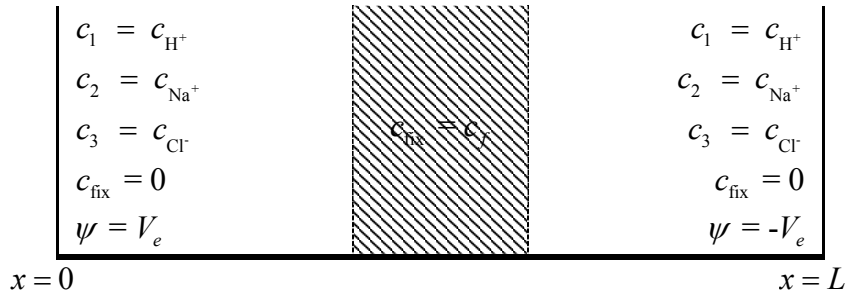

(b)

Figure 5.1 (a) Schematic illustration of the polyacidic (anionic) hydrogel swollen in aqueous solution under the influence of external DC electric current and (b) boundaries conditions for the numerical solution.

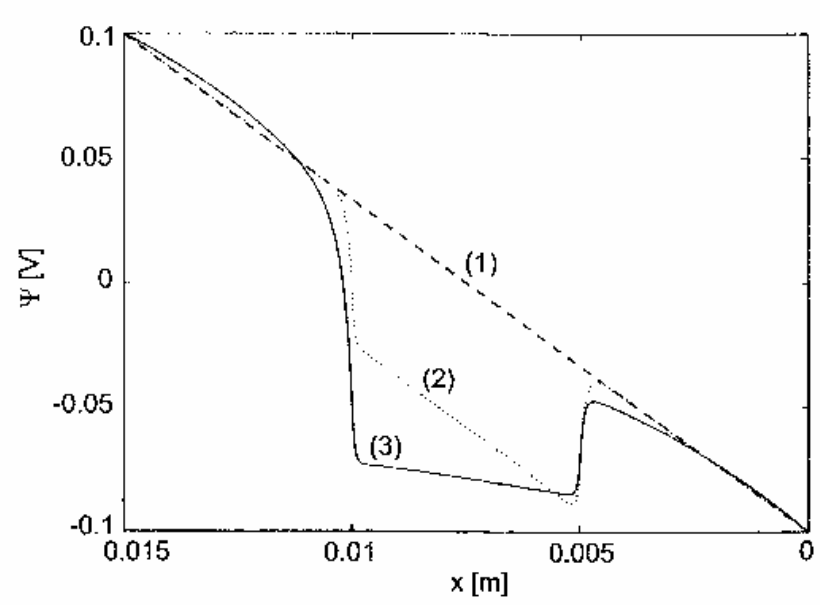

(a)

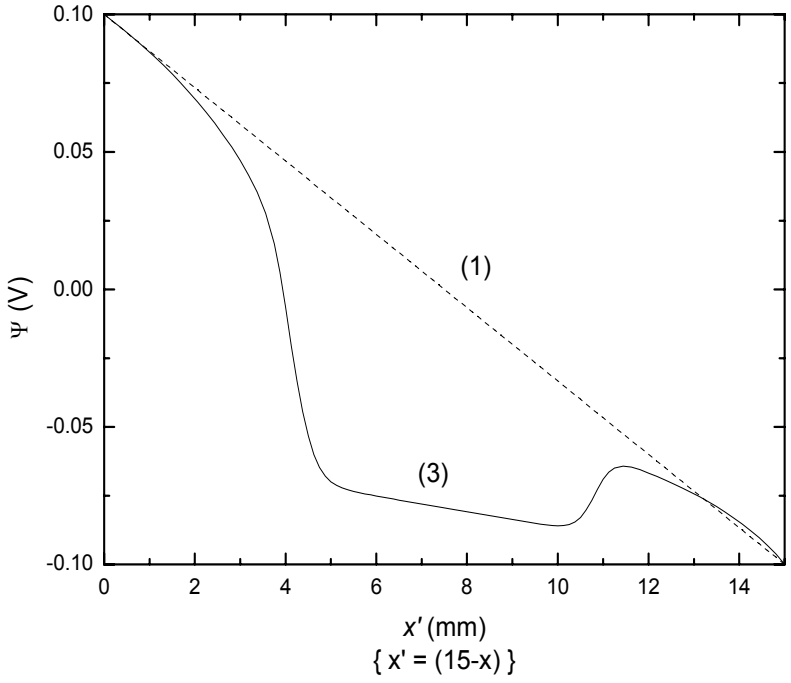

(b)

Figure 5.2 Comparison of electrical potential in the gel and bathing solution due to applied external electric field between (a) stabilized space-time FEM (Wallmersperger, 2001a) and (b) Hermite Cloud meshless method (Li, 2003).

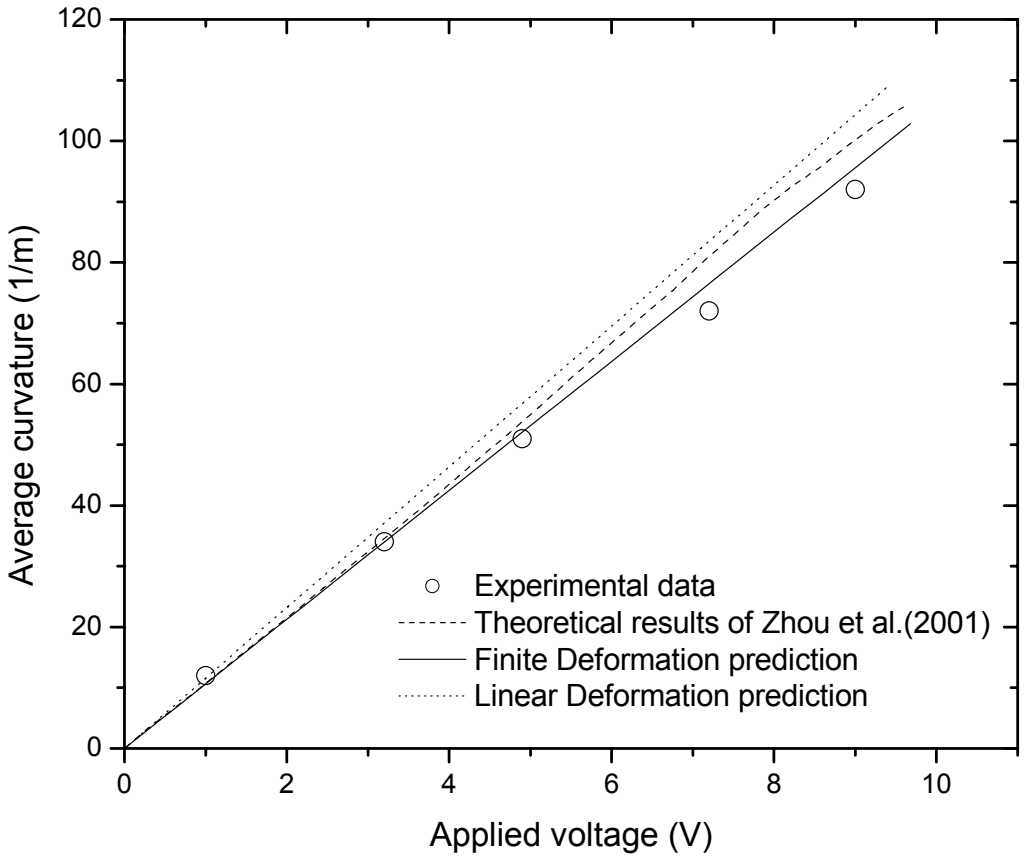

Figure 5.3 Comparison of the finite and linear deformation results of MECpH model with experimental data and theoretical results of Zhou et al.(2001).

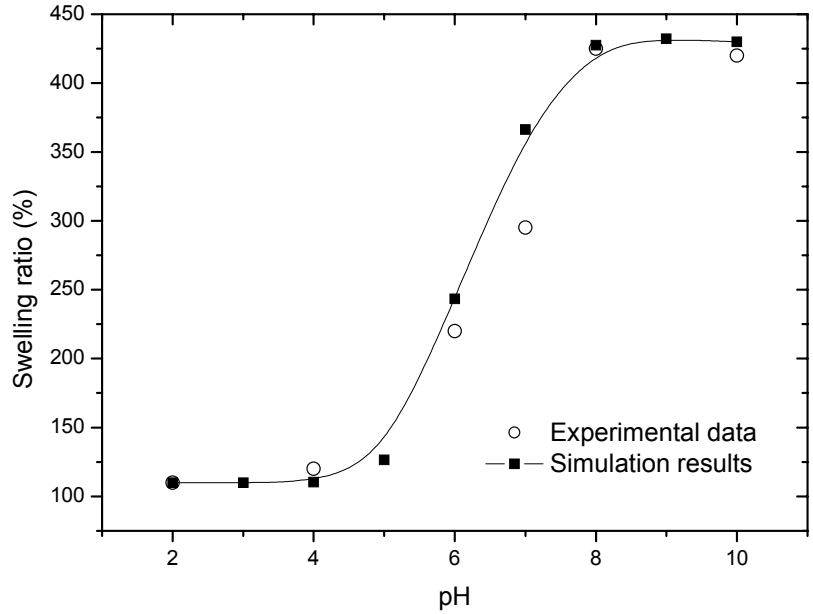

Figure 5.4 Comparison between simulation results and experimental data (Kim et al., 2004) for swelling ratio of PMAA/PVA IPN hydrogel as variation of pH environment.

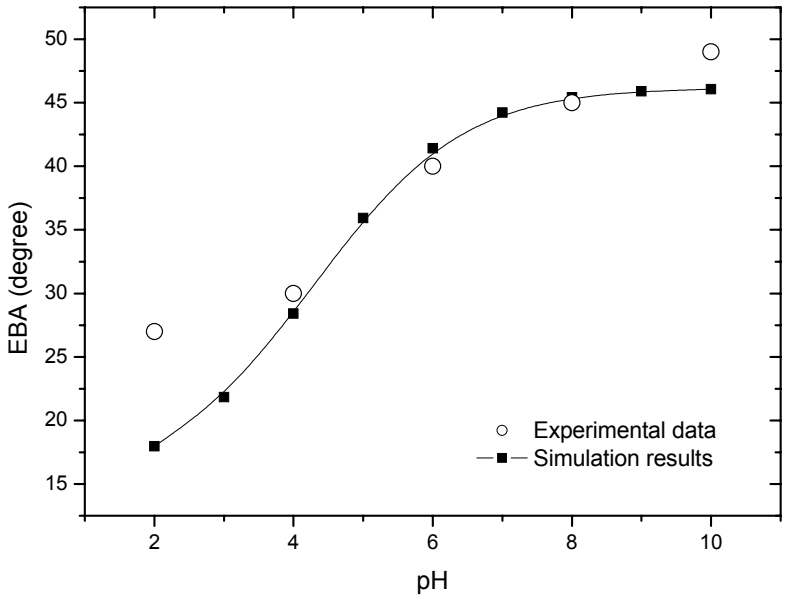

Figure 5.5 Simulation versus experiment (Kim et al., 2004) for equilibrium bending angle of PMAA/PVA IPN hydrogel as a function pH environment when constant voltage of 15V is applied across the hydrogel strip.

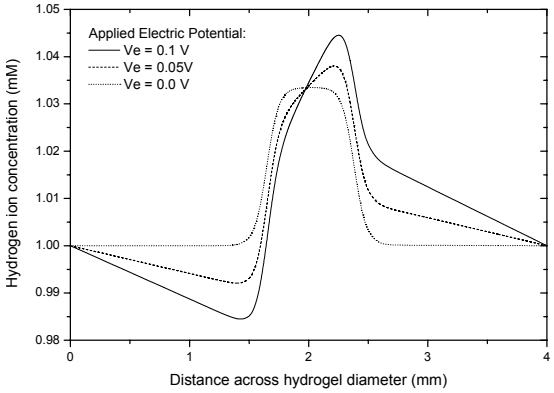

(a) Hydrogen ion (c_{H^+})

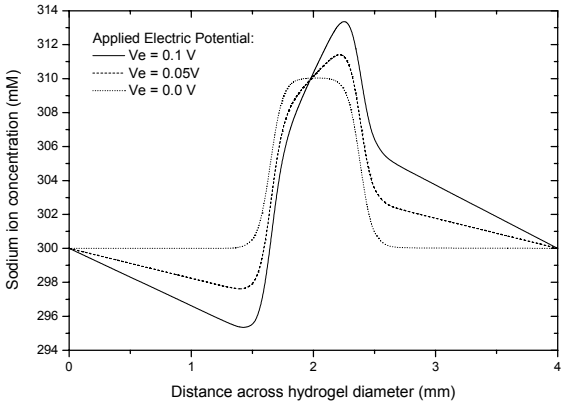

(b) Sodium ion (c_{Na^+})

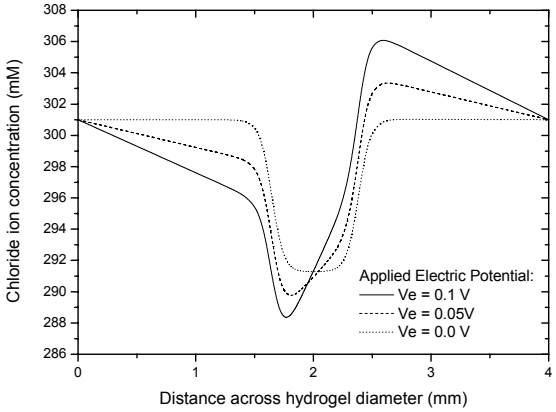

(c) Chloride ion (c_{Cl^-})

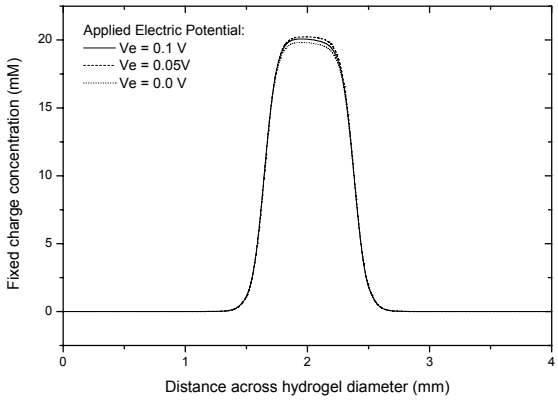

(d) Fixed charge group (c_f)

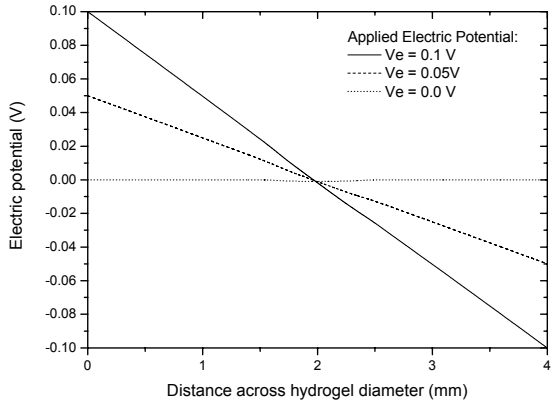

(e) Electric potential (ψ)

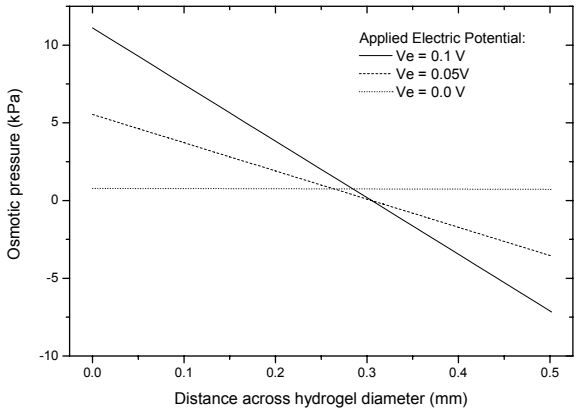

(f) Osmotic Pressure (P)

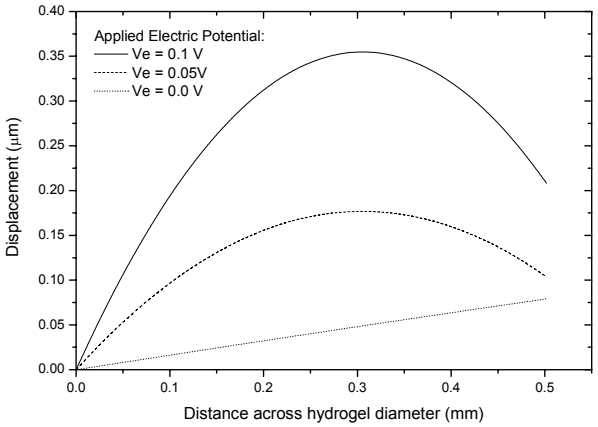

(g) Displacement (u)

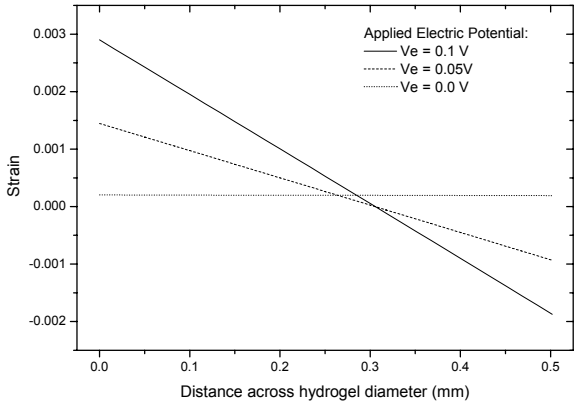

(h) Strain ($\varepsilon_{elastic}$)

Figure 5.6 Profiles of c_{H^+}, c_{Na^+}, c_{Cl^-}, c_f, ψ, P, u and $\varepsilon_{elastic}$ as a function of applied electric potential V_e. The PHEMA based hydrogel is equilibrated in an acidic medium of pH3 with NaCl added to control the ionic strength.

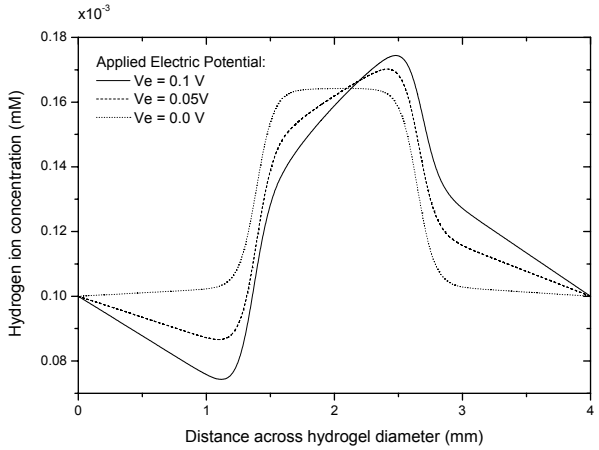

(a) Hydrogen ion (c_{H^+})

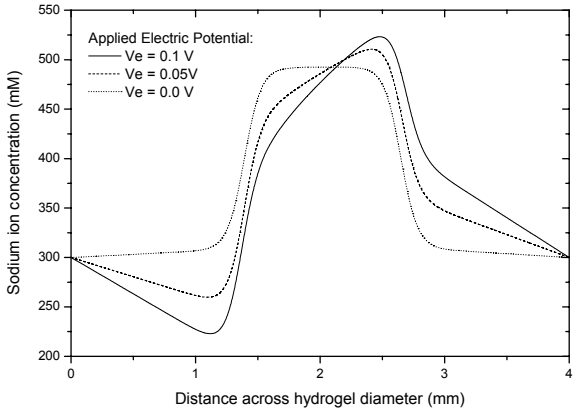

(b) Sodium ion (c_{Na^+})

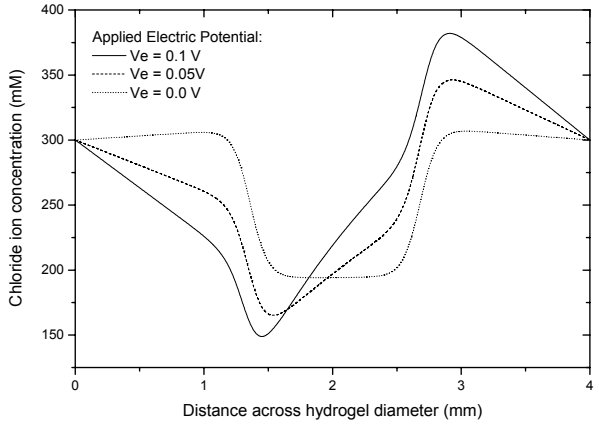

(c) Chloride ion (c_{Cl^-})

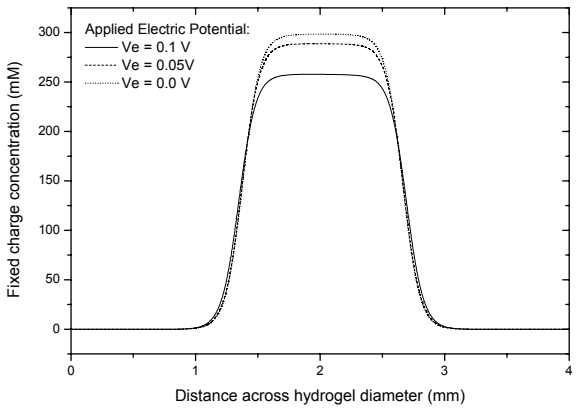

(d) Fixed charge group (c_f)

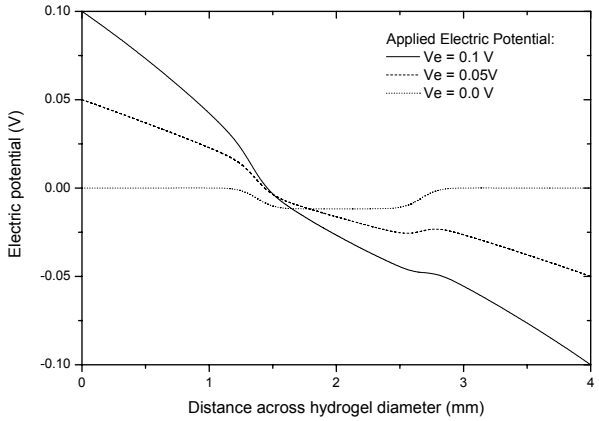

(e) Electric potential (ψ)

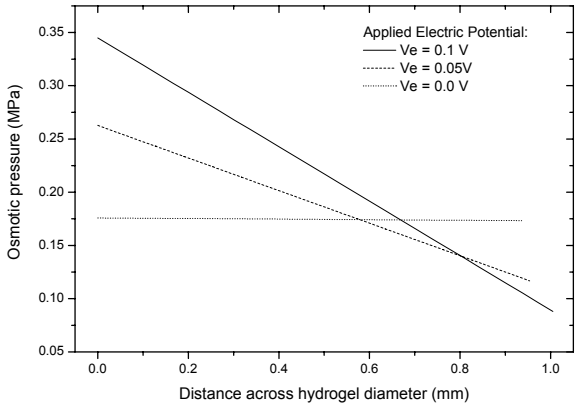

(f) Osmotic Pressure (P)

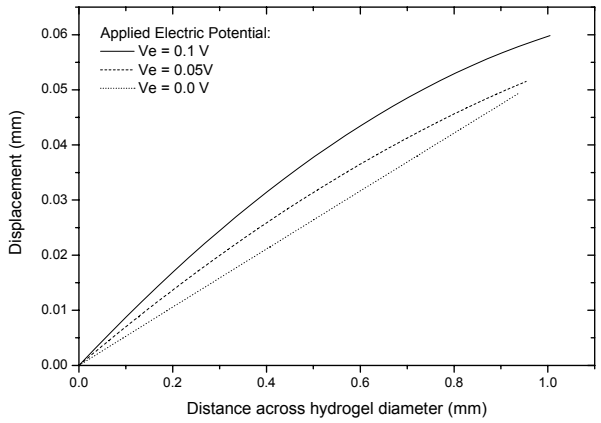

(g) Displacement (u)

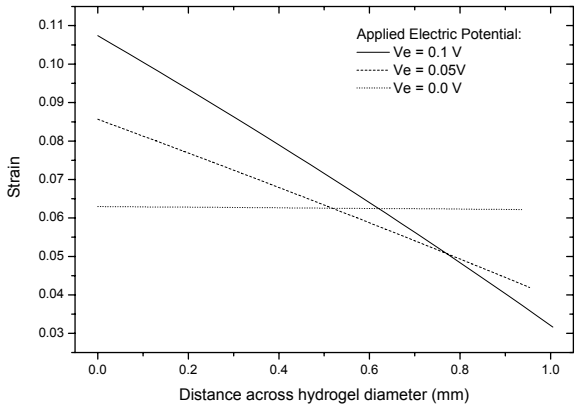

(h) Strain ($\varepsilon_{elastic}$)

Figure 5.7 Profiles of c_{H^+}, c_{Na^+}, c_{Cl^-}, c_f, ψ, P, u and $\varepsilon_{elastic}$ as a function of applied electric potential V_e. The PHEMA based hydrogel is equilibrated in an neutral medium with NaCl added to control the ionic strength.

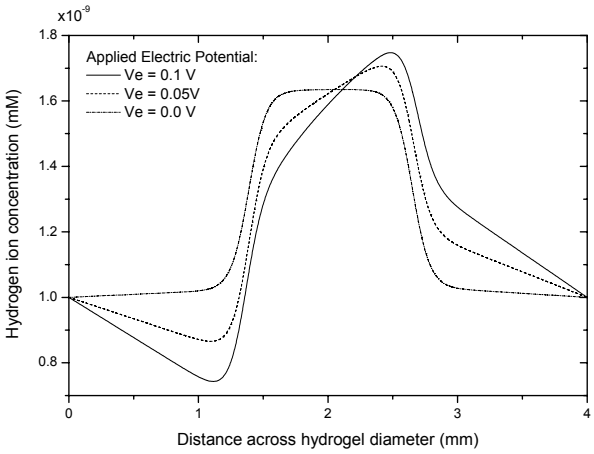

(a) Hydrogen ion (c_{H^+})

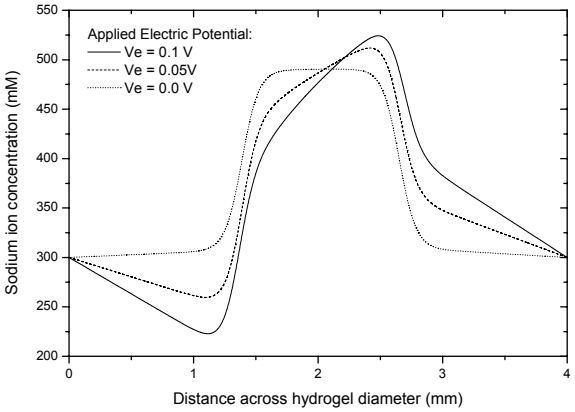

(b) Sodium ion (c_{Na^+})

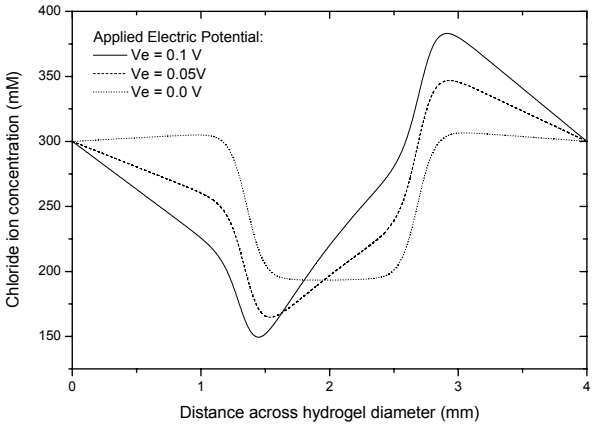

(c) Chloride ion (c_{Cl^-})

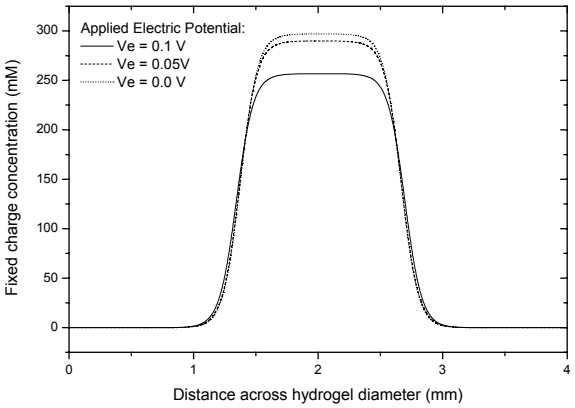

(d) Fixed charge group (c_f)

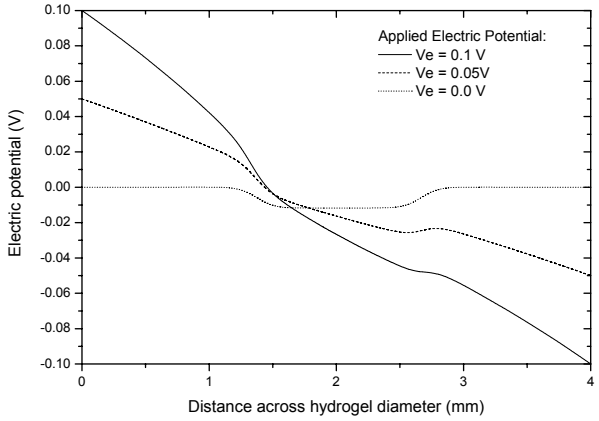

(e) Electric potential (ψ)

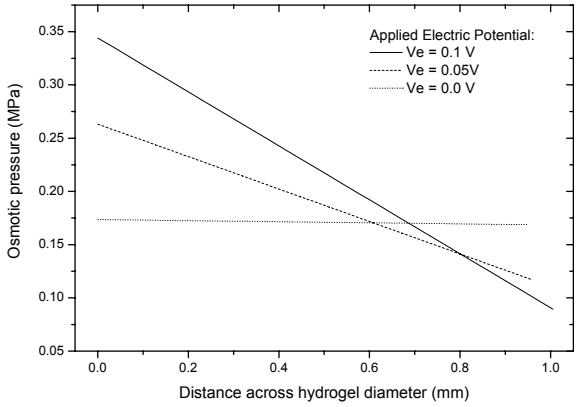

(f) Osmotic Pressure (P)

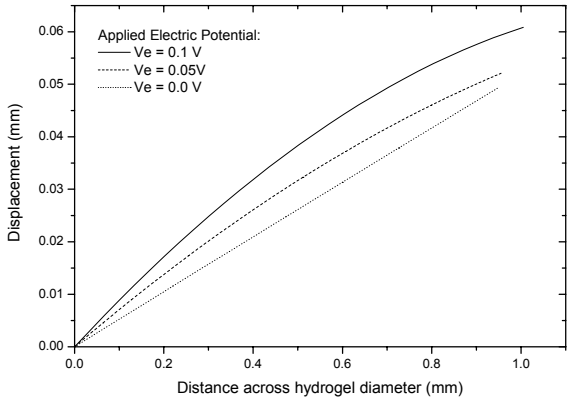

(g) Displacement (u)

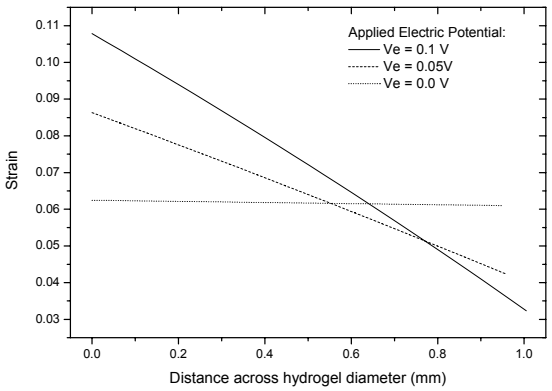

(h) Strain ($\varepsilon_{elastic}$)

Figure 5.8 Profiles of $c_{H^+}, c_{Na^+}, c_{Cl^-}, c_f, \psi, P, u$ and $\varepsilon_{elastic}$ as a function of applied electric potential V_e. The PHEMA based hydrogel is equilibrated in a basic medium of pH12 with NaCl added to control the ionic strength.

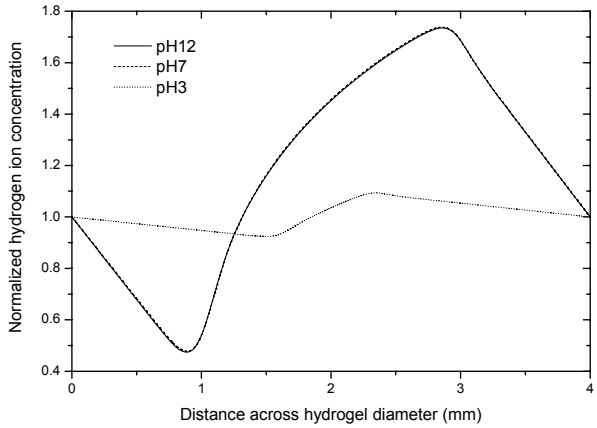

(a) Hydrogen ion (c_{H^+})

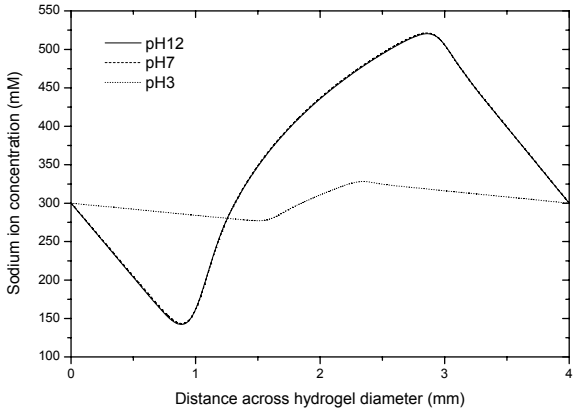

(b) Sodium ion (c_{Na^+})

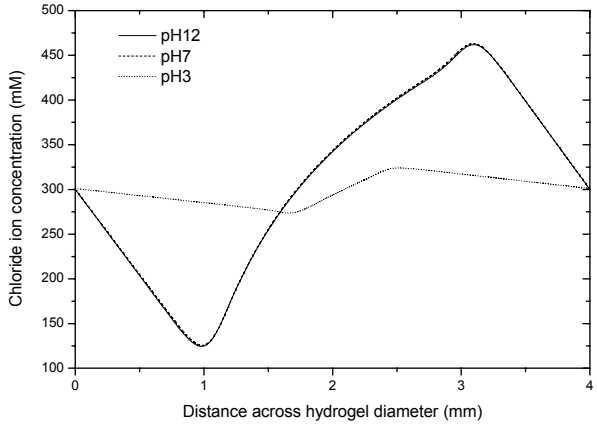

(c) Chloride ion (c_{Cl^-})

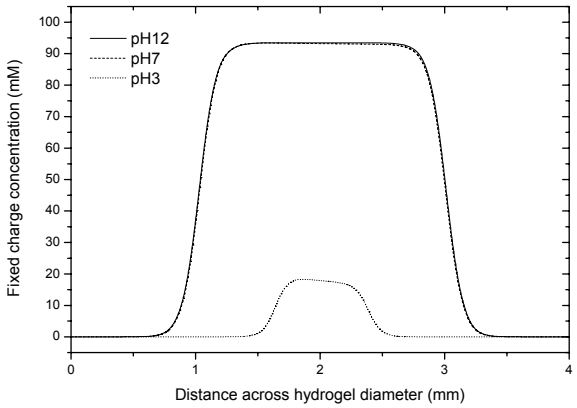

(d) Fixed charge group (c_f)

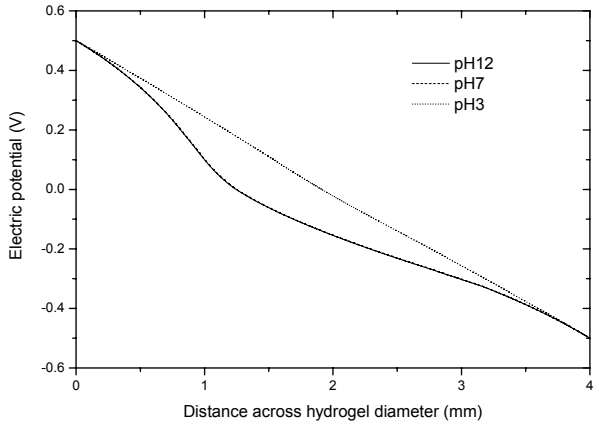

(e) Electric potential (ψ)

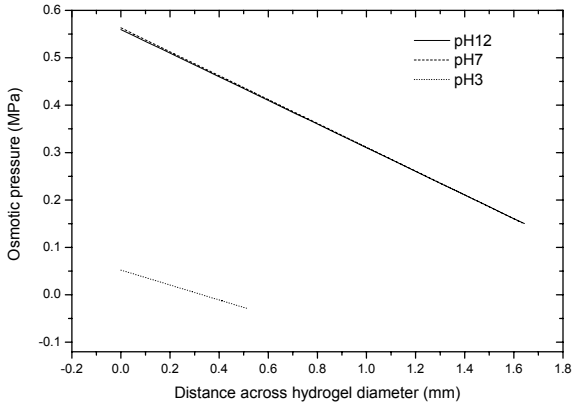

(f) Osmotic Pressure (P)

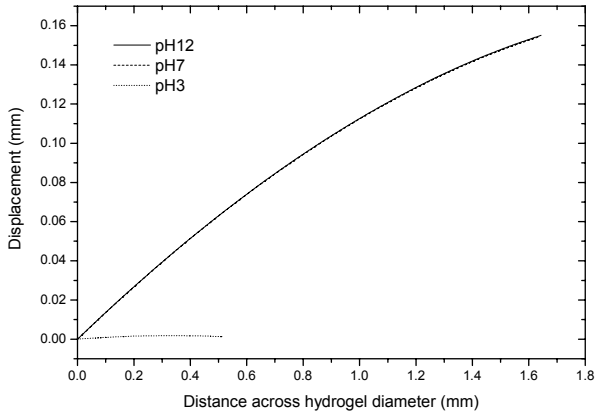

(g) Displacement (u)

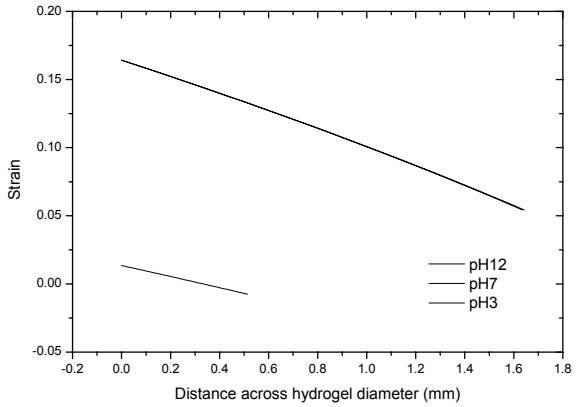

(h) Strain ($\varepsilon_{elastic}$)

Figure 5.9 Profiles of $c_{H^+}, c_{Na^+}, c_{Cl^-}, c_f, \psi, P, u$ and $\varepsilon_{elastic}$ as a variation of pH swelling medium. The PHEMA based hydrogel is equilibrated in NaCl electrolyte solution under the influence of applied voltage of 1.0V.

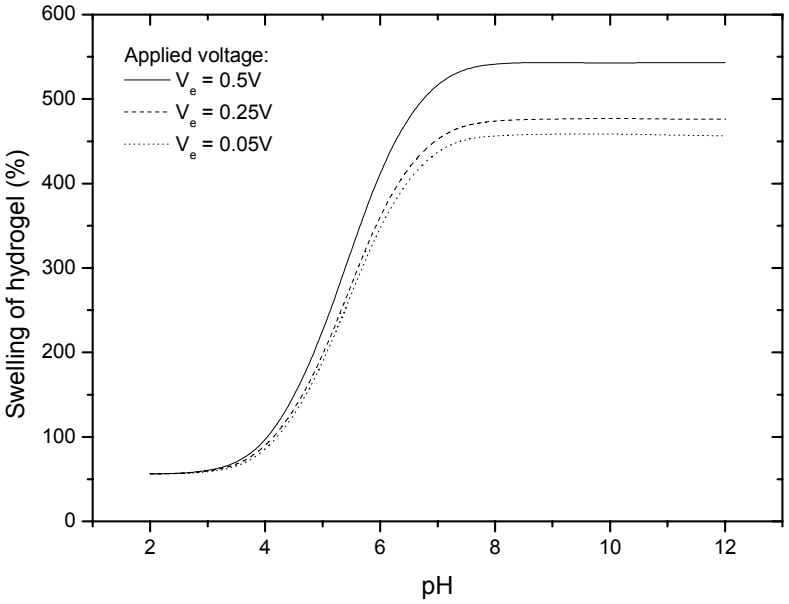

(a)

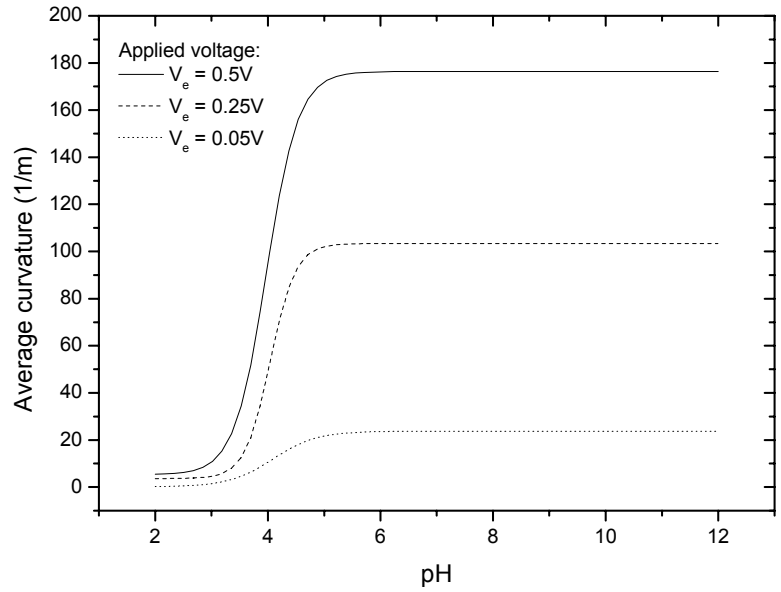

(b)

Figure 5.10 Effects of pH environment with varying applied voltage on (a) swelling equilibrium of hydrogel, (b) average bending curvature of hydrogel.

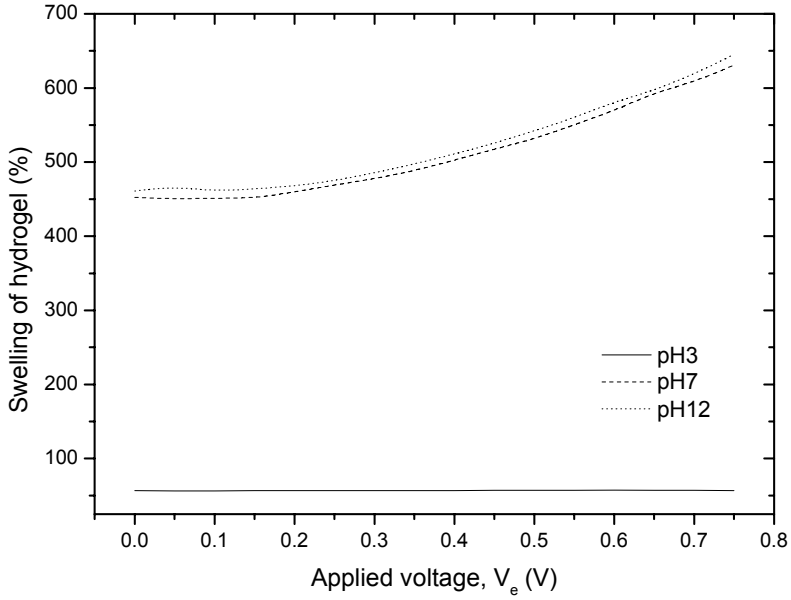

(a)

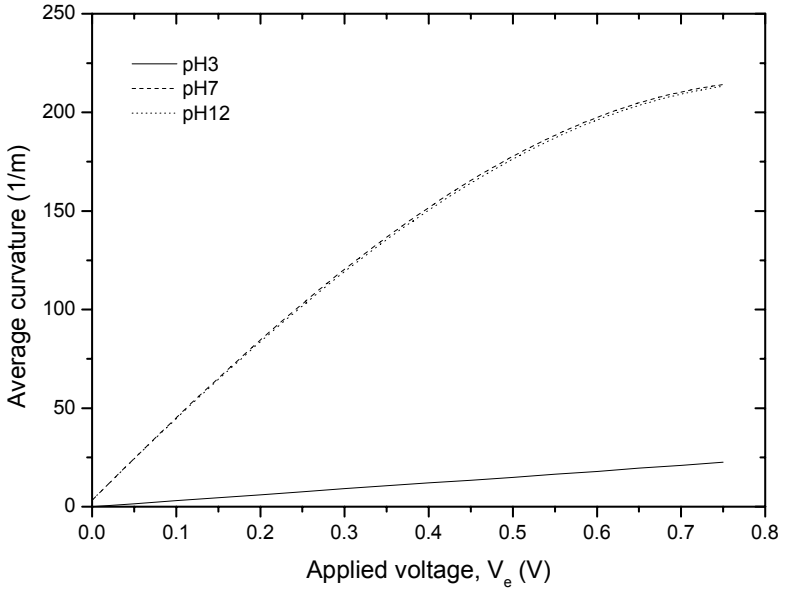

(b)

Figure 5.11 Effects of externally applied voltage on (a) swelling equilibrium of hydrogel, (b) average bending curvature of hydrogel; in acidic, neutral and basic solution.

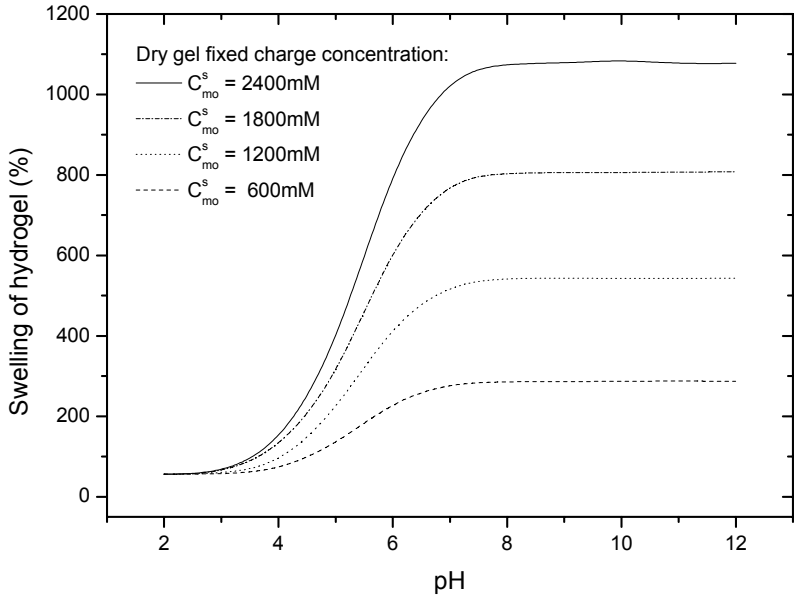

(a)

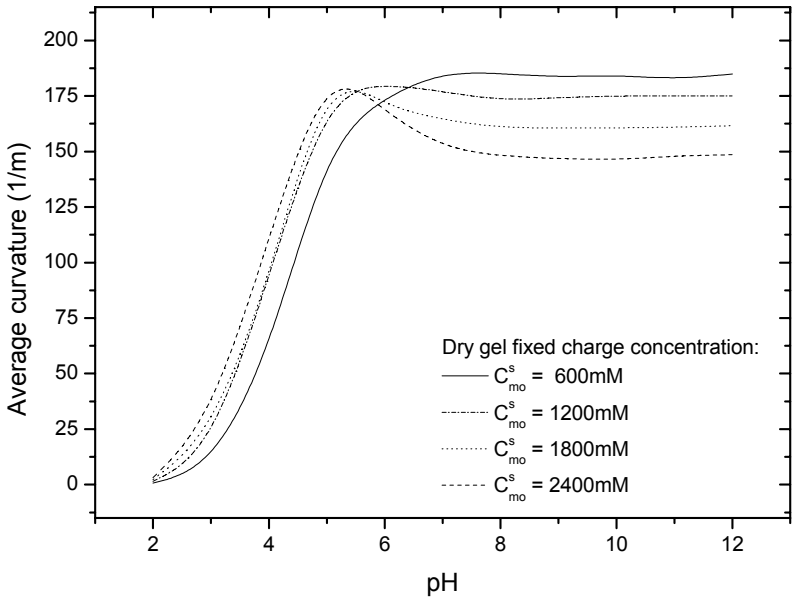

(b)

Figure 5.12 Effects of pH environment with varying ionizable fixed charge concentration on (a) swelling equilibrium of hydrogel, (b) average bending curvature of hydrogel; under the influence of applied voltage of 0.5V.

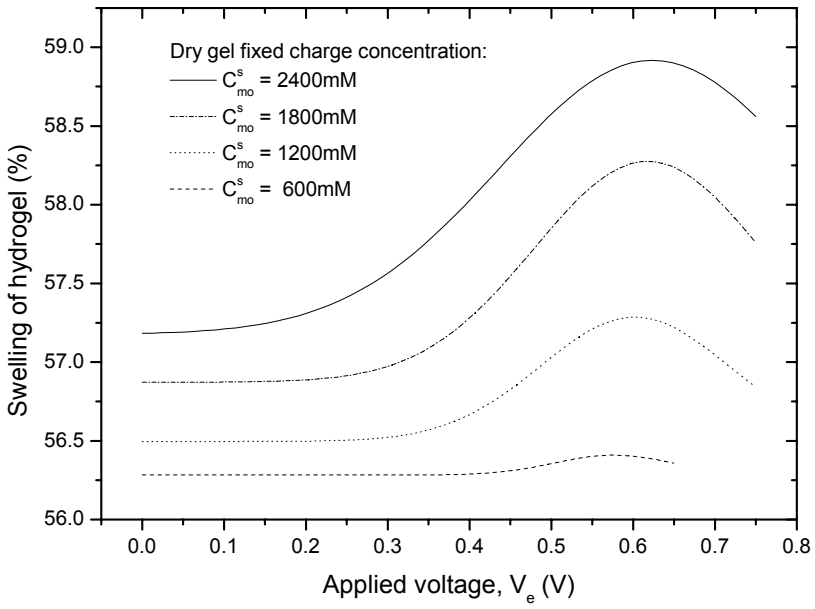

(a)

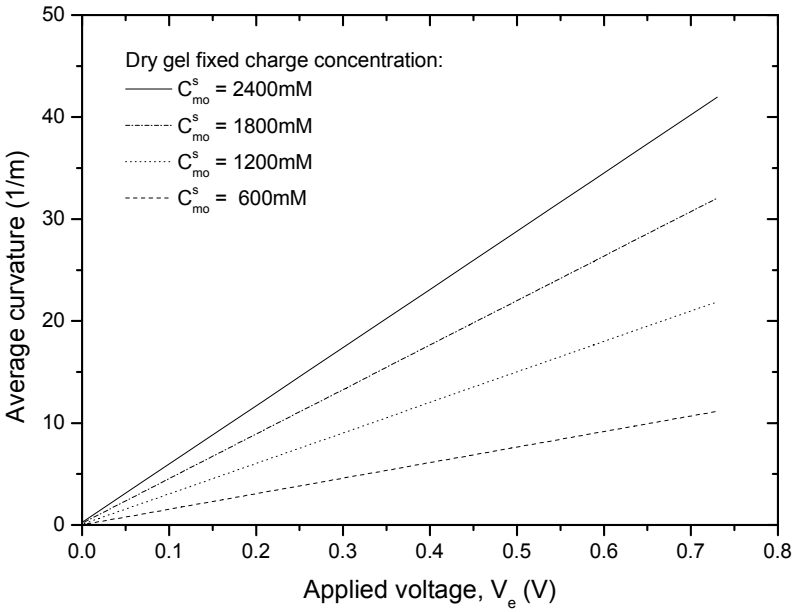

(b)

Figure 5.13 Effects of externally applied voltage with varying ionizable fixed charge concentration on (a) swelling equilibrium of hydrogel, (b) average bending curvature of hydrogel; in acidic swelling medium of pH3.

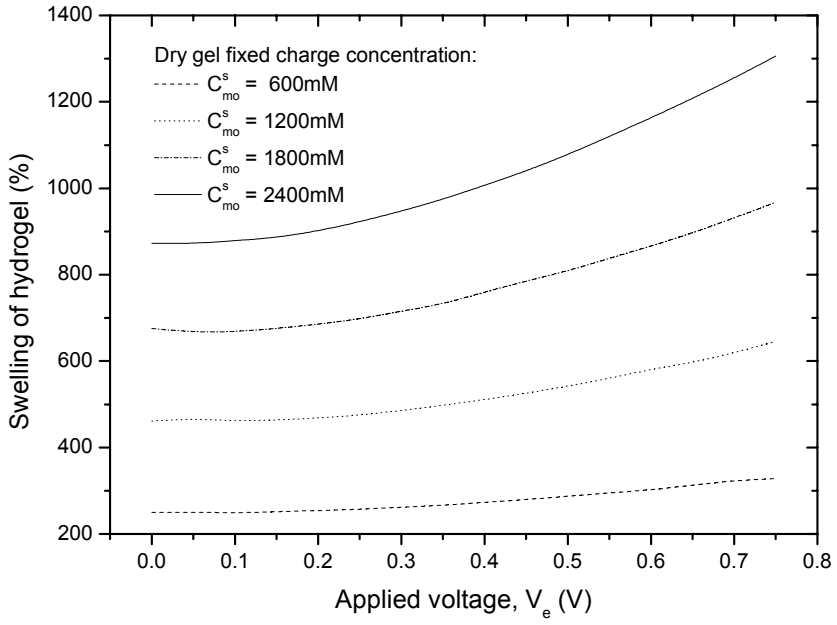

(a)

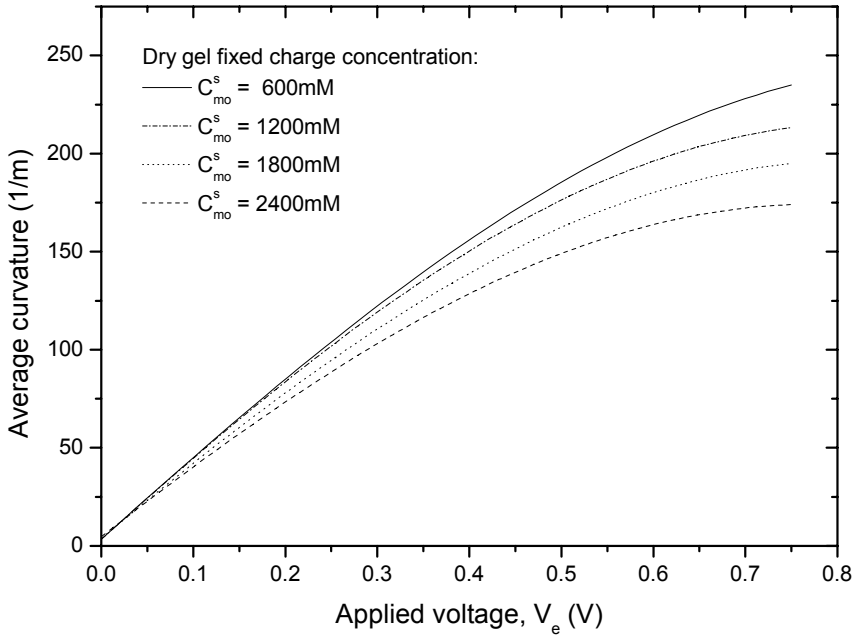

(b)

Figure 5.14 Effects of externally applied voltage with varying ionizable fixed charge concentration on (a) swelling equilibrium of hydrogel, (b) average bending curvature of hydrogel; in basic swelling medium of pH12.

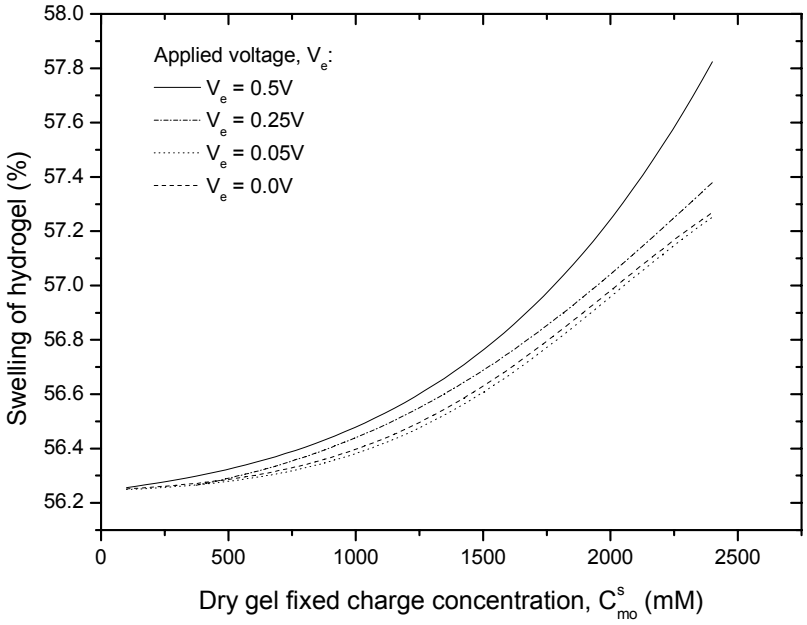

(a)

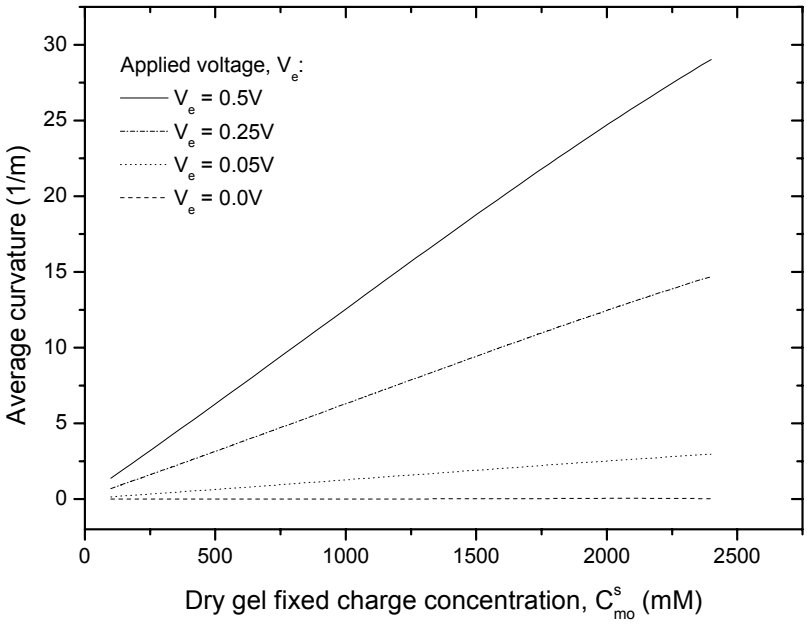

(b)

Figure 5.15 Effects of ionizable fixed charge concentration with varying applied voltage on (a) swelling equilibrium of hydrogel, (b) average bending curvature of hydrogel; in acidic swelling medium of pH3.

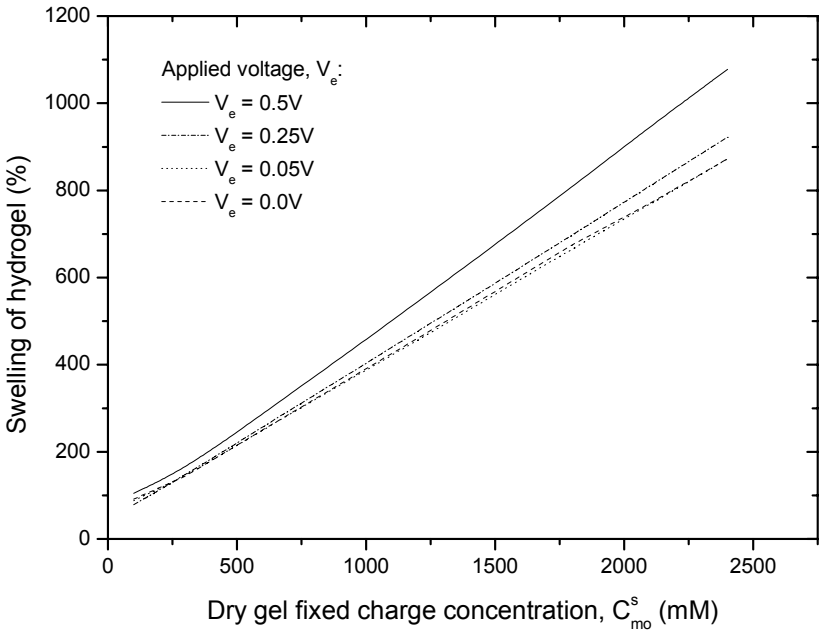

(a)

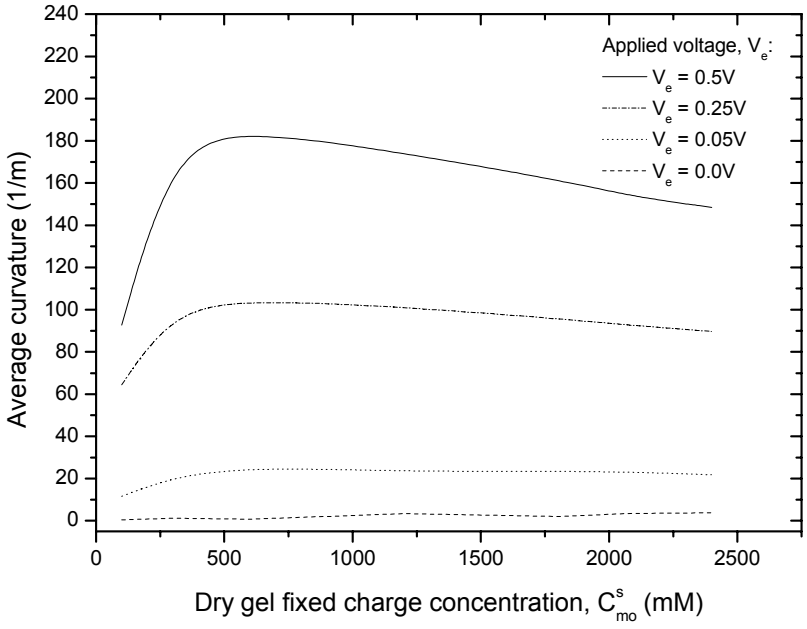

(b)

Figure 5.16 Effects of ionizable fixed charge concentration with varying applied voltage on (a) swelling equilibrium of hydrogel, (b) average bending curvature of hydrogel; in basic swelling medium of pH12.

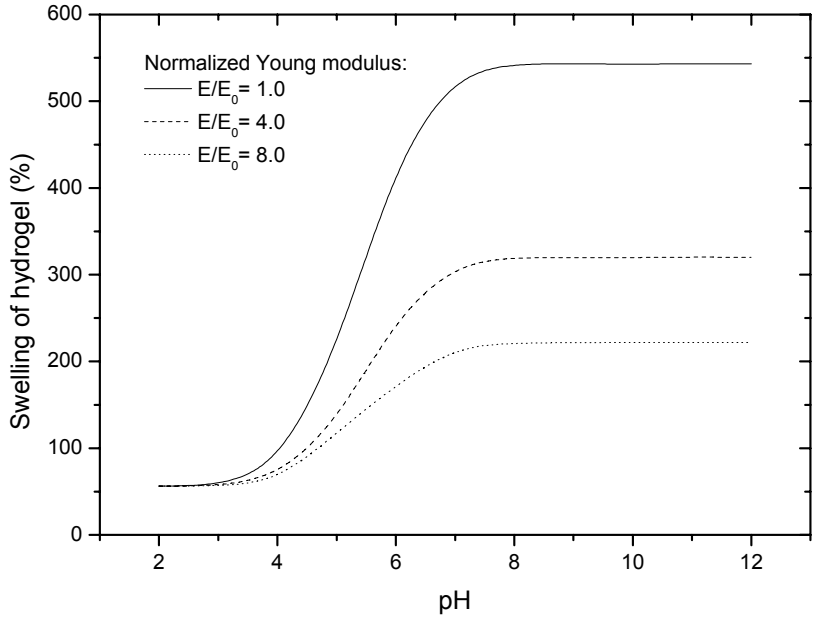

(a)

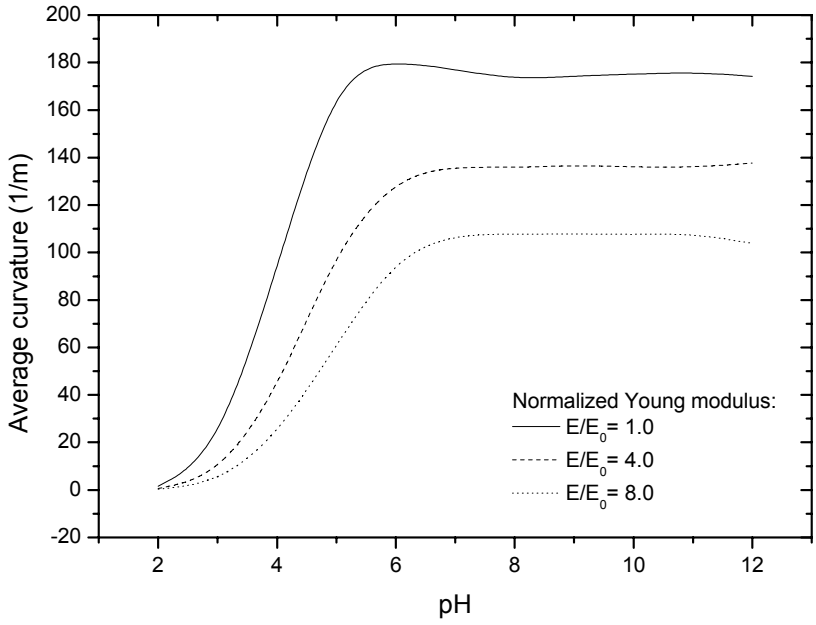

(b)

Figure 5.17 Effects of pH environment with varying normalized Young's modulus on (a) swelling equilibrium of hydrogel, (b) average bending curvature of hydrogel; under the influence of applied voltage of 0.5V.

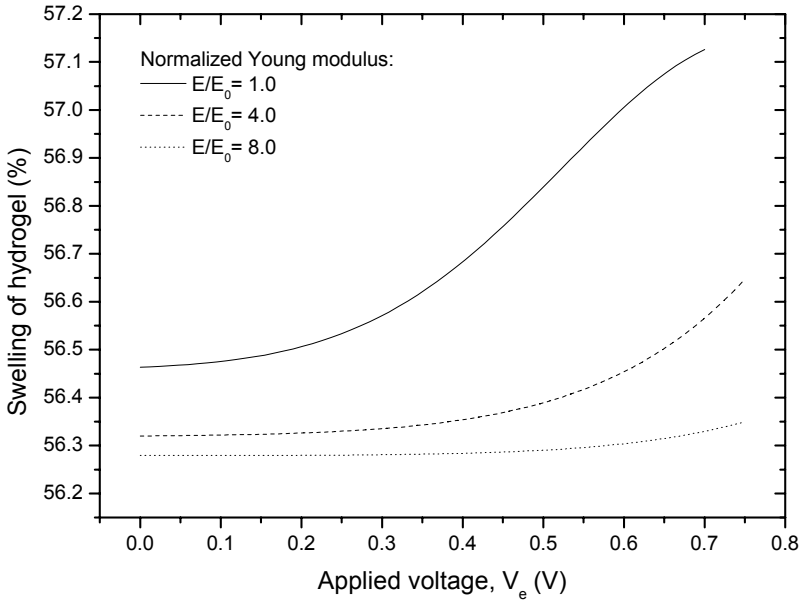

(a)

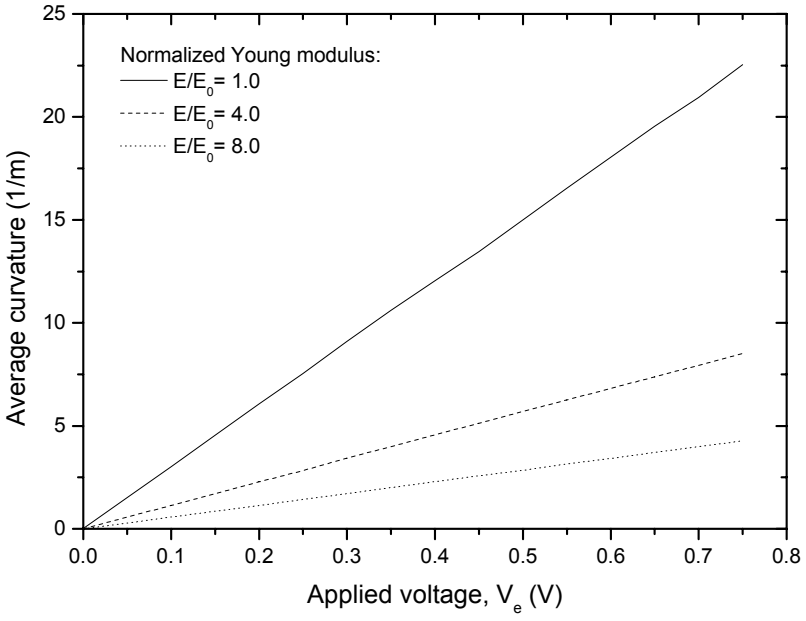

(b)

Figure 5.18 Effects of externally applied voltage with varying normalized Young's modulus on (a) swelling equilibrium of hydrogel, (b) average bending curvature of hydrogel; in acidic swelling medium of pH3.

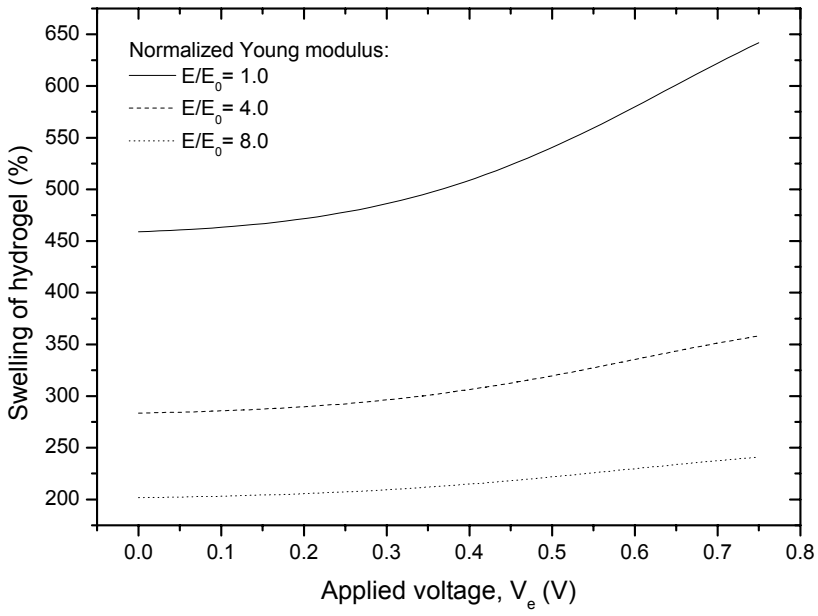

(a)

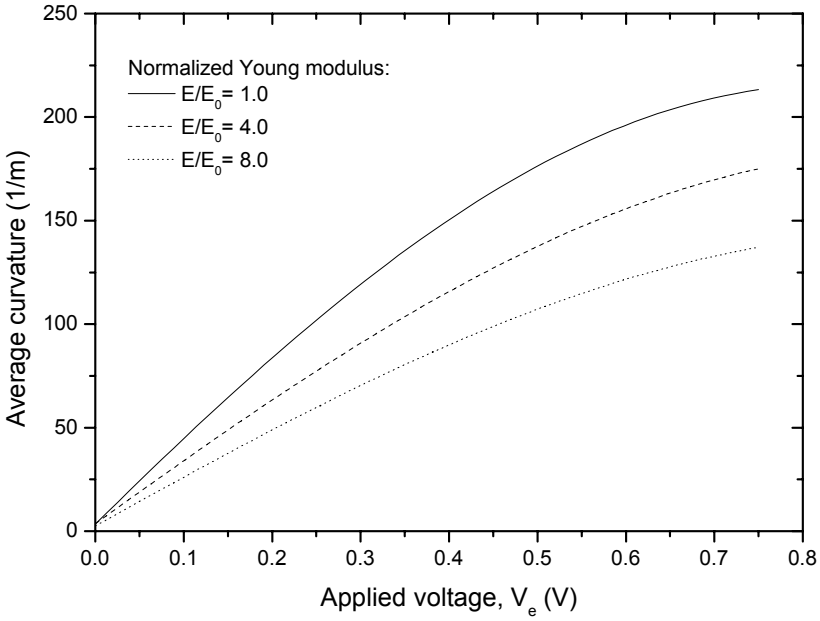

(b)

Figure 5.19 Effects of externally applied voltage with varying normalized Young's modulus on (a) swelling equilibrium of hydrogel, (b) average bending curvature of hydrogel; in basic swelling medium of pH12.

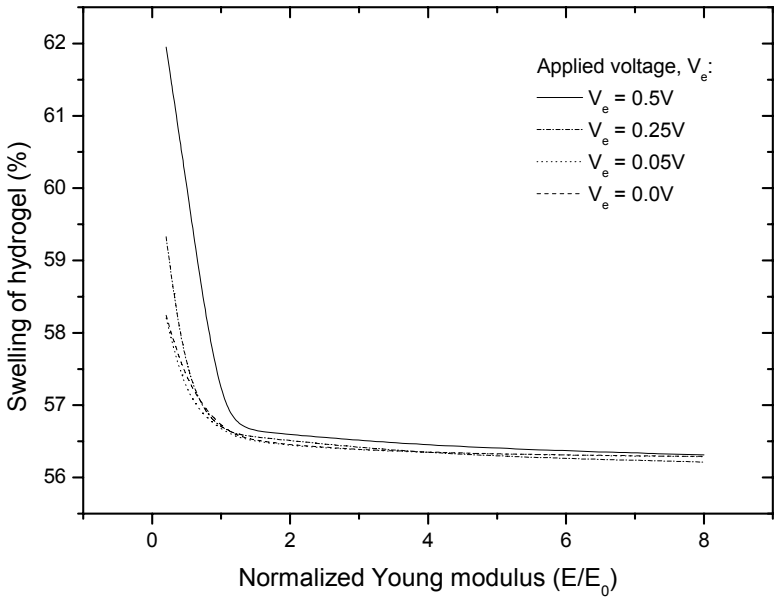

(a)

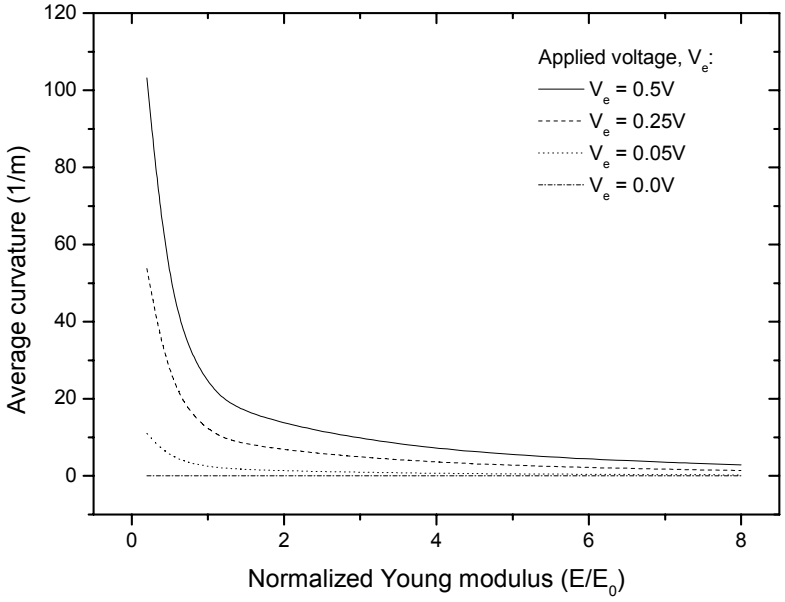

(b)

Figure 5.20 Effects of normalized Young's modulus with varying applied voltage on (a) swelling equilibrium of hydrogel, (b) average bending curvature of hydrogel; in acidic swelling medium of pH3.

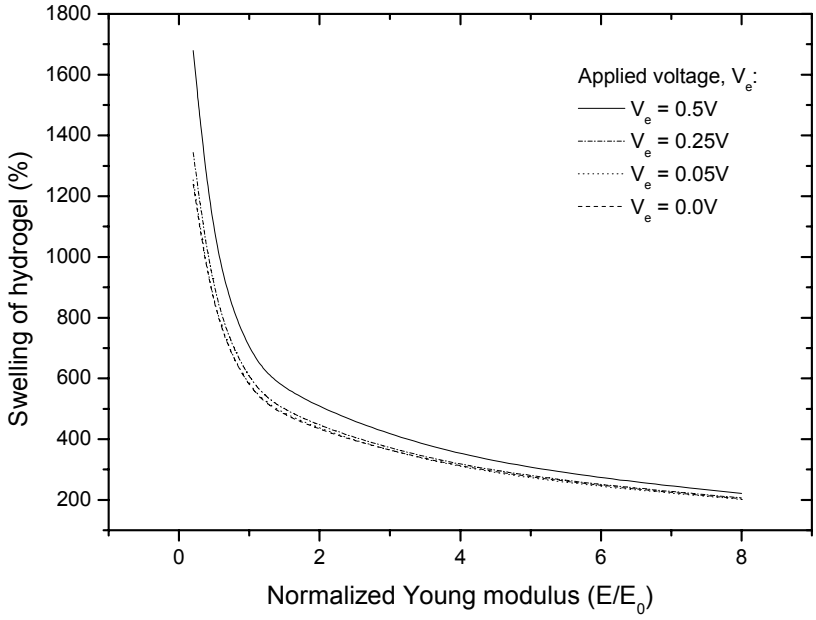

(a)

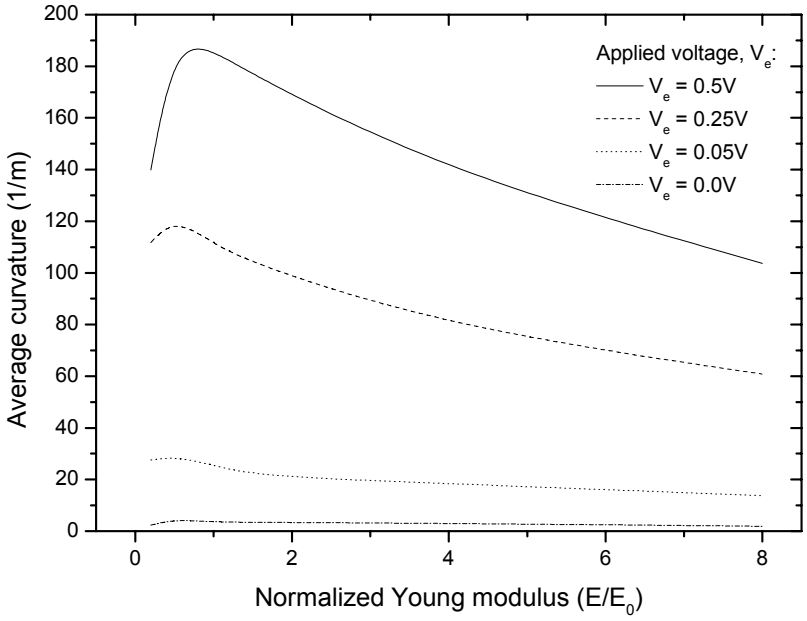

(b)

Figure 5.21 Effects of normalized Young's modulus with varying applied voltage on (a) swelling equilibrium of hydrogel, (b) average bending curvature of hydrogel; in basic swelling medium of pH12.

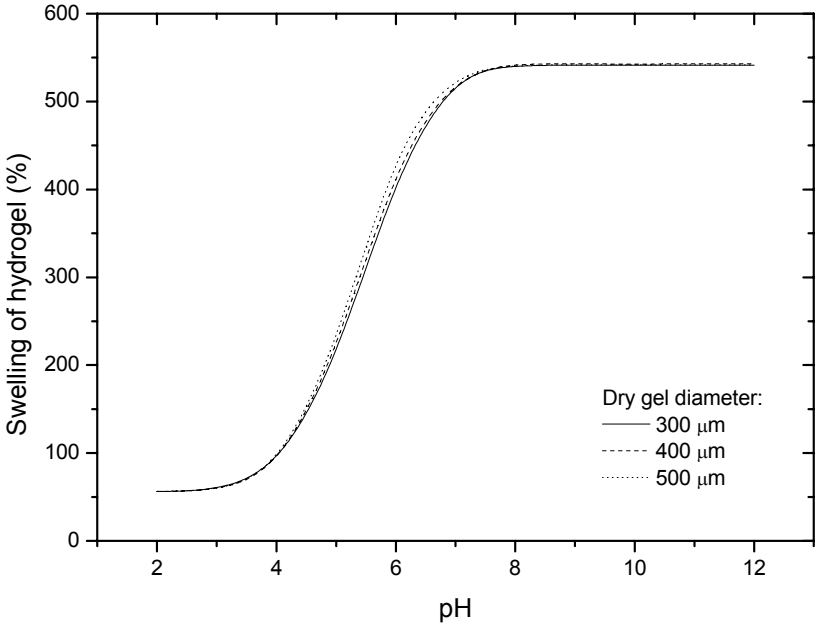

(a)

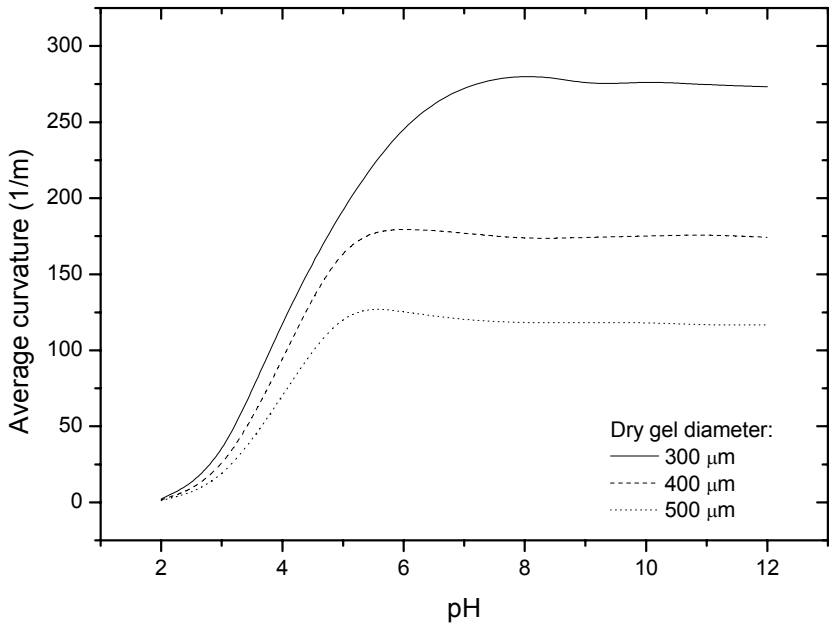

(b)

Figure 5.22 Effects of pH environment with varying dry-state gel thickness on (a) swelling equilibrium of hydrogel, (b) average bending curvature of hydrogel; under the influence of applied voltage of 0.5V.

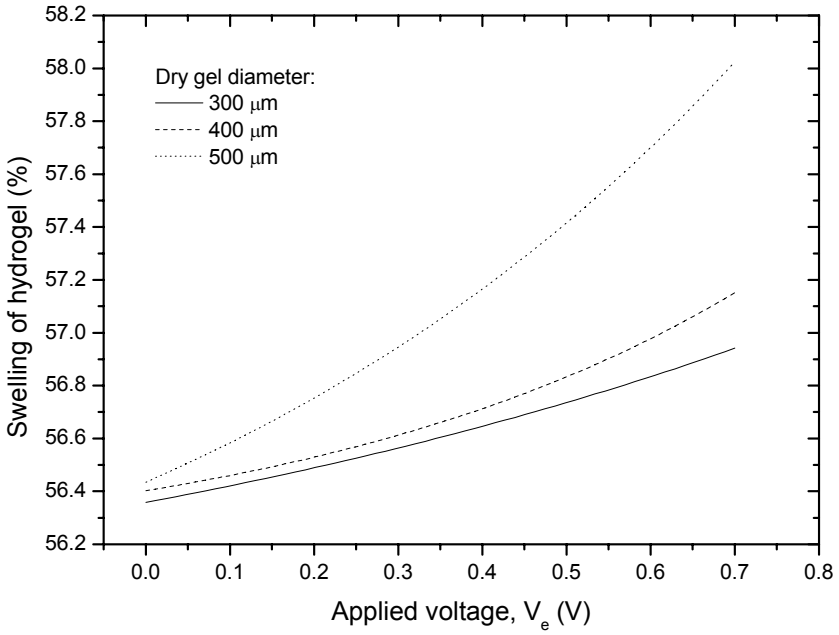

(a)

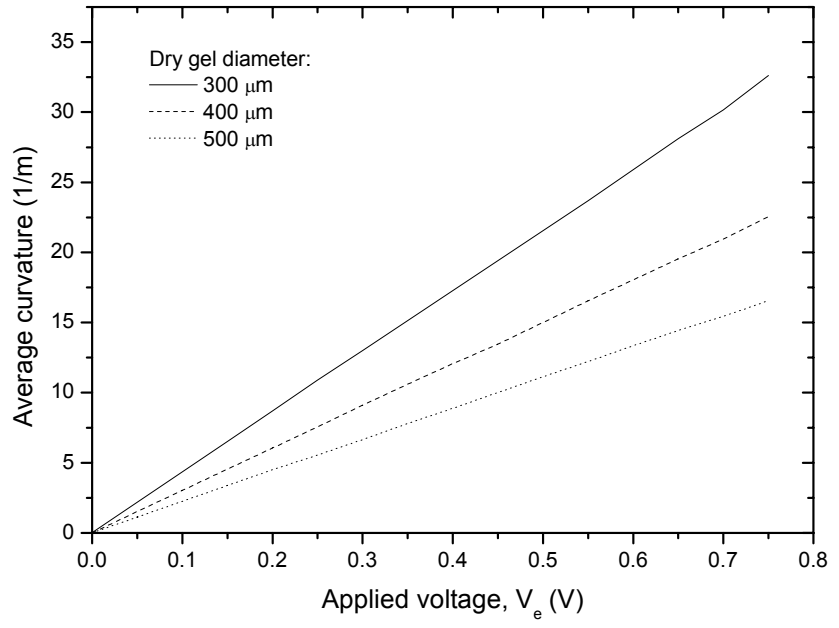

(b)

Figure 5.23 Effects of externally applied voltage with varying dry-state gel thickness on (a) swelling equilibrium of hydrogel, (b) average bending curvature of hydrogel; in acidic swelling medium of pH3.

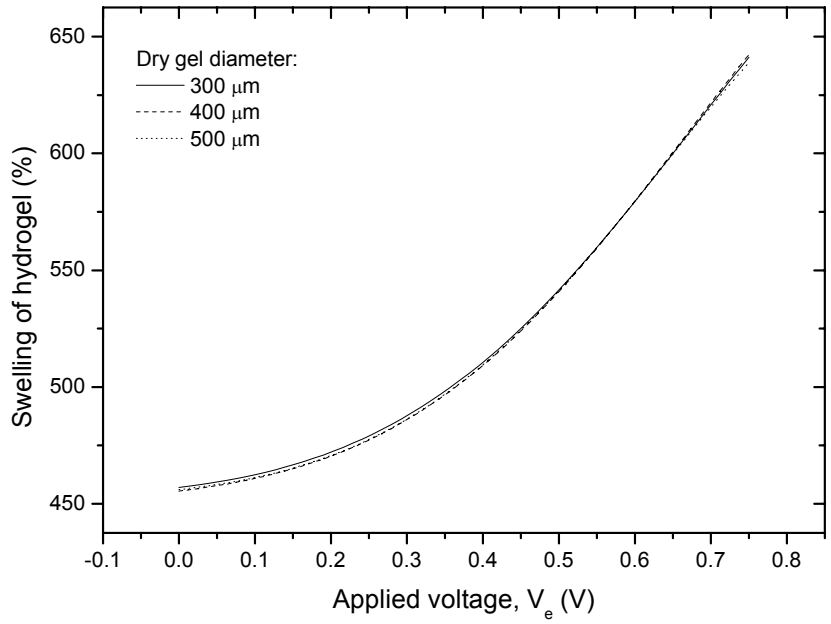

(a)

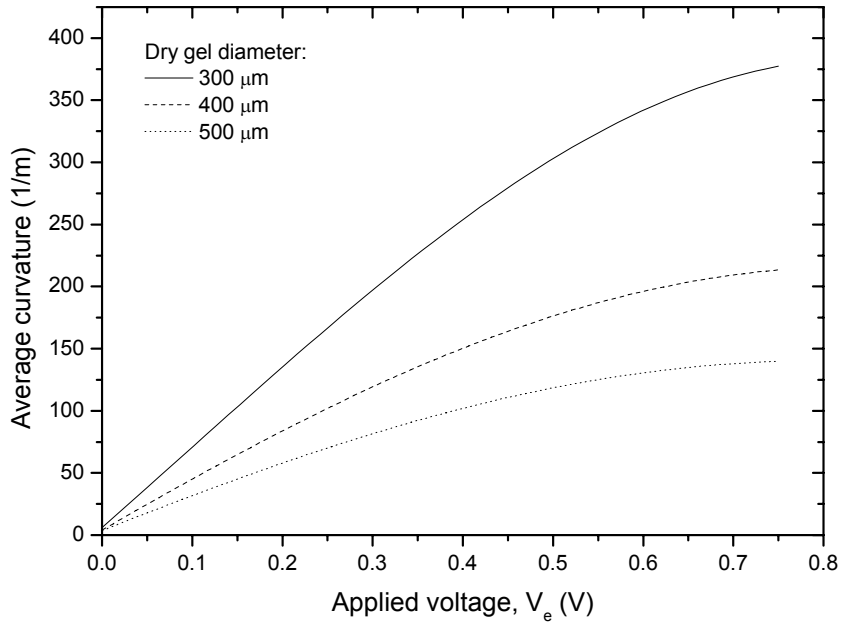

(b)

Figure 5.24 Effects of externally applied voltage with varying dry-state gel thickness on (a) swelling equilibrium of hydrogel, (b) average bending curvature of hydrogel; in basic swelling medium of pH12.

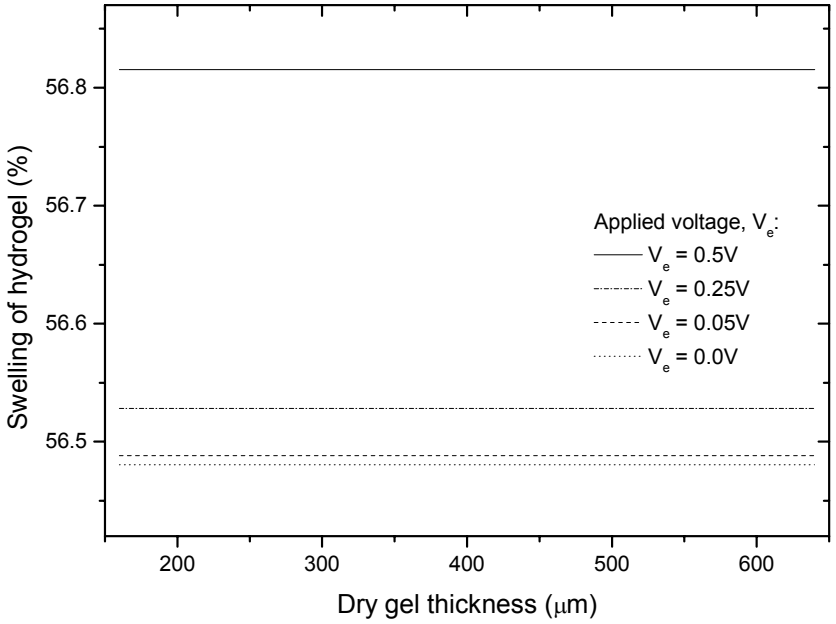

(a)

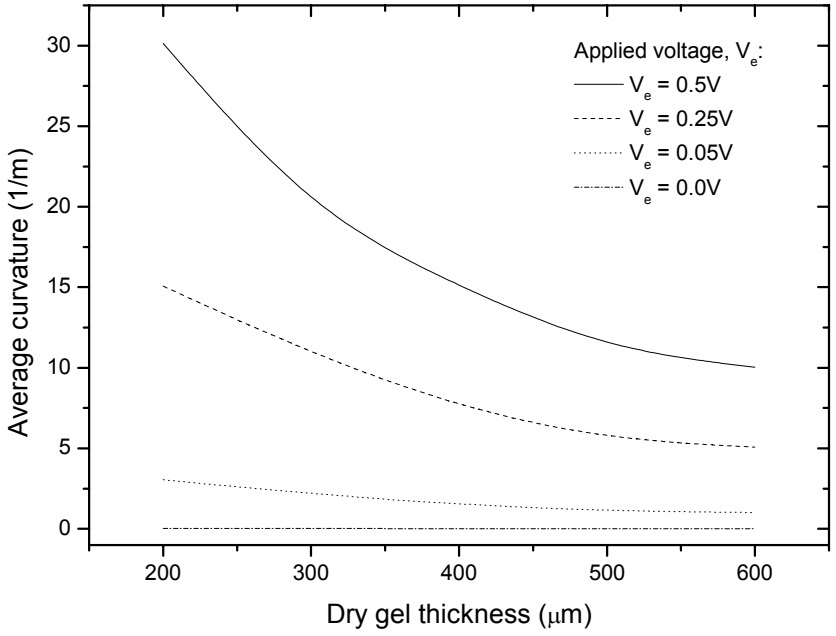

(b)

Figure 5.25 Effects of dry-state gel thickness with varying applied voltage on (a) swelling equilibrium of hydrogel, (b) average bending curvature of hydrogel; in acidic swelling medium of pH3.

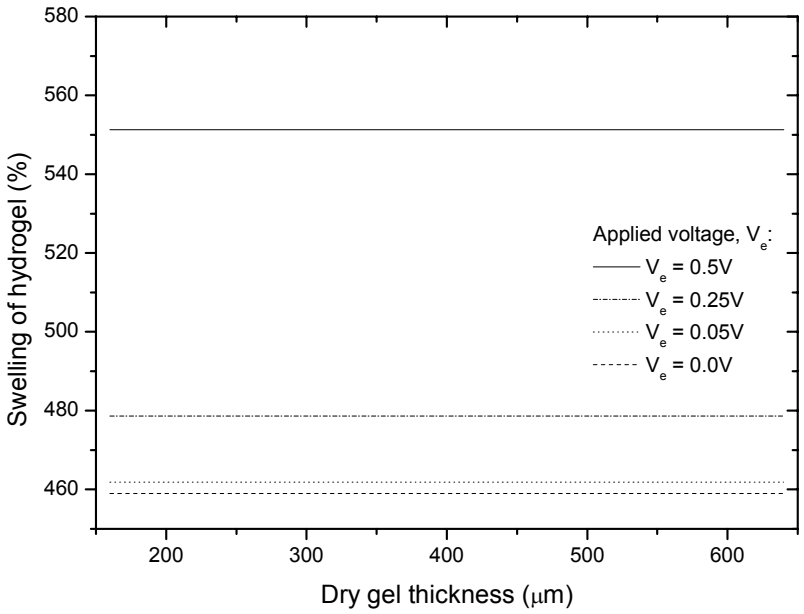

(a)

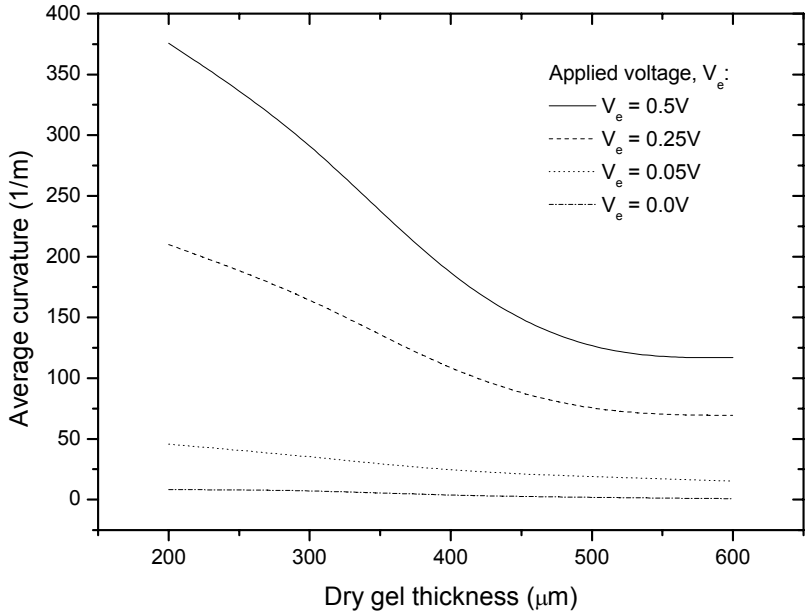

(b)

Figure 5.26 Effects of dry-state gel thickness with varying applied voltage on (a) swelling equilibrium of hydrogel, (b) average bending curvature of hydrogel; in basic swelling medium of pH12.

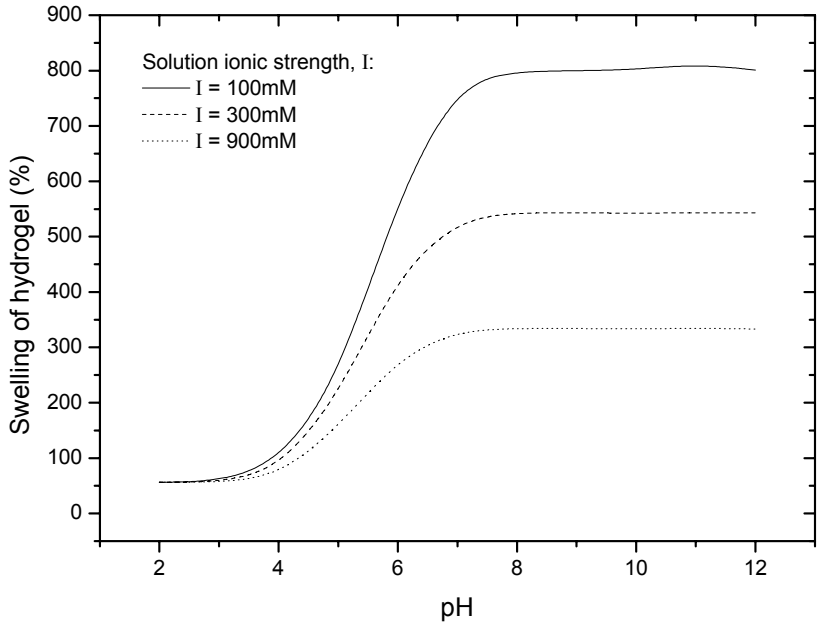

(a)

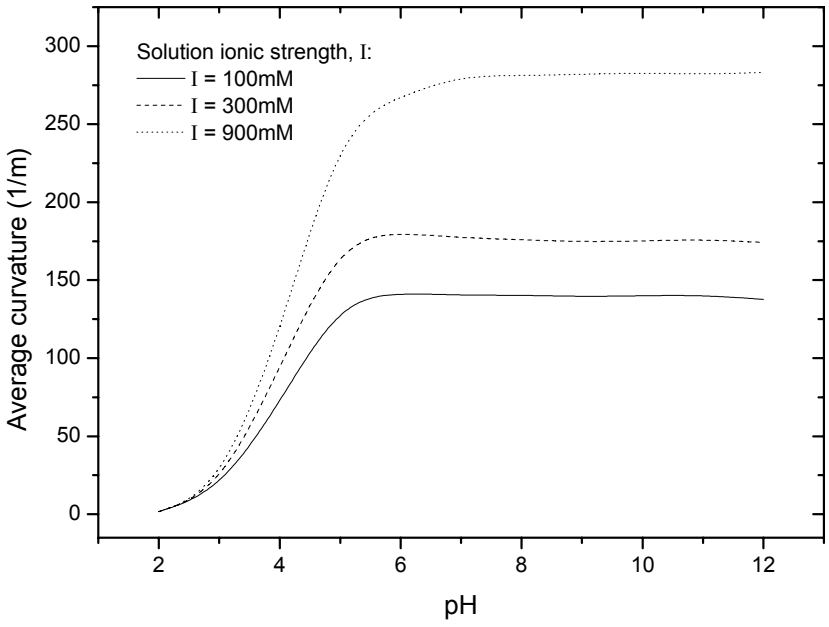

(b)

Figure 5.27 Effects of pH environment with varying solution ionic strength on (a) swelling equilibrium of hydrogel, (b) average bending curvature of hydrogel; under the influence of externally applied voltage of 0.5V.

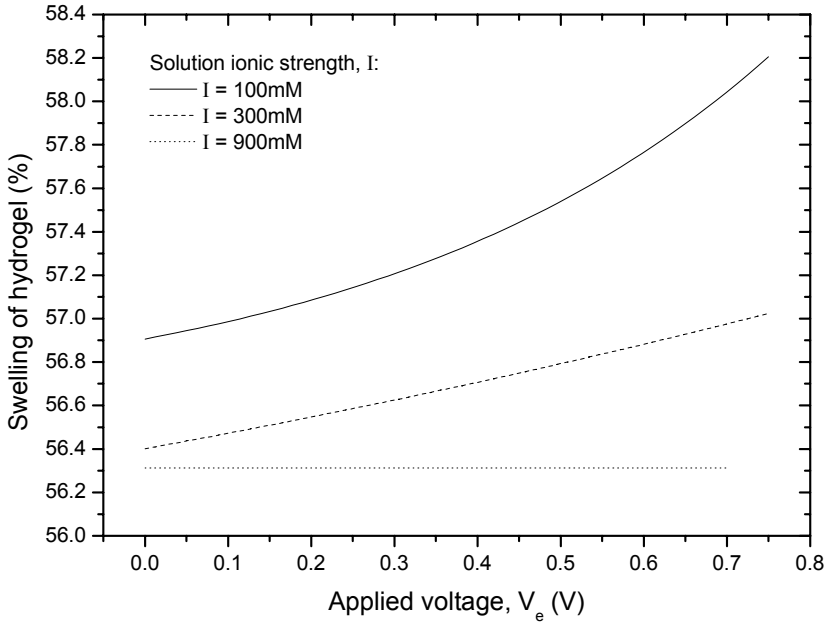

(a)

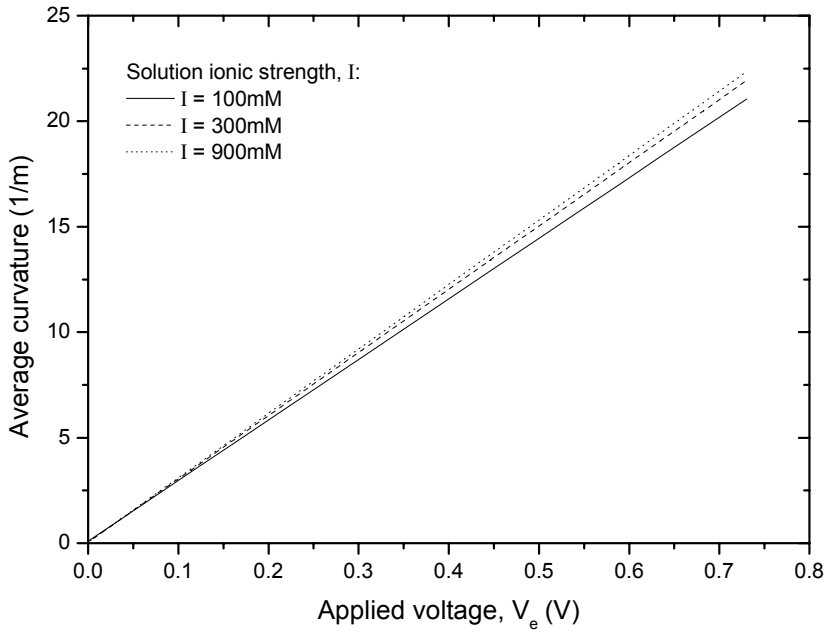

(b)

Figure 5.28 Effects of externally applied voltage with varying solution ionic strength on (a) swelling equilibrium of hydrogel, (b) average bending curvature of hydrogel; in acidic swelling medium of pH3.

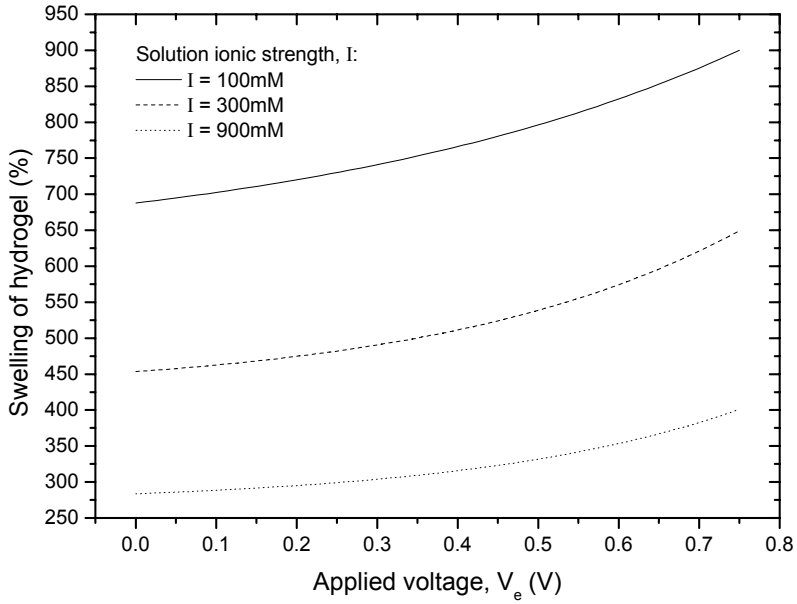

(a)

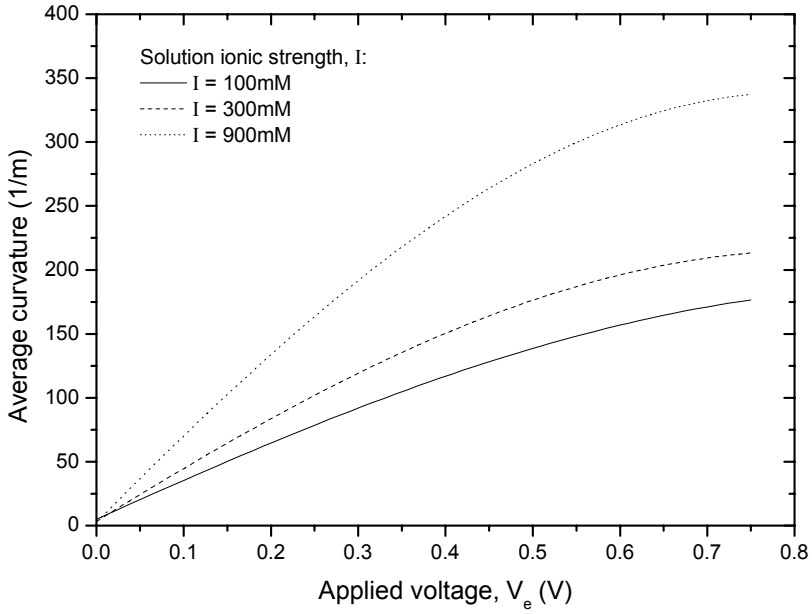

(b)

Figure 5.29 Effects of externally applied voltage with varying solution ionic strength on (a) swelling equilibrium of hydrogel, (b) average bending curvature of hydrogel; in basic swelling medium of pH12.

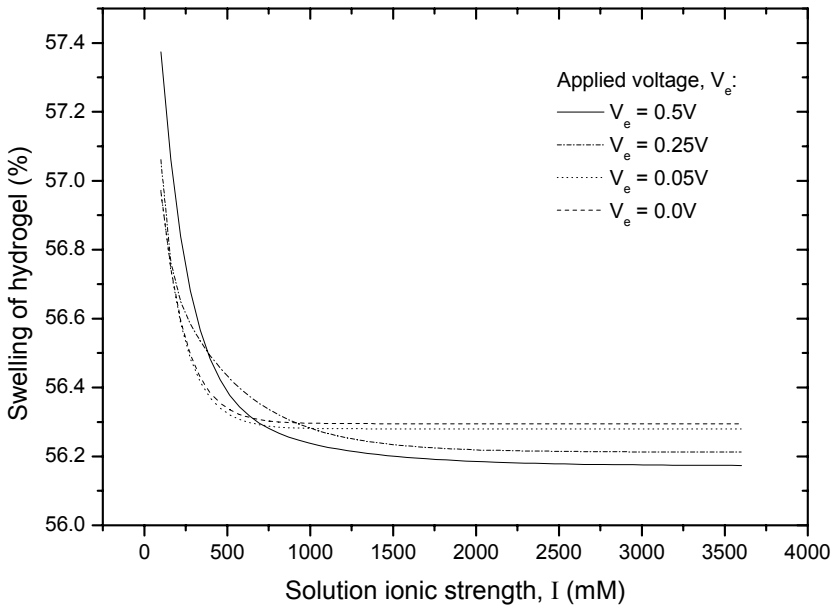

(a)

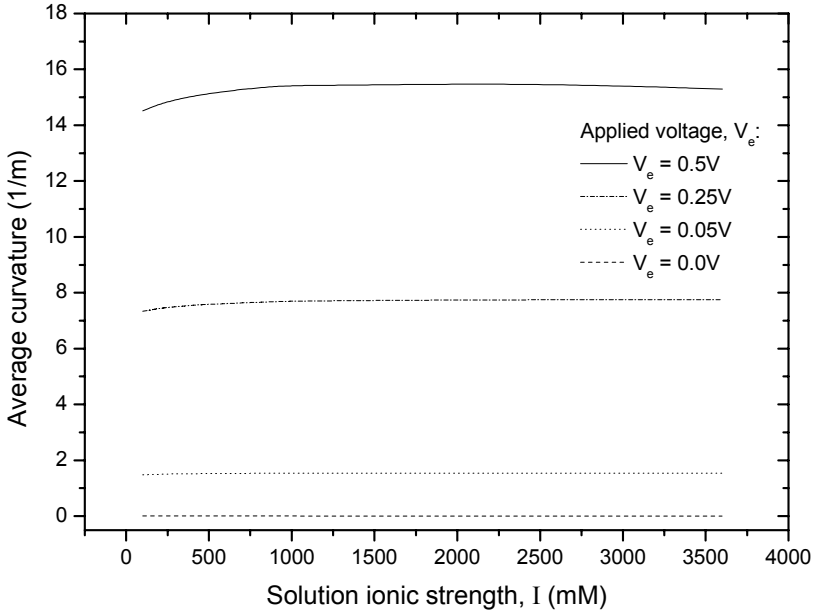

(b)

Figure 5.30 Effects of solution ionic strength with varying applied voltage on (a) swelling equilibrium of hydrogel, (b) average bending curvature of hydrogel; in acidic swelling medium of pH3.

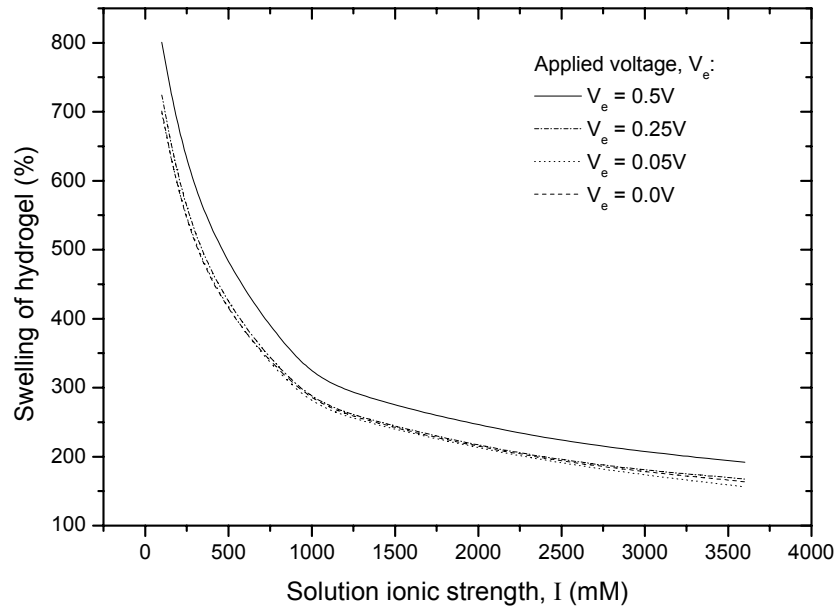

(a)

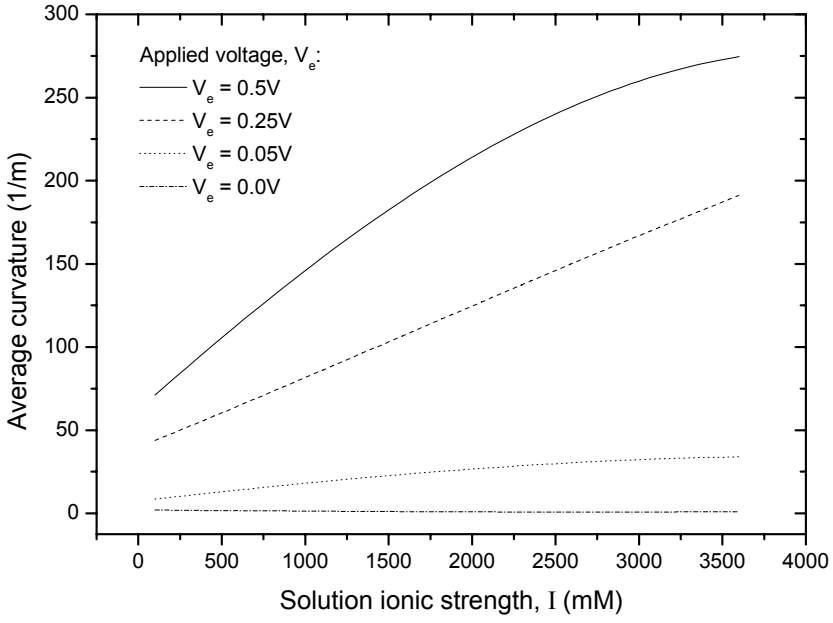

(b)

Figure 5.31 Effects of solution ionic strength with varying applied voltage on (a) swelling equilibrium of hydrogel, (b) average bending curvature of hydrogel; in basic swelling medium of pH12.

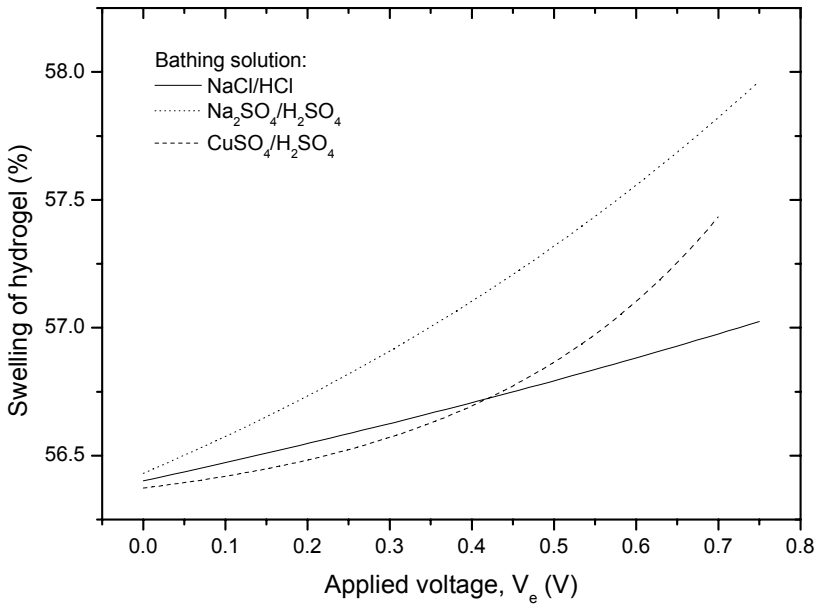

(a)

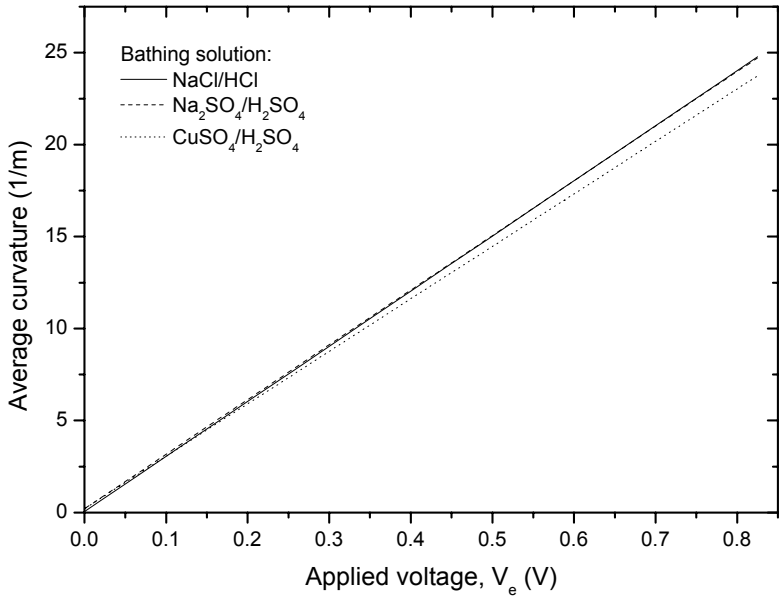

(b)

Figure 5.32 Effects of externally applied voltage with varying solution composition on (a) swelling equilibrium of hydrogel, (b) average bending curvature of hydrogel; in acidic swelling medium of pH3.

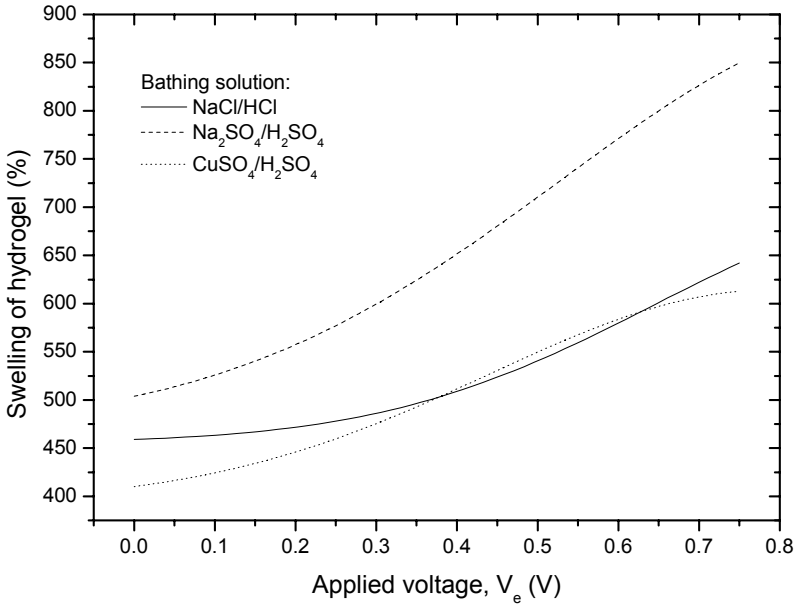

(a)

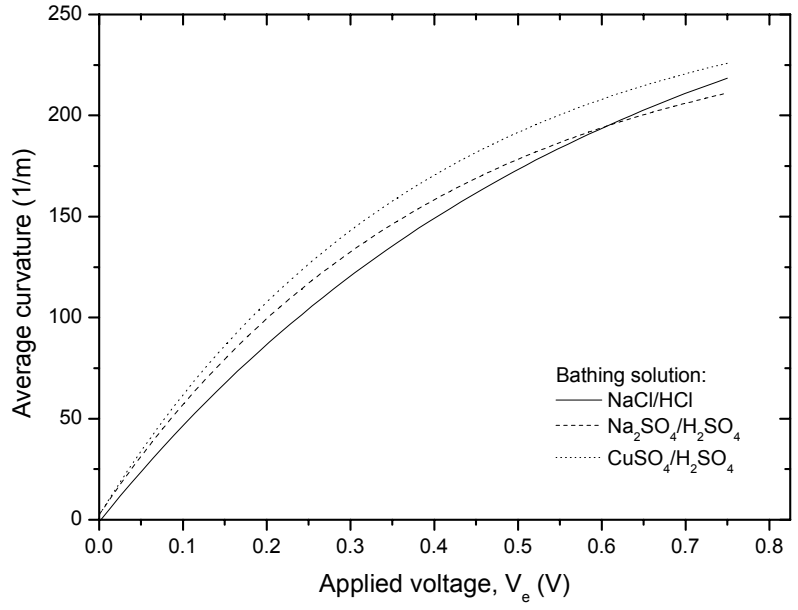

(b)

Figure 5.33 Effects of externally applied voltage with varying solution composition on (a) swelling equilibrium of hydrogel, (b) average bending curvature of hydrogel; in basic swelling medium of pH12.

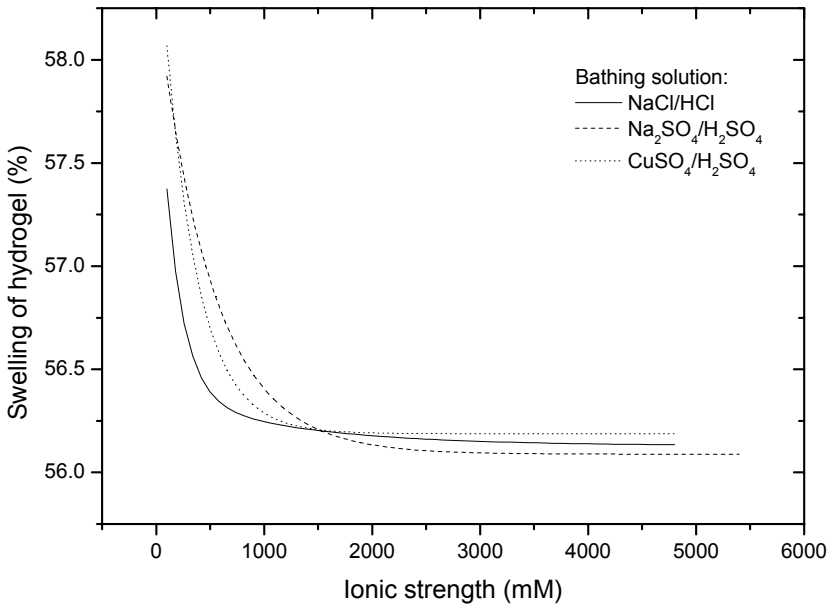

(a)

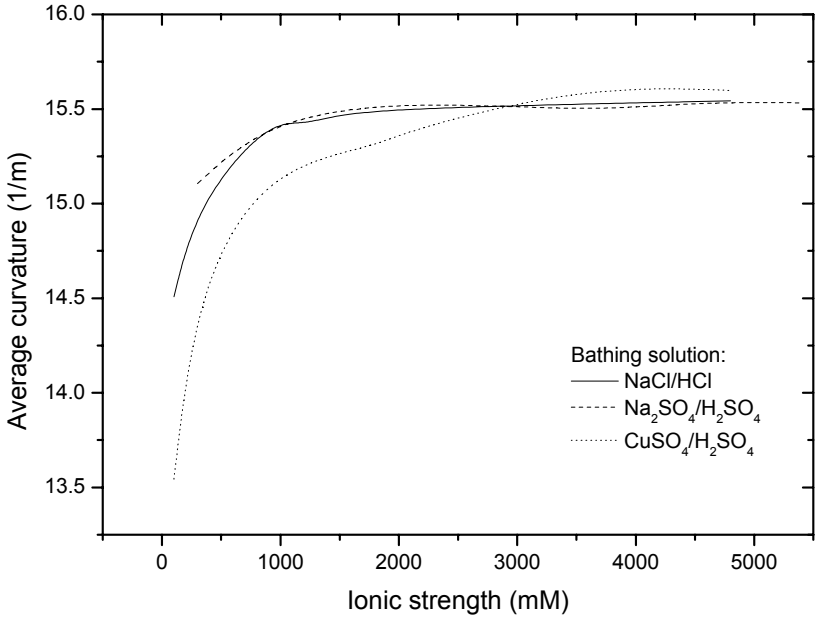

(b)

Figure 5.34 Effects of solution composition with varying applied voltage on (a) swelling equilibrium of hydrogel, (b) average bending curvature of hydrogel; in acidic swelling medium of pH3.

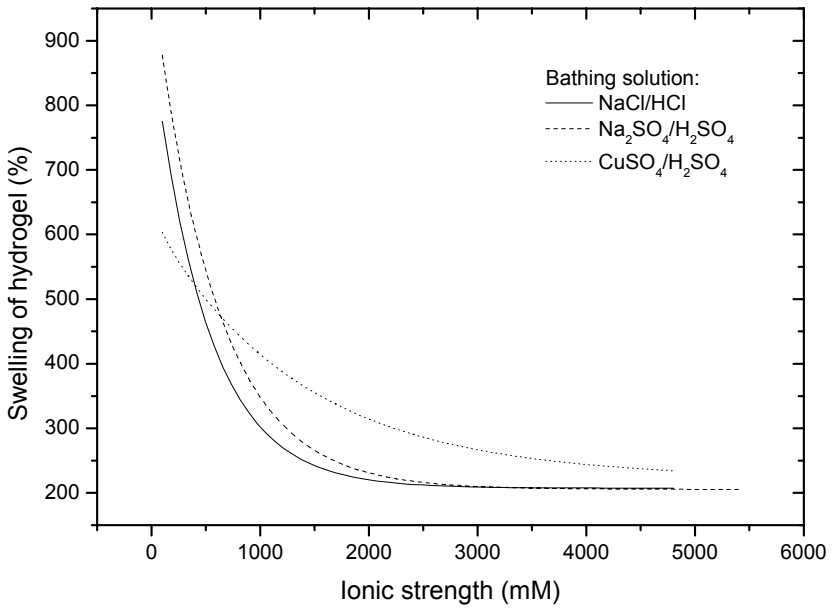

(a)

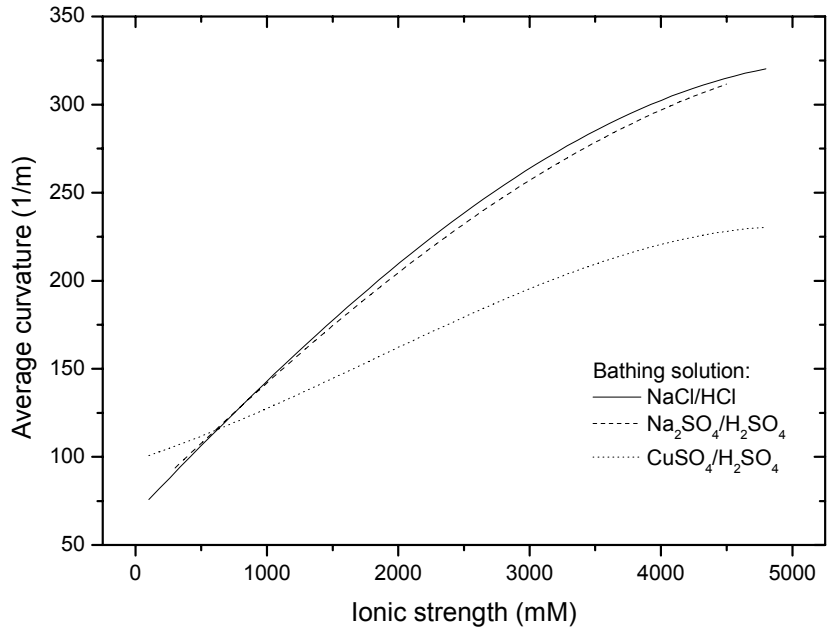

(b)

Figure 5.35 Effects of solution composition with varying applied voltage on (a) swelling equilibrium of hydrogel, (b) average bending curvature of hydrogel; in basic swelling medium of pH12.

CHAPTER 6

CONCLUDING REMARKS

6.1 SUMMARY

In this dissertation, a theoretical consideration related to the swelling, shrinking and bending behaviors of pH-responsive hydrogel has been presented. More specifically, this dissertation has dealt with chemo-electro-mechanical modeling in general and solving the equations of Poisson-Nernst-Planck coupled with the finite deformation in particular. The basic idea goes back to the multi-field formulation applied in charged membrane with elastic matrix. This model, termed the Multi-Effect-Coupling pH-stimulus (MECpH) model, accounts for the ions transport within both hydrogel and swelling medium, and the coupling between the electric field, ionic fluxes, and mechanical deformations of the hydrogel.

The first part of the numerical investigation, corresponding to Chapter 4 of this dissertation, the swelling equilibrium of pH-responsive hydrogel has been studied in the presence of chemical stimuli, i.e. pH and ionic strength. For the second part, namely Chapter 5, the deformation behavior (swelling, shrinking and bending equilibrium in particular) of the pH-responsive hydrogel has been studied in the concurrent presence of chemical and electric stimuli. Despite the complexity of the swelling behavior, plenty of physical insight can be obtained by systematically

investigating the physical and chemical nature of the hydrogel as well as its swelling medium.

Even though that the study of equilibrium swelling of charged, crosslinked hydrogel is not a new subject, this dissertation has contributed in some way to the advancements in this area of research. The main contributions of this dissertation include: outlined the steady-state behavior of swelling equilibrium of hydrogel on the basis of nonlinear chemoelectromechanical theories; incorporated the relationship of ionizable fixed charge groups with diffusive hydrogen ion in the formulation; introduced the finite deformation consideration into the mechanical formulation; gave a systematic analysis of the mechanisms governing the hydrogel deformation under the influences of chemical and electrical stimulations; calculated the changes of ions and electric field profiles of the hydrogel driven by chemical and electric stimuli, taking account of ion transports and electrochemical reactions; identified a few properties and geometrical parameters of hydrogel, as well as environmental conditions that might impact the deformation behavior of the hydrogel.

The reasonable agreements of the simulated and experimental swelling and bending (indicated by the diameters or hydration of the hydrogel and average curvature at the middle point of the hydrogel strip respectively) shown in: (1) Fig. 4.3 for PHEMA based hydrogel subjected to phosphate buffer solution with NaCl added to adjust the ionic strength; (2) Fig. 5.3 for polybasic hydrogel strip swollen in an acidic solution under the influence of externally applied electric voltage; (3) Figs. 5.4 and 5.5 for PMAA/PVA IPN hydrogel swollen in NaCl electrolyte solution in response to the electrochemical stimuli, suggest that the chemical-electrical-induced forces are attributable to diffusion and migration. The numerical predictions of MECpH are not in exact value with the real measured data; however, they are closely coherent with the

qualitative observations of the experimental data, and do provide a benchmark to the behavior of the pH-stimuli sensitive hydrogel under wide range of working environment which have been analyzed and illustrated in the parametric studies.

6.2 SUGGESTIONS FOR FUTURE WORKS

Due to the complexity of the chemoelectromechanical effects, the simulated results only serve as order of magnitude of estimatimation subjected to the limitations of the accuracy of the chosen model and assumptions and the values of the parameters used in conjunction with the simulations. Moreover, the present MECpH is not meant to reproduce exactly the data from experiment measurements but rather to provide a platform to observe the fundamental insight of the factors that constitute the swelling behavior of the pH-responsive hydrogel. Further improvement is inevitable with new understanding of the practical and theoretical phenomena of the hydrogel.

The researchs in the fild of polymer gel are still in the growing stage, henceforth, it will be of great benefits to the research communities if there are standard guides in presentating the experimental results and parameters in use. The candidate has come across few experimental and theoretical results published by other research groups; however, some of the crucial parameters are not given with sufficient details with the presented results. Hence, these reported experimental or theoretical results in most cases are difficult to replicate. Nevertheless, the efforts to compare the present model with the experimental or theoretical results from other research groups are encouraged.

The present mathematical model was derived under the condition of equilibrium, steady-state assumptions. Transient behavior of the swelling mechanism will be an interesting area to be explored in order to study time-varying mechanical responses of chemically or electrically driven hydrogel, on the other hand, to distinguish between these rate processes and those of interest which are intrinsic to the charged hydrogel itself. The continuity equations become important particularly for the dynamics of ion transport in heterogeneous non-equilibrium situation.

In this dissertation, the hydrogel was taken to be homogenous and symmetrical; hence, the possible effect from geometry irregularity has been neglected. Extension of the formulation to two- or three-dimensional model could be inserted into present model without much difficulty, nevertheless, to give some desirable improvement as compared to the one-dimensional model is still left to be proven in relative to the complexity.

The chemical reaction, for example, the electrolysis that occurs near to the electrodes could change the pH environment momentarily. When an electric field was applied across the hydrogel swollen in a buffer solution, electrochemical reactions occurred near to the electrode. The bending angle of a hydrogel may be further amplified by the local pH gradient attributed to water electrolysis.

Future developments could also be devoted to more specific application, for example, simulation of glucose-responsive delivery system for diabetes therapy systems (Albin et al., 1990). The systems can be based on the pH-sensitive hydrogel with immobilized glucose oxidase, and the saturated insulin solution will be encapsulated in the hydrogel. As glucose diffuses into the hydrogel, enzymatic reaction of glucose oxidase with glucose occurs where the glucose oxidase will catalyzes the glucose conversion to gluconic acid. The gluconic acid will in turn lower the pH in the

local environment of the hydrogel and causes the hydrogel to swell. Thereby, the insulin encapsulated in the hydrogel will permeate from the inner hydrogel into the outer medium.

REFERENCES

Aalberts, D. P. Microscopic Simulation of Phase Transition in Interacting Ionic Gels. *J. Chem. Phys.* **1996,** 104, 4309-4312.

Abe, K.; Koide, M.; Tsuchida, E. Selective Complexation of Macromolecules. *Macromolecules* **1977,** 10, 1259-1264.

Amsden, B. Solute Diffusion within Hydrogels: Mechanisms and Models. *Macromolecules* **1998,** 31, 8382-8395.

Andrews, A. T. *Electrophoresis: Theory, Techniques, and Biochemical and Clinical Applications, 2nd Ed.* Clarendon Press: Oxford, 1986.

Albin, G.; Horbett, T. A.; Ratner, B. D. Glucose-Sensitive Membranes for Controlled Release of Insulin. In *Pulse and Self-Regulated Drug Delivery*; Kost, J., Ed.; CRC Press: Boca Raton, 1990; pp 159-185

Alder, B. J.; Wainwright, T. E. Studies in Molecular Dynamics. I. General Method. *J. Chem. Phys.* **1959,** 31, 459-466.

Allen, M. P.; Tildesley, D. J. *Computer Simulation of Liquids*. Oxford University Press: New York, 1987.

Aluru, N. R. A Reproducing Kernel Particle Method for Meshless Analysis of Microelectromechanical Systems. *Comput. Mech.* **1999,** 23, 324-338.

Aluru, N. R. A Point Collocation Method Based on Reproducing Kernel Approximations. *Int. J. Numer. Methods Eng.* **2000,** 47, 1083-1121.

Aluru, N. R.; Li, G. Finite Cloud Method: A True Meshless Technique Based on A Fixed Reproducing Kernel Approximation. *Int. J. Numer. Methods Eng.* **2001,** 50, 2373-2410.

Aqvist, J.; Luzhkov, V. Ion Permeation Mechanism of the Potassium Channel. *Nature* **2000,** 404, 881-884.

Atluri, S.N.; Zhu, T. A New Meshless Local Petrov-Galerkin (MLPG) Approach in Computational Mechanics. *Comput. Mech.* **1998,** 22, 117-127.

Atluri, S.N. *The Meshless Method (MLPG) for Domain & BIE Discretizations*. Tech Science Press: Forsyth, GA, 2004.

Babuska, I.; Melenk, J. M. The Partition of Unity Method. *Adv. Comput. Math.* **1997,** 40, 727-758.

Babuska, I.; Banerjee, U.; Osborn, J. E. *Survey of Meshless and Generalized Finite Element Methods: A Unified Approach.* TICAM Report 02-40; The University of Texas: Austin, 2002.

Bajpai, S. K. Swelling Studies on Hydrogel Networks – A Review. *J. Sci. Ind. Res.* **2001,** 60, 451-462.

Bar-Cohen Y., Ed.; *Electroactive Polymer (EAP) Actuator As Artificial Muscles – Reality, Potential And Challenges*; SPIE Press monograph v. PM98; SPIE Press : Bellingham, Washington, 2001.

Basser, P. J.; Grodzinsky, A. J. The Donnan Model Derived from Microstructure. *Biophys. Chem*. **1993,** 46, 57-68.

Beebe, D. J.; Moore, J. S.; Bauer, J. M.; Yu, Q.; Liu, R. H.; Devadoss, C.; Jo, B. H. Functional Hydrogel Structures for Autonomous Flow Control inside Microfluidic Channels. *Nature* **2000a,** 404, 588-590.

Beebe, D. J.; Moore, J. S.; Yu, Q.; Liu, H.; Kraft, M. L.; Jo, B. H.; Devadoss C. Microfluidic tectonics: A Comprehensive Construction Platform for Microfluidic Systems. *Proceedings of the National Academy of Sciences of the United States of America*, **Dec 5 2000b,** *97*, 13488-13493.

Bell, C. L.; Peppas, N. A. Biomedical Membranes from Hydrogels and Interpolymer Complexes. In *Biopolymer II*; Peppas, N. A., Langer, R. S., Eds.; Advances in Polymer Science 122; Springer-Verlag: Berlin, 1995; pp 125-175.

Belytschko, T; Lu, Y. Y. A Curvilinear Overlay Method for High Gradient Problems. *Comput. Meth. Appl. Mech. Eng.* **1992,** 95, 383-396.

Belytschko, T.; Lu, Y. Y.; Gu, L. Element-Free Galerkin Methods. *Int. J. Numer. Methods Eng.* **1994,** 37, 229-256.

Belytschko, T.; Krongauz, Y.; Organ, D.; Fleming, M. Meshless Methods: An Overview and Recent Developments. *Comput. Meth. Appl. Mech. Eng.* **1996,** 139, 3-47.

Belytschko, T.; Liu, W. K.; Moran, B. *Nonlinear Finite Elements for Continua and Structures.* John Wiley & Sons: New York, 2000.

Binder, K. Applications of Monte Carlo Methods to Statistical Physics. *Rep. Prog. Phys.* **1997,** 60, 487-559.

Biot, M. A. General Solutions of the Equations of Elasticity and Consolidation for a Porous Material. *J. Appl. Mech.-Trans. ASME* **1956,** *23,* 92-96.

Bischoff, R.; Cray, S. E. Polysiloxanes in macromolecular architecture. *Prog. Polym. Sci.* **1999,** 24, 185-219.

Bockris, J. O. M.; Reddy-Amulya, K. N. *Modern Electrochemistry: Ionics*, 2nd ed.; Plenum Press: New York, 1998.

Boresi, A. P.; Chong, K. P.; Saigal, S. *Approximate Solution Methods in Engineering Mechanics.* John Wiley & Sons: New Jersey, 2003.

Bowen, R. M. Incompressible Porous Media Models by Use of The Theory of Mixture. *Int. J. Engng. Sci.* **1980,** 18, 1129-1148.

Brannon-Peppas, L.; Peppas, N. A. Equilibrium Swelling of pH-Sensitive Hydrogels. *Chem. Eng. Sci.* **1991a,** 46, 715-722.

Brannon-Peppas, L.; Peppas, N. A. Equilibrium Swelling Behavior of Dilute Ionic Hydrogels in Electrolytic Solutions. *J. Control. Release* **1991b,** 16, 319-330.

Brazel, C. S.; Peppas, N. A. Mechanism of Solute and Drug Transport in Relaxing, Swellable, Hydrophilic Glassy Polymers. *Polymer* **1999,** 40, 3383-3398.

Brock, D.; Lee, W., Segalman, D.; Witkowski, W. A Dynamic Model of a Linear Actuator Based on Polymer Hydroionic Polymeric Gel. *J. Intell. Mater. Syst. Struct.* **1994,** 5, 764-761.

Brondsted, H.; Kopecek, J. pH-Sensitive Hydrogels: Characteristics and Potential in Drug Delivery. In *Polyelectrolyte Gels: Properties Preparation and Applications;* Harland, R. S., Prud'homme, R. K., Eds.; ACS Symposium Series 480; American Chemical Society: Washington, DC, 1992; pp 285-304.

Burykin, A.; Schutz, C. N.; Villa, J.; Warshel, A. Simulations of Ion Current in Realistic Models of Ion Channels: The KcsA Potassium Channel. *Proteins.* **2002,** 47, 265-280.

Carnay, L. D.; Tasaki, I. Ion Exchange Properties and Excitability of the Squid Giant Axon. In *Biophysics and Physiology of Excitable Membranes*; W. J. Adelman Jr., Ed.; Van Nostrand Reinhold Co.: New York, 1971; pp 379-422.

Cascales, J. J. L.; Fernandez, A. J.; Otero, T. F. Characterization of the Reduced and Oxidized Polypyrrole/Water Interface: A Molecular Dynamics Simulation Study. *J. Phys. Chem. B* **2003,** 107, 9339-9343.

Chandrasekhar, S. Stochastic Problems in Physics and Astronomy. *Rev. Mod. Phys.* **1943,** 15, 1-89.

Chati, M. K.; Mukherjee, Y. X.; Mukherjee, S. The Boundary Node Method for Three-Dimensional Linear Elasticity. *Int. J. Numer. Methods Eng.* **1999,** 46, 1163-1184.

Chiarelli, P.; Umezawa, K.; De Rossi, D. A polymer Composite showing Electrocontractile Response. In *Polymer Gels: Fundamental and Biomedical*

Applications; DeRossi, D.; Kajiwara, K.; Osada, Y.; Yamauchi, A., Eds.; Plenum Press: New York, 1991.

Chu, Y.; Varanasi, P. P.; McGlade, M. J.; Varanasi, S. pH-Induced Swelling Kinetics of Polyelectrolyte Hydrogels. *J. Appl. Polym. Sci.* **1995,** 58, 2161-2176.

Coalson, R. D.; Kurnikova, M. G. Poisson-Nernst-Planck Theory Approach to the Calculation of Current through Biological Ion Channels. *IEEE Trans. Nanobioscience* **2005,** 4, 81-93.

Cooper, G. M.; Hausman, R. E. *The Cell: A Molecular Approach, 2nd Ed.* ASM Press: Washington, DC, 2000.

Cooper, K.; Jakobsson, E.; Wolynes, P. The Theory of Ion Transport through Membrane Channels. *Prog. Biophys. Mol. Biol.* **1985,** 46, 51-96.

Cussler, E. L. *Diffusion Mass Transfer in Fluid System, 2nd Ed.* Cambridge University Press: Cambridge, 1997.

Cussler, E. L.; Stokar, M. R.; Varberg, J. E. Gels as Size Selective Extraction Solvents. *AICHE J.* **1984,** 30, 578-582.

Dario, P.; De Rossi, D. Tactile Sensors and the Gripping Challenge, *IEEE Spectrum,* **1985,** 22, 46-52.

De, S.; Bathe, K. The Method of Finite Spheres. *Comput. Mech.* **2000,** 25, 329-345.

De, S.; Bathe, K. Displacement/Pressure Mixed Interpolation in the Method of Finite Spheres. *Int. J. Numer. Methods Eng.* **2001,** 51, 275-292.

De, S. K.; Aluru, N. R. A Chemo-Electro-Mechanical Mathematical Model for Simulation of pH Sensitive Hydrogels. *Mech. Mater.* **2004,** 36, 395-410.

De, S. K.; Aluru, N. R.; Johnson, B.; Crone, W.C.; Beebe, D. J.; Moore, J. Equilibrium Swelling and Kinetics of pH-Responsive Hydrogels: Models, Experiments and Simulations. *J. Microelectromech. Syst.* **2002,** 11, 544-555.

De Gennes, P. G.; Okumura, K.; Shahinpoor, M.; Kim. K. J. Mechanoelectric effects in Ionic Gels. *Europhys. Lett.* **2000,** 50, 513-518.

De Rossi, D.; Parrini, P.; Chiarelli, P.; Buzzigoli, G. Electrically Induced Contractile Phenomena in Charged Polymer Networks: Preliminary Study on the Feasibility of Muscle-like Structures. *Trans. Am. Soc. Artif. Intern. Organs* **1985,** XXXI, 60-65.

De Rossi, D.; Chiarelli, P.; Buzzigoli, G.; Domenici, G.; Lazzeri, L. Contractile Behavior of Electrically Activated Mechanochemical Polymer Actuators. *Trans. Am. Soc. Artif. Intern. Organs* **1986,** XXXII, 157-162.

De Rossi, D.; Nannini, A.; Domenici, G. Biomimetic Tactile Sensor with Stress Component Discrimination Capability. *J. Mol. Electron.* **1987,** 3, 173-181.

De Rossi, D.; Domenici, G.; Chiarelli, P. Analogs of Biological Tissues for Mechanoelectrical Transduction: Tactile Sensors and Muscle-Like Actuators. In *Sensors and Sensory Systems for Advanced Robots*; Dario, P., Ed.; NAATO ASI Series Vol. F43; Springer-Verlag: Berlin, 1988a.

De Rossi, D.; Nannini, A.; Domenici, G. Artificial Sensing Skin Mimicking Mechanoelectrical Conversion Properties of Human Dermis. *IEEE Trans. Biomed. Eng.* **1988b,** 35, 83-92.

DeRossi, D.; Kajiwara, K.; Osada, Y.; Yamauchi, A., Eds. Polymer Gels: Fundamental and Biomedical Applications, Proceedings of an International Symposium on Polymer Gels, Tsukuba, Japan, Sept 18-21, 1989; Plenum Press: New York, 1991.

DeVore, R. A.; Lorentz, G. G. Constructive Approximation: Polynomial and Splines Approximation; Grundlehren der Mathematischen Wissenschaften 303; Springer-Verlag: Berlin, 1993.

Doi, M.; Matsumoto, M.; Hirose, Y. Deformation of Ionic Polymer Gels by Electric Fields. *Macromolecules* **1992,** 25, 5504-5511.

Domenici, G.; De Rossi, D.; Bacci, A.; Bennati, S. Shear Stress Detection in an Elastic Layer by a Piezoelectric Polymer Tactile Sensor, *IEEE Trans. Electr. Insul.* **1989,** 24, 1077-1081.

Dobrynin, A. V.; Rubinstein, M.; Obukhov, S. P. Cascade of Transitions of Polyelectrolytes in Poor Solvents. *Macromolecules* **1996,** *29,* 2974-2979.

Dresner, L. Some Remarks on the Integration of Extended Nernst-Planck Equations in the Hyperfiltration of Multicomponent Solution. *Desalination* **1972,** 10, 27-46.

Duarte, C. A. *A Review of Some Meshless Methods to Solve Partial Differential Equations.* TICAM Report 95-06; The University of Texas: Austin, 1995.

Duarte, C. A.; Oden, J. T. An *h-p* Adaptive Method Using Clouds. *Comput. Methods Appl. Mech. Eng.* **1996,** 139, 237-262.

Dumitriu, S., Ed., *Polymeric Biomaterials, 2nd*. Marcel Dekker: New York, 2002.

Dusek, K., Ed. *Responsive Gels: Volume Transitions I*; Advances in Polymer Science Vol. 109; Springer-Verlag: Berlin, 1993a.

Dusek, K., Ed. *Responsive Gels: Volume Transitions II*; Advances in Polymer Science Vol. 110; Springer-Verlag: Berlin, 1993b.

Dusek, K; Patterson, D. Transition in Swollen Polymer Networks Induced by Intramolecular Condensation. *J. Polym. Sci. Part A2* **1968,** 6, 1209-1216.

Eisenberg, R. S. From Structure to Function in Open Ionic Channel. *J. Membrane Biol.* **1999,** 171, 1-24.

Elbert, D. L.; Hubbel, J. A. Surface treatments of Polymers for Biocompatibility. *Annu. Rev. Mater. Sci.* **1996,** 26, 365-394.

Ermak, D. J. A Computer Simulation of Charged Particles in Solution. I. Technique and Equilibrium Properties. *J. Chem. Phys.* **1975a,** 62, 4189-4196.

Ermak, D. J. A Computer Simulation of Charged Particles in Solution. II. Polyion Diffusion Coefficient. *J. Chem. Phys.* **1975b,** 62, 4189-4196.

Ermak, D. J.; McCammon, J. A. Brownian Dynamics with Hydrodynamic Interactions. *J. Chem Phys.* **1978,** 69, 1352-1360.

Erman, B.; Flory, P. J. Critical Phenomena and Transitions in Swollen Polymer Networks and in Linear Macromolecules. *Macromolecules* **1986,** 19, 2342-2353.

Escobedo, F. A.; Pablo, J. J. Molecular Simulation of Polymeric Networks and Gels: Phase Behavior and Swelling. *Phys. Rep.* **1999,** 318, 85-112.

Eyring, H. Viscosity, Plasticity, and Diffusion as Examples of Absolute Reaction Rates. *J. Chem. Phys.* **1936,** 4, 283-291.

Fasshauer, G. E. Solving Differential Equations with Radial Basis Functions: Multilevel Methods and Smoothing. *Adv. Comput. Math.* **1999,** 11, 139-159.

Fei, J.; Zhang, Z.; Gu, L. Bending Behavior of Electroresponsive Poly(vinyl alcohol)/ Poly(acrylic acid) Semi-interpenetrating Network Hydrogel Fibers under an Electric Stimulus. *Polym. Int.* **2002,** 51, 502-509.

Flory, P. J. Thermodynamics of High Polymer Solutions. *J. Chem. Phys.* **1942,** 10, 51-61.

Flory, P. J. *Principle of Polymer Chemistry*. Cornell University Press: New York, 1962.

Flory, P. J.; Rehner Jr., J. Statistical Mechanics of Cross-linked Polymer Networks. I. Rubberlike Elasticity. *J. Chem. Phys.* **1943a,** 11, 512-520.

Flory, P. J.; Rehner Jr., J. Statistical Mechanics of Cross-linked Polymer Networks. II. Swelling. *J. Chem. Phys.* **1943b,** 11, 521-526.

Fragala, A.; Enos, J.; LaConti, A.; Boyack J. Electrochemical Activation of a Synthetic Artificial Muscle Membrane. *Electrochim. Acta* **1972,** 17, 1507-1522.

Frenkel, D.; Smit, B. *Understanding Molecular Simulation: from Algorithm to Application*. Academic Press: San Diego, CA, 1996.

Freund, J. B. Electro-Osmosis in a Nanometer-Scale Channel Studied by Atomistic Simulation. *J. Chem. Phys.* **2002,** 116, 2194-2200.

Galaev, I; Mattiasson, B., Eds., *Smart Polymers for Bioseparation and Bioprocessing*; Taylor & Francis: London 2002.

Gehrke, S. H.; Cussler, E. L. Mass Transfer in pH-Sensitive Hydrogels. *Chem. Eng. Sci.* 1989, 44, 559-566.

Gillespie, D.; Eisenberg, R. S. Modified Donnan Potentials for Ion Transport Through Biological Ion Channels. *Phys. Rev. E* **2001,** 63, 061902.

Gillespie, D.; Eisenberg, R. S. Physical Descriptions of Experiemntal Selectivity Measurements in Ion Channels. *Eur. Biophys. J.* **2002,** 31, 454-466.

Gingold, R. A.; Monaghan, J. J. Smooth Particle Hydrodynamics: Theory and Applications to Non-Spherical Stars. *Mon. Not. R. Astron. Soc.* **1977,** 181, 375-389.

Gingold, R. A.; Monaghan, J. J. Kernel Estimates as a Basis for General Particle Methods in Hydrodynamics. *J. Comput. Phys.* **1982,** 46, 429-453.

Goldman, D. E. Potential, Impedance and Rectification in Membranes. *J. Gen. Physol.* **1943,** 27, 37-60.

Goldman, D. E. Excitability Models. In *Biophysics and Physiology of Excitable Membranes*; W. J. Adelman Jr., Ed.; Van Nostrand Reinhold Co.: New York, 1971; pp 337-358.

Gong, J. P.; Komatsu, N.; Nitta, T.; Osada, Y. Electrical Conductance of Polyelectrolyte Gels. *J. Phys. Chem. B* **1997,** 101, 740-745.

Gong, J. P.; Nitta, T.; Osada, Y. Electrokinetic Modeling of Contractile Phenomena of Polyelectrolyte Gels. One-Dimensional Capillary Model. *J. Phys.Chem.* **1994,** 98, 9583-9587.

Gong, J. P.; Osada, Y. Modeling and Simulation of Electrostatic Potential Distribution in Polyelectrolyte Gels. *Electrochimica Acta* **1995,** 40, 2445-2447.

Gosz, J.; Liu, W. K. Admissible Approximations for Essential Boundary Conditions in the Reproducing Kernel Particle Method. *Comput. Mech.* **1996,** 19, 120-135.

Grignon, J.; Scallan, A. M. Effect of pH and Neutral Slats upon the Swelling of Cellulose Gels. *J. Appl. Polym. Sci.* **1980,** 25, 2829-2843.

Grimshaw, P. E. Electrical Control of Solute Transport Across Polyelectrolyte Membranes. Ph. D. Thesis, Massachusetts Institute of Technology, MA, 1989.

Grimshaw, P. E.; Grodzinsky, A. J.; Yarmush, M. L.; Yarmush, D. M. Dynamic membranes for Protein Transport: Chemical and Electrical Control. *Chem. Eng. Sci.* **1989,** 44, 827-840.

Grimshaw, P. E.; Nussbaum, J. H.; Grodzinsky, A. J.; Yarmush, M. L. Kinetics of Electrically and Chemically Induced Swelling in Polyelectrolyte Gels. *J. Chem. Phys.* **1990,** *93*, 4462-4472.

Grodzinsky, A. J. Sc.D Thesis, Massachusetts Institute of Technology, MA, 1974.

Grodzinsky, A. J.; Melcher, J. R. Electromechanical Transduction with Charged Polyelectrolyte Membranes. *IEEE Trans. Biomed. Eng.* **1976,** 23, 421-433.

Grodzinsky, A. J.; Shoenfeld, N. A. Tensile Forces induced in Collagen by means of Electromechanochemical Transductive Coupling. *Polymer* **1977,** 18, 435-443.

Gu, W. Y.; Lai, W. M.; Mow, V. C. A Mixture Theory for Charged-Hydrated Soft Tissues Containing Multi-Electrolytes: Passive Transport and Swelling Behaviors. *J. Biomech. Eng.-Trans. ASME* **1998,** 120, 169-180.

Gulch, R. W.; Holdenried, J.; Weible, A.; Wallmersperger, T.; Kroplin, B. Polyelectrolyte Gels in Electric Fields. A Theoretical and Experimental Approach. In *Smart Structures and Materials 2000: Electroactive Polymer Actuators and Devices;* Bar-Cohen Y., Ed.; Proceedings of the SPIE 3987; SPIE Press: Bellingham, Washington, 2000.

Guldbrand, L.; Jonsson, B.; Wennerstrom, H.; Linse, P. Electrical Double Layer Forces. A Monte Carlo Study. *J. Chem. Phys.* **1984,** 80, 2221-2228.

Guldbrand, L.; Nordenskiold, L. Brownian Dynamics Simulation of Counterion Dynamics in Cylindrical Polyelectrolyte. *J. Phys. Chem*. **1987,** 91, 5714-5718.

Gunther, F. C.; Liu, W. K. Implementation of Boundary Conditions for Meshless Methods. *Comput. Methods Appl. Mech. Engrg.* **1998,** 163, 205-230.

Hanggi, P.; Talkner, P.; Borkovec, M. Reaction-Rate Theory: Fifty Years after Kramer. *Rev. Mod. Phys.* **1990,** 62, 251-339.

Hamlen, R. P.; Kent, C. E.; Shafer, S. N. Electrolytically Activated Contractile Polymer. *Nature* **1965,** 206, 1149-1150.

Harland, R. S.; Prud'homme, R. K., Eds., *Polyelectrolyte Gels: Properties Preparation and Applications;* Proceeding of American Chemical Society Symposium Series, Nov 11-16, ACS Symposium Series 480; American Chemical Society: Washington, DC. 1992.

Hasa, J.; Ilavsky, M.; Dusek, K. Deformation, Swelling, and Potentiometric Behavior of Ionized Poly(methacrylic acid). *J. Polym. Sci. Pt. B-Polym. Phys.* **1975,** 13, 253-262.

Helfferich, F. *Ion Exchange;* McGraw-Hill: New York, 1962.

Hicks, C. R.; Fitton, J. H.; Chirila, T. V.; Crawford, G. J.; Constable, I. J. Keratoprostheses: Advancing toward a True Artificial Cornea. *Surv. Ophthalmol.* **1997,** 42, 175-189.

Hille, B. *Ionic Channels of Excitable Membranes*; Sinauer Associates Inc.: Sunderland, MA, 1992.

Hirokawa, Y.; Tanaka, T.; Sato, E. Phase Transition of Positively Ionized Gels. *Macromolecules* **1985,** 18, 2782-2784.

Hladky, S. B. The Energy Barriers to Ion Transport by Nonactin Across Thin Lipid Membranes. *Biochim. Biophys. Acta* **1974,** 352, 71-85.

Hockney, R.W.; Eastwood, J.W. *Computer simulations using particles;* McGraw-Hill: New York, 1981.

Hodgkin, A. L.; Katz, B. The Effect of Sodium Ions on the Electrical Activity of the Giant Axon of the Squid. *J. Physiol.* **1949,** 108, 37-77.

Homma, M.; Seida, Y.; Nakano, Y. Evaluation of Optimum Condition for Designing High-Performance Electro-Driven Polymer Hydrogel Systems. *J. Appl. Polym. Sci.* **2000,** 75, 111-118.

Homma, M.; Seida, Y.; Nakano, Y. Effect of Ions on the Dynamic Behavior of an Electrodriven Ionic Polymer Hydrogel Membrane. *J. Appl. Polym. Sci.* **2001,** 82, 76-80.

Hon, Y. C.; Lu, M. W.; Xue, W. M.; Zhou, X. A New Formulation and Computation of the Triphasic Model for Mechno-Electrochemical Mixtures. *Comput. Mech.* **1999,** 4, 155-165.

Hooper, H. H.; Baker, J. P.; Blanch, H. W.; Prausnitz, J. M. Swelling Equilibrium for Positively Ionized Polyacrylamide Hydrogels. *Macromolecules* **1990,** 23, 1096-1104.

Huggins, M. L. Some Properties of Solutions of Long-Chain Compounds. *J. Phys. Chem.* **1942,** 46, 151-158.

Huyghe, J. M.; Janssen, J. D. Quadriphasic Mechanics of Swelling Incompressible Porous Media. *Int. J. Eng. Sci.* **1997,** 35, 793-802.

Hwang, Y.; Helfferich, F. Generalized Model for Multispecies Ion-Exchange Kinetics Including Fast Reversible Reactions. *React. Polym.* **1987,** 5, 237-253.

Ilavsky, M. Effect of electrostatic interactions on phase transition in the swollen polymeric network. *Polymer* **1981,** 22, 1687-1691.

Im W.; Roux, B. Brownian Dynamics Simulations of Ion Channels: A General Treatment of Electrostatic Reaction Fields for Molecular Pores of Arbitrary Geometry. *J. Chem. Phys.* **2001,** 115, 4850-4861.

Im W.; Roux, B. Ion Permeation and Selectivity of OmpF Porin: A Theoretical Study Based on Molecular Dynamics, Brownian Dynamics, and Continuum Electrodiffusion Theory. *J. Mol. Biol.* **2002,** 322, 851-869.

Irie, M. Photoresponsive Polymers. Reversible Bending of Rod-Shaped Acrylamide Gels in an Electric Field. *Macromolecules* **1986,** 19, 2890-2892.

Irie, M.; Kunwatchakun, D. Photoresponsive polymers. 8. Reversible Photostimulated Dilation of Polyacrylamide Gels having Triphenylmethane Leuco Derivatives. *Macromolecules* **1986,** 19, 2476-2480.

Jensen, P. S. Finite Difference Techniques for Variable Grids. *Comput. Struct.* **1980,** 2, 17-29.

Johansson, L.; Skantze, U.; Lofroth, J. E. Diffusion and Interaction in Gels and Solution. 6. Charged Systems. *J. Phys. Chem.* **1993,** 97, 9817-9824.

Johnson, B.; Niedermaier, D. J.; Crone, W. C.; Moorthy, J.; Beebe, D. J. Mechanical Properties of a pH Sensitive Hydrogel. *Proceedings of the 2002 SEM Annual Conference*, Milwaukee, June 10-12, 2002.

Johnson, B. D.; Beebe, D. J.; Crone, W. C. Effects of Swelling on the Mechanical Properties of a pH-sensitive Hydrogel for Use in Microfluidic Devices. *Mater. Sci. Eng. C-Biomimetic Supramol. Syst.* **2004a,** 24, 575-581.

Johnson, B. D.; Bauer, J. M.; Niedermaier, D. J.; Crone, W. C; Beebe, D. J. Experimental Techniques for Mechanical Characterization of Hydrogels at the Microscale. *Exp. Mech.* **2004b,** 44, 21-28.

Kajiwara, K.; Ross-Murphy, S. Synthetic Gels on the Move. *Nature* **1992,** 355, 208-209.

Katayama, S.; Ohata, A. Phase Transition of a Cationic Gel. *Macromolecules* **1985,** 18, 2781-2782.

Katchalsky, A. Rapid Swelling and Deswelling of Reversible Gels of Polymeric Acids by Ionization. *Experientia* **1949,** 5, 319-320.

Katchalsky, A.; Curran, P. F. *Nonequilibrium Thermodynamics in Biophysics.* Havard University Press: Massachusetts, 1965.

Katchalsky, A.; Lifson, S.; Eisenberg, H. Equation of Swelling for Polyelectrolyte Gels. *J. Polym. Sci.* **1951,** 7,571-574.

Katchalsky, A. Michaeli, I. Polyelectrolyte gels in Salt Solutions. *J. Polym. Sci.* **1955,** 15, 69-86.

Kato, M. Numerical Analysis of the Nernst-Planck-Poisson System. *J. Theor. Biol.* **1995,** *177,* 299-304.

Khare, A. R.; Peppas, N. A. Swelling/Deswelling of Anionic Copolymer Gels. *Biomaterials* **1995,** 16, 559-567.

Khokhlov, A. R. Swelling and collapse of polymer networks. *Polymer* **1980,** 21, 376-380.

Kim, B.; Peppas, N. A. Complexation Phenomena in pH-Responsive Copolymer Networks with Pendent Saccharides. *Macromolecules* **2002,** 35, 9545-9550.

Kim, D. W.; Kim Y. S. Point Collocation Methods Using the Fast Moving Least-Square Reproducing Kernel Approximation. *Int. J. Numer. Methods Eng.* **2003,** 56, 1445-1464.

Kim, I. C.; Torquato, S. Diffusion of Finite-Sized Brownian Particles in Porous Media. *J. Chem. Phys.* **1992,** 96, 1498-1503.

Kim, S. J.; Lee, K. J.; Kim, S. I.; Lee, Y. M.; Chung, T. D.; Lee, S. H. Electrochemical Behavior of an Interpenetrating Polymer Network Hydrogel Composed of Poly(propylene glycol) and Poly(acrylic acid). *J. Appl. Polym. Sci.* **2003,** 89, 2301-2305.

Kim, S. J.; Yoon, S. G.; Lee, S. M.; Lee, S. H.; Kim, S. I. Electrical Sensitivity Behavior of a Hydrogel Composed of Polymethacrylic Acid/Poly(vinyl alcohol). *J. Appl. Polym. Sci.* **2004,** 91, 3613-3617.

Kim, S. Y.; Shin, H. S.; Lee, Y. M.; Jeong, C. N. Properties of Electroresponsive Poly(vinylalcohol)/Poly(acrylic acid) IPN Hydrogels under an Electric Stimulus. *J. Appl. Polym. Sci.* **1999,** 73, 1675-1683.

Kishi, R.; Osada, Y. Reversible Volume Change of Microparticles in an Electric Field. *J. Chem. Soc. Faraday Trans.* **1989,** 85, 655-662.

Kishi, R.; Hasebe, M.; Hara, M.; Osada, Y. Mechanism and Process of Chemomechanical Contraction of Polyelectrolyte Gels under Electric Field. *Polym. Adv. Technol.* **1990,** 1, 19-25.

Konak, C.; Bansil, R. Swelling Equilibria of Ionized Poly(methacrylic acid) Gels in the Absence of Salt. *Polymer* **1989,** 30, 677-690.

Kremer, K. Numerical Studies of Polymer Networks and Gels. *Comput. Mat. Sci.* **1998,** 10, 168-174.

Krongauz, Y. PhD. Thesis, Northwestern University, IL, 1996.

Krongauz, Y.; Belytschko, T. Enforcement of Essential Boundary Conditions in Meshless Approximations Using Finite Elements. *Comput. Methods Appl. Mech. Engrg.* **1996,** 131, 133-145.

Kuhn, W.; Hargitay, B.; Katchalsky, A.; Eisenberg, H. Reversible Dilation and Contraction by Changing the state of Ionization of High-Polymer Acid Networks. *Nature* **1950,** 165, 514-516.

Kurauchi, T.; Shiga, T.; Hirose, Y.; Okada, A. Deformation Behaviors of Polymer Gels in Electric Fields. In *Polymer Gels*; DeRossi, D., Kajiwara, K., Osada, Y., Yamauchi, A., Eds, Plenum Press: New York, 1991; pp 237-246.

Kurnikova, M. G.; Coalson, R. D.; Graft, P.; Nitzan, A. A Lattice Relaxation Algorithm for Three-Dimensional Poisson-Nernst-Planck Theory with Application to Ion Transport through the Gramicidin A Channel. Biophysical Journal **1999,** 76, 642-656.

Kwon, I. C.; Bae, Y. H.; Kim, S. W. Electrically credible polymer gel for controlled release of drug. *Nature* **1991a,** 354, 291-293.

Kwon, I. C.; Bae, Y. H.; Okano, T.; Kim, S. W. Drug Release from Electric Current Sensitive Polymer. *J. Control. Release* **1991b,** 17, 149-156.

Lai, W. M.; Hou, J. S.; Mow, V. C. A Triphasic Theory for the Swelling and Deformation Behaviors of Articular Cartilage. *ASME J. Biomech. Eng.* **1991,** 113, 245-258.

Laio, A.; Torre, V. Physical Origin of Selectivity in Ionic Channels of Biological Membranes. *Biophys. J.* **1999,** 76, 129-148.

Lakshminarayanaiah, N. *Transport Phenomena in Membrane;* Academic Press: New York, 1970.

Lancaster, P.; Salkauskas, K. Surfaces Generated by Moving Least Squares Methods. *Math. Comput.* **1981,** 37, 141-158.

Lauger, P. Ion Transport Through Pores: A Rate-Theory Analysis. *Biochim. Biophys. Acta* **1973,** 311, 423-441.

Lauger, P. Microscopic calculation of Ion-Transport Rates in Membrane Channels. *Biophys. Chem.* **1982,** 15, 89-100.

Lee, C. R.; Grodzinsky, A. J.; Hsu, H. P.; Spector, M. Effects of a Cultured Autologous Chondrocyte-seeded Type II Collagen Scaffold on the Healing of a Chondral Defect in a Canine Model. *J. Orthop. Res.* **2003,** 21, 272-281.

Li, H.; Ng, T. Y.; Cheng, J. Q.; Lam, K. Y. Hermite-Cloud: A Novel True Meshless Method. *Comput. Mech.* **2003,** 33, 30-41.

Li, S. F.; Liu, W. K. Meshfree and Particle Methods and Their Applications. *Appl. Mech. Rev.* **2002,** 55, 1-34.

Li, Y.; Tanaka, T. Kinetics of Swelling and Shrinking of Gels. *J. Chem. Phys.* **1990,** 92, 1365-1371.

Lide, D. R., Ed. *CRC Handbook of Chemistry and Physics*, 83rd ed.; CRC Press: Boca Raton, 2002.

Liew, K. M., Ng, T. Y., Wu, Y. C. Meshfree Method for Large Deformation Analysis – A Reproducing Kernel Particle Approach. *Eng. Struct.* **2002,** 24, 543-551.

Liszka, T.; Orkisz, J. The Finite Difference Method at Arbitrary Irregular Grids and Its Application in Applied Mechanics. *Comput. Struct.* **1980,** 11, 83-95.

Liszka, T. J.; Duarte, C. M. A.; Tworzydlo, W. W. *hp*-Meshless Cloud Method. *Comput. Methods Appl. Mech. Eng*. **1996,** 139, 263-288.

Liu, G. R.; Gu, Y. T. A Point Interpolation Method for Two-Dimensional Solids. *Int. J. Numer. Methods Eng.* **2001,** 50, 937-951.

Liu, G. R. *Mesh Free Methods: Moving beyond the Finite Element Method*; CRC Press: Boca Raton, 2002.

Liu, G. R.; Liu, M. B. *Smoothes Particle Hydrodynamics*; World Scientific: Singapore, 2003.

Liu, G. R.; Gu, Y. T. A Meshfree Method: Meshfree Weak-Strong (MWS) form method for 2-D Solids. *Comput. Mech.* **2003,** 33, 2-14.

Liu, W. K.; Jun, S.; Zhang, Y. F. Reproducing Kernel Particle Methods. *Int. J. Numer. Methods Fluids* **1995a,** 20, 1081-1106.

Liu, W. K.; Chen, Y. J. Wavelet and Multiple Scale Reproducing Kernel Method. *Int. J. Numer. Methods Fluids* **1995b,** 21, 901-933.

Liu, W. K.; Jun, S.; Li, S. F.; Adde, J.; Belytschko, T. Reproducing Kernel Particle Methods for Structural Dynamics. *Int. J. Numer. Methods Eng.* **1995c,** *38*, 1665-1679.

Liu, W. K.; Chen, Y.; Chang, C. T.; Belytschko, T. Advances in Multiple Scale Kernel Particle Methods. *Comput. Mech.* **1996a,** 18, 73-111.

Liu, W. K.; Chen, Y. J.; Uras, R. A.; Chang, C. T. Generalized Multiple Scale Reproducing Kernel Particle Methods. *Comput. Methods Appl. Mech. Eng*. **1996b**, 139, 91-157.

Liu, W. K.; Li, S. F.; Belytschko, T. Moving Least-Square Reproducing Kernel Methods (I) Methodology and Convergence. *Comput. Methods Appl. Mech. Eng*. **1997,** 143, 113-154.

Lonergan, M .C.; Shriver, D. F.; Ratner, M. A. Polymer Electrolytes: The Importance of Ion-ion Interactions in Diffusion Dominated Behavior. *Electrochim. Acta* **1995,** 40, 2041-2048.

Lowman, A. M.; Peppas, N. A. Hydrogels. In *Encyclopedia of Controlled Drug Delivery*; Mathiowitz, E., Ed, Wiley: New York, 1999; pp 397-418.

Lu, Y. Y.; Belytschko, T.; Gu, L. A New Implementation of the Element Free Galerkin Method. *Comput. Methods Appl. Mech. Eng*. **1994,** 113, 397-414.

Lucy, L., “A numerical approach to testing the fission hypothesis.” Astron. J., 82:1013-1024, 1977.

MacGillivray, A. D. Nernst-Planck Equation and the Electroneutrality and Donan Equilibrium Assumptions. *J. Chem. Phys.* **1968,** *48*, 2903-2907.

MacGillivray, A. D.; Hare, D. Applicability of Goldman’s Constant Field Assumption to Biological Systems. *J. Theor. Biol.* **1969,** *25*, 113-126.

Mackie, J.S.; Meares, P. The Diffusion of Electrolytes in a Cation-Exchange Resin Membrane. I. Theoretical. *Proc. R. Soc. London, Ser A* **1955,** 232, 498-509.

Malmivuo, J.; Plonsey, R. *Bioelectromagnetism: Principles and Applications of Bioelectric and Biomagnetic Fields.* Oxford University Press: New York, 1995.

Malvern, L. E. *Introduction to the Mechanics of A Continuum Medium*. Prentice-Hall: Englewood Cliffs, NJ, 1969.

Mann, B. A.; Everaers, R.; Holm, C.; Kremer, K. Scaling in Polyelectrolyte networks. *Europhys. Lett.* **2004,** 67, 786-792.

Marchetti, M.; Prager, S.; Cussler, E. L. Thermodynamic Predictions of Volume Changes in Temperature-Sensitive Gels. 1. Theory. *Macromolecules* **1990,** 23, 1760-1765.

Marchiano S. L.; Arvia A. J. Diffusion in the Absence of Convection : Steady State and Nonsteady State. In *Comprehensive Treatise of Electrochemistry, Volume 6 Electrodics: Transport*; Yeager, E., Bockris, J. O’M., Conway, B. E., Sarangapani, S., Eds.; Plenum Press: New York, 1983; pp 65-132.

Mark, J. E. Some Recent Theory, Experiments, and Simulations on Rubberlike Elasticity. *J. Phys. Chem. B* **2003,** 107, 903-913.

Marry, V.; Grun, F.; Simon, C.; Jardat, M.; Turq, P.; Amatore, C. Structure and Dynamics in Colloidal and Porous Charged Media. *J. Phys.: Condens. Matter* **2002,** 14, 9207-9221.

Melenk, J. M.; Babuska, I. The Partition of Unity Finite Element Method: Basic Theory and Applications. *Comput. Methods Appl. Mech. Eng.* **1996,** 139, 289-314.

Metropolis, N.; Rosenbluth, A. W.; Rosenbluth, M. N.; Teller, A.H. Equation of State Calculations by Fast Computing Machines. *J. Chems. Phys.* **1953,** 21, 1087-1092.

Michaeli, I.; Katchalsky, A. Potentiometric Titration of Polyelectrolyte Gels. *J. Polym. Sci.* **1957,** 23, 683-696.

Mikos, A. G.; Peppas, N. A. Flory Interaction Parameter χ for Hydrophilic Copolymers with Water. *Biomaterials* **1988,** 9, 419-423.

Miyata, T.; Endo, A.; Ohmori, T.; Nakaiwa, M.; Kendo, M.; Kurumada, K. I.; Tanigaki, M. Brownian Dynamics Simulation Study of Self-Diffusion of Charged Particle in Swollen Counter-Charged Hydrogel Modeled as Cubic Lattice. *J. Chem. Eng. Jpn.* **2002,** 35, 640-648.

Monaghan, J. J. Why Particle Methods Work. *SIAM J. Sci. Stat. Comput.* **1982,** 3, 422-433.

Monaghan, J. J.; Lattanzio, J. C. A Refined Particle Method for Astrophysical Problems. *Astron. Astrophys.* **1985,** 149, 135-143.

Monaghan, J. J. An introduction to SPH. *Comput. Phys. Commun.* **1988,** 48, 89-96.

Monaghan, J. J. Smoothed Particle Hydrodynamics. *Annu. Rev. Astron. Astrophys.* **1992,** 30, 543-574.

Mow, V. C.; Kuei, S. C.; Lai, W. M.; Armstrong, C. Biphasic creep and Stress Relaxation of Articular Cartilage in Compression: Theory and Experiment. *ASME J. Biomech. Eng*. **1980,** 102, 73-84.

Mow, V. C; Wang, C. C.; Hung, C. T. The Extracellular Matrix, Interstitial Fluid and Ions as A Mechanical Signal Transducer in Articular Cartilage. *Osteoarthritis Cartilage* **1999,** 7, 41-58.

Mukherjee, Y. X.; Mukherjee, S. The Boundary Node Method for Potential Problems. *Int. J. Numer. Methods Eng.* **1997,** 40, 797-815.

Mukherjee, Y. X.; Mukherjee, S. On Boundary Conditions in the Element-Free Galerkin Method. *Comput. Mech.* **1997,** 19, 264-270.

Muller-Plathe, F. Diffusion of Penetrants in Amorphous Polymers: A Molecular Dynamics Study. *J. Chem. Phys.* **1991,** 94, 3192-3199.

Muhr, A. H.; Blanshard, J. M. V. Diffusion in Gels. *Polymer* 1982, 23, 1012-1026.

Nayroles, B.; Touzot, G.; Villion, P. Generalizing the Finite Element Method: Diffuse Approximation and Diffuse Elements. *Comput. Mech.* **1992,** 10, 307-318.

Nemat-Nasser, S.; Li, J. Y. Electromechanical Response of Ionic Polymer-Metal Composites. *J. Appl. Phys.* **2000,** 87, 3321-3331.

Netz, P. A.; Dorfmuller, T. Computer Simulation Studies of Diffusion in Gels: Model Structures. *J. Chem. Phys.* **1997,** 107, 9221-9233.

Ng, T. Y.; Li, Hua; Cheng, J. Q.; Lam, K. Y. A New Hybrid Meshless Differential Order Reduction (*h*M-DOR) Method with Applications to Shape Control of Smart Structures via Distributed Sensors/Actuators. *Eng. Struct.* **2003a,** 25, 141-154.

Ng, T. Y.; Li, Hua; Cheng, J. Q.; Lam, K. Y.; Yew, Y. K. A Novel True Meshless Numerical Technique (hM-DOR method) for the Deformation Control of Circular

Plate Integrated with Piezoelectric Sensors/Actuators. *Smart Mater. Struct.* **2003b,** 12, 955-961.

Noguchi, T.; Yamamuro, T.; Oka, M.; Kumar, P.; Kotoura, Y.; Hyon, S. H.; Ikada, Y. Poly(vinyl alcohol) Hydrogels as an Artificial Articular-Cartilage – Evolution of Biocompatibility. *J. Appl. Biomat.* **1991,** 2, 101-107.

Nussbaum, J. H. Electric Field Control of Mechanical and Electrochemical Properties of Polyelectrolyte Gels Membranes. Sc. D. Thesis, Massachusetts Institute of Technology, MA, 1986.

Nussbaum, J. H.; Grodzinsky, A. L. Proton Diffusion Reaction in Protein Polyelectrolyte Membrane and the Kinetics of Electromechanical Forces. *J. Membr. Sci.* **1981,** 8, 193-219.

Ohmine, I.; Tanaka, T. Salt effects on the phase transition of ionic gels. *J. Chem. Phys.* **1982,** 77, 5725-5729.

Oldiges, C.; Tonsing, T. Molecular Dynamic Simulation of Structural, Mobility Effects between Dilute Aqueous CH_3CN Solution and Crosslinked PAA. Part 1. Structure. *Phys. Chem. Chem. Phys.* **2002a,** 4, 1628-1636.

Oldiges, C.; Tonsing, T. Molecular Dynamics Simulation of Structural, Mobility Effects between Dilute Aqueous CH_3CN Solution and Crosslinked PAA. Part 2. Dynamics. *Phys. Chem. Chem. Phys.* **2002b,** 4, 5135-5141.

Onate, E.; Idelsohn, S.; Zienkiewicz, O. C.; Taylor, R. L. A Finite Point Method in Computational Mechanics. Applications to Convective Transport and Fluid Flow. *Int. J. Numer. Methods Eng.* **1996a,** 39, 3839-3866.

Onate, E.; Idelsohn, S.; Zienkiewicz, O. C.; Taylor, R. L.; Sacco, C. A Stabilized Finite Point Method for Analysis of Fluid Mechanics Problems. *Comput. Methods Appl. Mech. Eng*. **1996b,** 139, 315-346.

Osada, Y.; Hasebe, M. Electrically Activated Mechanochemical Devices Using Polyelectrolyte Gels. *Chem. Lett.* **1985,** 1285-1288.

Osada, Y.; Gong, J. P. Stimuli-Responsive Polymer Gels and Their Application to Chemomechanical Systems. *Prog. Polym. Sci.* **1993,** 18, 187-226.

Osada, Y.; Ross-Murphy, S.B. Intelligent Gels. *Sci. Am*. **May 1993,** 82-87.

Osada, Y.; Kishi, R.; Hasebe, M. Anomalous Chemomechanical Characteristics of Electro-Activated Polyelectrolyte Gels. *J. Polym. Sci. Part C* **1987,** 25, 481-485.

Osada, Y.; Gong, J. P.; Sawahata, K. Synthesis, Mechanism, and Application of an Electro-Driven Chemomechanical System Using Polymer Gels. *J. Macromol. Sci. Chem.* **1991,** A28, 1189-1205.

Osada, Y.; Okuzaki, H.; Hori, H. A Polymer Gel with Electrically Driven Motility.

Nature, **1992,** 355, 242-244.

Overbeek, J. T. G. The Donnan equilibrium. *Prog. Biophys. Biophys. Chem.* **1956,** 6, 57–84.

Panofsky, W. K.; Phillips, M. Classical Electricity and Magnetism, 2nd Ed.; Addison-Wesley: Reading, MA, 1964.

Park, H.; Park, K. Biocompatibility Issues of Implantable Drug Delivery Systems. *Pharm. Res*. **1996,** 13, 1770-1776.

Peppas, N.A., Ed., *Hydrogels in Medicine and Pharmacy*; CRC Press: Boca Raton, FL, 1987.

Peppes, N. A. Bures, P.; Leobandung, W.; Ichikawa, H. Hydrogels in Pharmaceutical Formulations. *Eur. J. Pharm. Biopharm.* **2000a,** 50, 27-46.

Peppas, N. A.; Huang, Y.; Torres-Lugo, M.; Ward, J. H.; J. Zhang. Physicochemical Foundations and Structural Design of Hydrogels in Medicine and Biology. *Annu. Rev. Biomed. Eng.* **2000b,** 2, 9-29.

Peters, A.; Candau, S. J. Kinetics of Swelling of Polyacrylamide Gels. *Macromolecules* **1986,** 19, 1952-1955.

Podual, K.; Doyle III, F. J.; Peppas, N. A. Preperation and Dynamic Response of Cationic Copolymer Hydrogels Containing Glucose Oxidase. *Polymer* **2000,** 41, 3975-3983.

Prange, M. M.; Hooper, H. H.; Prausnitz, J. M. Thermodynamics of Aqueous Systems Containing Hydrophilic Polymer or Gels. *AICHE J.* **1989,** 35, 803-813.

Press, W. H.; Teukolsky, S. A.; Vetterling, W. T.; Flannery, B. R. *Numerical Recipes in C: the Art of Scientific Computing,* 2nd ed.; Cambridge University Press: Cambridge, 1992.

Quinn, T.M.; A.J. Grodzinsky. Longitudinal Modulus and Hydraulic Permeability of Poly(methacrylic acid) Gels: Effects of Charge Density and Solvent Content. *Macromolecules* **1993,** 26, 4332-4338.

Randles, P. W.; Libersky, L. D. Smoothed Particle Hydrodynamics: Some Recent Improvements and Applications. *Comput. Methods Appl. Mech. Engrg.* **1996,** 139, 375-408.

Randles, P. W.; Libersky, L. D. Normalized SPH with Stress Points. *Int. J. Numer. Methods Eng.* **2000,** 48, 1445-1462.

Redondo, A.; LeSar, R. Modeling and Simulation of Biomaterial. *Annu. Rev. Mater. Res.* **2004,** 34, 279-314.

Ricka, J.; Tanaka, T. Swelling of Ionic Gels: Quantitative Performance of the Donnan Theory. *Macromolecules* **1984,** 17, 2916-2921.

Roux, B.; Allen, T.; Berneche, S.; Im, W. Theoretical and Computational Models of Biological Ion Channels. Q. Rev. Biophys. **2004,** 37, 15-103.

Rubinstein, I. *Electro-Diffusion of Ions*; SIAM Studies in Applied Mathematics; SIAM: Philadelphia, 1990.

Samson, E.; Marchand, J. Numerical Solution of the Extended Nernst-Planck Model. *J. Colloid Interface Sci.* **1999,** *215*, 1-8.

Samson, E.; Marchand, J.; Robert, J. L.; Bournazel, J. P. Modeling Ion Diffusion Mechanisms in Porous Media. *Int. J. Numer. Methods Eng.* **1999,** *46*, 2043-2060.

Schneider, S.; Linse, P. Monte Carlo Simulation of Defect-Free Cross-linked Polyelectrolyte Gels. *J. Phys. Chem. B* **2003,** 107, 8030-8040.

Segalman, D. J.; Witkowski, W. R.; Adolf, D.; Shahinpoor, M. Electrically-Controlled Polymeric Gels as Active Materials in Adaptive Structures. In Proceeding of the ADPA/AIAA/ASME/SPIE Conference on Active Materials and Adaptive Structures, Alexandria, VA, Nov 4-8, 1991; Knowles, G. J., Ed.; IOP Publishing: Bristol, 1992a.

Segalman, D. J.; Witkowski, W. R.; Adolf, D.; Shahinpoor, M. Theory and Application of Electrically Controlled Polymeric Gels. *Smart Mater. Struct.* **1992b,** 1, 95-100.

Segalman, D. J.; Witkowski, W. R.; Rao, R.; Adolf, D.; Shahinpoor, M. Finite Element Simulation of the 2D Collapse of a Polyelectrolyte Gel Disk. In *Smart Materials and Structures1993: Smart Material*, Proceeding of SPIE 1916, Albuquerque, NM, Feb 1-4, 1993; Varadan, V. K., Ed.; SPIE: Washington, 1993.

Selberherr, S. *Analysis and Simulation of Semiconductor Devices*; Springer: New York, 1984.

Shahinpoor, M. Nonhomogeneous Large Deformation Theory of Ionic Polymeric Gels in Electric and pH Field. In *Smart Materials and Structures1993: Smart Material*, Proceeding of SPIE 1916, Albuquerque, New Mexico, Feb 1-4, 1993; Varadan, V. K., Ed.; SPIE: Washington, 1993a.

Shahinpoor, M. A Relationship between the Volumetric Strain and the pH in Ionic Polymeric Gels. In *Smart Materials and Structures1993: Smart Material*, Proceeding of SPIE 1916, Albuquerque, New Mexico, Feb 1-4, 1993; Varadan, V. K., Ed.; SPIE: Washington, 1993b.

Shahinpoor, M. Continuum Electromechanics of Ionic Polymeric Gels as Artificial Muscles for Robotic Application. *Smart Mater. Struct.* **1994,** 3, 367-372.

Shahinpoor, M. Micro-electro-mechanics of Ionic Polymeric Gels as Electrically-Controllable Artificial Muscles. *J. Intell. Mater. Syst. Struct.* **1995,** 6, 307-314.

Shahinpoor, M.; Kim, K. J. Ionic Polymer – Metal Composites: III Modeling and Simulation as Biomimetic Sensors, Actuators, Transducers, and Artificial Muscles. *Smart Mater. Struct.* **1998,** 13, 1362-1388.

Shahinpoor, M.; Bar-Cohen, Y.; Simpson, J. O.; Smith, J. Ionic Polymer – Metal Composites (IPMCs) as Biomimetic Sensors, Actuators and Artificial Muscles – A Review. *Smart Mater. Struct.* **1998,** 7, R15-R30.

Shepard, D. A Two-Dimensional Interpretation Function for Irregularly-Spaced Data. In *Proceedings of the 23rd ACM National Conference;* ACM Press: New York, 1968.

Shibayama, M.; Tanaka, T. Volume phase transition and related phenomena of polymer gels. In *Responsive Gels: Volume Transitions I*; Dusek, K., Ed; Advances in Polymer Science Vol. 109, Springer-Verlag: Berlin, 1993; pp 1-62.

Shiga, T. Deformation and Viscoelastic Behavior of Polymer Gels in Electric Fields. In *Neutron Spin Echo Spectroscopy, Viscoelasticity, Rheology*; Edwards, S., Ed.; Advances in Polymer Science Vol. 134, Springer-Verlag: Berlin, 1997; pp 131-163.

Shiga, T.; Hirose, Y.; Okada, A.; Kurauchi, T. Bending of Poly(Vinyl Alcohol)-Poly(Sodium Acrylate) Composite Hydrogel in Electric Fields. *J. Appl. Polym. Sci.* **1992a,** 44, 249-253.

Shiga, T.; Hirose, Y.; Okada, A.; Kurauchi, T. Electric Field-Associated Deformation of Polyelectrolyte Gel Near a Phrase Transition Point. *J. Appl. Polym. Sci.* **1992b,** 46, 635-640.

Shiga, T.; Kurauchi, T. Deformation of Polyelectrolyte Gels under the Influence of Electric Field, *J. Appl. Polym. Sci.* **1990,** 39, 2305-2320.

Shoenfeld, N. A.; Grodzinsky, A. J. Contribution of Electrodiffusion to the Dynamics of Electrically Stimulated Changes in Mechanical Properties of Collagen Membranes, *Biopolymers* **1980,** 19, 241-262.

Siegel, R. A. pH Sensitive Gels: Swelling Equilibria, Kinetics and Applications for Drug Delivery. In *Pulse and Self-Regulated Drug Delivery*; Kost, J., Ed.; CRC Press: Boca Raton, 1990; pp 129-155.

Siegel, R. A.; Firestone, B. A. pH-dependent Equilibrium Swelling Properties of Hydrophobic Polyelectrolyte Copolymer Gels. *Macromolecules* **1988,** 21, 3254-3259.

Siegel, R. A.; Firestone, B. A.; Cornejo-Bravo, J.; Schwarz, B. Hydrophobic Weak Polybasic Gels: Factors Controlling Swelling Equilibrium. In *Polymer Gels: Fundamental and Biomedical Applications*; DeRossi, D.; Kajiwara, K.; Osada, Y.; Yamauchi, A., Eds.; Plenum Press: New York, 1991; pp 309-317.

Sjodin, R. A. Ion Transport across Excitable Cell Membranes. In *Biophysics and Physiology of Excitable Membranes*; W. J. Adelman Jr., Ed.; Van Nostrand Reinhold Co.: New York, 1971; pp 96-124.

Snita, D.; Paces M.; Lindner J.; Kosek J.; Marek M. Nonlinear behavior of simple ionic system in hydrogel in an electric field. *Faraday Discuss.* **2001,** 120, 53-66.

Snyder, J. F.; Shriver, D. F.; Ratner, M. A. Optimizing the Design of Polyelectrolytes Using Monte Carlo Simulations. *J. Electrochem. Soc.* **2001,** 148, A858-A863.

Snyder, J. F.; Ratner, M. A.; Shriver, D. F. Polymer Electrolytes and Polyelectrolytes: Monte Carlo Simulations of Thermal Effects on Conduction. *Solid State Ion.* **2002,** 147, 249-257.

Steinberg, I. Z.; Oplatka, A; Katchalsky, A. Mechanochemical Engines. *Nature* **1966,** 210, 568-571.

Suh, F. J. K.; Matthew, H. W. T. Application of Chitosan-based Polysaccharide Biomaterials in cartilage Tissue Engineering: A Review. *Biomaterials* **2000,** 21, 2589-2598.

Suleimenov, I. E.; Sigitov, V. B.; Kudaibergenov, S. E.; Didukh, A. G.; Fryasinova, T. S.; Bekturov, E. A. Influence of Combined Magnetic and Electric Fields on the Behavior of Polyelectrolyte Hydrogel. *Polym. Int.* **2001,** 50, 194-196.

Sun, D. N.; Gu, W. Y.; Guo, X. E.; Lai, W. M.; Mow, V. C. A mixed Finite Element Formulation of Triphasic Mechano-Electrochemical Theory for Charged, Hydrated Biological Soft Tissues. *Int. J. Numer. Meth. Engng.* **1999,** 45, 1375-1402.

Sussmann, M. V.; Katchalsky, A. Mechanochemical Turbine: A New Power Cycle. *Science* **1970,** 167, 45-47.

Suzuki, A.; Tanaka, T. Phase-Transition in Polymer Gels Induced by Visible-Light. *Nature* **1990,** 346, 345-347.

Swegel, J. W.; Attaway, S. W.; Heinstein, M. W.; Mello, F. J.; Hicks, D. L. *An Analysis of Smoothed Particle Hydrodynamics.* Sandia Report SAN93-2513; Sandia National Laboratories: Albuquerque, NM, 1994.

Syganow, A.; von Kitzing, E. The Drift Approximation Solves the Poisson, Nernst-Planck, and Continuum Equation in the Limit of Large External Voltages. *Eur. Biophys. J.* **1999,** 28, 393-414.

Takeda, H.; Miyama, S. M.; Sekiya, M. Numerical Simulation of Viscous Flow by Smoothed Particle Hydrodynamics. *Prog. Theor. Phys.* **1994,** 92, 939-960.

Tanaka, N.; Araki, M. Polymer-based Packing Materials for Reversed-Phase Liquid Chromatography . *Adv. Chromatogr.* **1989,** 30, 81-122.

Tanaka, T. Collapse of Gels and the Critical Endpoint. *Phys. Rev. Lett.* **1978,** 40, 820-823.

Tanaka, T. Phase Transition in Gels and Single Polymer. *Polymer* **1979,** 20, 1404-1412.

Tanaka, T. Gels. *Sci. Am.* **1981,** 244, 110-123.

Tanaka, T. Phase Transitions of Gels. In *Polyelectrolyte Gels: Properties Preparation and Applications;* Harland, R. S., Prud'homme, R. K., Eds.; ACS Symposium Series 480; American Chemical Society: Washington, DC, 1992; pp 1-21.

Tanaka, T.; Fillmore, D. Kinetics of Swelling of Gels. *J. Chem. Phys.* **1979,** 70, 1214-1218.

Tanaka, T.; Fillmore, D.; Sun, S. T.; Nishio, I.; Swislow, G.; Shah, A. Phase Transition in Ionic Gels. *Phys. Rev. Lett.* **1980,** 45, 1636-1639.

Tanaka, T.; Nishio, I.; Sun, S. T.; Ueno, S. Collapse of Gels in an Electric Field. *Science* **1982**, 218, 467-469.

Teorell, T. Transport Processes and Electrical Phenomena in Ionic Membranes. *Prog. Biophys.* **1953,** 3, 305-369.

Tieleman, D. P.; Berendsen, H. J. C. A molecular Dynamics Study of the Pores Formed by *Escherichia coli* OmpF Porin in a Fully Hydrated Palmitoyloleoylphosphatidylcholine Bilayer. *Biophys. J.* **1988,** 74, 2786-2801.

Tonsing, T.; Oldiges, C. Molecular Dynamic Simulation Study on Structure of Water in Crosslinked Poly(*N*-isopropylacrylamide) Hydrogels. *Phys. Chem. Chem. Phys.* **2001,** 3, 5542-5549.

Townshend, A., Ed.; *Encyclopedia of analytical science*, *Vol 1(A-Che)*; Academic Press: London, 1995.

Valiulin, R.; Skirda, V. Time Dependent Self-Diffusion Coefficient of Molecules in Porous Media. *J. Chem. Phys.* **2001,** 114, 452-458.

Van Gunsteren, W. F.; Berendsen, H. J. C. Computer Simulation of Molecular Dynamics: Methodology, Applications, and Perspectives in Chemistry. *Angew. Chem. Int. Ed. Engl.* **1990,** 29, 992-1023.

Victorov, A. I.; Radke, C. J.; Prausnitz, J. M. Molecular Thermodynamics for Swelling of Bicontinuous Gel. *Mol. Phys.* **2002,** 100, 2277-2297.

Viramontes-Gamboa, G.; Medina-Noyola, M.; Arauz-Lara, L. J. Brownian Motion of Colloidal Particles in Model Porous Medium. *Phys. Rev. E* **1995,** 52, 4035-4044.

Wallmersperger, T.; Kroplin, B.; Gulch, R. W. Modeling and Analysis of Chemistry and Electromechanics. In *Electroactive Polymer (EAP) Actuator As Artificial Muscles – Reality, Potential And Challenges*; Bar-Cohen Y., Ed.; SPIE Press monograph v. PM98; SPIE Press : Bellingham, Washington, 2001a; pp. 285-308.

Wallmersperger, T.; Kroplin, B.; Holdenried, J.; Gulch, R. W. A Coupled Multi-Field-Formulation for Ionic Polymer Gels in Electric Fields. In *Smart Structures and Materials 2001: Electroactive Polymer Actuators and Devices*, Proceeding of SPIE Vol. 4329, Bar-Cohen, Y., Ed.; SPIE: Washington, 2001b.

Wallmersperger, T.; Kroplin, B.; Gulch, R. W. Coupled Chemo-Electro-Mechanical Formulation for Ionic Polymer Gels – Numerical and Experimental Investigations. *Mech. Mater.* **2004,** 36, 411-420.

Wichterle, O.; Lim, D. Hydrophilic Gels for Biological Use. *Nature* **1960,** 185, 117-118.

Wilder, J.; Vilgis, T. A. Elasticity in Strongly Interacting Soft Solids: A Polyelectrolyte Network. *Phys. Rev. E* **1998,** 57, 6865-6874.

Woodson, H. H.; Melcher, J. R. *Electromechanical Dynamics. Part I: Discrete Systems*; John Wiley and Sons: New York, 1968.

Xu, Z. L. *Applied Elasticity*; Wiley Eastern Limited: New Delhi, 1992.

Yannas, I. V.; Grodzinsky, A. J. Electromechanical Energy Conversion with Collagen Fibers in An Aqueous Medium. *J. Mechanochem. Cell Motil.*, **1973,** 2, 113-125.

Yeager, E., Bockris, J. O'M., Conway, B. E., Sarangapani, S., Eds.; *Comprehensive Treatise of Electrochemistry, Volume 6 Electrodics: Transport*; Plenum Press: New York, 1983.

Yu, Q.; Bauer, J. M.; Moore, J. S.; Beebe, D. J. Responsive Biomimetic Hydrogel Valve for Microfluidics. *Appl. Phys. Lett.* **2001,** 78, 2589-2591.

Zhang, X.; Song, K. Z.; Lu, M. W.; Liu, X. Meshless Methods Based on Collocation with Radial Basis Functions. *Comput. Mech.* **2000,** 26, 333-343.

Zhao, B.; Moore, J. S. Fast pH- and Ionic Strength-Responsive Hydrogels in Microchannels. *Langmuir* **2001,** 17, 4758-4763.

Zhou, X.; Hon, Y. C.; Sun, S.; Mak, A. F. T. Numerical Simulation of the Steady-state Deformation of a Smart Hydrogel under An External Electric Field. *Smart Mater. Struct.* **2002,** 11, 459-467.

Zhu, T.; Zhang, J. D.; Atluri, S. N. A Local Boundary Integral Equation (LBIE) Method in Computational Mechanics and a Meshless Discretization Approach. *Comput. Mech.* **1998,** 21, 223-235.

PUBLICATIONS ARISING FROM DISSERTATION

Journal papers

1) Ng, T.Y.; Li, Hua; Cheng, J.Q.; Lam, K.Y.; Yew, Y.K. A Novel True Meshless Numerical Technique (*h*M-DOR Method) for the Deformation Control of Circular Plates Integrated with Piezoelectric Sensors/Actuators. *Smart Mater. Struct*. **2003,** 12, 955-961.
2) Yan, G.P.; Li, Hua; Cheng, S.X.; Bottle, S.E.; Wang, X.G.; Yew, Y.K.; Zhuo, R.X. Preparation, Properties, and Mathematical Modeling of Microparticle Drug Delivery Systems Based on Biodegradable Amphiphilic Triblock Copolymers. *J. Appl. Polym. Sci.* **2004,** 92, 3869-3873.
3) Li, Hua; Yew, Y.K.; Lam, K.Y.; Ng, T.Y. Numerical Simulation of pH-Stimuli Responsive Hydrogel in Buffer Solutions. *Colloid Surf. A-Physicochem. Eng. Asp*. **2004,** 249, 149-154.
4) Li, Hua; Ng, T.Y.; Yew, Y.K.; Lam, K.Y. Modeling and Simulation of the Swelling Behavior of pH-Stimuli-Responsive Hydrogels. *Biomacromolecules*. 2005, **6,** 109-120.
5) Li, Hua; Yew, Y.K.; Lam, K.Y. Meshless Steady-State Analysis for Swelling Equilibrium of pH-Sensitive Hydrogel in Buffered Solution. *J. Electroanal. Chem.* **2005,** 580, 161-172.
6) Lam, K.Y.; Li, Hua; Yew, Y.K.; Ng, T.Y. Structural Analysis via Meshfree Hermite-Cloud Method. *Int. J. Mech. Sci.* **2006,** 48, 440-450.
7) Yew, Y.K.; Li,Hua; Ng, T.Y.; Lam, K.Y. Analysis of pH Controlled Swelling of Hydrogel. *Biomedical Microdevices* (submitted)
8) Yew, Y.K.; Ng, T.Y.; Li, Hua; Lam, K.Y. Modeling of Electrochemically Functioning pH-Responsive Hydrogel *Biochimica et Biophysica Acta - General Subjects* (submitted)

Conference papers

1) Li, Hua; Ng, T.Y.; Yew, Y.K. Model Development and Behavior Simulation of pH-Stimulus-Responsive Hydrogels. *International Conference on Scientific and Engineering Computation, IC-SEC 2002*, 3-5th December 2002, Singapore.
2) Cheng, J.Q.; Li, H.; Lam, K.Y.; Ng, T.Y.; Yew, Y.K. A Hybrid Meshless-Differential Order Reduction (*h*M-DOR) Method for Deformation Control Analysis of Smart Circular Plate by Sensors/Actuators. *The 2nd International Conference on Structural Stability and Dynamics, ICSSD 2002,* 16-18th December 2002, Singapore.
3) Li, Hua; Yew, Y.K.; Ng, T.Y. Numerical Simulation of Hydrogel-Based pH-Responsive Biosensors in BioMEMS. *Symposium on Design, Test, Integration and Packing of MEMS/MOEMS, DTIP 2003,* 5-7th May 2003, Mandelieu-La Napoule, France.
4) Yew, Y.K.; Li, Hua; Lam, K.Y.; Ng, T.Y. Numerical Simulation of pH-Stimuli Responsive Hydrogel in Buffer Solutions. *First International Meeting on Applied Physics, Aphys 2003,* 13-18th October 2003, Badajoz, Spain.
5) Li, Hua; Yew, Y.K.; Lam, K.Y. Numerical studies of chemically and electrically controlled hydrogel for BioMEMS application. *The First International SBE Conference on Bioengineering and Nanotechnology, ICBN 2004,* 26-29th September 2004, Singapore.